Volume 12

# Multiscale Modeling of Pedestrian Dynamics

Emiliano Cristiani • Benedetto Piccoli • Andrea Tosin

MS&A

Modeling, Simulation & Applications

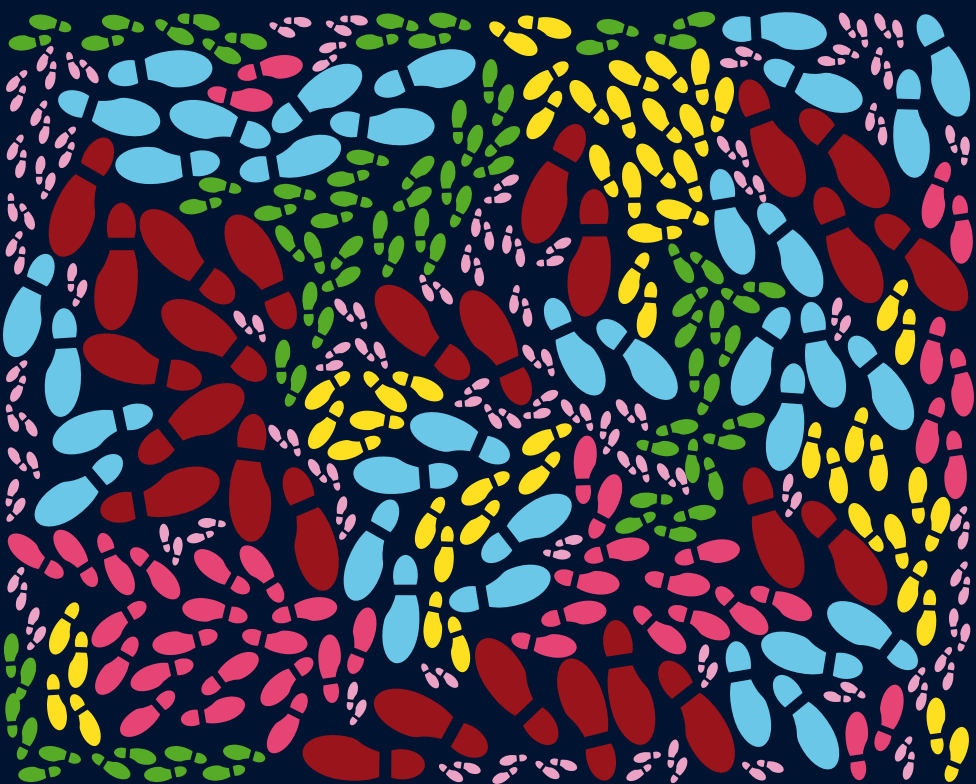

Springer

# MS&A

## Volume 12

Emiliano Cristiani • Benedetto Piccoli •
Andrea Tosin

# Multiscale Modeling of Pedestrian Dynamics

Springer

Emiliano Cristiani
Andrea Tosin
Consiglio Nazionale delle Ricerche
Istituto per le Applicazioni del Calcolo
M. Picone
Rome
Italy

Benedetto Piccoli
Department of Mathematical Sciences
Rutgers University
Camden, NJ
USA

ISSN 2037-5255 ISSN 2037-5263 (electronic)
MS&A – Modeling, Simulation & Applications
ISBN 978-3-319-06619-6 ISBN 978-3-319-06620-2 (eBook)
DOI 10.1007/978-3-319-06620-2
Springer Cham Heidelberg New York Dordrecht London

Library of Congress Control Number: 2014946611



Printed on acid-free paper

Springer is part of Springer Science+Business Media (www.springer.com)

*If people do not believe that mathematics is simple, it is only because they do not realize how complicated life is.*

John von Neumann

*To my newborn son Dario, who will soon be a pedestrian*

*To my son Edoardo*

*To my parents Rosanna and Dario*

# Preface

This book presents to researchers and graduate students mathematical models and numerical simulations of crowd dynamics. The book is addressed to scholars and professionals with different backgrounds, in particular applied mathematicians, physicists, engineers, system biologists, and psychologists, who can, for various reasons, be interested in mathematical modeling of crowd behavior and, more in general, of granular flows in living and nonliving complex systems from a multiscale point of view.

In a broader sense, this book is about the *science of mathematical modeling*, seen in action under the particular perspective of pedestrian dynamics modeling. The *leading idea* is that Applied Mathematics does not just consist in the application of existing models to practical case studies but, first and foremost, in the construction of *original mathematical approaches* motivated by often nonstandard problems continuously posed by the real world. In this respect, the cultural path followed in the book encompasses rigorous procedures of mathematization of reality, analysis of the mathematical structures thereby derived, and simulation of realistic scenarios which can constitute a basis for a fruitful dialogue with non-mathematical practitioners.

Research about crowd dynamics is fostered by both theoretical and practical reasons. On the one hand, many scholars want to understand the basic principles of pedestrian motion. Their insights can often be translated into mathematical models, which can be validated through simulations. On the other hand, practitioners are interested in faithful simulations of self-organized phenomena arising in pedestrian flows, especially in complex-shaped two-dimensional built environments. Indeed, it is well known that neglecting group behaviors can lead to major safety issues. Therefore, our interest is mainly focused on models which reproduce the spontaneously emerging *self-organized collective patterns* out of an accurate and realistic design of *individual interaction rules*. Namely, without resorting to the artificial inclusion of empirical features in the mathematical equations with the primary aim of reproducing target phenomena. In this respect, we note that crowd dynamics are often nicely visualized in computer graphics animations: Our approach is rather different, since we aim at a deeper understanding, through mathematical models, of the basic dynamical principles ruling crowd behaviors. To this goal, we consider two

points of view which have been classically taken in crowd dynamics modeling: The *microscopic* one, in which pedestrians are tracked individually, and the *macroscopic* one, in which pedestrians are assimilated to a continuum and observed through their average density. We present in detail and critically analyze selected existing models. Then, as a *core topic*, we develop a *multiscale paradigm*, which allows one to bridge the various scales, taking the most from each of them in terms of capturing the relevant clues of complexity of crowds. Our background idea is indeed that most of the complex trends exhibited by crowds are due to an intrinsic interplay between *individual* and *collective behaviors*, which are capable of affecting each other. The modeling approach we promote in this book pursues actively this intuition and profits from it for designing a general multiscale mathematical method susceptible of application also in fields different from the inspiring original one.

The book is divided in two parts and eight chapters, plus two appendices. The first part, mainly introductory, is dedicated to a broad audience. It features virtual experiments pointing out, on the one hand, the phenomenology of pedestrian behaviors we are interested in and, on the other hand, the ability of our multiscale model to address such phenomena. The second part, characterized by a more technical content, presents an overview of single-scale models and the details of our multiscale approach, together with analytical and numerical results, plus its generalization to different application fields.

The hallmarks of the present work, which make it different from other books on the same topic available in the literature, can be summarized as follows:

- This book promotes a true interplay among modeling, theory, and numerics for a cutting-edge multidisciplinary research topic. One of the leading principles is that models should originate from a correct interplay between real world and mathematics.
- This book offers an accurate review of models of crowd dynamics: Both seminal and the most relevant descending works are presented with a sufficient detail to allow readers to be quickly up-to-date with the state of the art in the field.
- This book focuses on a new multiscale description of crowd dynamics, based on measure theory, which covers the full path of Applied Mathematics: Model derivation, qualitative analysis, construction and analysis of numerical schemes, and application of the algorithms to the simulation of more and less standard benchmarks in pedestrian dynamics.
- Numerical tests highlight the effects of the interplay between small and large scales on pedestrian dynamics, suggesting that crowd modeling requires definitely a multiscale approach, in which scales truly integrate and complement.
- This book provides a ready-to-implement pseudo-code version of the multiscale algorithm.

Rome, Italy — Emiliano Cristiani
Camden, New Jersey, USA — Benedetto Piccoli
Rome, Italy — Andrea Tosin
July 4, 2014

# Acknowledgements

We thank Paolo Frasca, who contributed to the development of the model for social groups presented in Sect. 2.6; Francesco Rossi, who coauthored the research which led to the results presented in Chap. 7; Sauro Succi for insightful discussions about the application of the multiscale model to new fields, particularly to Quantum Mechanics; and Giovanna Nappo, who improved the quality of Sect. 8.4.

# Contents

# Part I
# Pedestrian Behavior: Phenomenology and Simulations

# Chapter 1
# An Introduction to the Modeling of Crowd Dynamics

**Abstract** In this chapter we begin the discussion about crowd dynamics from an informal phenomenological point of view. In particular, we put in evidence how simple interaction rules adopted independently by pedestrians generate, at a collective level, complex group behaviors featuring various forms of self-organization. Bearing in mind the ultimate goal of the book, which is mathematical modeling, we promote the idea that understanding such basic behavioral rules contributes to the modeling at all scales, also those not directly focused on single individuals. In the light of these arguments, we critically analyze the main scales of observation and representation which are typically used in mathematical modeling, namely the microscopic, the macroscopic, and the mesoscopic (or kinetic) scale. For each of them we discuss the advantages/drawbacks in catching/losing specific features of crowd dynamics, with a view also to the interplay with the available experimental knowledge about crowds. Finally we elucidate the role of the book in this cultural framework and we give reading directions through the various chapters targeted to a few different kinds of readerships.

## 1.1 Modeling-Oriented Phenomenological Issues

In this section we review the most important pedestrian behavioral rules which are usually taken into account in crowd modeling. As a complement, we discuss the concept of *self-organization* as a collective (and hardly predictable) result of those behavioral rules.

### *1.1.1 Behavioral Rules*

Modeling crowd dynamics requires to identify at least the most important behavioral rules pedestrians are subject to. It is plain that a pedestrian, as a complex living being, is basically unpredictable. Nevertheless, some guidelines can be drawn.

E. Cristiani et al., *Multiscale Modeling of Pedestrian Dynamics*, MS&A 12,
DOI 10.1007/978-3-319-06620-2_1,

#### 1.1.1.1 Target

In most of the cases, people move in a bounded space and have a desired destination to be reached. This destination, together with the geometry of the space, defines a *desired velocity field* which is exactly the velocity people would keep if they were alone in the domain. The desired velocity can be very different whether the pedestrian under observation knows the domain or moves in a unfamiliar environment. In the latter case, an exploration phase has to be taken into account. In the rest of the book, we will denote by $\Omega \in \mathbb{R}^d$ the walking area, $\Gamma \in \Omega$ the target, and $v_{\mathrm{d}} : \Omega \to \mathbb{R}^d$ the desired velocity field, where $d$ is the dimension of $\Omega$, usually $d = 2$.

The final velocity field pedestrians actually follow will be given by a suitable combination of the desired velocity field and the *interaction velocity field*, defined taking into account the following features of pedestrians.

#### 1.1.1.2 Repulsion

People want to avoid collisions, so they stop when they are too close to other people. Moreover, they have a tendency to avoid crowded regions, as well as to stay clear of walls and obstacles. Often mathematical models take into account this behavior by assuming the existence of a fictitious *repulsive force* which drives people toward clear spaces.

#### 1.1.1.3 Attraction

Sometimes people have the tendency to follow other people or simply stay in touch. This is the case of *social groups* like friends, families, tourist groups, and so on. For example, small groups of walking friends want to reach their destination all together, while keeping eye-contact and speaking with each other. Instead, tourist groups want primarily stay in touch with their guide (i.e. the sole person who knows the destination) and then keeping the group itself cohesive.

#### 1.1.1.4 Keeping Direction

People have the tendency to keep the same direction of motion, since changing direction is tiresome and usually inefficient. This is one the reason which makes walking through a crowd an annoying task.

#### 1.1.1.5 Visual Field

People have a limited visual field. It is usually assumed to be an angle of 170° or 180°, where the central area is sharper than the lateral ones. The line which divides

in two equal parts the visual field can coincide with the actual direction of motion or, instead, with the desired direction of motion, and it is obviously related to the head orientation. If, on the one hand, the assumption that people can see only in front is reasonable, on the other hand it must be noted that people can turn their head, thus perceiving almost all the space around, and that other senses than sight can be involved, like, e.g., hearing and touch. Visual field is also limited by any obstruction people can perceive, like walls, columns, and other pedestrians themselves.

#### 1.1.1.6 Sensory Regions

In normal conditions, people do not interact with the others by contact, as mechanical particles do. Rather, they observe the surrounding space and take decisions. Sensory regions, *which are in general different from the visual field*, represent the portion of the space effectively considered before taking a decision, and can be different from need to need. For example, pedestrians are mainly repulsed by other people walking both close and in front to them, or by people walking on a "collision course", while they are little or no repulsed by far-away pedestrians, even if they are in the visual field. Then, repulsive sensory region is usually short-range and anisotropic. Attraction, instead, can be much more extended in space, even up to the whole visual field.

Sensory regions are one of the main ingredients of the mathematical models and sometimes make the difference among them. Indeed, changing the shape of the sensory regions defined for the various tasks leads to major differences in the simulated pedestrian behavior.

In the rest of the book, we will denote a generic sensory region by $\mathscr{S}(x)$, where $x$ is the position of the pedestrian under observation.

#### 1.1.1.7 Metric vs Topological Sensory Regions

People have limited capabilities in processing information. They cannot perceive (and then respond to) many stimuli at the same time. This means that concurrent stimuli are processed one after the other, and complex situations are actually "simplified". In particular, people do not interact (by means of a repulsion force, for example) with more than a few people contemporaneously. If a *topological* definition of the sensory region $\mathscr{S}$ is applied, $\mathscr{S}$ is continuously enlarged or shrunk in order to include exactly the number of pedestrians who can reasonably be taken into account. This choice effectively models the limitations of the human brain in terms of processing information. On the contrary, if a *metric* definition of $\mathscr{S}$ is applied, the size of $\mathscr{S}$ is fixed once and for all, and the number of the observed pedestrians can be either less or more than the possible one. The latter choice is usually made for simplicity, but it can lead to unrealistic results, especially in case of large crowds.

#### 1.1.1.8 Panic

In case of panic, some of the behavioral rules described above change or cease to apply. The main difference with respect to the normal conditions is that interactions become *physical* and people start pushing. This obviously change the shape of the sensory regions. In addition, people move faster, change directions more often, are attracted to people who have a clear direction (in the hope they have found a safe way out), become more selfish stopping any kind of collaboration, and coordinated movements are lost.

### *1.1.2 Self-Organization*

We say that a crowd is "organized" when a *leader* (inside or outside of the crowd) decides its spatial distribution in order to maximize some global utility. Instead, we say that a crowd is "self-organized" when a coordinated spatial distribution arises by simply applying some local behavioral rules or one-to-one interactions among pedestrians. In the latter case, no one really decides the final shape of the crowd, and the shape which is finally assumed does not necessarily maximize some global utility. Nevertheless, it can happen that people take advantage of the organization which is spontaneously created.

Self-organization in pedestrians shows some important differences with respect to the same phenomenon observed in other biological systems, like animals or cells. As an example, let us consider the well known self-organizing phenomenon of trail formation in ants. In that case, the trail arises from two simple local rules followed by the ants: First, if an ant has found some food and it is coming back to the nest, then it drops on the ground a particular scent, which slowly evaporates. Second, if an ant smells the scent, it follows the trace. These two rules do not require any direct interaction among ants, and no long-range information about food location is spread around the ant colony by an informed individual. It must be noted that ants *are not aware* of forming or following a trail, which can be quite long if compared with the ant size. Then, the overall organization is not perceived by the ants.

It is very difficult to find among humans a phenomenon which shows a perfect analogy with the one mentioned above. Indeed, humans usually perceive and understand the global phenomenon they are part of, even if they did not want or was not able to forecast its emergence. Then, if a single pedestrian is not comfortable with the self-organized phenomenon she is contributing to form, she can rationally change the local rules which are the cause of that phenomenon. This makes pedestrians able to control the overall system, at least partially.

Having this in mind, we list here some self-organized patterns which are observed in crowds and often attempted to be reproduced by mathematical models, see Figs. 1.1–1.3.

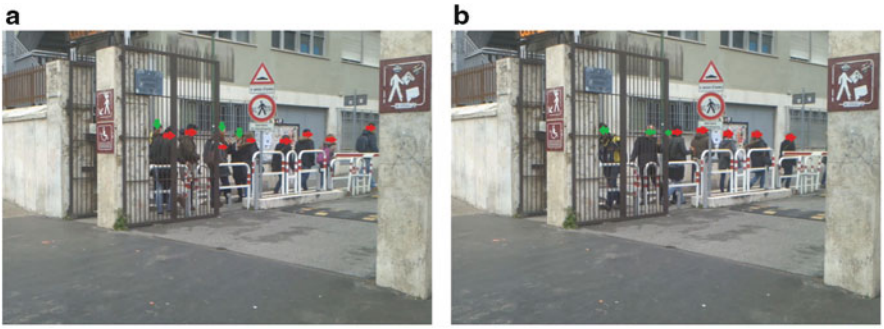


**Fig. 1.1** Intermittent flows. Photos taken on February 5, 2014 (Wednesday), lunch time, Sapienza – University of Rome. The gate does not allow the passage of two pedestrians at the same time. (**a**) The first group, marked with *green arrows*, has to wait for the passage of the second group, marked by *red arrows*; (**b**) as soon as the first group passed through, the first group moves ahead (©Emiliano Cristiani)


**Fig. 1.2** Arching. Photos taken on January 8, 2013 (Tuesday) in Tivoli (Rome), 8:00 a.m., train station. As soon as the train reaches the station, people run toward the nearest door. They are aware that last people in likely have to be standing for the entire 1-h journey because of lack of seats (©Emiliano Cristiani)

- Intermittent flows at shared bottleneck (Fig. 1.1). When two populations of pedestrians walking in opposite directions have to share a bottleneck, a sort of traffic light effect is observed: Some people of the first population passes the bottleneck, then they stop to allow some people of the other population to pass, and so on. The break of symmetry arises naturally, since there is no leader who settles the flows.
- Arching at bottlenecks (Fig. 1.2). When a large number of people has to pass quickly through a bottleneck (a small door, for example), the formation of a semi-circular arc just before the bottleneck is observed. In particular, people do not queue neatly one after the other. This arching effect can actually drop the efficiency of the overall dynamics.
- Lane formation in crossing flows (Fig. 1.3c). Two populations of pedestrians which walk in opposite directions self-organize in lanes. The space is divided in stripes, each of which is occupied by pedestrians moving in one direction only. This way diminishes the probability of encounters among pedestrian having opposite directions, thus improving the overall efficiency of both flows.


**Fig. 1.3** (**a**) V-like pattern. Photo taken on November 14, 2013 (Thursday), University of Rome "Tor Vergata". Three post-docs come back to their office after lunch; (**b**) teen wall. Photo taken on November 9, 2013 (Saturday) in Tivoli (Rome), 6 p.m., main shopping street; (**c**) lanes in crossing flows. Photo taken on February 5, 2014 (Wednesday), lunch time, Sapienza – University of Rome. Note that the crosswalk is partially obstructed by improperly parked cars, and the pedestrian traffic light is *red* (!). Forming lanes is the only way for pedestrians to cross the street sufficiently fast (©Emiliano Cristiani)

- V-like (Fig. 1.3a). Small social groups of walking friends or family members often assume a configuration which resembles a V, where the vertex is pointing against the direction of motion. This terminology comes from the biological literature, in particular that regarding migrating geese which show a V-like configuration where the vertex is directed toward the flying direction. By means of the V-like configuration each pedestrian finds a comfortable walking position supporting visual and verbal communication with the other group members. When the group has more than four members, it often split up in smaller groups.
- River-like and wall-like configuration (Fig. 1.3b). In social groups, V's are a good compromise between a short-range repulsion (to avoid collisions) and attraction (to stay together and communicate). When the surrounding crowd density reaches high levels, physical constraints prevail over social preferences and communications stop. People then start walking one behind the another,

forming a river-like pattern. An interesting exception is represented by groups of (hand-holding) teenagers. They are less susceptible to physical constraints and more interested in communicating and being noticed. Then, they can form outright moving walls orthogonal to the direction of motion, forcing the others to slow down and circumvent them.

In Sect. 3.2.3 we will come back on self-organization issues with a more detailed discussion which follows some psychological considerations about pedestrians as individuals.

## 1.2 Preliminary Reasonings on Mathematical Modeling

### *1.2.1 Crowds as a Living Complex System*

When attempting to describe new real world systems by mathematical equations one is normally faced with two possible approaches. The first one can be called the approach *by analogy*. One tries to figure out whether a more familiar system exists, which has already been successfully modeled, showing qualitatively comparable trends to those observed in the new system. Then one uses the models set up for the familiar system as a starting point for the mathematization of the new one. The second approach is instead based on the idea that the novelty itself of the new system should induce a mathematization ab initio, i.e., from very basic first principles.

The validity of either approach depends strongly on the peculiarities of the new system at hand. If there are reasons to suspect that the way in which it works is phenomenologically different from other better known systems then the first approach should be rejected in favor of the second one, despite the possible similarity of the observable behaviors. In fact, mathematical models should not limit themselves to reproducing observable behaviors. They should mainly identify the underlying less visible causes leading to such behaviors, so as to provide an essential explanation of the basic mechanisms ruling the system. Indeed, it is on this basis that reliable simulations and predictions can be grounded, also in scenarios not yet empirically tested. On the other hand, if the new system is clearly structurally similar to another one then the second approach should be rejected in favor of the first one, because it runs the risk of being uselessly time-consuming. In fact, there is no need for rediscovering from the beginning well consolidated mathematical structures. However, in both cases a preliminary careful analysis of the distinguishing features of the new system is the essential first step.

Human crowds can be classified, with good reasons, among the *new* systems which mathematics has started to deal with in relatively recent times. At the beginning, the main modeling approach was by analogy with particle systems of gas dynamics. Pedestrian dynamics were assimilated to those of gas particles described as a continuum flowing in space, the inspiration being drawn mainly from the similarity of the observed qualitative flow patterns in the two cases. Some

authors also borrowed a terminology proper of fluid dynamics, using expressions such as *laminar* and *turbulent* flow, for describing different regimes of crowd movement. However, more recently the idea of crowds as a *living complex system* has begun to impose itself, suggesting that an approach ab initio may be preferable for constructing more targeted mathematical models.

To say that crowds are a complex system means basically that one cannot expect to predict the behavior of *many* pedestrians from the detailed knowledge of the behavior of *one* pedestrian (as it happens instead for e.g., fluid particles). Indeed individual pedestrians modify continuously their local walking program due to interactions with neighboring people. This way they generate spontaneous collective trends not directly contained in the simple behavioral rules followed by each of them. It is as if repeated mutual interactions "amplified" the effect of the individual behavioral rules in a hardly controllable way. Even more important, all of this is made possible largely by the fact that crowds are *living* systems, i.e., they are not *passively* subject to the inertia law like the inert matter (e.g., again fluid particles). Actually, this does not mean that pedestrians elude the usual laws of Physics. Rather, they are able to influence the latter *actively* through personal decisions, whose impact is not necessarily assimilable to that of external force fields.

In view of the reasonings just proposed, it is of some importance to discuss a few basic complexity clues of crowds that mathematical models should cope with. In order for model to comply with them as much as possible, it can be guessed that methods traditionally used for describing the inert matter have to evolve, as already implied, in new mathematical ideas.

#### 1.2.1.1 Interactions and Multiscale Effects

Interactions among pedestrians pertain specifically to the scale of *single individuals*. Indeed, they are usually one-to-one, or at most one-to-few, as they involve immediate neighbors. On the other hand, the probably most striking effect of such interactions is the spontaneous emergence of self-organized *collective* flow patterns, clearly visible at a group level. This kind of influence of smaller on larger scales can be viewed as an *individuality-to-collectivity* scaling. Nevertheless, also the opposite influence is possible, namely the local collective state of the crowd (e.g., the local crowding of an area) can modify the individual interaction rules. Mathematical models should provide a way to link the individual point of view, which generates the dynamics, to a large-scale collective representation not necessarily focused on single pedestrians.

#### 1.2.1.2 Perception Ability and Expression of Behavioral Strategies

Pedestrians react to the neighboring crowd according to the *perception* they have of it. This is a subjective ability, which corresponds to the expression of a behavioral strategy. For instance, depending on the state of the surrounding environment

(including, but possibly not limited to, the number and localization of other nearby people) and on the travel purpose (leisure, commuters, rush hours, . . .), they can feel themselves facing either well-focused individualities or more blurred "packages" of walkers. Consequently, even if the elementary interaction rules are always the same, their global effect can be extremely different because of the *filtering* operated by pedestrian psychological perception. It is worth pointing out that the latter is an *active* ability of pedestrians as living agents, which can greatly impact on the effect of basic physical laws. From a complementary point of view, perception is the psychological consequence of the physical fact that crowds are extremely *granular* systems, i.e., systems in which the real dynamics originate at the level of single individuals. Mathematical models should explain how perception influences the usual dynamical laws and contributes to originate different observable outcomes.

#### 1.2.1.3 Large Deviations, Loss of Determinism, and Panic Onset

The expression of the aforesaid behavioral strategies, as well as their impact on standard laws of Physics, can be considered under either a deterministic or a stochastic point of view. The former is appropriate in *normal* conditions, i.e., when a standard rational attitude can be identified over which large deviations are not expected to occur. Conversely, the latter is suited for addressing cases in which irrational behaviors cannot be excluded, which might induce large deviations over the normal trends even up to *panic* onset. Mathematical models should account, at least at a qualitative level, for the transition from normal to panic conditions, namely explain how it can be triggered and how normal behavioral rules are modified in extremely critical situations. However, we anticipate that in this book we will be concerned only with crowd dynamics in normal conditions, so that an essentially deterministic approach is admissible.

At last, it is worth mentioning that models conceived for treating complex systems should deal with the above, and possibly also other, complexity clues within the standards of the mathematical reductionism. That is, the modeled system should not be as complex as the real one, for otherwise models are mostly ineffective for practical purposes. Therefore, a balance has to be sought between following the aforesaid guidelines and envisaging suitable strategies of complexity reduction by means of proper mathematical structures.

### *1.2.2 Scaling and Representation*

The first step of the modeling approach is the choice of the most appropriate scale for describing, by mathematical equations, the system at hand. This book is concerned with crowds as ensembles of interacting individuals, who, as discussed above, generate complex dynamics involving various scales. Therefore, its background idea is that the modeling approach should necessarily pursue a *multiscale* perspective.

However, various models exist in the literature which adopt a single-scale viewpoint. Hence it is important to explore the main characteristics of each modeling scale, also for a preliminary assessment of their possible links.

Traditionally, three types of mathematical descriptions are considered, corresponding to as many observation and representation scales.

#### 1.2.2.1 Microscopic Scale

The microscopic scale is the one at which the minimal entities composing a system, henceforth called *particles* for brevity, are visible. Here the adjective "minimal" stands for "atomic". That is, particles are regarded as the very fundamental constituents, further levels of detail being unnecessary for explaining the genesis of the dynamics exhibited by the system. In crowd dynamics, the microscopic scale corresponds to the level of single pedestrians, who can indeed be regarded as the atoms of a crowd. Mathematical models at the microscopic scale describe the movement of each single walker by means of proper *state variables*, normally position and velocity (at least in purely mechanical contexts). Since pedestrians are tracked one by one from their initial positions, this kind of description is also called *Lagrangian* (although such a terminology has no direct connection with the modeling scale).

Depending on the reference mathematical framework, microscopic models can be formalized in a few different ways. For instance, *differential* models use systems of ordinary differential equations which express the variation in time of the state variables attached to each pedestrian (much as in Rational Mechanics). On the other hand, *agent-based* models, such as e.g., Cellular Automata, update the microscopic states of pedestrians at discrete times according to mainly algorithmic evolution rules.

#### 1.2.2.2 Macroscopic Scale

As the name itself suggests, the macroscopic scale is just the opposite of the microscopic one. The focus is no longer on single particles, viz. pedestrians, but rather on their average distribution, which is described by means of a *density* in space, usually denoted by $\rho$, evolving in time. An immediate technical difference with the microscopic scale is that now space is, together with time, an independent variable. Indeed, one is not labeling anymore pedestrians one by one in order to track them along their paths. Rather, the space variable refers to arbitrary positions in the geometric space possibly crossed by different walkers at different times. This viewpoint is also called *Eulerian* as opposed to the Lagrangian one characteristic of the microscopic scale.

Ideally, the macroscopic picture is what is seen by a sufficiently far observer, who cannot distinguish individual pedestrians but detects just their collective mass. In order for this point of view to make sense, it is conceptually necessary that the

total number of pedestrians be so large that in every arbitrarily small portion of space there is still enough of them for a density to be defined. Indeed, $\rho$ is technically the limit of the ratio between the number of people contained in a reference volume centered at a point $x$ and the volume itself shrinking to zero:

$$\rho(x) = \lim_{\text{volume}\to 0} \frac{\text{number of people in volume}(x)}{\text{volume}(x)}.$$

This assumption is normally referred to as the *continuity of the matter*. It is plain that real crowds do not satisfy it so well as e.g., fluids do. However, it can be accepted as a mathematical abstraction which possibly provides useful approximations of the physical reality.

Models at the macroscopic scale focus on the evolution of the density and other average quantities, such as e.g., the *average velocity* of "packages" of pedestrians, which usually compare quite well with the available type of empirical information. They are generally formulated in terms of (systems of) partial differential equations using time and space as independent variables.

#### 1.2.2.3 Mesoscopic Scale

The mesoscopic (or *kinetic*) scale is more properly a scale of *representation* rather than of description. Indeed, it is based on the concept of *statistical distribution* of the states of the microscopic particles, viz. pedestrians, which is a quantity less tangible than the physical positions, velocities, and density typical of the other two scales presented above. In practice, in the mesoscopic approach the point of view on the physical system is intrinsically microscopic. Nevertheless, instead of labeling and tracking pedestrians one looks at the statistical distribution of the microscopic variables chosen to represent their state. Such a distribution is described by a *distribution function*, usually denoted by $f$. For instance, if the pedestrian microstate is constituted by the pair position-velocity, say in symbols $(x, v)$, then $f$ is a function of these two variables plus time $t$: $f = f(t, x, v)$. Specifically, $f(t, x, v)\, dx\, dv$ is the (infinitesimal) number of pedestrians that at time $t$ are located in the reference volume $dx$ centered at $x$ with a velocity comprised in the reference volume $dv$ centered at $v$. Models are then constructed by reinterpreting the physical laws responsible for microscopic dynamics in a probabilistic perspective, suitable to describe the causes that make the distribution function change in time.

The origins of the mesoscopic approach to the modeling of real world systems go back to the late 1800 with the kinetic theory of gases by Ludwig Boltzmann. In more recent times, this approach started to be used also in quite different contexts, to some extent closer to the contents of this book, such as e.g., modeling of vehicular traffic and, even more recently, of swarm dynamics. The conceptual advantage of this approach over the twos previously discussed is twofold. On the one hand, it allows one to still look at the physical system from a microscopic point of view, which is typically the most natural one for systems composed of several interacting

elements. On the other hand, it does not require that every single pedestrian be modeled. However, it does not provide directly average macroscopic quantities as a result of the equations. They need to be extracted a posteriori as suitable statistics from the distribution function once the latter is known.

### *1.2.3 Critical Analysis*

By comparing the discussions set forth in Sects. 1.2.1 and 1.2.2 it should be rather obvious that none of the usual scales addresses satisfactorily the complexity clues raised by crowds. In order to argue this criticism, we start from the basic consideration that a crowd is definitely a discrete system, say with a finite – though possibly quite large – number of particles. Hence the microscopic scale might seem the most appropriate modeling framework. However, large systems of equations induce typically nontrivial analytic and computational difficulties, which ultimately make the microscopic approach practically feasible only for relatively small numbers of pedestrians. Even more important, a small scale description can suffer from a large number of parameters, many of which are typically difficult to be estimated. Furthermore, it may hardly allow one to catch robustly the formation of collective self-organized patterns, because it is in general prone to fluctuations (e.g., in the initial or boundary data, which, as a matter of fact, are not known with deterministic precision). Finally, it does not provide a direct comparison with real world in terms of macroscopic measurements (such as e.g., of density, fluxes, ...), which often are the actually useful information for practical purposes. A posteriori averages in time or space can be computed but fluctuations cannot be avoided. On the other hand, neither the macroscopic scale is fully appropriate, because crowds do not fit the paradigms of continuity of the matter. Their discreteness makes it necessary to derive the main dynamics from individual-based considerations, which however are left out of macroscopic reasonings. In fact the latter normally resort to the idea that the behavior of *groups* of particles, regarded as elementary constitutive entities of the system, confined in arbitrarily small space volumes is sufficient to determine the behavior of the whole system. Therefore the modeling approach takes advantage of *constitutive relationships* instead of arriving at the detail of single particles. This is however in contradiction with the importance of granularity and perception in crowds. For instance, it makes it difficult to account for small inhomogeneities in the flow, which are mostly responsible for the spontaneous *symmetry breaking* triggering the formation of complicated self-organized patterns. Finally, the mesoscopic approach as it can be borrowed from standard gas dynamics is equally inappropriate to the representation of crowds, because the way in which it reinterprets probabilistically the microscopic dynamical laws assumes implicitly that the number of microscopic particles is so large that some heuristic approximations needed to close the equations are valid. In more detail, the main point is that any two particles of the system be sufficiently uncorrelated so that they

can be regarded as statistically independent. This can be a reasonable approximation for gas molecules subject to collisional dynamics, also in view of the high order of magnitude of the Avogadro number ($\sim 6 \cdot 10^{23}$ molecules per mole of gas), but it is clearly questionable for pedestrians in a crowd, who do not even interact through collisions.

In order to identify new modeling approaches, capable of profiting from the advantages and going beyond the limits of the classical ones, one can start from the consideration that in case of crowds the really useful quantitative information a model should provide is definitely the one concerning the collectivity. In fact, on the one hand it is less prone to globally unnecessary details; On the other hand it refers to quantities directly observable, which depict well the emergence of group behaviors and trends. However, this information should originate from the distinguishing features of individual pedestrians suitably translated into mathematical equations, according to the idea that one-to-one interactions generate spontaneously collective dynamics. In particular, the equations should account for the way in which individuals perceive the collectivity, which can greatly impact on the emergent group behaviors but, being a psychological ability of each walker, is better modeled at the level of single particles. This requires to identify proper mathematical structures by means of which the key concepts of *individuality*, *collectivity*, and *perceived collectivity* can be formalized. It is rather intuitive that such mathematical structures have to pertain to different observation and representation scales. Therefore the subsequent step is the elaboration of possibly nonstandard mathematical methods for linking them in an *embedded* multiscale perspective, that is one which makes possible the simultaneous presence and interplay of all levels of description.

## 1.3 The Interplay Between Modeling and Experimenting

It is a quite natural fact that Applied Mathematics be confronted with empirical investigations. Empirical data should serve for validating mathematical models, i.e., assessing the reliability of their predictions in some test cases, and for identifying their parameters. On the other hand, empirical data should not be artificially plugged into models for reproducing observed qualitative trends, because the latter should rather result from a correct interpretation of the inner system dynamics. Indeed, this is the correct use of a mathematical model as a tool for explaining essential, possibly non-evident, cause-effect links; Whereas the artificial insertion of data makes mathematical models simply a restatement of the original problem carrying almost no additional information. Concerning crowds, several types of data can be obtained from experiments. Some of them are similar to those measured for vehicular traffic while other are substantially different. We attempt now a rough classification and discuss their possible technical use in the modeling approach in view of an improvement of the quality of models.

### 1.3.1 Fundamental Diagrams

Fundamental diagrams are graphs plotting the average speed or flux (i.e., the product of speed and density) of pedestrians versus their density in uniform steady flow conditions. They are very much analogous to the fundamental diagrams used for vehicular traffic but for the fact that in case of crowds their shape can be considerably influenced by environmental conditions, which walkers are more sensitive to than cars. It has also been observed that flux diagrams of crowds may have two peak values, rather than just one like in vehicular traffic, the second at high pedestrian density being due to that walkers can still move even when they feel overcompressed. Information provided by such diagrams is mainly limited to one-directional flows, even when it is obtained from two-dimensional measurements. In particular, these data do not allow one to understand how pedestrians deviate from straight lines when looking for preferential paths.

### 1.3.2 Data on Emerging Collective Behaviors

Collective crowd behaviors emerge spontaneously mainly in the form of self-organized flow patterns (such as e.g., crowding at exits or obstacles, lane formation in counter-flows, traffic-light effect at bottlenecks). Data referred to such patterns do not provide information about the behaviors of single agents. Rather they describe their visible ensemble effect. It is worth stressing that emerging collective trends can be greatly different and much more complex than the behavioral rules followed by single individuals, due to the amplification produced by interactions and to the switch of point of view (from the inner one of individuals immersed in the crowd to the outer one on the collectivity as a whole). For this reason, these data are usually extremely sensitive to environmental conditions: Small variations in the arrangement of the walking area can induce large deviations on the observed collective patterns. As a partly counterintuitive example, it is known that placing a small obstacle in front of an exit can improve, under particular circumstances, the outflow of people by reducing the average egress time. In pedestrian traffic literature, this effect is known as the *Braess' paradox*.

### 1.3.3 Data on Individual Behaviors and on Interactions

These data are aimed at understanding how pedestrians individually react to other pedestrians and how such interactions determine the main dynamics. An example is the analysis of the spatial correlation among pedestrian speeds, which can provide information on the existence of a distance threshold, either metric or topological, beyond which group mates do not interfere with the individual walking choices.

This kind of empirical data can contribute to modeling at all scales, considering that interactions are at the core of the derivation of models not only at the microscopic scale. Indeed, models at the mesoscopic scale resort to a probabilistic interpretation of the physical laws governing the microscopic dynamics. Furthermore, clues about the physics of interactions are at the basis of modeling material behaviors, which characterize models at the macroscopic scale. Finally, it is evident that data on individual behaviors are mostly welcome in a multiscale perspective, too, for they can help ground the mathematical derivation of models at higher scales on sound phenomenological microscopic bases.

In general, the use of a specific type of empirical data in the modeling approach should be referred to a well-defined modeling scale. Even more, the available experimental information can influence in turn the assessment of the modeling scale, because validation and parameter estimation are impossible if models do not meet the scale of the data actually accessible. Nevertheless, we stress once again that models should reproduce empirical data used for their validation (fundamental diagrams, dependence on the environmental conditions, self-organized flow patterns) rather than being constructed on them. The latter practice amounts to modeling the effects rather than the causes, which cannot be the ultimate goal of mathematical modeling.

On the other hand, the discussion above has highlighted that a deep understanding of microscopic interactions is crucial for grounding models on the actual physics of crowds, including especially the complexity clues outlined in Sect. 1.2.1. Therefore, an effort has to be put in setting up experiments which shed light on qualitative and quantitative aspects of pedestrian behavior at an individual-based level. In doing this, pedestrian psychology cannot be ignored. Experiments cannot be conducted like with the inert matter, because human behavior cannot be exactly reproduced at one's pleasure. It might be biased if people know that they are being tested: For instance, human choice ability may be altered if people move in fake environments specifically conceived for recreating particular paths. Intuitively, this *caveat* applies even more so when pretending to simulate critical conditions, such as e.g., a panicky crowd, since simulated panic is probably very different from the actual one. Due to their relevance in the understanding of crowd dynamics, insights into pedestrian psychology will be examined in more detail in the dedicated Chap. 3.

## 1.4 Book Contribution

### *1.4.1 A Multiscale Approach*

This book is about the *science of mathematical modeling*. Its leading idea is that Applied Mathematics does not just consist in applying existing models but, first and foremost, in constructing new mathematical methods for applied sciences through a rigorous, and by far not obvious, process of mathematization of the reality.

Specifically, the book is motivated by the search for a mathematical approach capable of coping with the *multiscale* issues of crowd dynamics modeling. The starting points are mainly the first two complexity clues discussed in Sect. 1.2.1, which have both to do with the interplay between different scales:

- The scale of the *individualities*, which reflects the inner point of view of single pedestrians within the crowd. This can be identified with the *microscopic* scale of the system. It is at this scale that interaction dynamics have to be modeled by implementing through mathematical equations the essential behavioral rules discussed in Sect. 1.1.1.
- The scale of the *collectivity*, which corresponds to an outer point of view on the crowd, i.e., one of an ideal observer who can access the crowd at once as a group. This can be identified with the *macroscopic* scale of the system. It is at this scale that emergent self-organized trends can be sought, to be possibly compared with those known from empirical observations.
- The scale of the *perceived collectivity*, which serves as a bridge between the previous twos. It can be identified with the *mesoscopic* scale of the system. It is at this scale that individual perception enters the modeling approach as a behavioral characteristic which impacts on the way individuals relate to the collectivity.

The basic *phenomenological idea* of our approach is that microscopic pedestrians interact with the mesoscale of the surrounding collectivity, according to the bidirectional scaling between individuality and collectivity discussed in Sect. 1.2.1. In particular, collectivity is mathematically expressed by a *probability measure* over the distribution of the microscopic positions of pedestrians, which generalizes the concept of distribution function normally used in the kinetic approach. A measure is useful for handling various space structures of such a distribution, whereby we can translate different levels of perception of the individuals:

- An *atomic* mesoscopic distribution, viz. a Dirac delta-like probability measure, models a highly *granular* perception, corresponding to the ability of pedestrians to interact with other walkers one by one. This can happen in sparse crowds or for leisure-type travel purposes.
- An *absolutely continuous* mesoscopic distribution, viz. a probability measure with density (with respect to the usual Lebesgue measure in space), models a *bulky*, or *blurred*, perception, corresponding to the tendency of pedestrians to interact with surrounding subgroups of people as a whole. This can happen in dense crowds or for rush-hour-type travel purposes.

In addition, properly weighted *intermediate* levels of perception are possible, since a measure can include both an atomic and an absolutely continuous part at the same time.

It is worth pointing out that we do not see the mesoscale as a limit-like statistical description of the microscale when the number of microscopic particles is "sufficiently" high. Our mesoscale amounts rather to a representation of the particle dynamics in terms of transport of their probability distribution. As such, it is well defined for both large and small numbers of particles, the specific structure

of the probability distribution being dictated by the modeled perception level. By simple statistical arguments it is then possible to link the mesoscopic probability distribution to the *macroscopic mass* of the crowd, which is in turn represented by a finite measure (though in general not a probability) with the same space structure as the probability.

The possibility to *hybridize* the structure of the aforesaid measures is actually the *crucial point* of our approach. It makes it possible to *embed* discrete pointwise effects, which can be relevant for the emergence of particular self-organized patterns, in a continuous representation of the crowd. This is done via a *dedicated parameter* $\theta$, which can be chosen between 0 and 1 in order to fix the relative importance of the discrete and continuous contributions in the structure of the measures. This way, the discrete and continuous representations *coexist* in our model and *share information* dynamically. In this respect, they are indivisible.

This makes the difference from other ways of understanding multiscale approaches in the literature. Just to mention a few examples, we recall here: • *Multiscale geometric techniques*, sometimes used to represent geometrically complex systems such as e.g., those with a network structure. One specific part of the network is accurately modeled in three dimensions, whereas the rest is described by means of lumped zero-dimensional models. This enables one to account for the whole network while keeping the complexity of the model under control. • Multiscale methods implemented at a *numerical level* in connection with *domain decomposition*, in order to compute the solution to certain equations with different local accuracy. The general idea is to couple accurate but expensive calculations, performed by a microscopic (e.g., particle-based) solver in small and inhomogeneous regions, with less accurate but also less expensive ones, performed by a macroscopic (e.g., continuum) solver in large and homogeneous regions. The two solvers exchange information at the interface of the respective regions, which may be a fictitious internal boundary to be carefully described and numerically resolved. • *Scale alternation* for computing on the same system. In the resulting iterative algorithm the output of the microscopic simulation is used as input for the macroscopic simulation and vice versa. • *Upscaling procedures*, where the ultimate goal is to pass from a detailed but often inhomogeneous description of some quantities to a rougher but more homogeneous representation by averaging out inhomogeneities via homogenization techniques. • *Micro-macro decomposition of the distribution function* in the kinetic approach, used to obtain hybrid models together with related numerical schemes. In particular, the latter combine a fluid-dynamic solver in the whole domain with local kinetic corrections, which activate according to some transition conditions when the macroscopic description breaks down.

In our multiscale model, the probability (or mass) measure is finally the quantity which provides information about emergent collective behaviors. In order to compute it also at a practical level we build an ad hoc numerical scheme for producing simulations in a measure-valued framework. Finally, we provide a basic theory of well-posedness of initial-value problems and of convergence of the numerical

scheme. From such a qualitative analysis we extract a few guidelines, which can assist the construction of physically consistent and mathematically robust models.

### *1.4.2 Generalizations and Applications to Other Fields*

The basic multiscale approach just outlined can be technically evolved in various ways. The inspiring application may or may not always be crowd dynamics. In fact, once the measure-based model has been obtained, one can imagine also different uses of it aside from the motivations which led initially to its derivation. Specifically, the multi-faceted structure of a measure can be regarded, more in general, as a way of realizing a coupling between a *discrete* and a *continuous* description of a given particle system in which the intrinsic granularity, together with a locally finite and small number of particles, is expected to play a role in the resulting dynamics. Hence our measure-valued equations can constitute a technical paradigm for further interpretations of the multiscale approach to the modeling of interacting particles possibly different from pedestrians. Some prospective ideas, only partly developed in this book and to be possibly inserted in specific research programs, are outline in what follows:

- The extension of the crowd model to several interacting groups of pedestrians animated by different travel purposes. This simple improvement makes it possible to address a great variety of important case studies. We mention here, in particular, pedestrian counter-flows in straight corridors or through bottlenecks, where the multiscale model shows how important the level of perception itself can be for explaining the emergence of quite different self-organized collective behaviors out of the very same starting conditions. Other interesting applications concern the interaction of *many* with *few* individuals, when the latter are the only ones who know the way to go. Prototypical situations are e.g., a group of tourists following a guide or a group of people evacuating a room under the directions of a rescue team.
- A more detailed description of micro-meso interactions including the ability of pedestrians to adapt their behavioral strategy to the perceived distribution of both positions and *velocity* of the surrounding walkers. This implies conceiving phenomenological models based on *second order dynamics*, which use the pair position-velocity as descriptor of the microscopic state of pedestrians. Consequently, also the mesoscopic probability distribution is defined over a larger state space, typically a four-dimensional one (two components for the position and two for the velocity in case of crowds moving in two-dimensional domains). At that point, nontrivial computational difficulties arise in the numerical solution of the equations, which further motivate the search for mathematical structures at higher scales capable of reducing such a technical complexity.
- The application of the approach to *vehicular traffic*. Vehicular traffic used to be, and to some extent still is, a favorite reference background for modeling pedestrian traffic. In fact, it is an example of a system in which apparently

mechanical large-scale dynamics of inert matter (i.e., cars) are actually ruled by non-mechanical behavioral strategies of living matter (i.e., drivers) at smaller scales. Hence a multiscale model grounded on the idea of driver perception seems to be appropriate also in this case. In particular, the modeling method itself can profit from some specific features of the flow of cars, which can inspire interesting extensions.

For instance, the discrete and continuous descriptions need not refer to the same space dimension. Indeed, roads are essentially one-dimensional domains with respect to the main flow dynamics, especially if the latter are considered at a continuous level. Then a representation by means of one-dimensional longitudinal density waves can be sufficient. However, the number of cars along a road is locally sufficiently small for their granularity to have presumably an important impact on the flow. Therefore, a dynamically coupled discrete-continuous description is worth being considered, but the discrete part cannot ignore the two-dimensional nature of the road. Notice that such a *multidimensional multiscale coupling* can be viewed as the effect of the perception of drivers. When they look bulkily at cars ahead continuous effects of the one-dimensional stream dominate. On the other hand, when they follow the leaders ahead two-dimensional discrete effects, such as lane changes or overtaking, become important in assessing their behavioral strategy.

Another quite natural idea is that the discrete-continuous coupling varies in different sub-domains or can be triggered by the evolution in time of the state of the system itself. This amounts to converting the parameter $\theta$ mentioned in the previous section into a function of space and time, which can be either prescribed a priori or linked to the dynamics of the main system by means of proper constitutive relationships or evolution equations. For instance, one can guess that a continuous description is satisfactory along a one-way road, due to the essentially one-dimensional geometric constraint, whereas a discrete description is necessary at crossroads, where driver perception is sharpened by vehicles coming from different merging directions. As a matter of fact, this idea may apply also to crowds: The perception state of pedestrians can be continuously affected by the crowding in their surroundings as well as by changes in the arrangement of different walking areas they visit during a trip.

- *More general* discrete-continuous couplings. The discrete-continuous approach can also be definitively freed from the interpretation in terms of living agent perception and used per se. To this purpose, the minimal conceptual idea to be retained for a coherent use of our approach is simply that the discrete and continuous parts are *two copies* of the *same system* at different levels (viz. languages) of description. Then one can mix the two levels for studying the interplay of the specific information provided by each of them. For example, this point of view can be an original way of addressing the *wave-particle duality of light*, where the discrete part models electrons as pointwise massive particles while the continuous one models them as energy waves.
- The application of the approach to *Mathematical Biology*. Cells are another living complex system in which the interplay between small-scale granularity

and large-scale collective distribution can be essential to explain the emergence of self-organized dynamics. Specifically, in *cell migration phenomena*, especially those linked to morphogenesis which produce the formation of *visible patterns* (cf. e.g., vasculogenesis, angiogenesis, animal coat pattern formation), the number of involved cells can be locally rather small for individual behaviors to impact on group trends. In this case, the discrete/continuous dualism of the interaction of a single cell with some neighboring ones may not have a psychological empirical counterpart (like the perception of pedestrians and drivers) but can be rather based on the concept of *cell function*. Depending on its specific physiological function, a cell can have a different *level of activation*, which corresponds to a different way of being detected by other surrounding cells. Highly activated cells, which serve as leaders (the so-called *tip cells*), act as well-detected point masses, while little activated ones, which simply follow the leaders (the so-called *stalk cells*), behave as an indistinct subgroup. Models for the description of such phenomena may especially take advantage of the extension of our multiscale approach to several interacting populations, each cell population being identified by its function. It is also worth mentioning that cell-type biological problems can motivate nontrivial extensions of our multiscale approach to cases in which the mass of the system is not conserved in time. In fact, depending on the considered time scale, cell duplication/death events can come into play, which require to be handled in turn at a multiscale level without relying on the continuity equation only.

### *1.4.3 Purpose and Structure of the Book*

This book is intended to be read by scholars and professionals with different backgrounds. In particular applied mathematicians, physicists, engineers, but possibly also system biologists and psychologists as well as people interested in mathematical modeling and simulation of nonstandard complex systems of real world. The book is divided in two parts and eight chapters, plus two appendices. *The presentation in the two parts follows different styles, corresponding in principle to different target audiences*.

The first part, encompassing Chaps. 1–3, does not require specific technical skills, hence it is dedicated to a broad audience that can grasp the essential spirit and the potential contribution of mathematical modeling applied to crowd dynamics. It provides a general overview of the main phenomenological features of crowds and a preliminary assessment of the relevant methodological ideas constituting the cultural background of the mathematical approach promoted in the book. In addition, it offers to the reader virtual experiments which, on the one hand, visualize the main kinds of pedestrian behavior the book deals with and, on the other hand, point out the ability of mathematical models to address such phenomena.

The second part, encompassing Chaps. 4–8, is instead characterized by a more technical content and is therefore addressed to people with some mathematical background wanting to enter the details of modeling and model analysis. It opens with a critical overview of models available in the literature. Next, it examines in depth our multiscale approach including theoretical results of qualitative and numerical analysis related to it. Finally, it discusses the generalization and application of the approach to other real world systems, possibly also distant from crowd dynamics, which can be tackled in an original manner under a multiscale perspective.

We describe now in some detail the content of the remaining book chapters:

- Chapter 2 presents numerical simulations performed by means of the multiscale model, which will be technically described later in Chap. 5. The purpose is to visualize some typical phenomena in crowds while demonstrating the potential of the model to catch and reproduce them. Specifically, the chapter contains a collection of virtual experiments mimicking typical real world situations. Some of them aim at showing qualitatively the *emergence of collective self-organized patterns*, such as lane formation and intermittent flow at bottlenecks generated by pedestrian counter-flows in free and built environments. Others address more quantitative issues, such as the *estimate of the average outflow time* of a crowd leaving a room, in order to point out the differences in the model predictions due to different levels of individual perception, viz. of discrete-continuous coupling. Finally, others consider less standard pedestrian dynamics such a those exhibited by *social groups*.
- Chapter 3 presents some psychological aspects of pedestrian behavior, which can be taken into account in the mathematical models in order to make them more truthful. Specifically, it reports and discusses the most important experimental findings about the way in which pedestrians choose their path and interact with external structures, thereby completing the phenomenological picture.
- Chapter 4 introduces mathematical models of pedestrian flow at the various scales discussed in the present chapter, namely microscopic, macroscopic, and mesoscopic. The goal is by no means to review thoroughly the state-of-the-art on the subject, which is evolving quite quickly, but rather to outline, through selected examples along the mainstreams of the current literature, the cultural context in which the book is set. In addition, this overview of single-scale models can contribute to a deeper understanding of the multiscale approach promoted in the book.
- Chapter 5 details the multiscale modeling approach, including its numerical treatment, which is the core topic of the book. The proposed derivation, however, does not cover entirely the path across the various scales outlined above in Sect. 1.4.1. The style is rather that of an "educated guess" leading directly to the final measure-valued equation, which then allows one to play with the space structure of the pedestrian distribution. In particular, the key point is the reinterpretation of the classical continuity equation in terms of abstract measures, the measure of a given set referring heuristically to the number of pedestrians contained in the space region individuated by that set. The reason for this

approach is that it is a more "user-friendly" first glance at the problem, especially in view of its extension to other contexts possibly distant from crowd dynamics. On the other hand, the rigorous multiscale derivation of the equations for crowd dynamics will be proposed in the subsequent chapter as an introduction to the theoretical treatment of measure-valued models.

- Chapter 6 is devoted to a theoretical analysis of the mathematical structures presented in Chap. 5. It opens with the formal derivation of the measure equations out of a microscopic particle description of the system. Then it presents results (with proofs) concerning the well-posedness of related initial-value problems and the convergence of the numerical scheme specifically conceived for approximating them and producing simulations (such as those shown in Chap. 2). Out of such a theoretical analysis, it also provides indications, to be possibly regarded as modeling guidelines, for the construction of particular models fitting the scope of the developed theory, hence not only physically consistent but also mathematically robust. This chapter assumes that the reader has been exposed to measure theory and functional analysis. Practitioners not interested in technical mathematical aspects should be able to skip it without loosing much of the understanding of the contents of the book.
- Chapter 7 pushes forward the theoretical analysis of the models initiated in Chap. 6 by investigating more in depth the properties of dynamical evolutions in Wasserstein spaces. Motivations are provided for supporting the idea that such spaces are more suited than classical $L^p$ spaces to study problems of interacting agents. In particular, the chapter shows that the Wasserstein metric is a more proper tool than the $L^1$ metric not only from the modeling point of view but also as far as the theoretical properties of the models are concerned. For instance, it demonstrates by means of an explicit example that the $L^1$ metric may fail in giving the uniqueness of the solution while the $W_p$ metric does not. Moreover, it discusses a few other numerical schemes for the approximation of the solutions of models from both Lagrangian and Eulerian perspectives and addresses further interaction models that fit the general theory. Finally, it proposes a well-posedness theory in measure for *transport equations with source*, technically mass balance (rather than conservation) equations. This implies, in particular, *extending the usual Wasserstein metric* to measure which do not carry the same mass. It is worth stressing that transport equations with source play an important role in modeling a lot of physical systems, including the one which constitutes the main target of this book. Sources (or sinks) of pedestrians can be indeed a good way of describing mathematically e.g., stairs connecting floors of a building, which produce an injection (or removal) of people in the domain. Chapter 7 assumes that the reader is provided with a quite solid background in measure theory and functional analysis. A quick account of the basic concepts can be found in Appendix A. Readers not interested in advanced theoretical issues can feel free to skip this chapter with no consequences on the understanding of the rest of the book.
- Chapter 8 offers conceivable improvements and generalizations of the multiscale structures presented in the book, up to their use for problems much different from

the original one which motivated them. In more detail, it deals with: • The derivation of measure-valued equations out of a microscopic modeling of Newtonian-like dynamics (i.e., ones involving the concept of *acceleration* of the particles), so as to export the ideas of individuality, collectivity, and perception also to the so-called *second order models*. • The extension of the perception-based discrete-continuous coupling to cases in which the agent perception, hence their behavioral strategy, evolves in time and space possibly under the influence of the system itself. Remarkably, the chapter shows how this idea can be suitable to model driver behavior in vehicular traffic by coupling an essentially one-dimensional continuous perception on straight roads to a genuinely two-dimensional granular perception at crossroads. • Finally, the application of the measure-based discrete-continuous coupling to a toy problem conceptually different from crowd dynamics, namely a *wave-particle complementary description* of the Brownian motion, having in mind the well-known analogous dualism of light.

The following chart illustrates three possible *reading paths* through the chapters of the book, corresponding to three different types of readership: a more modeling-oriented path (red line), a path which emphasizes analytical aspects (blue line), and finally a path specifically concerned with phenomenological and experimental issues of crowd dynamics.

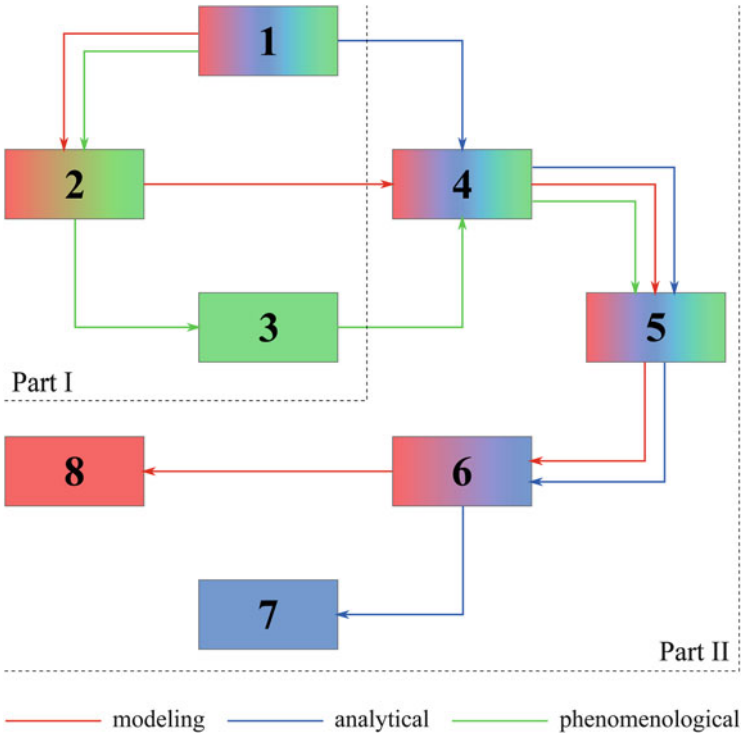

The book is completed by two appendices. Appendix A provides for the reader's convenience some basic background material about measure, probability, and transport theory, which should help grasp the essential ideas necessary to understand the contents of Chaps. 6 and 7. Appendix B reports instead a conceptual pseudo-code which should facilitate the implementation, in one's own favorite programming language, of the multiscale numerical scheme introduced in the book (and actually used to produce all simulations presented in Chaps. 2 and 8).

## 1.5 Bibliographical Notes

Section 1.1.1 For the behavioral rules of pedestrians in mathematical models we refer the reader to the references of Chap. 4, especially those regarding microscopic models. Here we just point out three papers: The one by Cristiani et al. [46] clearly elucidates the separation between visual field and sensory region, and investigates the effects of different sensory regions; The paper by Ballerini et al. [11] is a good recent reference about the distinction between metric and topological interactions, although these concepts were well known for a long time in the biological literature; The paper by Helbing et al. [85] is a good source of information for panic conditions in pedestrians.

Section 1.1.2 From the experimental literature, we mention, among others, Helbing et al. [84] and Moussaïd et al. [126] for the lane formation in crossing pedestrians; Moussaïd et al. [128] and references therein for the V's and river-like patterns; Daamen and Hoogendoorn [53] and Seyfried et al. [157] for arching at bottlenecks. Helbing et al. [84] for intermittent flows at bottlenecks.

Section 1.2.2 We will dwell on the specific literature about microscopic, macroscopic, and mesoscopic models of pedestrian dynamics in the bibliographical notes of Chap. 4. Here we simply recall that the seminal works in which methods of the kinetic theory are applied to *vehicular traffic* are those by Prigogine [147] and Prigogine and Herman [148]. On the same line are also the works by Klar, Wegener, and coauthors, see [110] for a comprehensive review. Concerning *swarm dynamics*, Degond and Motsch [60] describe from a kinetic point of view some Vicsek-type microscopic models of flocking (cf. Vicsek et al. [164]). Similarly, Carrillo et al. [33] and Ha and Tadmor [78] use Vlasov-type (i.e., mean field) kinetic models to study the microscopic model by Cucker and Smale [51, 52].

Section 1.3 See Chap. 4 (Sect. 4.2.1) of this book for further discussion and examples of fundamental diagrams. A nice reference for a review of the main self-organized group patterns produced by pedestrians is instead Helbing et al. [83]. The Braess' paradox was introduced in [22] in 1969 (see [23] for a reference in English). Finally, see Chap. 3 of this book for an overview of psychological research, both theoretical and experimental, about pedestrian path selection and movement in organized environments.

Section 1.4.1 Besides the present one, a few *other books* treating various aspects of the dynamics of crowds are currently available. We recall here the book by Adamatzky [1], which focuses on the mental dynamics driving the fusion of individualities into the collectivity during the formation of a crowd; The book by Kachroo et al. [107], which, starting from the extensive research available on vehicular traffic, develops two-dimensional macroscopic models for the control of crowd behavior in connection with the implementation of evacuation strategies; The books by Pelechano et al. [139] and by Thalmann [159], variously concerned with the simulation of virtual crowds for computer animation purposes.

Multiscale modeling/simulation has become nowadays a so popular concept in many different application fields that nearly everyone has his own way of understanding and implementing it. For the reader's convenience, and without claiming to be thorough, we give here a few clues, to be used as starting points for further personal bibliographical search, which exemplify *other multiscale approaches* more or less distant from the one promoted in this book. Quarteroni and Veneziani [149] use a multiscale geometric approach to the network-structured circulatory system. Donev et al. [66] and Weimar [169] use multiscale algorithms coupling particle-based and continuous solvers for reaction-diffusion systems in fluid dynamics and crystallography. Kraft [113] adopts a scale alternation in a problem of solidification for reducing the global computational effort. Bresch et al. [24] use homogenization techniques for solving the Stokes equations in a rough domain by deducing macroscopic pressure coefficients incorporating the effect of the microscopic rugosity. Finally, Degond et al. [58, 59] and Herty and Moutari [92] propose macro-kinetic models and solvers for fluid flows and vehicular traffic, respectively, aiming at a better description and numerical resolution of localized non-equilibrium regions (e.g., crossroads in vehicular traffic) where empirical constitutive relationships valid in equilibrium conditions are strongly violated.

Section 1.4.2 See Chaps. 5 and 8 of this book for a preliminary treatment of some of the generalizations of the multiscale approach. In particular: Sect. 5.6 for the extension to two interacting populations; Sect. 8.1 for the derivation of second order measure-valued models; Sects. 8.2 and 8.3 for the application to vehicular traffic problems; Sect. 8.4 for a prototypical example of multiscale treatment of the wave-particle duality based on Brownian motion. Moreover, the paper by Piccoli and Rossi [142] provides a theoretical contribution toward measure-valued models based on the mass balance equation with source for possible applications in Mathematical Biology.

# Chapter 2
# Problems and Simulations

**Abstract** In this chapter we give an informal introduction to the multiscale model and present some case studies of interest for applications, along with related numerical simulations. Results presented here are somehow complementary to those usually presented by physicists, engineers, and computer scientists. Indeed, we aim at showing how mathematical modeling can help in developing truthful pedestrian models, and at giving a sample of phenomena which can be simulated without the introduction of artificial or ad hoc effects.

## 2.1 An Informal Introduction to the Multiscale Model

We present here the main ideas of our multiscale model, avoiding heavy technicalities and advanced mathematical tools. A more rigorous scale-free description of the model will be given in Chap. 5, within a measure-based modeling framework. Basically, we assume that we have two models which describe the *same* physical phenomenon at *different* scale. To fix the ideas, we assume that the first model is microscopic (agent-based) and the second one is macroscopic (continuous). Moreover, without loss of generality, we assume that they are both first order models, which means that we model the *velocity* of the agents (as a nonlinear function of their positions), and not their *acceleration* as in classical Newtonian frameworks.

Hereafter, we focus on pedestrian motion (see Sect. 8.4 for a different application). We denote by $N$ the number of pedestrians under observation, by $X^k(t) \in \mathbb{R}^2$ the position of the $k$-th pedestrian, by $X := (X^1, \dots, X^N)$ the vector of the positions, and by $X^{-k} = (X^1, \dots, X^{k-1}, X^{k+1}, \dots, X^N)$ the vector of the positions but the $k$-th. We also denote by $\rho(t, x)$ the average density of pedestrians at position $x \in \mathbb{R}^2$ and time $t > 0$. As usual, we assume that the microscopic model is constituted by a system of ordinary differential equations of the form

$$\dot{X}^k(t) = v_m[X^{-k}(t)](X^k(t)) \qquad k = 1, \dots, N, \tag{2.1}$$

E. Cristiani et al., *Multiscale Modeling of Pedestrian Dynamics*, MS&A 12,
DOI 10.1007/978-3-319-06620-2_2,

where $v_m[X^{-k}](x)$ is the microscopic velocity field at $x$, which also depends implicitly or explicitly on the positions of all the other pedestrians. The velocity $v_m$ takes into account all the desired features of the model, such as the target, the repulsion from the other pedestrians, the sensory region, etc. The macroscopic model is instead assumed to be constituted by a conservation law of the form

$$\frac{\partial}{\partial t}\rho(t,x) + \nabla \cdot \big(\rho(t,x)\, v_M[\rho(t,\cdot)](x)\big) = 0, \qquad t > 0, \quad x \in \mathbb{R}^2, \tag{2.2}$$

where $v_M[\rho](x)$ is the macroscopic velocity field at $x$, which, similarly to the microscopic case, depends on the density $\rho$ in all the space (nonlocal dependence) at time $t$. However, the specific form of the models is not essential to define the multiscale model. The *condicio sine qua non* is the explicit presence of the velocity fields $v_m$ and $v_M$, or, analogously, the presence of the acceleration fields in the case of second order models.

The multiscale model is based on a suitable combination of the microscopic and macroscopic velocity fields. To get it, $v_m$ and $v_M$ have to be defined on the same domain. The macroscopic velocity $v_M$ is already defined at any $x \in \mathbb{R}^2$, then it can be simply computed at the points $X^k$ in order to use it in (2.1) in place of $v_m$. The case of the microscopic velocity is instead more complicated. Indeed, $v_m$ is only defined at the pedestrians' positions, and not everywhere in the space. This can be fixed in several ways depending on the specific applications. In our case it is convenient introducing the concept of *test pedestrian*, i.e. a $(N+1)$-th fictitious pedestrian who is temporarily placed at the point of interest just to compute the velocity field she would be subject to. Following this approach, in order to use $v_m$ in (2.2) in place of $v_M$, we consider a test pedestrian located at $X^{N+1} = x \in \mathbb{R}^2$, and then we compute $v_m[X](x)$. Once the two velocity fields are made directly comparable, they are coupled by defining a *multiscale velocity field* as a linear combination of the two, i.e.

$$v[X,\rho] := \theta v_m[X] + (1-\theta) v_M[\rho], \qquad \theta \in [0,1]. \tag{2.3}$$

Note that $v$ will depend on both the positions of all the single pedestrians and their density in all the space, and can be defined at any $x \in \mathbb{R}^2$, included at $X^k$'s.

Finally, the new velocity field $v$ takes the place of both $v_m$ and $v_M$ in (2.1)–(2.2), so that both the single pedestrians and their density evolve by means of the *same* velocity. As a consequence, single pedestrians and the density should be considered as a whole, since *they are driven by the same velocity field, which, in turn, is computed with the contribution of both of them*.

The key parameter of the multiscale model is the number $\theta \in [0,\ 1]$, which controls the contribution of the discrete and continuous components in the computation of the velocity field. Namely, $\theta$ plays the role of an interpolation parameter, in the following way. If $\theta = 0$, single pedestrians and their density evolve considering only the continuous density of pedestrians. This approach is similar to one often used in literature in which the evolution of a system is firstly computed by a macroscopic

model, and *then* a number of Lagrangian particles are tracked by means of the pre-computed velocity field. Conversely, if $\theta = 1$ single pedestrians and their density evolve considering only the positions of the single pedestrians. This approach is much less usual. Finally, if $0 < \theta < 1$ the two scales are fully coupled, and both discrete individuals and continuous density contribute to the velocity field.

In Chap. 5 the multiscale model will be recovered following a measure-theoretic approach. The main advantage of this (more abstract) approach is that the model is completely scale-free, meaning that the evolution equation describing the pedestrian motion can be written with no a priori choice of the scale of observation. The model can be later specialized in order to follow single pedestrians (discrete point of view), or their density (continuous point of view), or both individuals and density at the same time.

In the simulations which follow, we make use of our multiscale model. As particular cases of it, we also consider purely continuous ($\theta = 0$) and discrete ($\theta = 1$) model. A precise definition of the velocity field can be found in Sect. 5.2. Here we just reveal that we take into account the following pedestrian features (cf. Sect. 1.1.1): Target (desired velocity), repulsion and relative sensory region, attraction and relative sensory region, and metric/topological interactions. Panic conditions are not considered.

## 2.2 Effects of Repulsion

To begin with, in the frame of a purely macroscopic model we investigate the self-organization spontaneously emerging from repulsion within a group of pedestrians in motion in a clear environment. The group is initially compact and has a homogeneous density (Fig. 2.1a), and the desired velocity (see definition in Sect. 1.1.1) coincides with the unit vector in the horizontal direction, i.e. the group is walking rightward. No attraction is assumed between individuals, so that, as soon as people start to interact, the model predicts an expansion of the crowd in consequence of the repulsion among group mates. At the same time, the density decreases and becomes inhomogeneous due to the anisotropy of the sensory region, which is here restricted in front (Fig. 2.1b). Front-rear symmetry is lost, and most people remain initially concentrated in the rear part of the group, where the influence of the mass ahead is stronger. By consequence, in this zone the velocity is lower, hence, as time goes by, the group elongates in the horizontal direction until the distribution of people again becomes almost homogeneous (Fig. 2.1c). Only the motion of the leaders seems to be basically unperturbed (Fig. 2.1b, c), coherently with the fact that they simply follow the desired velocity because nobody is in front of them.

Remarkably, in a purely microscopic setting we can qualitatively reproduce the same spontaneous organization of the crowd. Starting from a regular square configuration (Fig. 2.2a), pedestrians move rightward and interact only with pedestrians in front of them. In Fig. 2.2b we show the final configuration, directly comparable with that in Fig. 2.1c.

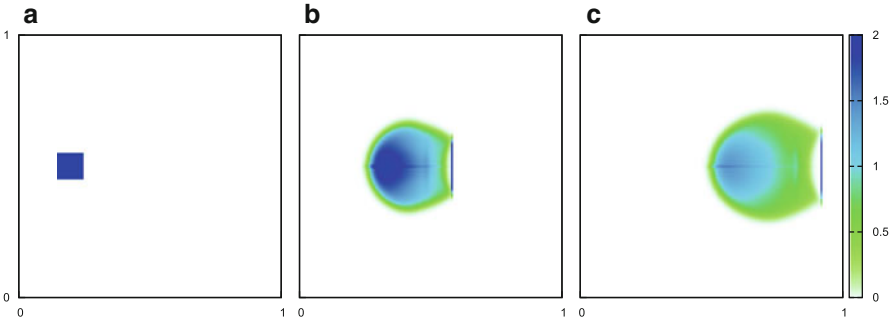


**Fig. 2.1** Spontaneous arrangement of a macroscopic crowd. Starting from a compact cluster, the group expands and the density decreases. Leaders tend however to maintain the initial configuration

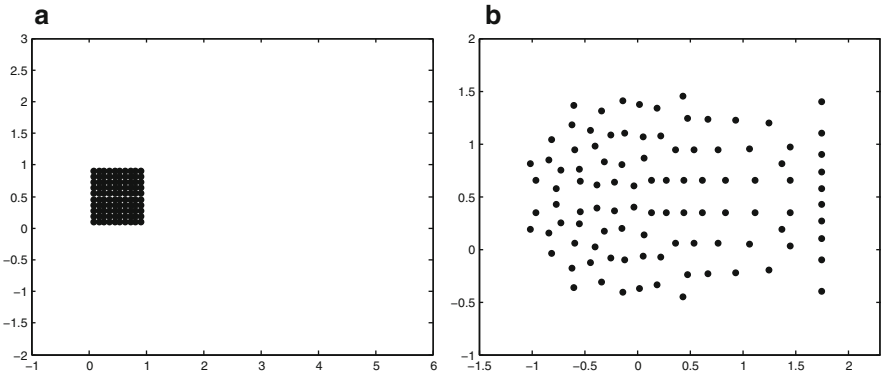


**Fig. 2.2** Spontaneous arrangement of a microscopic crowd. Starting from a compact cluster, the group expands and the density decreases. Leaders tend however to maintain the initial configuration

Those results show that the discrete and the continuous dynamics may lead, at least in some cases, to the same results. This observation motivates and justifies a coupled multiscale approach. Let us now turn on the multiscale features of the model, showing both the continuous and the discrete components of the crowd. We also switch the desired velocity off, so that the total velocity coincides with that caused by the interactions among pedestrians. Starting again from the homogeneous initial condition, shown in Fig. 2.3a, the simulation expands the group as predicted by the multiscale model choosing the interpolation parameter $\theta$ equal to 0, 0.3, and 1. The simulation runs until a fixed final time, common to all cases, is reached; Results are shown in Fig. 2.3b–d.

The main features of the dynamics outlined above are caught at all scales. In particular, the effect of the only frontal repulsion is visible at the head of the group, where pedestrians stay aligned on a vertical line as they are initially, because there is none in front of them. This effect clearly shows up looking both at the density distribution at the macroscopic scale (Fig. 2.3b) and at the individual pedestrians at the microscopic scale (Fig. 2.3c).

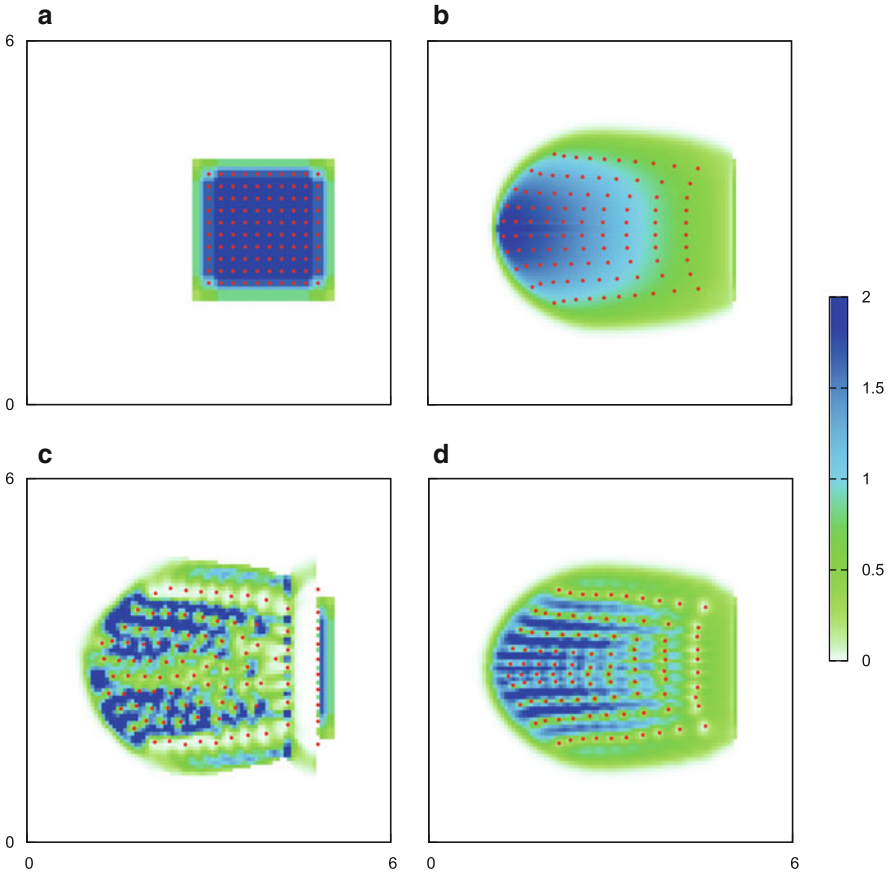


**Fig. 2.3** (**a**) Initial condition. Crowd distribution at the final time computed by the multiscale model with (**b**) $\theta = 0$, (**c**) $\theta = 1$, and (**d**) $\theta = 0.3$

As an interesting effect of the microscopic scale driving the macroscopic dynamics, we notice some kind of "density holes" near every microscopic pedestrian in the case $\theta = 1$ (Fig. 2.3c). They are actually small areas of very low density, caused by the fact that microscopic repulsion has a great impact at the macroscopic scale. Indeed, the microscopic granularity is seen as a singularity in the average crowd distribution, and in the discrete model the evolution of the macroscopic density is fully ruled by the microscopic scale. With the choice $\theta = 0.3$ (Fig. 2.3d) the hole effect is instead limited, and a good compromise between the two scales is reached. Furthermore, in Fig. 2.3d pedestrians are less scattered than in Fig. 2.3c, meaning that the contribution of the continuous model on the overall dynamics has, in a sense, a homogenizing effect. Conversely, in Fig. 2.3d the macroscopic density is more scattered than in Fig. 2.3b, thus the microscopic scale destroys the macroscopic smoothness and introduces a non-negligible granular effect in the overall dynamics.

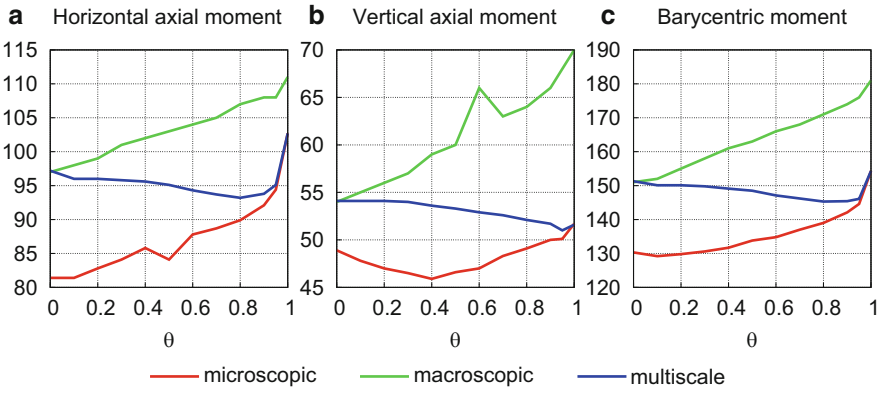


**Fig. 2.4** Moments of inertia of the crowd distribution as functions of the interpolation parameter: (**a**) horizontal axial moment $I_1$; (**b**) vertical axial moment $I_2$; (**c**) barycentric moment $I_G$. Note that $I_1 + I_2 = I_G$

These novel behaviors show that the multiscale approach is not a mere exercise to match two existing models, but it can effectively model a wider set of flow instances, with new results and insights.

## *Scale Interpolation and Group Shape*

In this paragraph, in order to investigate more in depth the intercorrelation between the scales, we study how the crowd shape depends on the interpolation parameter $\theta$. We study the shape of the crowd by computing the *moments of inertia* $I$ of the crowd. Indeed from classical mechanics it is known that moments of inertia provide quantitative information on the shape of a body. We denote by $I_1$, $I_2$ and $I_G$ the horizontal axial, vertical axial and barycentric moments of inertia, respectively.

Referring to the simulation setup of Fig. 2.3, we compute the significant moments of inertia of the final configuration of pedestrians. The graphs in Fig. 2.4 show the trend of the three moments of inertia of the crowd mass as functions of the interpolation parameter $\theta$. Notice that the moments of inertia of the multiscale mass are linear interpolations of the corresponding moments of inertia of the discrete and the continuous masses. The latter are therefore also plotted in the graphs for reference. The most relevant fact is that the multiscale moments of inertia are almost constant with respect to interpolation parameter (aside from small border effects, especially close to the fully discrete case). This fact indicates that the distribution of the mass is essentially independent of the scale, and therefore the discrete and the continuous dynamics arising from pedestrian interactions are compatible with each other and allow a coupled approach by scale interpolation.

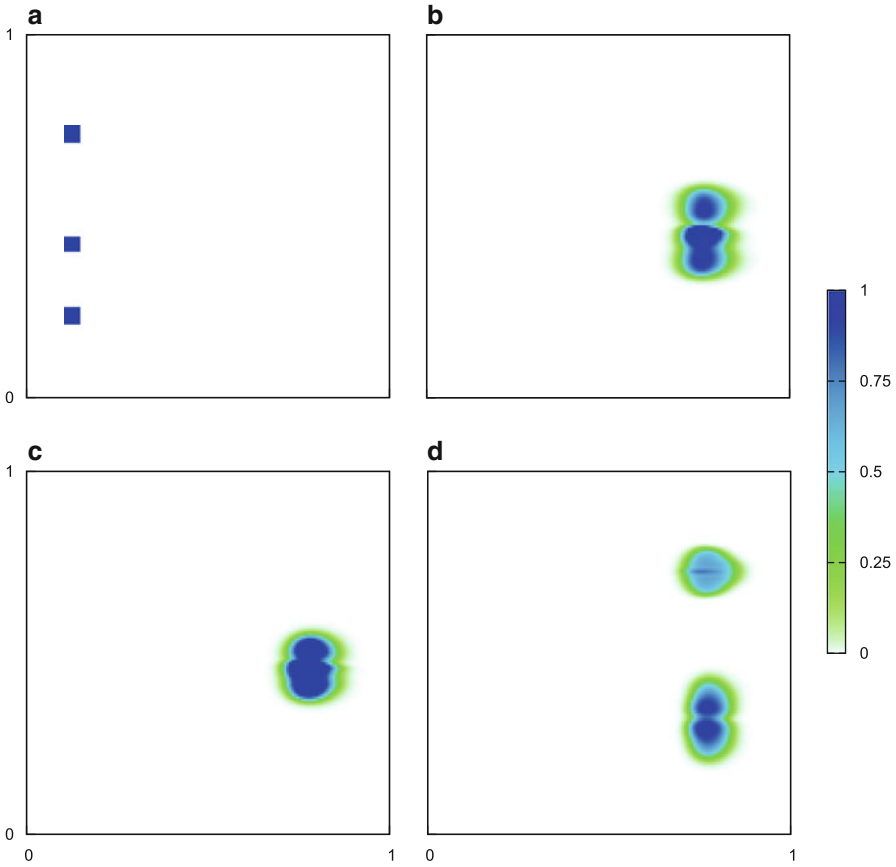


**Fig. 2.5** Effect of attraction in walking pedestrians. (**a**) Initial condition; (**b**) topological attraction makes the three clusters merge without compressing it; (**c**) metric attraction with large radius gives a result qualitatively similar to the topological one, but with more compression; (**d**) when attraction is metric with small radius, merging of clusters is limited to those which are sufficiently close

## 2.3 Metric vs. Topological Attraction

In this section we investigate the effect of attraction in a purely continuous framework. The interaction velocity now also includes an attractive component toward group mates (cf. Sect. 1.1.1), with a strength significantly greater than that of repulsion, along with an isotropic sensing domain for attraction spanning the whole space around the agents.

The initial condition features three clusters of pedestrians at the same homogeneous density, located a certain distance away from one another along the left side of the domain (Fig. 2.5a), who walk rightward. We first consider the case of a topological correction (cf. Sect. 1.1.1), meaning that pedestrians are allowed to

adjust the amplitude of their zone of attraction so as to interact with a predefined number of people, which in this simulation is set at 66 % of the total mass initially present in the domain. Then the three clusters tend to merge in a unique group, as shown in Fig. 2.5b. If instead we do not include any topological correction, the dynamics depend on the size of the metric interaction neighborhood (i.e., the sensory region). In particular, for a large radius of attraction (Fig. 2.5c) the result is qualitatively similar to that obtained with topological attraction but shows a higher level of compression, while for a small radius (Fig. 2.5d) only the two clusters initially sufficiently close merge, the third one being instead unaffected by the presence of other agents in the domain.

This test clearly shows that topological attraction between pedestrians greatly affects the resulting pattern. This does not mean that it is impossible to obtain similar structures with a purely metric attraction, by duly tuning its radius. However, the topological correction is essential in order to deal with a large value of the allowed interaction distance. Indeed a metric upper bound to the radius of attraction exists, which translates the fact that pedestrians are in no case concerned with very far mates, and which should necessarily coincide with the fixed radius of attraction in a purely metric approach. Now, such an upper bound is in general rather large, because pedestrians are able to see quite far, and can be attracted even by far fellows if necessary. Therefore, once the group is formed, a purely metric attraction with a large radius would imply attraction with an exceedingly large number of pedestrians. Thus, the topological correction is the only way to stay cohesive with a reasonable number of group mates while keeping a large interaction neighborhood. As a further confirmation of this, the test shows that a small interaction neighborhood in the purely metric approach disrupts cohesion, and aggregation is only partial, since far individuals may not be seen.

## 2.4 Flow Through a Bottleneck

As the first example, we consider the case of a group of pedestrians who want to go through a single narrow passage, obtained by placing two obstacles in front of each other as in Fig. 2.6.

In this simulation attraction is not active and a quite strong repulsion is restricted in front. Sliding boundary conditions are imposed along the boundaries of the obstacles. The initial condition is an inhomogeneous density of people, confined in the left area of the domain (Fig. 2.6a). The crowd then moves rightward, and when approaching the bottleneck (Fig. 2.6b), people initially pass through at the maximum speed (Fig. 2.6e). However, as all pedestrians cannot access the bottleneck at the same time, an obstruction builds up soon (arching effect, Fig. 2.6c). As a consequence, speed before the bottleneck is low, and some individuals in the middle of the group are even forced to stop, whereas beyond the bottleneck it attains its maximum again (Fig. 2.6f). After a certain time, the whole group flows through the bottleneck and the obstruction is depleted (Fig. 2.6d, g).

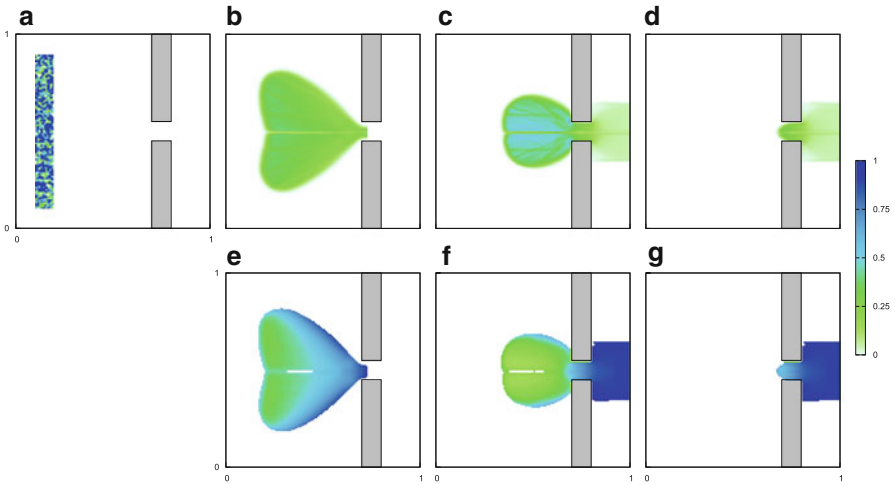


**Fig. 2.6** Pedestrian dynamics in presence of obstacles: a crowd wants to reach the right edge of the domain, going through a bottleneck. *Upper row*: density map. An obstruction forms as pedestrians try to access the passage (arching effect), until all people flow to the opposite side. *Lower row*: speed map. The speed of the crowd is inhomogeneous, with a sharp transition from low to high values across the bottleneck in correspondence of the opposite transition in the values of the density

The second example considers a more complicated environment, in which pedestrians have to flow through either of two bottlenecks, which are located beside one another. In particular, pedestrians must choose one of the bottlenecks in order to reach their final destination. This problem may model, for instance, the flow of passengers exiting the cars of a subway and then heading for the exit of the station via an escalator.

Simulations show that at the beginning people tend to access the closer passage (Fig. 2.7b), but later on some individuals, pushed sideway by the crowd at the entrance of the first bottleneck, decide to take the other passage (Fig. 2.7c). This gives rise to a flow also in the second bottleneck: Pedestrians branch off at the separation of the two bottlenecks (Fig. 2.7d), until all of them have entered either passage (Fig. 2.7e).

This is consistent with experimental observations: A typical station may have two (or even more) adjacent escalators that pedestrians can use to reach the ground level, however it is commonly observed that, on average, they prefer to take the closest one to their starting point. This behavior is clearly caught by the model, indeed Fig. 2.7a–f show a lower crowd density in the farthest passage.

Let us come back to the first example and investigate the influence of the coupled microscopic and macroscopic effects on the estimated average outflow time, i.e. the time pedestrians need to pass the bottleneck. This will provide meaningful insights into the way in which the microscopic granularity works within the macroscopic flow. The scenario of the simulation is depicted in Fig. 2.8.

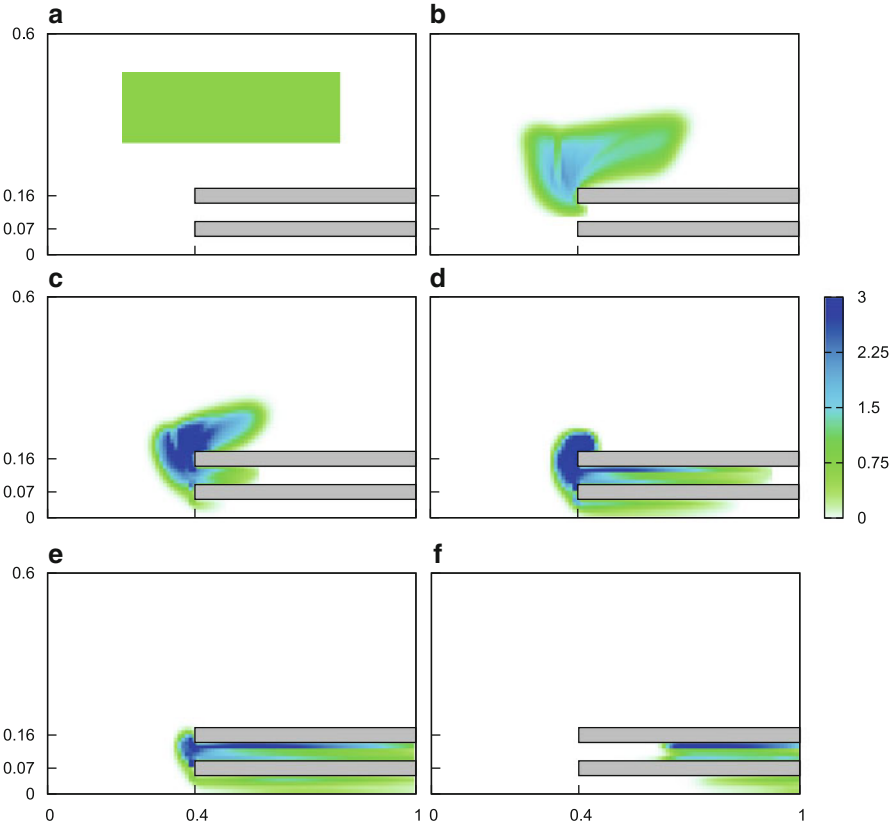


**Fig. 2.7** Evolution of the density of pedestrians at successive time instants for the problem of two narrow passages

We consider an estimator of the outflow time defined as the average time needed to empty the left room weighted by the percent mass of crowd that, at each time instant, still has to leave the room. In this way the estimator is mainly affected by the behavior of the majority of pedestrians, and is not very sensible to the behavior of the very last pedestrians, which could instead largely influence the classical outflow time (i.e., the time needed by *all* pedestrians to leave the room). The graphs of Fig. 2.9 show the trend of this estimator as a function of the interpolation parameter for a small crowd of 10 pedestrians and a large crowd of 100 pedestrians. In both cases, the two analogous curves, computed by using only the discrete or the continuous mass, are plotted for suitable reference. The multiscale average outflow time is the linear interpolation of the corresponding microscopic and macroscopic times.

The trend of the average outflow time is qualitatively similar for both the small and the large crowd, in particular it is decreasing with the interpolation parameter $\theta$.

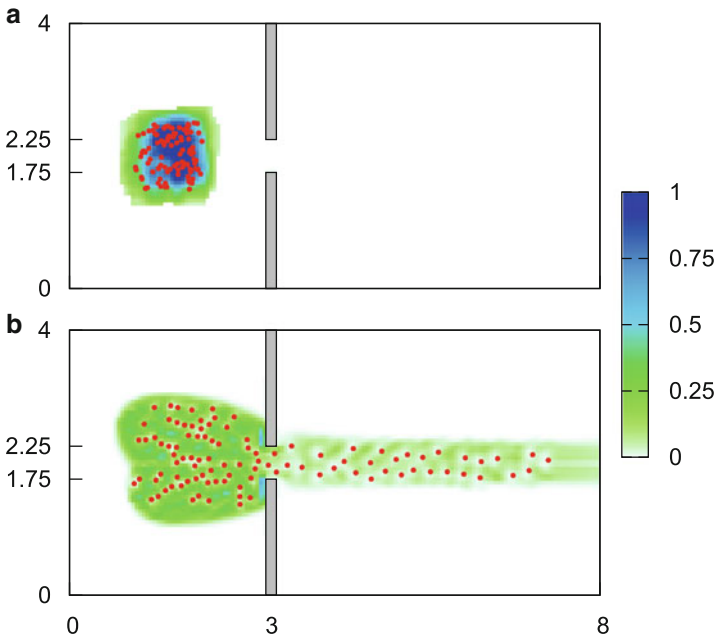


**Fig. 2.8** A crowd leaving a room through a door, initial condition (**a**) and underway outflow (**b**)

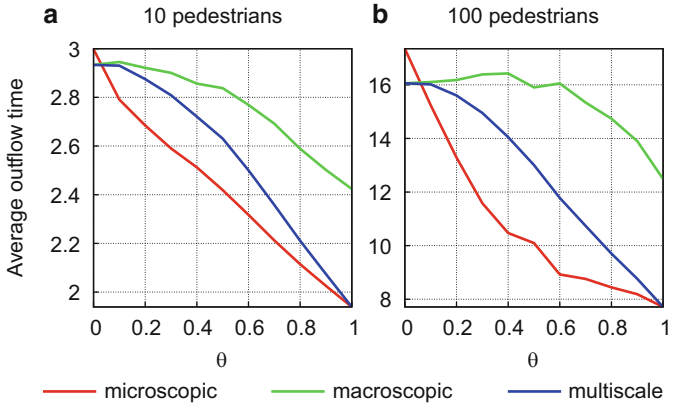


**Fig. 2.9** (**a**) Average outflow time as a function of the interpolation parameter $\theta$ for a crowd of 10 pedestrians and (**b**) 100 pedestrians

This elucidates the role played by a more influential microscopic granularity within the macroscopic flow: The more the multiscale coupling is biased toward the microscopic scale, the more fluent the crowd stream becomes (and consequently the average outflow time decreases). This can be explained considering that the interpolation parameter $\theta$ can be viewed as the percent mass shifted from the

macroscopic to the microscopic scale in consequence of the multiscale coupling. Subtracting interacting macroscopic mass from the system progressively reduces the action of the macroscopic interactions while enhancing that of the microscopic ones. Since the latter are less distributed in space, because the microscopic mass is clustered in single points, this ultimately results in fewer deviations from the desired velocity and the desired paths.

## 2.5 Crossing Flows

Here we study the problem of two groups of people walking in opposite directions toward one another.

### *2.5.1 Lane Formation*

In order to model crossing flows we need two densities describing the spatial distribution of the two pedestrian groups. Each group has its own desired velocity, which is unaffected by the desired velocity of the opposite group. On the other hand, each interaction velocity now depends on both pedestrian distributions, indeed the dynamics triggered by encounters among individuals belonging to different populations plays a relevant role in this problem. Specifically, we assume that pedestrians of either population feel uncomfortable when too close to pedestrians of the opposite population, due to their different walking targets. Therefore, they try to keep away from areas of high concentration of people coming in the opposite direction, aiming at gaining room for their walking direction. We assume no interaction among pedestrians belonging to the same population, so as to focus specifically on the effect of the interactions between the two oppositely walking groups. We model two uninterrupted flows of pedestrians. One population enters the domain from the left boundary while the other enters from the right boundary. The desired velocity is $(1, 0)$ for the first population and $(-1, 0)$ for the second one, that is first population is walking rightward and second population leftward.

Let us begin with a purely macroscopic approach. Figure 2.10 shows the prediction of the model in the case the two populations are equal, so that the behavior is expected to be perfectly *symmetric*. Indeed, the symmetry of the initial datum is preserved. Although the result is rather satisfactory from the mathematical point of view, the final stable configuration is quite unrealistic, meaning that it is not observed in actual pedestrians. Figure 2.11 shows the results in the case in which the two populations are not equal. More precisely, the first one is larger than the second one. It is clear that the difference between the two populations leads to the break of the left-right symmetry. This test shows the ability of the model to reproduce the alternate walking lanes, which are experimentally observed as a characteristic self-organization phenomenon in crossing flows. A question naturally arises: Why

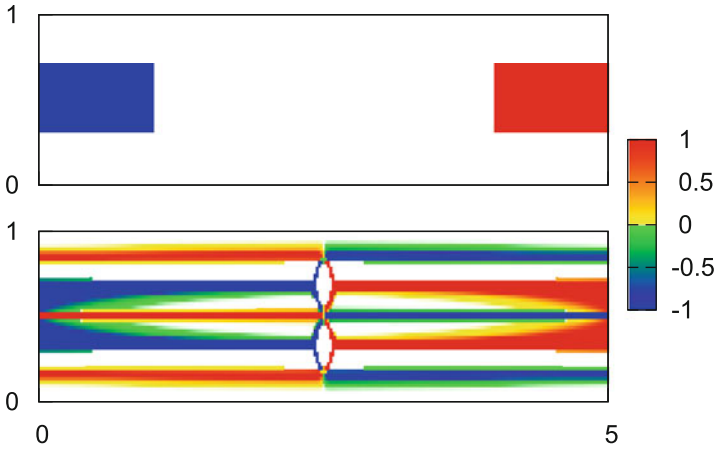


**Fig. 2.10** Two uninterrupted symmetric flows of macroscopic pedestrians. Initial (*top*) and final (*bottom*) configuration. Left-right symmetry is not lost although each population breaks in more than one group

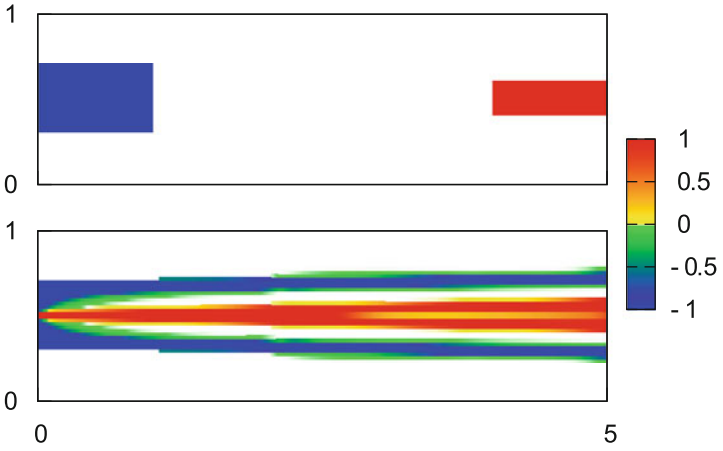


**Fig. 2.11** Two uninterrupted asymmetric flows of macroscopic pedestrians. Initial (*top*) and final (*bottom*) configuration. $2 + 1$ lanes are formed

we observe exactly two and one lanes respectively, instead of a different number of lanes? Figures 2.12 and 2.13 answer this question, showing that the number of lines depend on the extension (in the vertical direction) of the two populations. In the tests of Figs. 2.11 ($2 + 1$ lanes), 2.12 ($3 + 2$ lanes) and 2.13 ($4 + 3$ lanes) the first population has a vertical extension of 0.4, 0.6 and 0.8 respectively, while the difference between the extensions of the two populations is kept fixed to 0.2.

We recall that the mathematical model has *not* been conceived with the specific purpose of describing the walking lanes addressed here. Rather, we stress that the

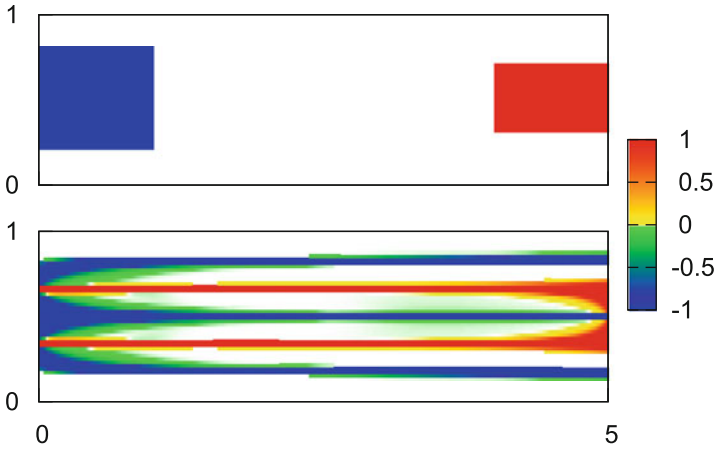


**Fig. 2.12** Two uninterrupted asymmetric flows of macroscopic pedestrians. Initial (*top*) and final (*bottom*) configuration. $3 + 2$ lanes are formed

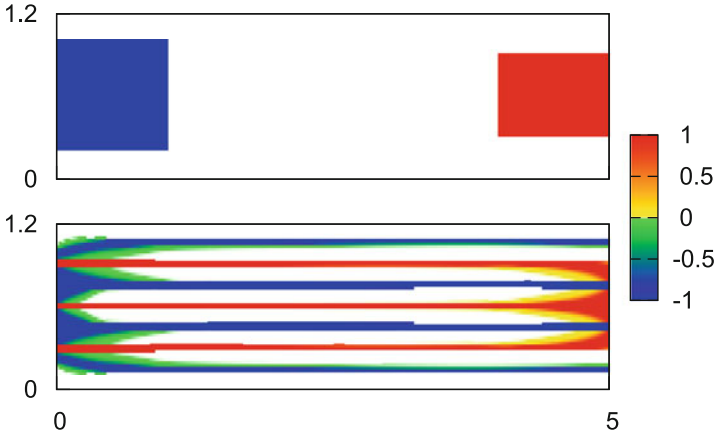


**Fig. 2.13** Two uninterrupted asymmetric flows of macroscopic pedestrians. Initial (*top*) and final (*bottom*) configuration. $4 + 3$ lanes are formed

model is able to catch this behavioral custom as a by-product of much more general and elementary modeling principles (cf. Sect. 1.1.1), resorting ultimately to the basic idea of nonlocal interactions among pedestrians.

In the frame of a microscopic model we obtain similar results, in particular we observe again the appearance of the lanes. It is instead impossible to get a perfectly symmetric result as the one shown in Fig. 2.10, due to the intrinsic inhomogeneous granular effects characterizing microscopic models. Figure 2.14 shows the outcome of the simulation in the case of two populations formed by the same number of agents randomly distributed in a symmetric portion of the domain. Figure 2.15

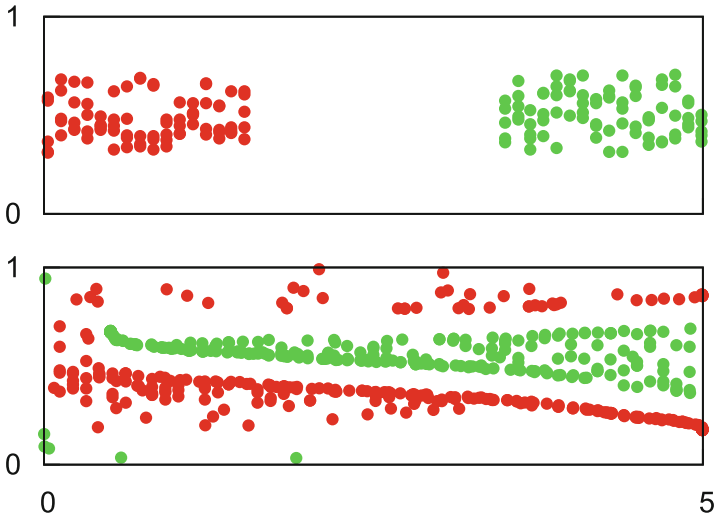


**Fig. 2.14** Two uninterrupted symmetric flows of microscopic pedestrians. Initial (*top*) and final (*bottom*) configuration. Symmetry is broken by the granularity

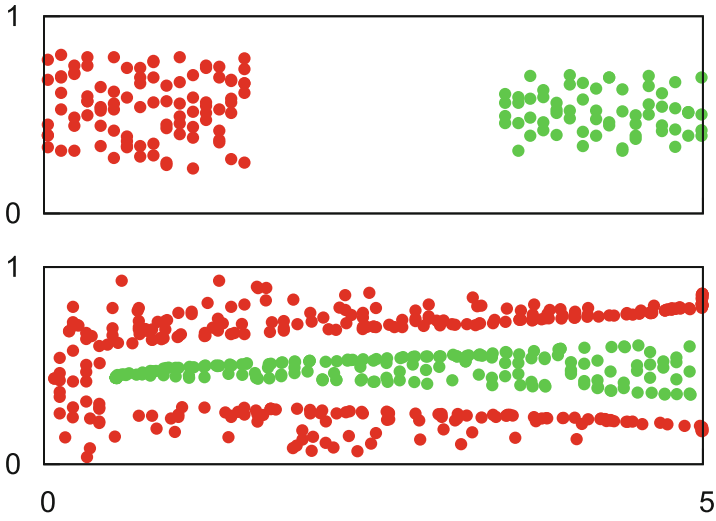


**Fig. 2.15** Two uninterrupted asymmetric flows of microscopic pedestrians. Initial (*top*) and final (*bottom*) configuration. $2 + 1$ lanes are formed

shows the outcome of the simulation in the case the two populations are non equal, to be compared with Fig. 2.12.

Let us now switch to the multiscale features of the model, showing both the continuous and the discrete components of the crowd, and consider again the test

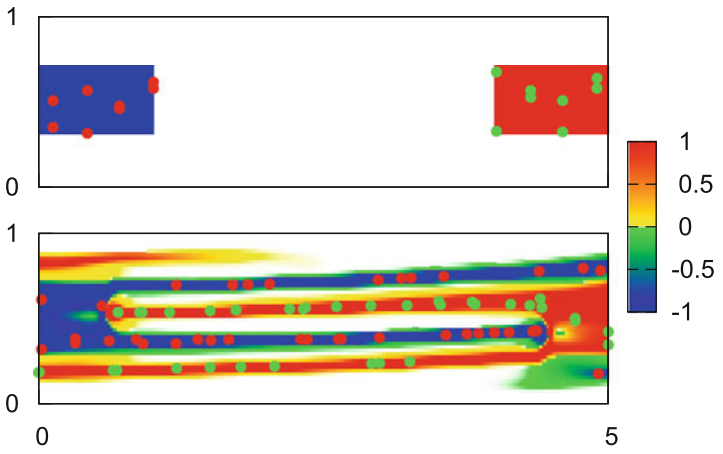


**Fig. 2.16** Two uninterrupted symmetric flows of microscopic and macroscopic pedestrians. Initial (*top*) and final (*bottom*) configuration. The effect of a few microscopic pedestrians are sufficient to break the left-right symmetry

described in Fig. 2.10. We aim at catching one of the main advantages of the multiscale model, i.e., the introduction of the *granularity* in a purely macroscopic setting in a form which is fully justifiable from the mathematical and physical point of view (see Chap. 5 for details). From Fig. 2.10 it is clear that a purely macroscopic approach is not able to break the left-right symmetry as it is expected by actual pedestrians. In order to get realistic results, the right amount of granularity must be introduced in the model. Figure 2.16 shows the outcome of the simulations performed by the multiscale model in the perfectly symmetric case. It is remarkable that the introduction of a few microscopic pedestrians is sufficient to break the symmetry of the density of pedestrians. Indeed, after the first interaction in the middle of the domain, two lanes per population are immediately formed, and then they remain stable.

### 2.5.2 *Intermittent Flow*

In the following test we investigate the behavior of two crossing populations who share a narrow passage (e.g., a door). The setting of the problem is displayed in the snapshot of Fig. 2.18a. In particular the blue crowd with red microscopic pedestrians, say population 1, walks rightward whereas the yellow one with green microscopic pedestrians, say population 2, walks leftward. Let us begin from the case in which the macroscopic scale leads the dynamics. The bottleneck tends to clog (Fig. 2.17a): No density nor microscopic pedestrians flow through, except for a small mass which is able to pass at early times, when the passage is still free. This is well confirmed by the time trend of the macroscopic flux across the bottleneck

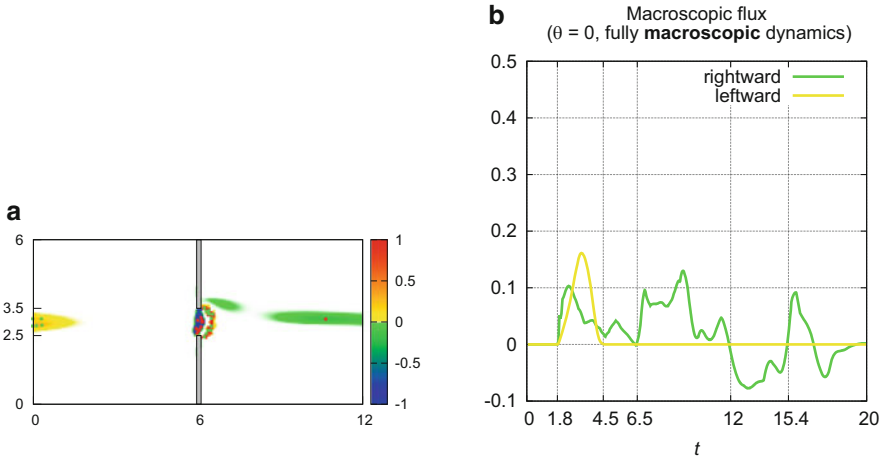


**Fig. 2.17** (**a**) Clogging at the bottleneck; (**b**) corresponding macroscopic fluxes arising with the fully macroscopic dynamics

(Fig. 2.17b): That of population 2 is permanently zero for $t \geq 4.5$, whereas that of population 1 oscillates between small positive and negative values, which implies that population 1 is pushed backward by population 2 as soon as it tries to cross.

By realizing a multiscale coupling between the continuous and the discrete model ($\theta = 0.3$), we obtain the dynamics depicted in Fig. 2.18 and summarized in Fig. 2.19 via the time trend of the macroscopic and microscopic fluxes across the bottleneck. The model produces a traffic light effect, i.e. an intermittent flow through the bottleneck. In more detail, starting from the initial condition depicted in Fig. 2.18a, pedestrians of population 2 are induced to stop at the bottleneck while those of population 1 go through at one side (Figs. 2.18b and 2.19 for $4.5 \leq t \leq 8.5$). After some time, population 2 reorganizes itself and stops the flow of population 1 (Figs. 2.18c and 2.19 for $8.5 \leq t \leq 11$), then its larger mass stuck at the bottleneck locally gives it the necessary strength for repelling opposite walkers and gaining room in the middle (Figs. 2.18d and 2.19 for $11 \leq t \leq 15$). Some walkers of population 1 remain trapped by the stream of population 2 and cannot access the passage (Figs. 2.18e and 2.19 for $t \approx 15$) until most of population 2 has flowed through (Figs. 2.18f and 2.19 for $15 \leq t \leq 17.5$).

From the modeling point of view, the difference with the previous fully macroscopic case is that the multiscale coupling shifts some macroscopic mass onto the microscopic pedestrians, all other parameters and initial conditions being unchanged. The inhomogeneous distribution of this microscopic mass induces a break of symmetry between the interfacing populations, which finally leads to an alternate occupancy of the passage according to the repulsion prevailing locally in space and time.

Shifting the whole mass onto the microscopic pedestrians we obtain that the microscopic scale leads the dynamics, which produces the outcome displayed in

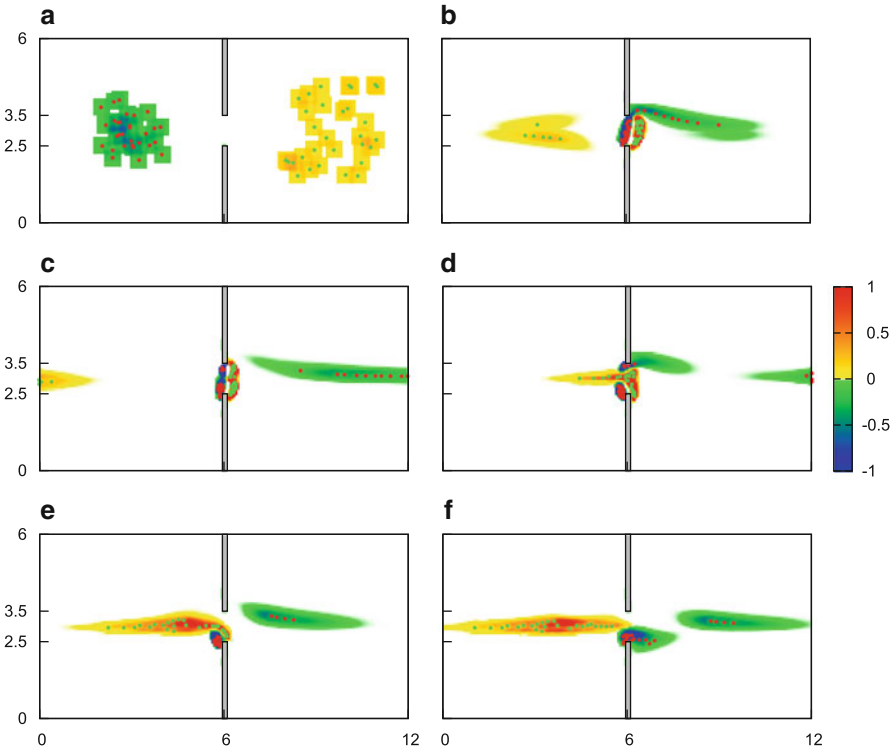


**Fig. 2.18** Alternate flows at the bottleneck in the multiscale model. Negative values of the density of the population walking rightward are for pictorial purposes only

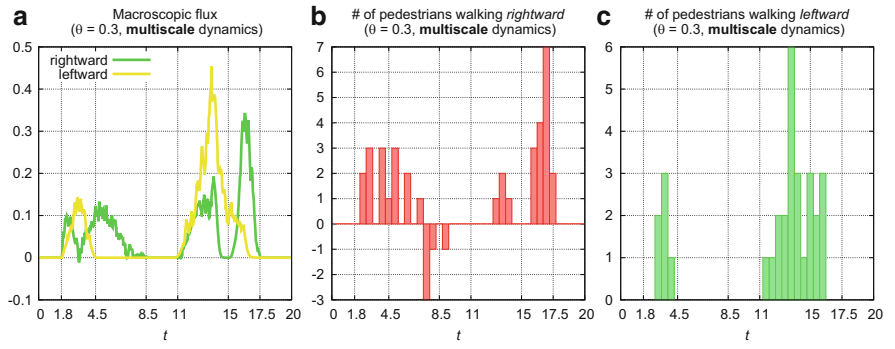


**Fig. 2.19** Multiscale model: (**a**) macroscopic fluxes across the bottleneck; (**b**)–(**c**) number of microscopic pedestrians crossing the bottleneck rightward and leftward, respectively

Fig. 2.20. Now the microscopic granularity fully dominates and the stream is the fluentest one. As a result, the bottleneck interferes less with the stream than in the previous cases, and the model reproduces the alternate oppositely walking lanes (Fig. 2.20a) extensively observed as one of the main effects of self-organization

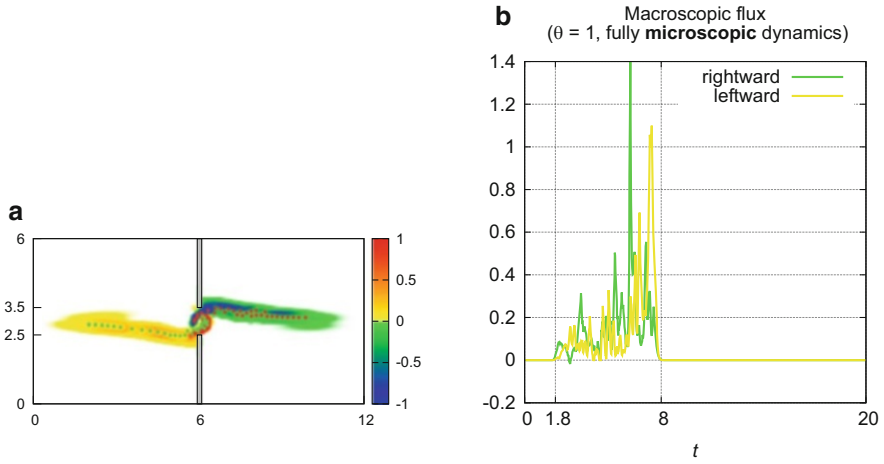


**Fig. 2.20** (**a**) Alternate lanes through the bottleneck; (**b**) corresponding macroscopic fluxes emerging with the fully microscopic dynamics. Notice that both fluxes are identically zero for $t \geq 8$ because by then both populations have completely flowed across the door

in real crowds. The time trend of the macroscopic flux across the bottleneck (Fig. 2.20b) confirms that the two populations flow simultaneously through the passage, with comparable fluxes, in the interval $1.8 \leq t \leq 8$. After the time $t = 8$ the macroscopic fluxes are identically zero because by then both populations have completely flowed across the door.

## 2.6 Social Groups and One-Many Interactions

In this section we show the combined effects of attraction and repulsion in describing the walking behavior of social groups of pedestrians. The typical scenario is a family or a group of friends having a leisure walk in a commercial walkway or a mall. Walking social groups have some distinctive features: First, their members want to stay together, keeping visual contact and reaching the destination at the same time. Second, they want to keep verbal contact, i.e. every group member wants to hear what the others say. In this context, the attraction force is employed to guarantee the cohesion of the group. Repulsion force instead has a twofold effect: If short-range, it allows to avoid collisions. If medium-range and directed against the direction of motion, it prevents each group member from having a mate behind, thus making impossible verbal communication.

We first simulate small social groups moving in the right direction in a free environment. As illustrated in Sect. 1.1.2, small groups (3–4 members) deploy themselves in a V-like formation. Figure 2.21 shows the result of purely microscopic simulation for 3, 4, and 12 pedestrians. Attraction and short-range repulsion is

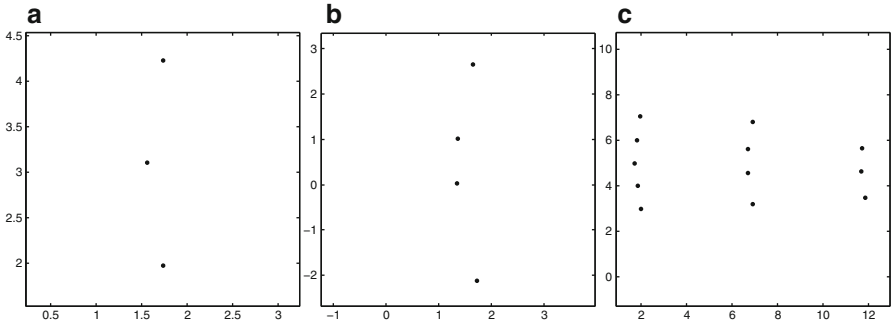


**Fig. 2.21** V-like formations in walking social groups. The pattern is obtained by means of an isotropic attraction and an anisotropic repulsion. The patterns created by large groups are less stable than those formed by small groups. (**a**) 3 members; (**b**) 4 members; (**c**) 12 members

all-to-all, while medium-range repulsion is limited to an angle of 160° centred in the opposite direction of motion. In all cases V-like formation arises, being much more stable in small groups rather than large groups. In the latter case, instability leads to the break of the pattern and several V's arise in place of a unique large V.

When social groups move in a crowded environment, their shape changes. The ease of communication becomes secondary, and the need for keeping some contact with the rest of the group actually leads the behavior. Figure 2.22 shows the results of a purely microscopic simulation for 5 and 10 pedestrians, respectively. The group first walks in a free environment, then it enters a crowded region. We assume here a frontal metric attraction and repulsion among the group members, which are active before and after the group enters the crowd. In the uncongested area the group takes an irregular circular-like shape. When the group reaches the mass of strangers (frozen in the simulation) the group quickly re-arranges itself taking a river-like configuration, cf. Sect. 1.1.2. As for V's, river-like pattern is not stable for large groups. Indeed, large groups have the tendency to split up in two or more lanes (Fig. 2.22d).

The group entering the crowd is clearly better described in a multiscale fashion. As we did in Sect. 2.5, we consider two populations: The first one, modeled with $\theta = 1$ (evolution guided by the single pedestrians) moves to the right and describes a 7-member social group. The second one, modeled with $\theta = 0$ (evolution guided by the macroscopic density) moves slightly to the left and describes the crowd. The interactions are modeled as follows:

- Pop. 1 vs Pop. 1: frontal metric long-range attraction and short-range repulsion.
- Pop. 1 vs Pop. 2: frontal metric medium-range repulsion.
- Pop. 2 vs Pop. 1: frontal metric short-range repulsion.
- Pop. 2 vs Pop. 2: frontal metric medium-range repulsion.

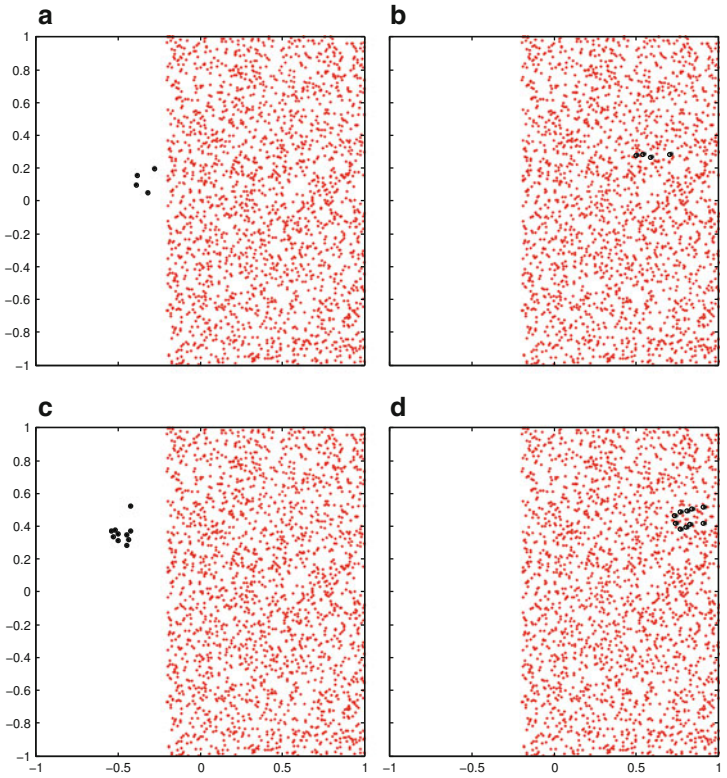


**Fig. 2.22** A social group walks into a crowded region. (**a**)–(**b**) A small group with 5 members; (**c**)–(**d**) a large group with 10 members

The main difference with respect to the previous test is that here the crowd is not frozen, but has its own dynamics. In particular, there is an internal repulsion which makes the crowd come back to the original shape after the passage of the social group (otherwise the "wake" left by the group in the crowd would last forever). The repulsion makes also the crowd expand to fill the whole space and, until the equilibrium is reached, the density in the inner part is higher than the density in the outer part of the crowd. Figure 2.23 shows the result of the simulation. As before, the shape of the group changes after the interaction with the crowd and a river-like configuration shows up. Since the group is repulsed from the crowd, it tends to move toward its boundary, where the density is lower.

As a last example of social group, we consider the case of a crowd following a leader, for instance a group of tourists and their guide. The leader is a microscopic pedestrian who behaves in a different way with respect to all of the other group members: She is the only one *informed* of the way to go, hence she walks with a pre-assigned velocity to the right, independently of the others (i.e., she does not interact with the rest of the group). She only stops when her distance from the

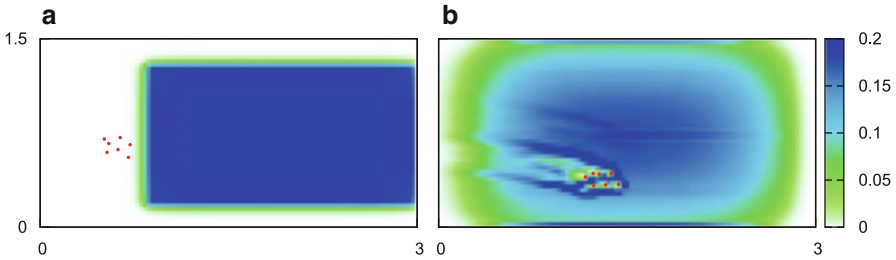


**Fig. 2.23** A 7-members social group walks into a crowded region. Only the scale leading the dynamics is plotted. (**a**) Before the interaction; (**b**) after the interaction

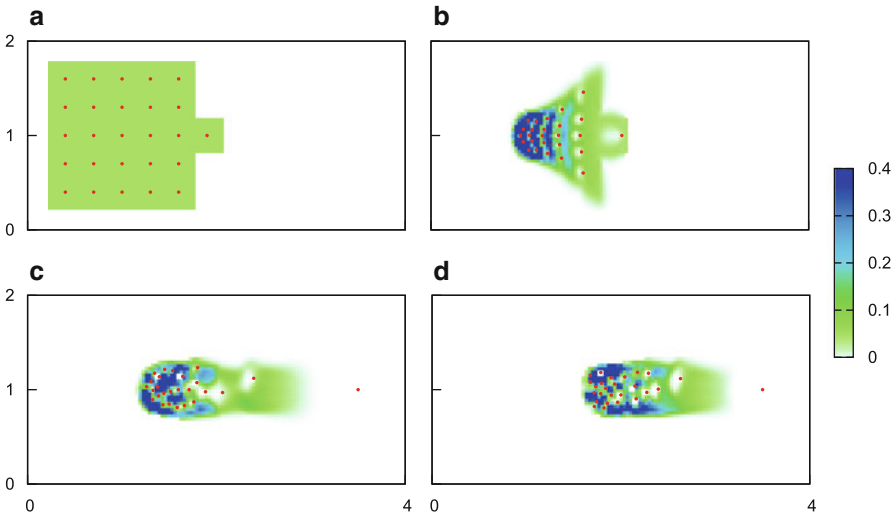


**Fig. 2.24** (**a**) Initial condition; (**b**) the group assumes an elongated configuration; (**c**) the group is formed and follows the leader; (**d**) the leader waits for the group while the group moves on

group becomes too large. The followers have no desired velocity, because they are not informed of the way to go, and experience both frontal attraction and frontal repulsion with their group mates, including the leader. Attraction acts against group dispersion, and is needed especially in order for the crowd to follow the leader. Instead, repulsion is intended for collision avoidance among group mates. The sensory region for the attraction is so small that the tail of group does not feel the leader ahead.

The group starts from the square-shaped distribution depicted in Fig. 2.24a, with the leader in front. Then, after a transient (Fig. 2.24b), it assumes a horizontally elongated shape (Fig. 2.24c) as a result of joint attractive and repulsive effects. With no leader such a configuration would be an equilibrium, as attraction and repulsion balance. However, as soon as the leader starts moving forward undisturbed, pedestrians at the front, who can feel her directly, are attracted and move forward

in turn. At the same time, pedestrians at the rear are attracted toward group mates in front. This makes the information on the way to go travel backward across the group, which ultimately moves forward as a whole (Fig. 2.24d).

It is worth stressing that *at the macroscopic scale there is no counterpart of the microscopic leader*. This implies that the macroscopic velocity field is not affected by the microscopic leader, therefore the macroscopic mass feels the latter only through the microscopic velocity field.

## 2.7 Bibliographical Notes

Section 2.1 The idea of coupling microscopic and macroscopic scales into a *multiscale model* has been developed in the paper by Cristiani et al. [48]. Here we presented the theory in a simplified manner, without referring to the measure theory. A full description of the model is given in Chap. 5.

Section 2.2 Simulations presented in Figs. 2.1 and 2.2 are from Cristiani et al. [47]; those presented in Figs. 2.3 and 2.4 are instead from Cristiani et al. [48].

Section 2.3 The terminology *topological interactions*, as opposed to metric ones, has been borrowed from the papers by Ballerini et al. [11,12], which give experimental evidence of topological interactions in animal groups (particularly flocks of starlings). The authors also provide simulation results (cf. [11, Figure 4]) which are consistent with those we presented in Fig. 2.5. The interested reader is further referred to the recent paper by Bellomo and Soler [18] for a kinetic model of swarm implementing analogous ideas. The simulation presented in Fig. 2.5 is from Cristiani et al. [47].

Section 2.4 The macroscopic simulation of the *flow through a bottleneck* (Fig. 2.6), which is from Cristiani et al. [47], compares qualitatively well with that obtained by Helbing et al. [85] by means of a microscopic model. The multiscale version of the same simulation (Figs. 2.8 and 2.9) is from Cristiani et al. [48]. The scenario of the *subway station* is thoroughly described in the paper by Piccoli and Tosin [144] and further delved into in the paper by Bruno et al. [27].

Section 2.5 *Crossing flows* have been addressed by several authors, mostly by means of microscopic models. The models in the literature show in general a good agreement between the experimental features of this kind of flow and their predictions. In the papers by Helbing and Johansson [86], Helbing et al. [89] and by Hoogendoorn and Daamen [98], Hoogendoorn et al. [99], which are a valuable source of empirical information on pedestrian behavior, particular attention is payed to typical patterns emerging in crossing pedestrian flows. The microscopic models proposed by Helbing and Molnàr [88], Hoogendoorn and Bovy [95], and Maury et al. [121] have also proved to be successful in reproducing such experimental evidences. The simulations presented in Figs. 2.17–2.20 are from Cristiani et al. [48], the others instead appear for the first time in this book.

Section 2.6 The results about *V-like and river-like formations* are presented for the first time in this book, and are motivated by the work by Moussaïd et al. [128]. The motion of social groups within a crowd has been little investigated in the literature, compared to the motion of crowds composed of single individuals. The simulation results in Moussaïd et al. [128] are qualitatively similar to those presented here, although the former are obtained through a second order model, based on social forces. It is of note that somewhat dual configurations can be obtained by imposing within the social group a repulsion force against group mates in front. The only difference is that in the latter case inverted-V formations emerge, i.e., the vertex of the formation is in front of the group. Inverted-V formations often appear in animal groups, for example in migrating geese. These results strongly suggest that the main advantage of V-like formations is not the aerodynamic effect, but instead the improvement of the communication between individuals, see Cristiani et al. [46] and references therein. Finally, the simulation of the *group of tourists with guide* (Fig. 2.24) is from Cristiani et al. [48].

# Chapter 3
# Psychological Insights

**Abstract** The aim of this chapter is to take another point of view in the modeling of the crowd. Namely, here we report some approaches focusing on pedestrians as individuals. Then it is of paramount importance to take into account the psychological aspects of the problem, distinguishing moving humans from "particles" or even from self-propelled agents (e.g., birds). Such psychological components show up both in the choice of walking strategies and preferences and in interaction rules with other pedestrians. The focus will be mainly on investigations addressing the behavior of the single pedestrian moving in an organized environment. Moreover, we will discuss some models proposed by works in different fields, not limited to psychology. However, the latter are more of qualitative nature, as opposed to mathematically advanced ones discussed in Chaps. 4 and 5. Then we will deal with experiments and measurements. In particular we will discuss how the experimental setting influences results because of expected *psychological bias*. Also a view on the most used measurement tools is included, since this may also affect the perception of experiment participants. Finally, we will compare some experimental setting, showing how sensitive to them measurements can be.

## 3.1 Wide Literatures

To deal with the various aspects of studying and modeling walking humans a number of researchers from different fields wrote relevant papers, thus producing a very wide literature. It is beyond the scope of this chapter to provide an exhaustive compendium. We rather want to underline how the problem interested a few different fields including:

- Applied Mathematics.
- Architecture.
- Biology.
- Cognitive Science.

E. Cristiani et al., *Multiscale Modeling of Pedestrian Dynamics*, MS&A 12,
DOI 10.1007/978-3-319-06620-2_3,

- Medicine and Physical Therapy.
- Physics, such as particle systems and Statistical Mechanics.
- Psychology.
- Sociology.
- Transportation engineering.

In the following sections we will report results from various papers in different domains, but always with the main intention of underlying specific characteristics which are relative to the movement of the single pedestrian and focused on psychological aspects. Notice that we do not exclude to deal with interactions pedestrian-pedestrian if this involves social or other rules, which can not be captured by pure mechanistic models. However, the results we want to discuss are not confined to work by psychologists or cognitive scientists. As an example, let us mention the early literature in Transportation Engineering.

Among the first studies and measures of pedestrian behavior are those by transportation engineers. In particular empirical studies, such as in metro stations or other areas, appeared since the 1950s. The interest of researchers was in producing a systematic approach to comfort and safety of pedestrian facilities, introducing, for instance, the concept of *level-of-service*, *design elements* and *planning guidelines*.

This literature is mainly based on measures of quantities such as average velocity and total flow (number of pedestrian per unit of time). The main point was to reach simple formulas relating such quantities to the size of the facility, so to have explicit formulas to use in design and planning. An example is the relation between the longitudinal space used and the average speed of pedestrians. However, these approaches were not capturing the richness of dynamic features, as those illustrated in Sect. 3.2.3. Still also this literature addressed questions related to personal characteristics of pedestrians, such as purposes of walking, age, gender, size and others, and characteristics of the trip, such as walking purpose, route familiarity, presence of luggage and alike.

## 3.2 Specific Characteristics of Pedestrians

The aim of this section is to focus on emerging behavior of pedestrians which can be justified only by social and psychological insight. As explained in Chap. 1, many approaches are based on frameworks originally used in gas and fluid dynamics. However, there are profound differences among gas particles and agents which are able to measure the system state and take decisions. These observations apply to many groups of agents such as animals or robots, however there are some specific issues which are relevant only for pedestrians as human beings. Here we deal with these issues.

### 3.2.1 Cognitive Maps

When walking, humans use representations of the environment created by their brains and known as *cognitive maps*. In other words, unless they use a map or technological devices (such as GPS), humans make choices based on virtual representations of the reality.

The creation of a cognitive map is mostly a subconscious process, based on observations of the environment. The process of knowing the environment is dynamic and information is continuously updated, taking into account the short term and long term purposes of the walker. More precisely, the information is typically gathered in two ways: *Route-based knowledge*, acquired during exploration of the environment by performing travels, or *survey knowledge*, acquired by watching the environment from a special position (e.g. elevated), consulting maps, photographs and other information on the environment as, more recently, GPS equipped devices. Most people develop a two dimensional knowledge of the environment even if the route-based process is mainly one dimensional. The map creation process thus integrates information coming from a number of different sources and at different moments in time.

The most basic source of knowledge is thus sensorimotor apprehension of information from the body or from the environment during locomotion. The direct measurements of distances of environmental size is impossible from a single location. Thus the elaboration process can be highly complicated and use a variety of practices, such as triangulations, estimations from known locations and others. Landmarks represent one of the key components of cognitive maps, maybe the fundamental component, and are also the main tool toward constructing the maps. More precisely, landmarks may be used as centroid of regions, nodes of a network or as indicator of nearby point of interest. For instance, a very visible building may serve as landmark for a specific city area.

Great differences show up among individuals in gaining environmental knowledge. For route-based knowledge, the literature reports various differences in the learning process, including gender based: Women apparently spend more time scanning the sidewalk than men do. For survey knowledge, the process is highly affected by the used mean and the way it is used. For instance the orientation of a geographical map with respect to the observed environment influences the ability of users to correctly use the information. Moreover, sufficient information should be provided on the map to help identifying all the relevant locations. Regarding new technology, it was observed that GPS users are highly ineffective with respect to map users and even more with respect to experienced users, showing longer distance traveled, slower motion, more stops and larger direction errors. In experiments GPS users rated wayfinding tasks as highly difficult and more challenging than users with direct knowledge of the environment.

Cognitive maps are most probably created in an Euclidean type metric space, at least in many western countries, and consist of points, lines and areas. However, cognitive maps do not satisfy the usual axioms of Euclidean geometry.

Cognitive maps are influenced by many factors and can be substantially different from a geographical map, in particular producing errors in the estimation of distances and other measures of the environment.

The most common observed alterations of measures are usually called *distortion* and *fuzziness*. Distortion is defined as the displacement of a location from its actual position, while fuzziness measures the dispersion of the estimate of a location. For instance one may locate a building entrance 100 m away from the actual location or provide an estimate within a 30 m range. Various studies reported systematic distortions in cognitive maps. In particular some common elements are the following:

- Distances are generally overestimated.
- Shorter distances are exaggerated with respect to longer distances.
- Cognitive maps are usually rotated to align to landmark axes, such as major transportation axes.
- Reference points (as home location) affect the estimation and also the retrieval of information from cognitive maps.
- Fuzziness is higher for peripheral locations.

Also the errors are influenced by personal characteristics. In particular, one can compose aggregate cognitive maps by collecting measures from groups with common characteristics. It was observed that such aggregate maps are affected by the group residences. For instance, people living in centrally located neighborhoods are more likely to show higher level of aggregate precision with respect to directions, rather then people living in peripheral neighborhoods. However, this major precision is not occurring in measuring distances. Concluding, home and landmark locations appear to be a major factor affecting the accuracy of aggregate cognitive maps, in particular for the spatial distribution of errors.

### *3.2.2 Geographical and Social Features*

Some researchers argued that a high degree of cooperation between pedestrians is an intrinsic part of pedestrian behavior. Even more, that most of pedestrian flows in large facilities would be impossible without a high level of cooperation. On this regard, the tacit agreement to maintain walking lanes is one way to increase the efficiency of the overall flows. This justified the study of various differences among *social rules* observed when walking. Being social phenomena, such rules are also differentiated geographically.

Let us start discussing geographic differences. It is reported that in central Europe pedestrians have a slight tendency to walk on the right-hand side. This preference is in line with the car driving rules. However, the same happens also in London, while in Great Britain drive is on the left-hand side. Moreover in Japan both cars and pedestrians stay on the left-hand side, while Korea provides last combinatorial possibility with cars driving on right-hand side and pedestrian preferring left-hand

side. However, the structure of the formed lanes is quite stable independently of the preferred walk side. One has to notice that these preferences are reported in various studies, but explicit and robust quantitative measurements are often lacking, thus these preferences are rather observed on an anecdotal basis.

Notice also that the preference apparently shows up mostly when interacting with other pedestrians and is less pronounced when individuals are walking alone. The main reason is that such preferences, even if mild, are sufficient for symmetry-breaking phenomena as observed in Chap. 2. It is still very debatable if the efficiency of the resulting self-organized configuration is a cause or consequence of the behavioral convention. Various arguments as reinforcement learning and differential games models were proposed in favor of the first hypothesis. In this respect, reinforcement learning is compatible with the appearance of different preferences in different geographical areas. The main reasoning for differential games goes as follows: Initially individuals would split equally among left and right when interacting. However, when random deviations occur, it is more probable that the subsequent choices are biased leading to an increasingly marked preference. Apparently this argument should predict that lanes in high crowding interacting flows should appear on both sides and this is somehow confirmed by experiments. We will go back on this issue of handiness in pedestrian routes in Sect. 3.4.3.

For what concerns social behavior, generally speaking groups are usually granted more space than single pedestrians. Some studies also report gender differences, claiming that more space is usually granted to males. Other social differences include the appearance, with studies reporting of higher distance to well dressed women than sloppy dressed. The latter effect was referred to as *power of beauty*, however it seems more linked to social reputation because of the dressing style. Also it was observed that persons and small groups look for larger groups and various other studies addressed social, gender and even racial characteristics. If caution is in order for the geographical differences and habits, it is even more imperative for social and other differences. Along this line, it was proposed that in most of cases manoeuvrability may indeed be the main reason for observed choices with very minor bias due to characteristics of the interacting pedestrians.

### *3.2.3 Self-Organization and Re-organization*

An effect of the highly complex behavioral rules of interaction among pedestrians is the appearance of the so-called *self-organization* phenomena, see Sect. 1.1.2. The superposition of the interaction rules gives rise to special geometric characteristics of the position and dynamics of the whole group, without centralized controllers or organized agreement (such as by signs or verbal alerts) which act on purpose for that. As for the cognitive maps, most interaction decisions must happen at a subconscious level, rather than being high level strategic decisions. This is probably one of the reasons why even relatively simple models can reproduce them.

Self-organization is observed in a number of different fields, including animal groups. In this section we want to stress how the special features of pedestrian cognitive aspects can further trigger the phenomenon towards dynamical advantages for the whole group on the move.

On the other side, we will also point out some *unwanted* situations, mainly due to *panic* (or other non normal conditions). However, beside reporting various self-organized configurations, we want also to briefly address the ability to re-organize the group in case of need.

Among various self-organization phenomena, the mostly relevant and observed ones are the following:

- Lane formation in unidirectional flows.
- Walking couples, clusters and V's.
- Capacity drops at bottlenecks.
- Clogging and arches in stampedes and panic situations.
- Slower-is-faster effect and Braess' paradox for obstacles.
- Zipper configurations at bottlenecks.
- Coexisting lanes formation in opposite flows.
- Circular flows at cross intersections.
- Intermittent flows (or traffic light effect) at shared bottlenecks.

Many of the above phenomena occur mainly when the crowd density is sufficiently high. In particular, beside lanes of walking pedestrians, one may also observe shock-like waves, i.e., queue formations where the end of the queue is moving backwards (the latter are well accepted in vehicular traffic literature).

Some specific formations were also noticed when walking in groups. Couples walking together are particularly common, while small groups tend to dispose themselves in a V-like formation. More precisely, the shape is that of a V if observed from above with pedestrians moving upward in the camera image. The terminology "(inverted) V" comes from comparison with migrating birds, which also display a V formation but in opposite position with respect to the flying direction.

In case of flows having opposite walking directions, many researchers observed the formation of alternate lanes of pedestrian having the same direction of walk. The case of pedestrian crossing roads is the most commonly studied. This lane formation phenomenon diminishes the probability of encounters among pedestrian having opposite directions, thus improving the overall efficiency of both flows. In particular the walking velocity increases by removing breaking and avoidance manoeuvres. Such self-organization happens without verbal communication. Moreover, the presence of obstacles, such as columns, favors the formation of lanes, with the side preference showing up more consistently.

Bottlenecks typically produce capacity drops in many type of flows including vehicular ones. If the density exceeds a given threshold, then the flow starts to decrease up to possibly reaching a stuck. Capacity dropping in pedestrian flows at bottlenecks, such as narrowing of aisles, was observed but not so neatly as in the case of vehicular traffic. There are at least three reasons which could explain this:

1. The difficulty in measuring pedestrian flows (we will go back to this in Sect. 3.4).
2. The capability of pedestrians to re-organize so as to mitigate the drop (see the zipper configuration below).
3. The discomfort of sharing space with other pedestrians, which prevents from creating too high densities in normal conditions.

These three reasons do not apply to the case of stampedes and panic situations. If people feel in danger in a given environment and consider the egress the only way to be safe, then they start to rush to exits creating cloggings. In this situation the flow is completely disorganized (somehow turbulent) and the capacity drop of exits is dramatic. In some extreme cases exits could be completely blocked with no pedestrian flowing through even if the area after the exit is completely empty. This situation occurs when pedestrian are trying to use the exit at the same time and the precise configuration could be explained only by a three dimensional model of pedestrian bodies. It is referred to also as a *slower-is-faster effect*, in the sense that a lowering of rush to the exit would indeed improve the functioning of the exit itself. Moreover, in these circumstances, pedestrians may fall to the floor, thus completely changing the scenario and, unfortunately, often giving rise to casualties. On the other side, two dimensional models and data report the formation of *arches*: Semi-circular shapes before the exit.

Going back to normal conditions, it was observed that bottleneck capacity depends on the specific geometry. The problem of optimizing the shape of a given bottleneck site is highly nontrivial, since complete quantitative models for the interactions pedestrian-environment do not take into account all cognitive and re-organization phenomena. However, some researchers suggested funnel-shaped aisles as a way to improve the capacity.

It is often agreed that obstacles on the way to exit and near doors can be of help in easing the flow. This is sometimes referred to as the *Braess' paradox*, for the similarities with the paradox observed in vehicular traffic. (The latter consists in the fact that adding links to networks, the overall equilibrium traffic flow may lower; So, formulated inversely, removing space can improve the flow.) In particular, columns serve this purpose well and the precise consequences depend on the specific positions with respect to exits. The effect is similar to wave breakers with crowd pressure somehow absorbed by the obstacle. Obviously, the obstacles are functioning as long as they do not create a major obstruction to the natural flow.

Another way of improving the flow through bottlenecks occurs naturally because of the ability of pedestrians to use space in a *zipper* like fashion. Representing the area occupied by a pedestrian as an ellipse, the obtained configuration has the same shape of a zipper with pedestrian areas representing teeth, see Fig. 3.1. More precisely, two lanes are formed with pedestrians walking diagonally behind each other. Geometrically this allows a better use of space. This is opposed to the situation of large sites, where pedestrians tend to maximize the distance from walls. The ability of pedestrians to quickly self-organize in these shapes affects the capacity of the bottleneck and so the possible delays. Moreover, the flow happens to be proportional to the bottleneck width, starting from the minimal size for allowing the

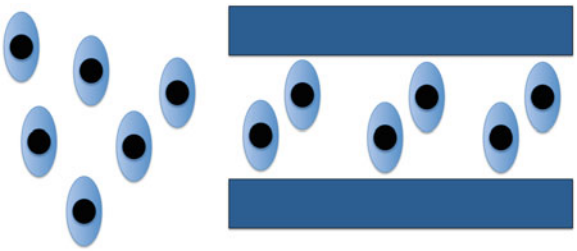

**Fig. 3.1** A graphical representation of the zipper effect

zipper effect and consistently for different kinds of bottleneck and entering flow. An anticipation effect was also observed, i.e. in the vicinity of the bottleneck, but before it, pedestrians tend to dispose themselves so as to occupy only a space equivalent to the dimension of the bottleneck, with the crowd spreading out upstream. While some researchers argued that appropriate geometries could then avoid or reduce capacity drops, others showed that the zipper effect is so strong that the exact geometry of the bottleneck has only a minor influence on the flow. Extrapolating from these studies, different relations among the flow and the crowd density were proposed, but a general agreement on a precise formulation is still lacking.

## 3.3 Models for the Single Pedestrian

Here we review some possible approaches in modeling the single pedestrian. In most of works proposing advanced modeling of crowd dynamics, the motion of the single pedestrian is simply reduced to determining a *desired velocity* and prescribing a dynamics with velocity relaxing to the preferred one. On the other side, in psychological literature and some of the mathematics, physics, and engineering ones, models are available for the strategy of the single pedestrian, relying on a number of objective functions.

### *3.3.1 The 2/3 Power Law and Other Empirical Laws*

Some researchers, mainly in the fields of cognitive sciences and psychology, noticed that various human movements tend to verify the so called $2/3$ (two third) power law. More precisely, various measurements confirmed that velocity is proportional to curvature to the power $2/3$. This gives rise to specific geometric properties of the trajectories followed by these movements or, better to say, to the speed at which humans perform some given geometric curves.

A number of papers were devoted to the kinematic of handwriting. The power law being verified by simple and complicate curves, such as letters and pictures, performed by people when writing and drawing. Some researchers found that the

same power law is respected, at least to some extent, also by the movements of pedestrians.

One has to notice that the $2/3$ power law seems to be ubiquitous in human movements or at least to be a good predictor in many experimental conditions. However, measurements are not always so precise and the risk of a false myth is not negligible. In particular, a few experiments have shown that the law does not apply to all graphic movements. The law was indeed mainly verified for elliptic movements, while for complex movements segmentation is necessary. The latter introduce some arbitrariness in the way quantities are measured. Some researchers proposed specific conditions under which the law would be satisfied.

The cognitive origin of the $2/3$ power law is not known. Some researchers argued that it is of mechanistic origin, other proposed it as a decision taken at the level of central nervous systems. There are some evidence for the first argument.

### *3.3.2 Models of Path Choice*

There are a wide number of models that were proposed for the choice of paths made by pedestrian, mainly when walking in structured environment but free of other pedestrians or moving obstacles. Here we will not discuss more quantitative models, on the contrary we report on more qualitative approaches.

It is interesting to notice that a large number of criteria were proposed as possible explanation of some path choice. Among others, we mention the following (clustered by choice criteria):

- Optimization criteria: Shortest path, least time, shortest leg first, longest leg first, straighter leg first.
- Sensational criteria: Most scenic, most aesthetic, clearest.
- Comfort criteria: Fewest turn, minimal angular deviation, most comfortable.
- Knowledge criteria: Most known, first noticed, different from previously taken.

See Fig. 3.2 for a pictorial illustration of some of them.

It is interesting to notice that some of these criteria are often in contrast and some are effectively one the opposite of the other. Thus it is difficult to obtain a clear picture of the most used or valid criteria, however, the set of criteria can be considered in an organized modeling effort. One has to notice that in every day walking there are a number of additional criteria one may indeed consider, such as visibility, chance of accidents, patrol by authorities, safety in general and other. For instance it was shown that criteria such as longest leg first or minimal angular deviation depends on the visibility of the final goal. This renders even more complicated a clarification of the main guiding causes for path choice.

The problem of choosing a path with multiple destinations was also addressed in a number of papers. Regarding these studies, researchers noticed that closed paths (with final destination equal to initial point) tended to be of circular type, that is corresponding to the boundary of the convex hull of the given multiple destinations

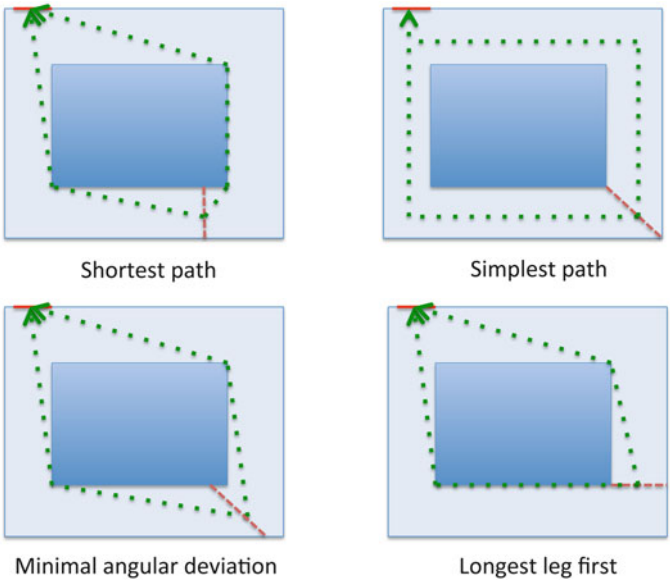


**Fig. 3.2** Some criteria by which single pedestrians choose their path

as points on the plane. On the other side, more local strategy as choosing the nearest neighbors failed to explain results. Most experiments were run by showing a map to individuals, thus may be affected by the experimental setting, see also Sect. 3.4.

Some researchers pushed these criteria to a more quantitative level. For instance, critical decisions are obviously taken at junctions and crossing, thus can be measured more precisely. A strong correlation was noticed among these decisions and angles of incidence of roads at junctions. In particular, individuals tend to keep the linearity of their path or, as listed above, to minimize the angular deviations. The discussion reported in a number of studies does not give rise to certain conclusions, but rather expresses the difficulty of a simple model to take into account the complex process of decision making operated by pedestrians.

## 3.4 Experimental Settings and Measurements

The knowledge about pedestrian walking is achieved by experiments. Because of the cognitive aspect of the decision making processes during walking, it is of paramount importance to take into account the experimental setting and to critically analyze experimental results. In particular *the presence of psychological bias may affect strongly the observed results*. It is also known that cultural influences and the composition of pedestrian crowds in terms of age, gender, and trip purpose can significantly influence pedestrian behavior.

Despite this evidence, a large majority of experimental studies are performed in settings where the biases can be very important if not dramatic. Some researchers reach the conclusion that values of fundamental variables, measured in laboratory experiments, simply cannot be used for design recommendation, so even less for management. On the other side, some qualitative results of experiments can be used to increase the general understanding of crowd dynamics, when a large number of pedestrians gives rise to complex phenomena.

## *3.4.1 Experimental Setting*

The most used experimental settings are the following:

- Interviews.
- Virtual reality.
- Artificial environments.
- Natural environments.

In the following we briefly discuss the different experimental settings.

### 3.4.1.1 Interviews

Some aspects of the pedestrian behavior in route navigation and the formation of cognitive maps can be obtained by interviews. Generally speaking, individuals will be exposed to a real environment or a picture/map and will be asked about choices they would perform in that environment. Since it is quite well agreed that the process of walking and also cognitive map construction happen at unconscious level, there are serious limitation of this tool. Other care should be taken when presenting a map to individuals, because of the significant differences among geographical and cognitive maps, see Sect. 3.2.1.

### 3.4.1.2 Virtual Reality

Virtual reality is extensively used, especially in psychological and cognitive science literature. The main reasons are the convenience of the experimental setting and the low cost.

Virtual reality allows to test many different landscapes and environments via graphical software. This allows to test many different hypotheses with a considerably simple modification of the experiments. We will not enter the difficult discussion of the differences between the perceptions of artificial and real environments, but a number of results confirm the validity of this approach, at least for some specific hypothesis testing. Still psychological bias is a serious risk.

In this direction, specialized websites, such as *experimental or mechanical turks*, provide new extensive tools for performing experiments in virtual setting. Researchers however usually need to somehow filter the information.

#### 3.4.1.3 Artificial Environments

Real environments may present major difficulties for running large size experiments, with many pedestrians involved, or for using advanced tech instruments. In particular, it is hard to find suitable places allowing one to observe both dense and undisturbed pedestrian flows, while, on the other side, cameras, antennas, sensors and other devices may not be easily placed outdoor. These are the main reason why many researchers resort to artificial environments. Usually lab space equipped with cameras and other devices and with features resembling real structured environments.

To reduce the psychological bias, researchers do not communicate to the subjects the experiment purpose and the expected results. Often participants are given time to familiarize with experimental setup, so as to reproduce as closely as possible the every day conditions. Moreover, sometimes pedestrians are divided into groups with different instructions on routes and goals so as to mimic a real life situation.

In large crowd experiments some care is also taken on the composition of the crowd in terms of age and gender. In particular researchers try to have population groups which would be statistically similar to those of the residents.

Some experiments even tried to reproduce panic situation, when pedestrians are urged to exit and break the normal interaction rules.

Also in this case some major psychological bias are unavoidable. For instance, in artificial environment doors may be replaced by frames and aisles by moving barriers, providing a completely artificial perception experience and surely affecting cognitive maps.

In some cases pedestrians are provided with distinction signs such as numbers, tags, coloured hats or other. In other cases pedestrians are equipped with various technological devices, which can range from small detectors to complicated equipments.

In experiments involving a large number of pedestrians, groups are formed and a group leader is chosen. The role of the leader is to guide the group through the experiment following precise instructions provided by researchers. In particular the leader also takes care of the timing of group movements. Clearly, this departs strongly from every day life conditions.

On the same line, one has to notice that large experiments are typically performed once or in a very limited time range. This probably causes a sensitive limitation in the variability of crowd behavior.

#### 3.4.1.4 Natural Environments

There is a limited number of studies using surveillance cameras placed in transportation sites or other surveilled areas (opposed to cameras placed in lab experiments as for artificial environments). In this case the behavior of pedestrians is directly observed in natural environment, thus overcoming the main difficulties of possible psychological bias.

The setting brings obvious advantages in testing specific hypotheses and in measuring pedestrian behavior. Measurements can be performed in a similar way as for artificial environment if, in that setting, no devices were applied to participants bodies.

With the increasing number of surveillance cameras available, we expect this to become an increasingly important instrument for experiments.

### *3.4.2 Measurements*

Beside the experimental setting, researchers need to design or use tools for measuring quantities which are relevant to describe pedestrian motions. The first task is to decide which quantities must and can be measured. These are strictly related to the final purpose of experiments, thus can be focused on macroscopic quantities, such as flow of a crowd in motion, microscopic quantities, such as discrete choice of pedestrians at junctions, or even nanoscopic quantities, such as posture of the pedestrian.

On the other side, among the most used measurement tools we mention the following:

- Pictures: manual counting or image analysis.
- Videos cameras: Manual measurements and image analysis.
- GPS sensors.
- Accelerometers.
- Infrared sensors.
- Bluetooth antennas.

We now briefly discuss the different tools and measurements. From pictures researchers can measure the position of pedestrian at a given time instant or can identify trails of pedestrians (such as on snow or on grass field). Images can be used either to count manually, for instance the number of pedestrians in a given area, or to process the image via ad hoc software. Sometimes pictures are collected in series to provide a view of a whole trajectory of a given pedestrian. The images are often processed manually, thus rendering the approach very labor-intensive.

Similarly videos are used both to directly observe and measure a phenomenon or to be processed via image analysis. A number of different approaches may be used in the latter case. For instance, researchers designed elaboration composed of various steps, including advanced mathematical techniques such as Kalman filter and others. In order to facilitate the analysis, often participants are wearing specific clothes (colored hats) or objects over clothes (such as ping-pong balls). This allows the tracking of whole trajectories, thus giving a dynamic information. Such trajectories can be determined at a very high level of precision, often at a resolution of centimeters and fraction of seconds. In turn this provides a number of measurable quantities, such as velocity, acceleration, curvature of the trajectory, . . .

GPS sensors and other "probes" can be used to determine position and velocity of pedestrians equipped with such devices. The technique is useful also to infer the properties of a whole crowd from sampling a limited number of individuals.

Accelerometers (sometimes included in mobile phone devices) provide information at the nanoscale, producing a signal related to the body movements of a single pedestrian. Then appropriate signal analysis techniques must be applied, sometimes combined with machine learning in order to determine the characteristics of gait and thus infer other information. Here the literature includes medical studies related to both the physiological aspect of walking and the need of measuring energy consumption.

New types of sensors are nowadays used to replace manual counting, such as infrared sensors, measuring the heat energy of infrared radiation naturally emitted by pedestrians, and Bluetooth antennas to detect wireless communicating devices, many of which are becoming ubiquitous (e.g., smart phones).

### *3.4.3 Comparison of Different Experimental Settings*

As already pointed out, researchers are aware of the differences which are expected to arise naturally between artificial and virtual environments on one side and the natural one on the other side. This issue seriously limits the reliability of precise measures, still leaving some validity for the observation of some aggregate phenomena. To further illustrate this problem, we report some results of direct observations and use of surveillance cameras from a project performed on the Camden Campus of Rutgers – The State University of New Jersey.

Thousands of students walk on the Campus area of Rutgers – Camden every day. The area is equipped with surveillance cameras and the public is informed by signs. However, students, faculty and staff walk on the Campus area every day during the academic year, thus they are not expected to pay much attention to the cameras (which are placed in elevated spots) or to exhibit unusual behavior because of that.

A site was identified with a path presenting a turn with an angle of approximately 135° and surrounded by grass, see Fig. 3.3. Pedestrians walking in the path were observed to *cut* naturally the angle, thus finding themselves on the left part of the

**Fig. 3.3** Experimental setting in campus area of Rutgers-Camden (©Benedetto Piccoli)

trail. This is consistent with various theories, including the $2/3$ power law and the minimal angular deviation. On the other side, keeping the left is in contrast with the supposed right-hand preference in United States, thus the experiments intended to determine which effect was the dominant one.

To have simple measurements, an obstacle (high orange cone) was placed just after the corner at a distance of 406 cm (corresponding to two pavement tiles) in the center of the path. Thus pedestrians were forced to choose to pass to the left or the right of the obstacle. The interpretation is that passing to the left would be compatible with various path choice models, while passing to the right with the social agreement on keeping the right.

The experiment was performed in three settings:

- Setting A. Pedestrians were observed while walking on the path, not interacting with any other pedestrian and not carrying heavy objects. They were not aware of being observed.
- Setting B. Pedestrians were informed that they were going to be observed while walking but not informed about which measurements were going to be taken.
- Setting C. Pedestrians walking on the path were stopped and interviewed about the choice they would have made with respect to passing the obstacle.

All the other conditions of the experiments were identical and for each setting more than 200 persons were involved in the experiment. The results were the following:

- Setting A. 27 % of pedestrians walked to the right of the obstacle.
- Setting B. 52 % of pedestrians walked to the right of the obstacle.
- Setting C. 62 % of pedestrians walked to the right of the obstacle.

The results show *the strong influence of the experimental setting* and the importance of the psychological bias, well beyond possible random fluctuations. Moreover, it was confirmed by other measurements in similar settings.

## 3.5 Bibliographical Notes

Section 3.1 As mentioned, a complete account of the various literatures is beyond the scope of this monograph, the same holding true also for this bibliographical notes. We can distinguish among two broad categories, the more *quantitative* (e.g., by engineers, physicists, biologists, some of the psychologists, etc.) and the more *qualitative* (e.g., by sociologists, architects, and some of the psychologists). A quite extensive account of the contributions from physicists and the early ones from transportation engineers can be found in Daamen and Hoogendoorn [53], Helbing et al. [84], Papadimitriou et al. [137]. The early work in transportation engineering are probably among the first in the quantitative category, see Fruin [72], Hankin and Wright [79], Navin and Wheeler [129]. In particular, Fruin [72] is among the first discussing a concept of *level of service*, thus asking for advanced design of pedestrian facilities. For other papers we refer the reader to the list of references in Daamen and Hoogendoorn [53], Helbing et al. [84], Papadimitriou et al. [137]. On the more qualitative side, we may cite few works by sociologists and psychologists, as Dabbs jr. and Stokes III [54], Goffman [74], Golson and Dabbs [76], Wolff [172].

Section 3.2.1 The discussion of cognitive maps was mainly inspired by Golledge [75], Ishikawa and Montello [104], Lloyd and Heivly [119], Montello [125]. For a discussion on the use of geographical maps see Levine et al. [116, 117]. For experiments with GPS see Ishikawa et al. [103].

Section 3.2.2 Information about geographical and social issues can be found in Daamen and Hoogendoorn [53], Helbing et al. [84] and references therein. The distortion of maps related to geographical position of homes was pointed out in Lloyd and Heivly [119]. Discussion about sociological issues can be found in Dabbs jr. and Stokes III [54], Goffman [74].

Section 3.2.3 The phenomenon of self-organization is well explained and reported in Helbing et al. [84]. Specific issues about bottlenecks and re-organization can be found in Cepolina and Tyler [34], Daamen and Hoogendoorn [53], Schadschneider and Seyfried [156], Seyfried et al. [157]. See also Sect. 1.1.2 of this book.

Section 3.3.1 For general discussion about $2/3$ power law we refer to Viviani and Flash [168], while for pedestrian locomotion to Vieilledent et al. [165]. See also Plamondon and Guerfali [146] and Schaal and Sternard [155] for a discussion about the origin of such a law and additional critical analysis.

Section 3.3.2 An extensive discussion of path choice can be found in Golledge [75], while a specific discussion about angular deviations can be found in Dalton [56]. For multiple destinations see also Vickers et al. [163].

Section 3.4 Most of the above references are about experiments performed in different settings. For artificial environment see in particular Daamen and Hoogendoorn [53], Helbing et al. [84]. The importance of introducing cognitive aspects in quantitative modeling was also pointed out recently in Moussaïd

et al. [127]. One of the few studies using surveillance cameras is Cepolina and Tyler [34].

Section 3.4.2 Video elaboration techniques are explained in Hoogendoorn et al. [99], Willis et al. [171]. For the use of probes see Kamareddine and Hughes [108], Koshak and Fouda [111]. Accelerometers were used to determine gaits for instance in Ailisto et al. [2], Aminian et al. [7] and to infer crowd dynamics in Roggen et al. [152]. For infrared sensors see Ozbay et al. [136], while for Bluetooth see O'Neill et al. [135].

# Part II
# Modeling and Mathematical Problems

# Chapter 4
# An Overview of the Modeling of Crowd Dynamics

**Abstract** In this chapter we review some of the most important models at microscopic, macroscopic, and mesoscopic scale, which, in our opinion, represent milestones in their respective fields or are of particular interest for this book. We also report some models for rational pedestrians, which make use of techniques from optimal control theory. For the sake of convenience, we present all models in two space dimensions.

## 4.1 Microscopic Models

The description of the pedestrian dynamics at the microscopic scale is based on the assumption that every single person can be tracked individually, and her trajectory can be forecast. Microscopic models can be *differential*, if they are based on ordinary differential equations, or *nondifferential*, otherwise.

### *4.1.1 Force Models*

Force models are second order differential models. In general, a two-dimensional force model for $N$ pedestrians is constituted by a system of $4N$ scalar ordinary differential equations. The $k$-th pedestrian is described by means of her time-dependent position $X^k(t) \in \mathbb{R}^2$ and velocity $V^k(t) \in \mathbb{R}^2$. The model has a structure analogous to that of Newtonian dynamics, i.e.,

$$\begin{cases} \dot{X}^k(t) = V^k(t) \\ \dot{V}^k(t) = F^k(t,\, X^1,\, \ldots,\, X^N,\, V^1,\, \ldots,\, V^N), \end{cases} \qquad k = 1,\, \ldots,\, N. \tag{4.1}$$

The equation above is complemented with suitable initial conditions for the positions $X^k(0)$ and velocities $V^k(0)$, for $k = 1,\, \ldots,\, N$.

E. Cristiani et al., *Multiscale Modeling of Pedestrian Dynamics*, MS&A 12,
DOI 10.1007/978-3-319-06620-2_4,

Force models are based on the assumption that acceleration and deceleration of pedestrians are the reaction to the perceived information that they obtain about the environment. Although the environment does not really exert any force on pedestrians, they are motivated to act in a certain way by the environment, so that one can say that pedestrians actually act *as if* they were subject to external forces.

Force models are characterized by different choices of $F^k$. Some models assume pedestrians to be volumeless points, while other assume, more realistically, that pedestrians occupy a finite volume. In the former case, some issues can arise. For example, implementations of the repulsive force between pedestrians require additional elements to guarantee realistic behavior, especially in high density situations, since strong overlapping of pedestrians or backward/high velocities occur as artifacts of the force-based description.

An important assumption of force models is that the total force exerted on the pedestrian is simply given by the *sum* of all forces, as in classical mechanics. This assumption often leads to undesired effects. For example, in some situations pedestrians perform repetitive backwards and forwards movement due to e.g. high repulsive forces. In real situations pedestrians either stop, when they evaluate the situation as blocked, or change direction.

Finally, we mention that these models contain many free parameters that must be adequately calibrated to achieve a good quantitative description.

#### 4.1.1.1 Magnetic Force Model

The magnetic force model assumes that pedestrians behave as magnets or electrically charged particles. Any kind of attractive/repulsive point, including pedestrians themselves, generate a field in the surrounding space. Then, pedestrians simply move in the space following the Coulomb's law

$$F^k(t) = \sum_P C q^k q^P \frac{X^k(t) - X^P(t)}{\left|X^k(t) - X^P(t)\right|^3}, \tag{4.2}$$

where $C$ is a constant, $q^k$ is the "charge" of pedestrian $k$, and $P$ is the interacting point located at $X^P$ with "charge" $q^P$. Each pedestrian is a positive point source ($q > 0$) so that they are repulsed from each other. Columns and obstacles in general are positive point source as well. Instead, targets are negative point sources. Walls are modeled as a number of positive point sources on a straight line at regular intervals. A magnetic dipole is used to conduct pedestrians through a gate.

If pedestrians are not assumed to be volumeless, overlapping can occur. To introduce collision avoidance features, the model considers a *body zone*, which is a space that cannot be occupied by anything else than the pedestrian herself. The model considers also a *judge zone*, which is the zone in which the influence of other pedestrians is taken into account (cf. the definition of sensory region given in Sect. 1.1.1). Both body and judge zone are circular, the former being centered

at the individual, while the latter being shifted ahead in the direction of motion. At each time step, the positions of pedestrians are updated according to the motion equation (4.1)–(4.2), then, if an overlap occurred, the position is corrected as the nearest admissible position. This is done for both pedestrian-pedestrian and pedestrian-structure interactions.

The magnetic force model is able to reproduce quite well the group behavior (crossing flow of two or more pedestrians with or without columns, crossing at intersections, passage through a bottleneck, etc.). It is also able to catch self-organizing lane formation in crossing groups of pedestrians.

#### 4.1.1.2 Social Force Model

In the social force model the total force exerted on a pedestrian is

$$F^k = F_{\mathrm{d}}^k + \sum_{h \neq k} F_{\mathrm{r}}^{kh} + \sum_{A} F_{\mathrm{a}}^{kA} + \sum_{Q} F_{\mathrm{r}}^{kQ} + \xi^k, \tag{4.3}$$

where the terms in the above equation are defined and discussed in the following.

Each pedestrian has a *desired direction* of motion $v_{\mathrm{d}}^k$. This velocity depends on the geometry of the domain and takes into account the desired final destination. The presence of fixed obstacles can be also taken into account. The trajectory of a single undisturbed pedestrian is simply given by the solution of $\dot{X}^k(t) = v_{\mathrm{d}}^k(X^k)$. A deviation of the actual velocity from the desired velocity due to whatever cause leads to a tendency to restore the desired velocity with a certain relaxation time $\tau$. This gives an acceleration term of the form

$$F_{\mathrm{d}}^k(X^k, V^k) = \frac{v_{\mathrm{d}}^k(X^k) - V^k}{\tau}.$$

The motion of pedestrians is influenced by other pedestrians. In particular, they try to keep a certain distance from each other, since they feel increasingly uncomfortable the closer they get to a strange person, and, in any case, they try to avoid collisions. This results in a *repulsive force* $F_{\mathrm{r}}^{kh}$ which is a monotonic decreasing function of the distance of two pedestrians $k$ and $h$. This function can also depend on the velocities $V^k(t)$ and $V^h(t)$ and can take into account the fact that pedestrians require more space in the direction of motion. A simple choice is given by an exponential decay of the repulsive force,

$$F_{\mathrm{r}}^{kh}(|X^k - X^h|) = -C_1 \exp -\frac{|X^k - X^h|}{C_2} \tag{4.4}$$

where $C_1$, $C_2$ are two parameters of the model. The presence of a sensory region $\mathscr{S}(X^k(t))$ (see Sect. 1.1.1) can be included modifying the above definition. In particular, a dependence on the mutual position of the $k$-th and the $h$-th pedestrian

can be introduced, in order to take into account whether pedestrian $h$ is seen by pedestrian $k$.

Pedestrians are sometimes attracted to other pedestrians (friends, tourist guide, etc.) or objects. If $A$ is a point of interest located at $X^A$ (it can coincide with a pedestrian's position), one can define the *attractive force* $F_{\mathrm{a}}^{kA}$ as a monotonic increasing function of the distance $|X^k - X^A|$. Again, it can be weighted taking into account the sensory region.

Pedestrians avoid *obstacles* (walls, columns, etc.). If $Q$ is an obstacle, an ad hoc repulsive force $F_{\mathrm{r}}^{kQ}$ can be introduced. It can be exponentially decreasing with respect to the distance between the pedestrian and the nearest point $X^Q$ of the obstacle.

Finally, individual *random fluctuation* reflecting unsystematic behavioral variations are modeled by adding a random variable $\xi^k$.

Panic conditions can be also modeled by adding proper social forces, and assuming that pedestrians have a finite volume. In such a case, physical interaction forces come into play when pedestrians get so close to each other that they have physical contact. One can add a *body force* counteracting body compression and a *sliding friction force* preventing relative tangential motion.

The social force model describes quite realistically some observed phenomena. It allows one to reproduce various spatio-temporal patterns that are not externally prescribed by, e.g., traffic signs, laws, or behavioral conventions. Instead, patterns emerge due to the nonlinear interactions of pedestrians and are often caused by a spontaneous break of symmetry. Among the self-organized patters which can be reproduced, we mention the *lane formation*, the *oscillations at bottlenecks* (or traffic light effect) and *arching* behind an exit door. In panic conditions, simulations also show some paradoxical but realistic effects like the *freezing-by-heating* effect (people continuously and irrationally change direction finally keeping their position practically unchanged) and the *faster-is-slower* effect (cf. the Braess' paradox).

#### 4.1.1.3 Centrifugal Force Model

The centrifugal force model differs from the social force model mainly in the definition of the repulsive force (4.4). In order to introduce the new repulsive force, let us define

$$e^{kh} = \frac{X^h - X^k}{\left|X^h - X^k\right|}$$

and $a^+ = \frac{1}{2}(a + |a|)$, for every $a \in \mathbb{R}$. Then, we have

$$F_{\mathrm{r}}^{kh} = -m^k \frac{(V^k \cdot e^{kh})^+}{\left|V^k\right|}[((V^k - V^h) \cdot e^{kh})^+]^2 \frac{1}{\left|X^h - X^k\right|} e^{kh}$$

where $m^k$ is the mass of the $k$-th pedestrian. The term

$$(V^k \cdot e^{kh})^+$$

plays the role of the visual field, vanishing the effects of any pedestrian behind the considered one, while the term

$$((V^k - V^h) \cdot e^{kh})^+$$

is introduced to translate the fact that if pedestrian $h$ walks faster than pedestrian $k$, there are no repulsive effects, even if pedestrian $h$ is ahead of and visible by pedestrian $k$. Finally, the exponential term in (4.4) is substituted by

$$\frac{1}{\left|X^h - X^k\right|}.$$

Centrifugal force model assumes that pedestrians are not just points, rather they occupy a certain volume. Then, a *collision avoidance* technique is employed in addition to the basic model to deal with the problem of overlapping pedestrians. The technique is rather simple and can be described as follows: First, it is assumed that collision has not occurred and the pedestrian's position is updated. Then, it is detected whether a collision has occurred. If this is the case, the pedestrian is moved back to the original position and then, among the admissible velocities, the velocity closest to the original one is found. If there is no way to move forward and a step back would be required, the pedestrian just stops.

### *4.1.2 Maury and Venel's Model*

The Maury and Venel's model is a collision avoidance first order differential model described by $2N$ scalar ordinary differential equations

$$\dot{X}^k(t) = V^k(t, X^1, \ldots, X^N), \qquad k = 1, \ldots, N. \tag{4.5}$$

Here $X^k(t)$ is the position of the $k$-th pedestrian at time $t$. In this case the velocity of pedestrians is assigned directly, without referring to their acceleration. The model assumes pedestrians to be circular-shaped, and proposes a method to avoid contacts among them, i.e., pedestrians are imposed to never collide. For simplicity, assume that it is given a pedestrian-independent desired velocity field $v_\mathrm{d}$. Then, each pedestrian moves with a velocity $V^k$ which corresponds to the projection of $v_\mathrm{d}(X^k)$ on a space of admissible velocities. This space takes into account the fact that the pedestrians cannot collide with each other.

Let us define the vectors

$$X := (X^1, \ldots, X^N), \quad \text{and} \quad V_\mathrm{d}(X) := (v_\mathrm{d}(X^1), \ldots, v_\mathrm{d}(X^N)).$$

Moreover, let us denote by $r^1, \ldots, r^N$ the radii of the $N$ pedestrians and define the distance between two agents as

$$d^{kh}(X) := |X^k - X^h| - r^k - r^h.$$

The model imposes that the vector $X(t)$ satisfies the constraint

$$X(t) \in Q_0 := \{Y \in \mathbb{R}^{2N} \ : \ d^{kh}(Y) \geq 0, \quad \forall\, k, h, \quad k \neq h\}, \quad \forall\, t > 0.$$

Let us define the cone of admissible velocities as

$$C(X) := \left\{ W \in \mathbb{R}^{2N} \ : \ d^{kh}(X) = 0 \quad \Rightarrow \right.$$
$$\left. W^k \cdot \frac{X^k - X^h}{\left|X^k - X^h\right|} + W^h \cdot \frac{X^h - X^k}{\left|X^k - X^h\right|} \geq 0, \quad \forall\, k < h \right\}.$$

Note that the set $C(X)$ is defined in a such a way that whenever two pedestrians $k$ and $h$ touch each other, their actual (admissible) velocities will make their mutual distance $d^{kh}$ immediately increase, thus avoiding hard collision. The dynamics of all pedestrians are then given by

$$\dot{X}(t) = P_{C(X)}(V_{\mathrm{d}}(X)) \qquad k = 1, \ldots, N$$

where $P_{C(X)}$ is the projection operator on the set $C(X)$.

A macroscopic version of this model was also proposed, see Sect. 4.2.4.

### *4.1.3 Cellular Automata Models*

Cellular Automata (CA) models are time- and space-discrete microscopic models which do not rely on differential equations. The domain of computation is discretized by means of a mesh. Each cell $C$ of the mesh is associated to a certain status, usually *on* or *off*, that changes at each time step according to the status of the neighboring cells. CA models for pedestrian flow usually assume that each cell can be either empty (off) or occupied by a single pedestrian (on).

The attractiveness of using CA models is that the interactions of the entities are based on intuitively understandable behavioral rules which are more easily translated in algorithms than in mathematical functions. As a consequence, rules can be given "by words" and can be understood by people with no mathematical background. They are easily implemented on computers, and compared to differential models, run very fast. This last property allows one to run large-scale simulations otherwise intractable. As a drawback, we mention that these models are often very

simple and do not allow a theoretical a priori analysis of their properties. Indeed, it is difficult going further than a purely algorithmic level of the discussion.

Each CA model is characterized by its *matrix of preferences*. Assume for simplicity that each pedestrian is allowed to move one cell away only. In this case, one can associate to each cell $C$ a $3 \times 3$ matrix $M_C$, whose entries represent the probabilities to move in one of the eight neighboring cells or not to move at all. The matrix $M_C$ can be used to model the desired direction of motion, can be both time- and cell-dependent, and, if distinguishing more than one pedestrian group is needed, it can be also group-dependent.

Collisions are avoided in a natural way, preventing two pedestrians to move in the same cell at the same time. In particular, if the target cell is occupied, the pedestrian does not move. If it is not occupied and no other pedestrian targets the same cell, the move is executed. If more than one pedestrian share the same target cell, only one is chosen according to the relative probabilities with which each pedestrian chose their target. The winner moves while its rivals for the same target keep their position.

A CA model is hardly able to reproduce collective phenomena and let self-organization arise. This is due to the fact that interactions are basically local (short-range). On the other hand, allowing pedestrians to move many cells away in one time step makes the model (and the code) much more complicated, since many cases have to be managed.

An interesting concept which helps CA model reproduce complex behavior is that of *floor field*. It can be used to define a desired velocity field or, more interesting, long-range interactions. In the last case, the interplay between CA and floor field gives rise to a hybrid model which may have some flavors of a multiscale approach. Let us assume that the floor field is a *scalar* field $\Phi(t, x)$ defined at every point $x$ of the domain at any time $t > 0$. The function $\Phi$ affects the transition probabilities, i.e., for every cell $C$, the nine values of $M_C$ depend on the value $\Phi(t, x_C)$, where $x_C$ is the center of the cell $C$. The function $\Phi$ has its own dynamics, which can be dependent on or independent from the status of the cells. To fix the ideas, let us consider the case in which $\Phi$ is used to model long-range attraction among pedestrians. Here, any pedestrian leaves a "trace" on the ground that can be perceived by the others. The intensity of the trace at cell $C$ and time $t$ is given by $\Phi(t, x_C)$. The function $\Phi$ has a double evolution equation: The first one is continuous and macroscopic, for example a standard diffusion-decay equation

$$\frac{\partial \Phi}{\partial t} = D \triangle \Phi - \delta \Phi,$$

where $D$ and $\delta$ are the diffusion and the decay coefficient, respectively. This evolution let the trace spread around and decay in time. The second is instead discrete-in-time and agent-based. It can be defined by

$$\Phi(t + \Delta t, x) = \Phi(t, x) + G(x, \Phi(t, x)), \quad \forall\, x \in C, \ \forall\, C,$$

where $\Delta t$ is the CA time step and the function $G$ is positive if $x$ belongs to an occupied cell and vanishes if $x$ belongs to an empty cell. In practice, the second

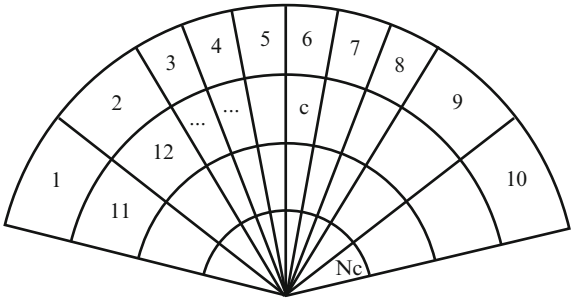


**Fig. 4.1** Discrete choice models: possible choices of a pedestrian and corresponding probabilities to make those choices

equation models a discrete-time source for the first equation. This evolution lets the single pedestrians leave the trace on the ground while moving. Finally, the transition probabilities are increased where $\Phi$ is large, so that pedestrians tend to follow the traces left by the others.

### *4.1.4 Discrete Choice Models*

Discrete choice models join the simplicity of cellular automata models with a continuous-in-space representation of pedestrians. They are suitable to model short-range interactions only, although a desired direction toward a target can be imposed as a datum of the problem. Initially, pedestrians are located at generic positions $\{X^k(0)\}_k$, $k = 1, \ldots, N$. Then, at any time iteration, the space around each pedestrian is divided in $N_c > 0$ small cells (or *choices*). Each center of the cells corresponds to a location that pedestrian can reach in the next iteration. Each cell $c = 1, \ldots, N_c$ is associated to the probability $p_c \in [0, 1]$ to make that choice, see Fig. 4.1. More precisely, at each iteration the probabilities $p_c$ are computed on the basis of pedestrian's preferences, some of them are listed in the following:

1. Avoid obstacles (obstacles make some cells unavailable, i.e., $p_c = 0$).
2. Avoid crowded cells.
3. Propensity to maintain the current direction of motion.
4. Propensity to reach a given destination.
5. Propensity to follow some pedestrians identified as leaders.

## 4.2 Macroscopic Models

The description of pedestrian dynamics at the macroscopic scale is based on the assumption that the number of agents is large enough to be described by locally averaged quantities, typically density $\rho$ and velocity $v$, regarded as dependent variables of time and space.

Let us stress that, in some cases, macroscopic models for pedestrian flow simply extend the one-dimensional approaches proposed for vehicular traffic. The main addition to the models of pedestrian dynamics is a *desired velocity* vector field $v_\mathrm{d} : \Omega \to \mathbb{R}^2$, where $\Omega$ is the domain the pedestrians are free to move in. The desired velocity is introduced to model the presence of a *target* (the exit or a meeting point) that people want to reach, and depends on the geometry of the domain. The desired velocity $v_\mathrm{d}$ is generally given as a datum and it is time-independent. It corresponds to the velocity that pedestrians would set to reach the target if they did not experience mutual interactions (this is the case, e.g., if only one pedestrian is present). In some more complicated control-based models, $v_\mathrm{d}$ is an additional unknown of the problem and it expresses a *strategy* to reach the target in an optimal manner, see Sect. 4.4.

*First order models* are usually constituted by one conservation law of the form

$$\frac{\partial \rho}{\partial t} + \nabla \cdot q(\rho) = 0, \quad t > 0, \quad x \in \Omega, \tag{4.6}$$

where $\rho$ represents the pedestrian density and $q(\rho)$ is their flux, which has to be given as a function of the density in order to close the model. Since the following definition holds true:

$$q(\rho) := \rho v(\rho),$$

where $v$ is the velocity field, one can alternatively prescribe $v(\rho)$. The equation basically states that the mass of pedestrians moves following the nonlinear velocity field $v(\rho)$ and is conserved in time. The equation is complemented by an initial condition $\rho(0, x) = \bar{\rho}(x)$ and, if $\Omega$ is bounded, by some boundary conditions at $\partial\Omega$ for any $t > 0$.

*Second order models* are usually constituted by a system of partial differential equations for $\rho$ and $v$ of the form

$$\begin{cases} \dfrac{\partial \rho}{\partial t} + \nabla \cdot (\rho v) = 0, & t > 0, \quad x \in \Omega \qquad \text{(4.7a)} \\[2ex] \dfrac{\partial v}{\partial t} + (v \cdot \nabla) v = a(\rho, v), & t > 0, \quad x \in \Omega \qquad \text{(4.7b)} \end{cases}$$

where, denoting by $(v^1, v^2)$ the two components of $v$ and by $(x^1, x^2)$ the two components of $x$, we have

$$(v \cdot \nabla) v = \left( v^1 \frac{\partial v^1}{\partial x^1} + v^2 \frac{\partial v^1}{\partial x^2},\ v^1 \frac{\partial v^2}{\partial x^1} + v^2 \frac{\partial v^2}{\partial x^2} \right).$$

The function $a$ in (4.7b) represents the *acceleration* of pedestrians and has to be given as a function of the two unknowns in order to close the system. Equation (4.7a)

models the conservation of the mass, while (4.7b) accounts for the conservation of the momentum. The system (4.7a)–(4.7b) is complemented by initial conditions $\rho(0,x) = \bar{\rho}(x)$, $v(0,x) = \bar{v}(x)$, and, if $\Omega$ is a bounded, by some boundary conditions at $\partial\Omega$ for any $t > 0$.

*Remark 4.1 (first vs. second order models).* Pedestrian behavior is only marginally determined by (pseudo-)mechanical cues, a more relevant role being played by decisional abilities. For this reason, an inertia-based framework does not appear to be the most natural setting. To support this claim, we consider, as an example, that in pedestrian motion impulsive effects are often present: A walker can suddenly decide to change her velocity to face environmental conditions, such as the presence of other walkers. Normally, she reaches in a very short time her final velocity, which then remains constant for a while, until new interactions occur. Nevertheless, there are some reasons to include acceleration in the models: First, acceleration has a direct effect on movement since people in a crowd can be pushed around. Second, acceleration is a perceptible input to the cognitive system and a major source of information in an information-starved situation. Third, and most important, acceleration carries the consequences of injuries among pedestrians and it can be directly considered as a measure of danger and overcompression.

Before listing some of the most important models available in literature, it is helpful introducing an important ingredient which often recurs in macroscopic models, namely the *fundamental diagram*.

### 4.2.1 Fundamental Diagram

Let us assume that the velocity has the form

$$v = sw \tag{4.8}$$

where $s$ (standing for *speed*) is a scalar function and $w$ is a vector field. For simplicity, one can assume that $s$ is the modulus of $v$ and $w$ is a unit vector giving the direction of motion.

The fundamental diagram expresses the relationship between the flux $q$ and the density $\rho$. This relationship was widely studied in one-dimensional traffic flow, where many experimental measurements were performed and many functions were proposed. In the pedestrian case, which is instead two-dimensional, it is simpler referring to the relationship between the speed $s$ and the density $\rho$.

Here we present some possible choices for the function $s = s(\rho)$ among the simplest ones, assuming that both the speed and the density are normalized, i.e., $s, \rho \in [0, 1]$, see Fig. 4.2. Note that many choices are directly derived from the vehicular traffic literature. It can be also assumed that $s$ depends on $\rho$ and $\nabla\rho$.

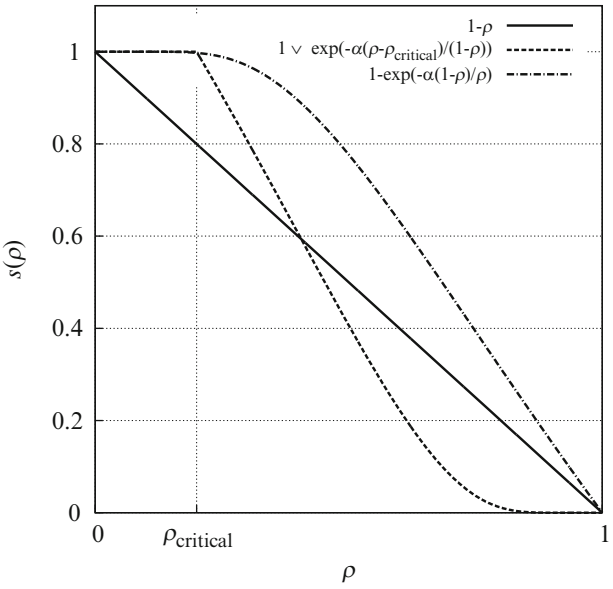


**Fig. 4.2** Graphs of some functions $s(\rho)$ representing possible speed diagrams for first order models

$$s(\rho) = 1 - \rho$$

$$s(\rho) = \begin{cases} 1, & 0 \le \rho \le \rho_{\text{critical}} \\ \exp\left(-\alpha \frac{\rho - \rho_{\text{critical}}}{1-\rho}\right), & \rho_{\text{critical}} < \rho \le 1 \end{cases}, \quad \alpha > 0, \quad \rho_{\text{critical}} \in (0,1)$$

$$s(\rho) = 1 - \exp\left(-\alpha \frac{1-\rho}{\rho}\right), \quad \alpha > 0$$

$$s(\rho, \nabla\rho) = 1 - \rho - \varepsilon \frac{1}{\rho} \frac{\partial \rho}{\partial w}, \quad \varepsilon > 0$$

where $\frac{\partial \rho}{\partial w}$ represents the directional derivative of $\rho$ with respect to the direction $w$.

### *4.2.2 Coscia and Canavesio's Model*

The Coscia and Canavesio's model is a first order model characterized by a particular choice of the flux $q$ in (4.6). It is assumed that

$$q = q(x, \rho, \nabla\rho) = \rho v(x, \rho, \nabla\rho), \quad \text{with} \quad v(x, \rho, \nabla\rho) = s(\rho, \nabla\rho) w(x, \nabla\rho),$$

where $s$ is a scalar function (corresponding to the fundamental diagram, see Sect. 4.2.1) and $w$ is a vector giving the direction of motion. Note that here $w$ is not in general a unit vector. Moreover, the actual density $\rho$ can be replaced with the *fictitious* or *perceived* density

$$\rho^*(\rho, \nabla\rho) := \rho\left(1 + \varepsilon(1-\rho)\frac{\partial\rho}{\partial w}\right),$$

where $\frac{\partial\rho}{\partial w}$ represents the directional derivative of $\rho$ with respect to the direction $w$. The choice of the fictitious density translates the fact that pedestrians actually perceive a density which is larger (resp., smaller) than the actual one if it is increasing (resp., decreasing) in their direction of motion.

The function $w(x, \nabla\rho)$, instead, is assumed to have the form

$$w(x, \nabla\rho) = v_{\mathrm{d}}(x) + C\, v_{\mathrm{i}}(\nabla\rho)$$

where $C$ is a parameter, $v_{\mathrm{d}}(x)$ (desired velocity) is simply a unit vector pointing towards the desired target, and $v_{\mathrm{i}}(\nabla\rho)$ (interaction velocity) is defined as the direction of the minimum directional derivative of $\rho$:

$$v_{\mathrm{i}}(\nabla\rho) = \arg\min_{\xi\in\mathscr{S}(x)}\left\{\frac{\partial\rho}{\partial\xi}\right\},$$

where $\mathscr{S}(x)$ is a suitable sensory region, see Sect. 1.1.1. This particular choice of $w$ models the fact that pedestrians try to reach their target, while, at the same time, try to escape crowded region.

### 4.2.3 Colombo and Rosini's Model

The Colombo and Rosini's model is a first order one-dimensional model conceived to catch some special features of the pedestrian behavior in panic conditions. If, on the one hand, a one-dimensional model cannot be realistic for modeling pedestrian flow, on the other hand it can shade light on some interesting effects that can arise, and then serves as a starting point for further generalizations.

A standard one-dimensional conservation law of the form

$$\frac{\partial\rho}{\partial t} + \frac{\partial q}{\partial x} = 0, \quad t > 0, \quad x \in \mathbb{R}, \tag{4.9}$$

is complemented by a non-standard choice of the closure relationship $q(\rho)$. Indeed it is assumed that there exist two "maximal" densities $\rho_{\max}$ and $\rho_{\max}^{\mathrm{panic}}$, with $\rho_{\max}^{\mathrm{panic}} > \rho_{\max}$, such that:

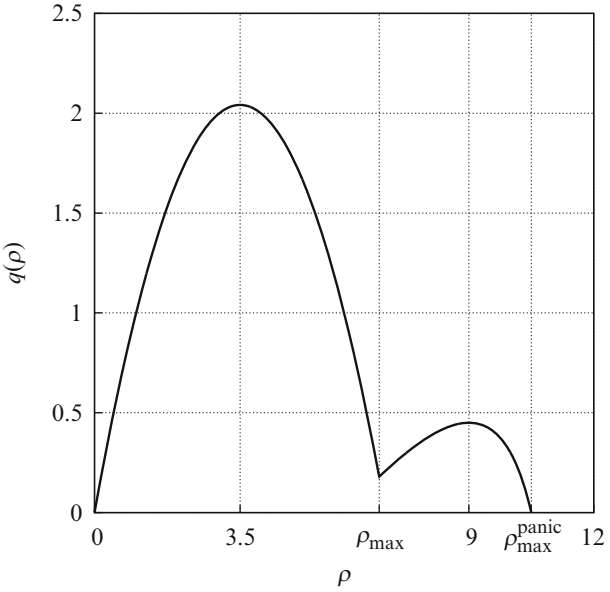


**Fig. 4.3** Fundamental diagram taking into account normal and panic conditions. The assumed values of the maximal densities are $\rho_{\max} \sim 6.84\,\text{ped/m}^2$ and $\rho_{\max}^{\text{panic}} = 10.5\,\text{ped/m}^2$

1. $q : [0,\ \rho_{\max}^{\text{panic}}] \to [0,\ +\infty)$.
2. $q(\rho) = 0$ if and only if $\rho = 0$ or $\rho = \rho_{\max}^{\text{panic}}$.
3. Restrictions of $q$ to the intervals $[0, \rho_{\max}]$ and $[\rho_{\max}, \rho_{\max}^{\text{panic}}]$ are strictly concave.

A function $q$ satisfying the above assumptions is

$$q(\rho) = \max\left\{\frac{\rho(7-\rho)}{6},\ \frac{3(\rho-6)(2\rho-21)}{20(\rho-12)}\right\},$$

see Fig. 4.3. This choice has a clear physical meaning: In normal conditions, pedestrians density varies in $[0, \rho_{\max}]$, but, contrary to traffic flow, they do not stop completely when the maximal density is reached. Rather, they enter the panic state and keep moving, reaching a second maximal flow, until the actual maximal density is reached (corresponding to an *overcompression*, and possibly death, of pedestrians). Such a trend of the fundamental diagram $q(\rho)$ was experimentally confirmed. Nevertheless, the flux $q$ used here and the experimental data cannot be compared directly since they have different units. Experimental data assume $[\rho] = \text{m}^{-2}$ and $[q] = \text{m}^{-1}\,\text{s}^{-1}$, while in this model one has $[\rho] = \text{m}^{-1}$ and $[q] = \text{s}^{-1}$.

Standard solutions of (4.9) satisfy a sort of "maximum principle", i.e., if the initial datum $\rho(0, x)$ is in $[\rho_m,\ \rho_M]$, then the solution $\rho(t,\ x)$ stays in $[\rho_m,\ \rho_M]$ for all $t > 0$. This property prevents de facto the arising of panic conditions. The problem is solved by allowing the equation to have nonclassical solutions, i.e.,

solutions satisfying (4.9) in its weak (or integral) form, but possibly violating the other usual admissibility conditions found in the literature, such as Lax inequalities, the vanishing viscosity criterion or the various entropy conditions.

### 4.2.4 Maury et al.'s Model

The Maury et al.'s model is a first order model which can be seen as a macroscopic version of the Maury and Venel's model described in Sect. 4.1.2. The pedestrian population is described by a density $\rho$ which is subject to remain below a certain maximal value (equal to 1 in what follows). This constraint represents the macroscopic counterpart of the hard-collision avoidance.

Given a desired velocity $v_d$, the model uses (4.6) with $q(\rho) = \rho v(\rho)$, choosing

$$v(\rho) = P_{C(\rho)}(v_d),$$

where $P$ is the projection operator (here the projection is meant in the $L^2$ sense), and the set $C(\rho)$ corresponds to all those velocity fields which do not increase $\rho$ on the already saturated zone, namely where $\rho = 1$. It is defined by

$$C(\rho) := \left\{ w \in (L^2(\Omega))^2 \ : \ \int_\Omega w \cdot \nabla \phi \leq 0 \quad \forall \phi \in H^1_+(\Omega), \phi = 0 \ \text{ a.e. in } \ \{\rho < 1\} \right\} \tag{4.10}$$

with

$$H^1_+(\Omega) = \{\phi \in H^1(\Omega; \mathbb{R}) \ : \ \phi \geq 0 \ \text{ in } \ \Omega\}.$$

The particular choice of $C(\rho)$ translates the fact that $v$ cannot have any component directed from a point where $\rho < 1$ to a point where $\rho = 1$. Indeed, $\nabla \phi$, if not equal to 0, points toward a region of the space where density is saturated. Equation (4.10) can be understood as the weak formulation of the following constraint:

$$\nabla \cdot w \geq 0 \quad \text{in} \quad \{\rho = 1\}$$

which says that the crowd cannot be further compressed in the region where the maximal density has already been reached.

### 4.2.5 Nonlocal Models

Pedestrians look ahead up to several meters and take decisions considering the distribution of the neighbors. Therefore, a realistic model should be *nonlocal*.

From the mathematical point of view, this is translated by assuming that the velocity $v = v[\rho]$ depends on values of the density $\rho$ *around* $x$ (square brackets denote functional dependence) and not only *at* $x$. In the following we list three possible choices for the velocity $v$.

A first possible choice for the velocity $v$ is

$$v[\rho] = s(\rho, \nabla\rho)(v_{\mathrm{d}} + v_{\mathrm{i}}[\rho]). \tag{4.11}$$

Here $s$ is a scalar function (corresponding to the fundamental diagram, see Sect. 4.2.1), $v_{\mathrm{d}}$ is a given desired direction, and $v_{\mathrm{i}}$ is the interaction velocity, defined by

$$v_{\mathrm{i}}[\rho] = -\varepsilon \frac{\nabla(\rho * \eta)}{\sqrt{1 + |\nabla(\rho * \eta)|^2}} \tag{4.12}$$

where $\varepsilon > 0$ is a parameter, $*$ is the convolution operator, and $\eta$ is a mollifier which possibly contains information on the sensory region $\mathscr{S}(x)$ (see Sect. 1.1.1). This choice translates the fact that individuals deviate from the desired path avoiding the direction of maximal increase of the averaged density.

A second possible choice for the velocity $v$ is

$$v[\rho](t,\, x) = v_{\mathrm{d}}(x) + v_{\mathrm{i}}[\rho](t,\, x), \qquad v_{\mathrm{i}}[\rho](t,\, x) = -\int_{\mathscr{S}(x)} C \frac{y - x}{|y - x|^2} \rho(t,\, y)\, dy \tag{4.13}$$

where $C > 0$ is a parameter. This choice translates the fact that pedestrians are repulsed from other pedestrians. The strength of the repulsion is inversely proportional to their mutual distance and directly proportional to the density itself. Notice that this choice gets rid of the fundamental diagram, since the function $s(\rho)$ does not appear.

A third possible choice for the velocity $v$ is

$$v[\rho](t,\, x) = s(\rho(t,\, x_p)) \left(\theta v_{\mathrm{d}}(x) + (1 - \theta) v_{\mathrm{i}}(x, x_p)\right). \tag{4.14}$$

Here $\theta \in [0,\, 1]$ is a dimensionless parameter that weights pedestrian attitude to give priority to the walking area layout or to the crowd conditions, and $x_p \neq x$ is a point that has to be understood as the location where crowding is more influential, according to some specific perception criterion. Once the point $x_p$ is found, the interaction velocity is simply given by

$$v_{\mathrm{i}}(x,\, x_p) = -\frac{x_p - x}{|x_p - x|}$$

meaning that pedestrians want to steer clear of the point where crowd is more influential. The point $x_p$ can be defined in several ways:

1. Pedestrians evaluate the perceived density a step forward in the desired direction:

$$x_p(x) = x + C v_{\mathrm{d}}(x)$$

   where $C > 0$ is a parameter.
2. Pedestrian attention is drawn by the point where the maximum value of $\rho$ is attained:

$$x_p[\rho](t,\, x) = \arg \max_{y \in \mathscr{S}(x)} \rho(t,\, y).$$

3. Pedestrians evaluate $x_p$ as the center of mass of the whole crowd:

$$x_p[\rho](t,\, x) = \frac{\displaystyle\int_{\mathscr{S}(x)} y\rho(t,\, y)\, dy}{\displaystyle\int_{\mathscr{S}(x)} \rho(t,\, y)\, dy}.$$

All these choices *delocalize* the evaluation of the velocity (both modulus and direction), making the model nonlocal.

### 4.2.6 Bellomo and Dogbé's Model

The Bellomo and Dogbé's model is a second order model characterized by some particular choices of the acceleration term $a$ in (4.7b).

A first simple version of the model is given by the choice

$$a(\rho,\, v) = C\big(s(\rho)v_{\mathrm{d}} - v\big) - \frac{K^2(\rho)}{\rho}\frac{\partial \rho}{\partial v_{\mathrm{d}}} v_{\mathrm{d}} \tag{4.15}$$

where $C$ is a parameter, $v_{\mathrm{d}}$ is the desired velocity, $s(\rho)$, $K^2(\rho)$ are scalar functions to be defined ($s$ corresponds to the fundamental diagram, see Sect. 4.2.1), and $\frac{\partial \rho}{\partial v_{\mathrm{d}}}$ represents the directional derivative of $\rho$ with respect to the direction $v_{\mathrm{d}}$. The first term at the right-hand side models the trend to the equilibrium velocity $s(\rho)v_{\mathrm{d}}$, while the second term represents the action of the density gradient along $v_{\mathrm{d}}$. In the end, both the local value of the density and its local changes in direction $v_{\mathrm{d}}$ are taken into account. Note that both terms locally induce pedestrians to align with the desired velocity.

A second version of the model is given by the choice

$$a(\rho,\, v) = C\big(s(\rho)w - v\big) - \frac{K^2(\rho)}{\rho}\frac{\partial \rho}{\partial w} w \tag{4.16}$$

with

$$w = v_{\mathrm{d}} + v_{\mathrm{i}} \quad \text{and} \quad v_{\mathrm{i}}(\nabla\rho,\, x) = \arg\min_{\xi\in\mathscr{S}(x)} \left\{ \frac{\partial\rho}{\partial\xi} \right\},$$

where $\mathscr{S}(x)$ is the sensory region, see Sect. 1.1.1. In this case the preferred direction of movement can be modified by the presence of other pedestrians, since the interaction velocity make pedestrians steer toward regions of low density. More precisely, the direction of the minimal directional derivative of the density is computed and used to correct the desired velocity.

A third version of the model is derived from the one-dimensional Aw and Rascle's model for traffic flow, and it is based on the conservation of a new quantity usually referred to as the *pseudo-pressure* $P$, which replaces the relaxation term in (4.15). In the two-dimensional setting the pseudo-pressure is a vector $P = (P^1, P^2)$ and the system has the form

$$\begin{cases} \dfrac{\partial\rho}{\partial t} + \nabla\cdot(\rho v) = 0 \\ \dfrac{\partial}{\partial t}\left(v^1 + P^1 v_{\mathrm{d}}^1\right) + v^1\dfrac{\partial}{\partial x^1}\left(v^1 + P^1 v_{\mathrm{d}}^1\right) + v^2\dfrac{\partial}{\partial x^2}\left(v^1 + P^1 v_{\mathrm{d}}^1\right) = \rho\alpha\left(s(\rho)v_{\mathrm{d}}^1 - v^1\right) \\ \dfrac{\partial}{\partial t}\left(v^2 + P^2 v_{\mathrm{d}}^2\right) + v^1\dfrac{\partial}{\partial x^1}\left(v^2 + P^2 v_{\mathrm{d}}^2\right) + v^2\dfrac{\partial}{\partial x^2}\left(v^2 + P^2 v_{\mathrm{d}}^2\right) = \rho\alpha\left(s(\rho)v_{\mathrm{d}}^2 - v^2\right). \end{cases} \tag{4.17}$$

The pseudo-pressure $P$ has to be given as a function of $\rho$ and $v$ in order to close the system. It can be chosen in several ways, for example

$$P(\rho,\, v) = \frac{\rho^{1+\gamma}}{C - \rho^{1+\gamma}} v$$

where $C$ is large enough to ensure that $C - \rho^{1+\gamma} > 0$, or

$$P(\rho,\, v) = s(\rho)v_{\mathrm{d}}. \tag{4.18}$$

Panic conditions can be handled by all the models described above. Authors suggest to increase the maximal speed of pedestrians while changing sign in front of the density gradient in (4.15) or (4.16). Indeed, in panic conditions, attractive accelerations become predominant with respect to repulsive ones because people tend to follow other walkers in the hope that they have found a way out.

## 4.3 Mesoscopic Models

Mesoscopic (or *kinetic*) models are based on a *statistical* representation of the crowd in the space of the *microscopic* states of pedestrians by means of the so-called (*one-particle*) *distribution function* $f$. If we assume, to fix the ideas, that the microstate of

a pedestrian is defined by the pair position-velocity $(x, v) \in \mathbb{R}^2 \times \mathbb{R}^2$ understood as independent variables, then the function $f$ is written as $f = f(t, x, v)$ and is such that $f(t, x, v)\, dx\, dv$ is, at time $t$, the (infinitesimal) average number of pedestrians located in the reference space volume $dx$ centered at $x$ with a velocity belonging to the reference volume $dv$ centered at $v$. For the sake of clarity, we point out that in one space dimension (i.e., $(x, v) \in \mathbb{R} \times \mathbb{R}$) this is read as the (infinitesimal) average number of pedestrians located between $x - \frac{1}{2}dx$ and $x + \frac{1}{2}dx$ with a speed comprised between $v - \frac{1}{2}dv$ and $v + \frac{1}{2}dv$.

The distribution function satisfies the following *kinetic equation*

$$\frac{\partial f}{\partial t} + v \cdot \nabla_x f + \nabla_v \cdot (F[f]f) = J[f], \tag{4.19}$$

where $\nabla_x$, $\nabla_v \cdot$ denote, respectively, the gradient with respect to $x$ and the divergence with respect to $v$, and moreover:

- The first two terms at the left-hand side form the *convective derivative*, which simply states that the distribution function is transported in the space of microscopic states by the velocity of the pedestrians themselves (hence, in practice, that $f$ is a *material quantity* for pedestrians).
- The third term at the left-hand side and the one at the right-hand side model the acceleration acting on pedestrians due to either external actions or mutual *microscopic* interactions.

The operator $F$ typically describes a *mean field acceleration* exerted on the generic pedestrian with microstate $(x, v)$, that we will henceforth call *test pedestrian*, by other surrounding walkers, called *field pedestrians*, within the sensory region $\mathscr{S}(x)$ of the former:

$$F[f](t, x, v) = \iint_{\mathscr{S}(x)\times\mathbb{R}^2} \mathscr{F}(x, y, v, w)\, f(t, y, w)\, dy\, dw, \tag{4.20}$$

where $\mathscr{F}$ gives the pairwise interaction between the test pedestrian $(x, v)$ and the field pedestrian $(y, w)$.

The operator $J$ describes instead binary *stochastic* interactions that can lead pedestrians to gain or loose, in probability, the test state $(x, v)$ according to some *transition probabilities*. Specifically, $J$ is written as:

$$J[f](t, x, v) = G[f, f](t, x, v) - f(t, x, v)L[f](t, x, v), \tag{4.21}$$

where $G$ is the (bilinear) *gain operator* and $L$ the (linear) *loss operator*. Detailed forms of $\mathscr{F}$, $G$, and $L$ will be discussed later with reference to specific models.

In practice, mesoscopic models do not distinguish pedestrians individually, like microscopic models. However, unlike macroscopic models, they still allow one to describe pedestrian behaviors at a microscopic individual level, albeit only in terms of probabilities. Furthermore, once the distribution function is known, macroscopic

observable quantities can be computed as moments of $f$ with respect to the variable $v$. For instance, density and flux are respectively obtained as:

$$\rho(t,\, x) = \int_{\mathbb{R}^2} f(t,\, x,\, v)\, dv, \qquad q(t,\, x) = \int_{\mathbb{R}^2} v\, f(t,\, x,\, v)\, dv, \tag{4.22}$$

whence also the macroscopic velocity in the point $x$ at time $t$ can be recovered as $q(t,\, x)/\rho(t,\, x)$.

### 4.3.1 Dogbé's Model

Dogbé's model is based on (4.19) with some particular choices of the operators $F$ and $J$.

First, the acceleration term $F$ is assumed to contain, besides a mean field contribution like (4.20), an additional *macroscopic* contribution expressed in the form:

$$\phi(\rho,\, \nabla\rho,\, v,\, v_{\mathrm{d}}),$$

where $\rho$ is the macroscopic density given in (4.22), $\nabla\rho$ is its gradient in space, $v$ is the actual microscopic velocity, and $v_{\mathrm{d}}$ is the desired velocity pointing in the direction of the locally preferred destination. The function $\phi$ can include, for instance, a relaxation of $v$ toward an equilibrium velocity given in terms of the local crowd density $\rho$, plus a trend to avoid density gradients along the desired path. In this case, its expression can be taken fully analogous to (4.15), after duly reinterpreting the symbol $v$ appearing there in the present mesoscopic context. Alternatively, the action of the density gradient can be generalized by considering in $\phi$ a term of the form:

$$\frac{\partial\varphi}{\partial v_{\mathrm{d}}} v_{\mathrm{d}} = \varphi'(\rho) \frac{\partial\rho}{\partial v_{\mathrm{d}}} v_{\mathrm{d}},$$

where the function $\varphi : \mathbb{R}_+ \to \mathbb{R}$ is chosen according to specific attraction/repulsion dynamics to be modeled. For instance, $\varphi(\rho) = -\rho^2$ may be used to model a stronger repulsion for increasing crowd density, while $\varphi(\rho) = \log\rho$ may model gregarious pedestrians who like to be close to one another.

As far as the mean field contribution is concerned, cf. (4.20), the proposed pairwise interaction term $\mathscr{F}$ in Dogbé's model is as follows:

$$\mathscr{F}(x,\, y,\, v,\, w) = -\beta_1 \left( \frac{d_c - |y - x|}{|y - x|} \right) e^{-\beta_2 (d_c - |y-x|)^2} \frac{y - x}{|y - x|},$$

hence it does not depend explicitly on the velocities of the test and field pedestrians and changes sign when the actual distance $|y - x|$ between the latter crosses a critical threshold $d_c > 0$. In particular, given that $\beta_1$, $\beta_2$ are nonnegative coefficients, the pairwise mean field microscopic interaction is repulsive if $|y - x| < d_c$, i.e., if the two pedestrians are too close to one another, and is attractive if $|y - x| > d_c$, i.e., if they are far from each other. The exponential function is used for producing a decay of the interaction with the distance.

Finally, stochastic interactions linked to state transition dynamics are modeled by means of the following classical forms of the gain and loss operators (cf. (4.21)):

$$\begin{aligned} G[f, f](t, x, v) = &\iiint_{\mathscr{S}(x)\times\mathbb{R}^2\times\mathbb{R}^2} \eta(x, y, v_*, w) A(v_* \to v | v_*, w) \omega(x, y) \\ &\times f(t, x, v_*) f(t, y, w)\, dy\, d v_*\, dw \\ L[f](t, x, v) = &\iint_{\mathscr{S}(x)\times\mathbb{R}^2} \eta(x, y, v, w) \omega(x, y) f(t, y, w)\, dy\, dw, \end{aligned} \tag{4.23}$$

where:

- $\eta$ gives the frequency of encounters, hence of interactions, among pedestrians on the basis of their microscopic position and velocity. A possible choice borrowed from the classical kinetic theory is $\eta(v_*, w) = |w - v_*|$.
- $A$ is the transition probability density associated with a velocity transition event from a generic $v_*$ to the test velocity $v$ in consequence of an interaction with a pedestrian with velocity $w$.
- $\omega$ is a weight function over the distance between the interacting pedestrian within the sensory region $\mathscr{S}(x)$.

### 4.3.2 Bellomo and Bellouquid's Model

The mesoscopic crowd model by Bellomo and Bellouquid differs from the previous one in that it aims at revisiting and adapting the mathematical structures of the classical kinetic theory in the light of some modeling issues specifically raised by crowds. The main two points that this model addresses are:

- The *microscopic granularity*, typical of both sparse and dense crowds (cf. the discussion set forth in Chap. 1, particularly in Sects. 1.2.1, 1.2.3, and 1.4.1), which makes it questionable to assume a continuous statistical distribution of the microscopic states of pedestrians.
- The complexity of microscopic interactions, which are viewed as *nonlinearly additive stochastic games*, meaning that they are described by the operator $J$ as opposed to the mean field operator $F$ and that they take into account the influence

of the local collective distribution of pedestrians on the behavioral rules applied by single individuals.

The microscopic granularity is introduced in the model by referring to a particular structure of the distribution function, namely:

$$f(t,\, x,\, \theta,\, s) = \sum_{i=1}^{n} \sum_{j=1}^{m} f_{ij}(t,\, x) \delta_{\theta_i}(\theta) \otimes \delta_{s_j}(s), \tag{4.24}$$

where $s$ is the speed of the test pedestrian and $\theta$ is the angle which identifies her direction of motion, so that the velocity can be recovered as $v = s(\cos\theta,\, \sin\theta)$ (cf. (4.8)). The symbol $\delta$ denotes the Dirac delta distribution, thus the representation (4.24) assumes that pedestrian microscopic velocity can distribute only over a finite set of values, also called *velocity classes*, identified by a lattice of normalized speeds $I_s = \{s_1 = 0,\, \ldots,\, s_m = 1\}$ and a lattice of angular directions $I_\theta = \{\theta_1 = 0,\, \ldots,\, \theta_n = 2\pi\}$ in the plane.

In (4.24) the functions $\{f_{ij}(t,\, x)\}_{i=1,\ldots,n,\, j=1,\ldots,m}$, are the *discrete kinetic distribution functions*, such that $f_{ij}(t,\, x)\, dx$ is the (infinitesimal) average number of pedestrians that at time $t$ are located in the elementary space volume $dx$ centered at $x$ and are walking with velocity $v_{ij} = s_j(\cos\theta_i,\, \sin\theta_i)$. In other words, $f_{ij}(t,\, x) = f(t,\, x,\, \theta_i,\, s_j)$ in distributional sense.

A system of evolution equations for the new unknowns $\{f_{ij}(t,\, x)\}_{i=1,\ldots,n,\, j=1,\ldots,m}$ is obtained by plugging the representation (4.24) into (4.19) with $F = 0$ (no mean field interactions) and $J$ given formally by (4.21)–(4.23). After some technical calculations, this yields:

$$\begin{aligned} \frac{\partial}{\partial t} f_{ij}(t,\, x) + v_{ij} \cdot \nabla f_{ij}(t,\, x) = \sum_{h,k=1}^{n} \sum_{p,q=1}^{m} \int_{\mathscr{S}(x)} \eta[\rho](t,\, y) A^{ij}_{hp,kq}[\rho](t,\, y) \omega(x,\, y) \\ \times f_{hp}(t,\, x) f_{kq}(t,\, y)\, dy \\ - f_{ij}(t,\, x) \sum_{k=1}^{n} \sum_{q=1}^{m} \int_{\mathscr{S}(x)} \eta[\rho](t,\, y) \omega(x,\, y) f_{kq}(t,\, y)\, dy, \end{aligned} \tag{4.25}$$

where it is further assumed that both the frequency of the interactions $\eta$ and the transition probabilities $A^{ij}_{hp,kq} = A(v_{hp} \to v_{ij} | v_{hp},\, v_{kq})$ depend on the macroscopic density $\rho$. The latter, in turn, depends on the whole set of discrete kinetic distribution functions, as it can be easily seen by inserting (4.24) into the first of (4.22):

$$\rho(t,\, y) = \sum_{i=1}^{n} \sum_{j=1}^{m} f_{ij}(t,\, y).$$

This ultimately makes microscopic interactions nonlinearly additive. Indeed the terms encoding the microscopic behavioral rules of pedestrians bring technically further nonlinearities in the right-hand side of (4.25) as they are affected by the collective state of the crowd within the sensory region of the interacting individuals.

At last, it is worth spending a few words to discuss in which sense the interactions expressed by the right-hand side of (4.25) can be assimilated to *stochastic games*. The coefficients $A^{ij}_{hp,kq}$ give the probability that a pedestrian with velocity $v_{hp} = s_p(\cos\theta_h, \sin\theta_h)$, called in this context *candidate pedestrian*, jumps to the test velocity $v_{ij} = s_j(\cos\theta_i, \sin\theta_i)$ in consequence of an interaction with a field pedestrian with velocity $v_{kq} = s_q(\cos\theta_k, \sin\theta_k)$ within her sensory region. Candidate and field pedestrians can be viewed as two *players* who play a game at each interaction, their *game strategies* being the respective velocities $v_{hp}$, $v_{kq}$. The *payoff* of the game is the new velocity $v_{ij}$ that the candidate pedestrian can get after the interaction. Such a payoff is not known deterministically from the knowledge of the strategies of the two players because it depends on personal behaviors which are better described in probabilistic terms. From this point of view, the transition probabilities $A^{ij}_{hp,kq}$ form actually the probability distributions of such *stochastic payoffs* conditioned to the game strategies (viz. the pre-interaction velocities) of the two players/pedestrians. Remarkably, the payoff of the game is, at the same time, the *new strategy* that the candidate pedestrian will use in approaching future interactions. Therefore, such a description of the microscopic interactions reflects the evolution in time of the behavioral strategy of pedestrians.

## 4.4 Models for Rational Pedestrians

Are pedestrians fully rational? Is their way to move the result of some optimal strategy to reach their targets? In general, the answer is no for several reasons. First, they do not always have a priori knowledge of the environment they move in, so they cannot choose their path in an optimal manner. Second, they are not completely able to forecast the behavior of other pedestrians, especially for long time. Third, and most important, they are selfish: Individuals try to reach their goal regardless of the wills of the others, and rarely consider the fact that a collaboration can in fact be advantageous, in particular if the collaboration requires (counterintuitively) to stop or slow down for some time. On the other hand, in some special situations (e.g., well known walking area, routine itinerary) pedestrians can actually show good predictive abilities and an optimal behavior.

Keeping this in mind, it can be interesting to model the *ideal* fully rational behavior of pedestrians in order to better understand the role of rationality in the final behavior, and also to set the rational behavior as a sort of a "target" for normal pedestrians.

In the following we briefly describe five models for rational pedestrians. The first one is "nanoscopic", meaning that it considers the *internal* dynamics of the single pedestrian. The second one is microscopic, the third and the fourth ones

are macroscopic, and the last one has a multiscale flavor. Before describing the macroscopic models, we will recall some features of the *eikonal equation*, since it is an important ingredient of such models.

### 4.4.1 The Arechavaleta et al.'s Model

The Arechavaleta et al.'s model is a control-based model which deals with a pedestrian moving in a free environment, thus does not take into account the presence of other pedestrians and obstacles. It was originated as a way of studying human locomotion and to reproduce that in robots. The model is defined at the *nano* scale, since it is based on information on the internal dynamics of the single pedestrian.

The main idea is that the pedestrian decides her trajectory by acting linearly with two controls: the first affecting the velocity and torsion of her body and the second affecting the curvature. The motion is then decided by minimizing the square of the control norm. Indicating by $(x, y)$ the position of the body's torso in given reference system, by $\theta$ its angle with respect to the first coordinate axis and $\kappa$ its curvature, the equations are written as:

$$\begin{cases} \dot{x} = u_1 \ \cos(\theta) \\ \dot{y} = u_1 \ \sin(\theta) \\ \dot{\theta} = u_1 \kappa \\ \dot{\kappa} = u_2 \end{cases}$$

where the first control $u_1(t) \in [a, b]$ and the second control $u_2(t) \in [-c, c]$, for a suitable choice of the parameters $a, b, c$. The optimal control problem is given by:

$$\min_{u_1, u_2} \frac{1}{2} \int_0^T \left(\alpha \ u_1^2 + \beta \ u_2^2\right) dt$$

where $\alpha, \beta$ are other two parameters and $T$ is the final time. Solutions to the optimal control problem are given by concatenations of arc of clothoids.

### 4.4.2 Hoogendoorn and Bovy's Microscopic Model

The Hoogendoorn and Bovy's microscopic model is based on the assumption that pedestrians can forecast to a certain extent the behavior of the others, and then choose their direction of motion on the basis of the forecast. It consists of two main ingredients: A force based model (see Sect. 4.1.1) and a cost functional to be minimized, which translates the "cost" (in terms of discomfort due to proximity

of other pedestrians, straying from the desired direction, etc.) associated to every possible trajectory joining the current position to the desired target. Recalling (4.1), the model has the form

$$\begin{cases} \dot{X}^k(t) = V^k(t) \\ \dot{V}^k(t) = F^k(t) + U^k(t) \end{cases} \qquad k = 1, \ldots, N, \tag{4.26}$$

where $U^k$ is a *control* variable which can be freely chosen by each pedestrians in a given set of admissible controls $\mathscr{U}^k$. System (4.26) is complemented by initial conditions $X^k(\tau)$, $V^k(\tau)$ at some initial (generic) time $t = \tau$, for $k = 1, \ldots, N$.

Let us denote the complete state of the system by

$$Z := (X^1, \ldots, X^N, V^1, \ldots, V^N)$$

and define

$$V := (V^1, \ldots, V^N), \quad F := (F^1, \ldots, F^N), \quad U := (U^1, \ldots, U^N).$$

Then, we can rewrite the complete dynamics in a short form as

$$\dot{Z}(t) = f(Z, U) := \begin{pmatrix} V \\ F + U \end{pmatrix}. \tag{4.27}$$

Each pedestrian has her own cost functional of the form

$$J^k(U; \tau) := \int_\tau^\infty e^{-\lambda s} L^k(s, Z^{U,\tau}(s), U(s))\, ds,$$

where $\tau \geq 0$ is any initial time, $\lambda \geq 0$ is a discount factor translating the fact that a short-term saving is preferable to a long-term saving, $L^k$ is the cost function which takes into account any modeling assumptions about preferences of pedestrians, and $Z^{U,\tau}(t)$ is the solution of (4.27) with initial time $\tau$ and control $U$.

At any time $\tau$, pedestrian $k$ is assumed to behave in the following way. First, she predicts the choice of the controls of the others, i.e., it is assumed that she knows the vector

$$U^{-k}(t) := (U^1(t), \ldots, U^{k-1}(t), U^{k+1}(t), \ldots, U^N(t)), \qquad \forall\, t \geq \tau$$

which is the vector $U(t)$ where the $k$-th component is removed. Then, she finds

$$U^{k,*} = \arg \min_{U^k \in \mathscr{U}^k} J((U^1, \ldots, U^N); \tau).$$

Finally, she moves following (4.26) and employing the control $U^{k,*}$.

The knowledge of $U^{-k}(t)$ for any $t \geq \tau$ can be obtained in several ways. The simplest choice proposed by the authors of the model is $U^{-k}(t) = 0$, which translates, e.g., the fact that pedestrians have no idea on the response behavior of the others to the current state of the system. Another possibility is that pedestrians predict the behavior of the others by assuming that the latter behave according to some (given) feedback mechanism, i.e., $U^{-k}(t) = U^{-k}(Z(t))$.

### 4.4.3 Eikonal Equation and Minimum Time Problems

The eikonal equation often appears as a crucial ingredient of macroscopic models. This is due to its relation to minimum time problems. Let us consider a single pedestrian who can move in the domain $\Omega$ and denote her position at time $t$ by $X(t)$. Assume that her starting point is $\bar{X} \in \Omega$ and that she wants to reach a given target $\Gamma \subset \Omega$ in minimal time (for example an emergency exit). Moreover, assume that her dynamics is given by

$$\begin{cases} \dot{X}(t) = v(X(t), u(t)) = s(X(t))\, u(t), \qquad u(t) \in B_1(0) \\ X(0) = \bar{X} \end{cases} \tag{4.28}$$

where $B_1(0) \in \mathbb{R}^2$ is the unit two-dimensional ball, $s : \Omega \to \mathbb{R}$ is a *given* scalar function, and $u$ is the control variable. Here we denoted by $v$ the velocity of the pedestrian and by $s$ the modulus of $v$. Note that the speed (and then the velocity) *does not depend explicitly on time*. The pedestrian is assumed to be free to decide her direction of motion, i.e., she can choose the control $u \in B_1(0)$ at any time. The question arises which is the optimal direction of motion $u^*(\cdot)$ which let the pedestrian reach the target in minimal time (the optimal direction will not be, in general, the straight line joining $\bar{X}$ and $\Gamma$ since $s$ is space-dependent).

The eikonal equation allows one to find the optimal direction $u^*$ in feedback form, i.e., depending on the space, i.e. one can compute the function $u^* = u^*(x)$ for *any* $x \in \Omega \setminus \Gamma$, such that the minimal time trajectory to the target is given by the solution to

$$\begin{cases} \dot{X} = s(X)u^*(X), \\ X(0) = \bar{X}. \end{cases}$$

By means of the Dynamic Programming principle, under suitable conditions, it is possible to characterize the optimal direction $u^*$ as

$$u^*(x) = -\frac{\nabla\phi(x)}{|\nabla\phi(x)|}, \quad x \in \Omega \setminus \Gamma$$

where $\phi$ is the unique *viscosity solution* of the following eikonal equation (which in this context is seen as a particular Hamilton-Jacobi-Bellman equation)

$$\begin{cases} s(x)\,|\nabla\phi(x)| = 1, & x \in \Omega \setminus \Gamma \\ \phi(x) = 0, & x \in \Gamma \end{cases} \tag{4.29}$$

complemented with suitable boundary conditions at $\partial\Omega$. The value $\phi(x)$ corresponds to the minimal time to reach the target starting from any point $x \in \Omega\setminus\Gamma$ and employing the optimal direction of motion.

If the speed depends also on time, i.e., $v = v(t,\, x,\, u) = s(t,\, x)u$, two approaches can be followed:

1. The time variable is simply seen as a *parameter*. The eikonal equation is

$$\begin{cases} s(\tau,\, x)\,|\nabla\phi(\tau,\, x)| = 1, & x \in \Omega \setminus \Gamma \\ \phi(\tau,\, x) = 0, & x \in \Gamma \end{cases} \tag{4.30}$$

   and it is solved for any fixed time $\tau$. At each time $\tau$, the optimal direction is

$$u^*(\tau,\, x) = -\frac{\nabla\phi(\tau,\, x)}{|\nabla\phi(\tau,\, x)|}, \quad x \in \Omega \setminus \Gamma.$$

2. The time variable is treated in the same way as the space variables and the minimum time problem is reformulated in the space-time. The target is extended as $\Gamma' = \{t > 0\} \times \Gamma$ and the new three-dimensional velocity field is

$$v'(t,\, x,\, u) := \begin{pmatrix} 1 \\ s(t,\, x)u \end{pmatrix}, \qquad u \in B_1(0). \tag{4.31}$$

   Note that pedestrians "move" in time with fixed speed 1 since time travel is (so far) impossible. The Hamilton-Jacobi-Bellman equation associated to the new problem is

$$\begin{cases} \max\limits_{u\in B_1(0)} \{-v'(t,\, x,\, u)\cdot\nabla_{t,\,x}\,\phi(t,\, x)\} = 1, & (t,\, x) \in (\mathbb{R}_+ \times \Omega) \setminus \Gamma' \\ \phi(t,\, x) = 0, & (t,\, x) \in \Gamma' \end{cases} \tag{4.32}$$

   where $\nabla_{t,\,x}$ denotes the gradient with respect to both space and time variables. In this case $\phi$ is the minimal *fictitious time* to reach the target $\Gamma'$ in the space-time. The optimal direction is

$$u^*(t,\, x) = \arg\max_{u\in B_1(0)} \{-v'(t,\, x,\, u)\cdot\nabla_{t,\,x}\,\phi(t,\, x)\}, \quad (t,\, x) \in (\mathbb{R}_+ \times \Omega) \setminus \Gamma'.$$

   This way, the optimal direction is computed taking into account the fact that the speed varies in space and time.

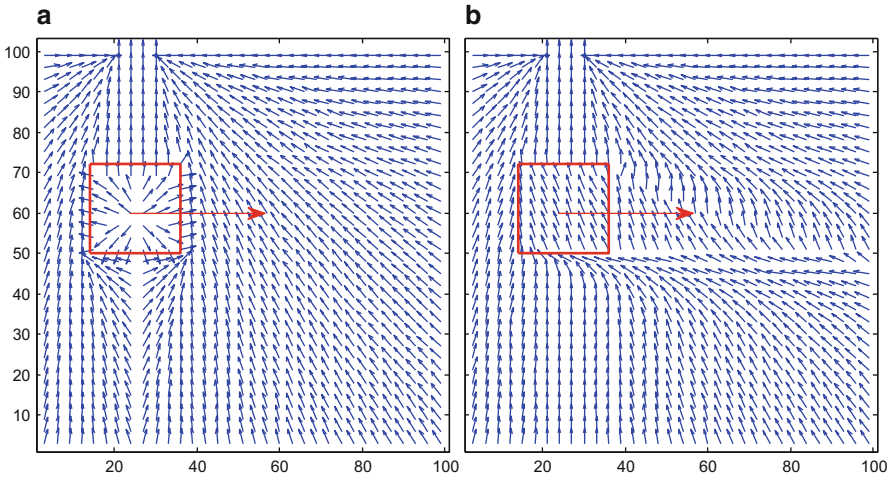


**Fig. 4.4** Optimal velocity fields to reach the exit on the *upper side* from any point of the room at $t = 0$. The *red square* represents a slow region moving to the *right* with constant speed. (**a**) Parametrized eikonal equation; (**b**) space-time eikonal equation

To better elucidate the difference among the two approaches, we show in Fig. 4.4 two optimal velocity fields computed by the parametrized eikonal equation (4.30) and its space-time extended version (4.32). We considered a room with one exit (target) on the upper side, to be reached in minimal time. Pedestrians are freely to move in the room with speed 1, but for a square region $R$ (say, a crowded area) moving rightward, in which pedestrians have to slow down ($R$ moves with its own prescribed dynamics, embedded in the function $s$). Both velocity fields shown in Fig. 4.4 correspond to the initial time $t = 0$. If time dimension is not taken into account, the optimal velocity field prescribes to circumvent $R$ whenever $R$ is in between the starting point and the target. Conversely, if the dynamics of $R$ is taken into account in the computation of the optimal velocity, pedestrians starting behind and sufficiently far from $R$ move immediately to the target in a straight line, since they predicted that once they will have reached the initial position of $R$, it will be moved to the right, and the way will be clear.

### *4.4.4 Hughes' Model*

The Hughes' model describes pedestrians by means of two quantities, their density $\rho(t, x)$ and their (two-dimensional) velocity $v(t, x)$, with $t > 0, x \in \mathbb{R}^2$. The model is based on the assumption that pedestrians want to reach their destination, denoted by $\Gamma$, as soon as possible but temper this behavior to avoid high densities. This result is obtained by coupling a conservation law for the density and an eikonal

equation for the velocity. Referring to the notations used in Sect. 4.4.3, we have that the speed $s(t, x) = |v(t, x)|$ of pedestrians is a *given* function of the density $\rho$, i.e.,

$$s(t, x) = s(\rho(t, x)) \tag{4.33}$$

corresponding to the fundamental diagram, see Sect. 4.2.1.

The velocity $v$ is given by

$$v[\rho, \phi](t, x) = s(\rho(t, x))w[\phi](t, x), \qquad w[\phi](t, x) = -\frac{\nabla\phi(t, x)}{|\nabla\phi(t, x)|}, \tag{4.34}$$

where $\phi$ is an auxiliary function, called *potential*. The model is constituted by a conservation law for $\rho$

$$\frac{\partial\rho}{\partial t} + \nabla \cdot (\rho v[\rho, \phi]) = 0, \qquad t > 0, \quad x \in \Omega \tag{4.35}$$

with initial conditions $\rho(0, x) = \bar{\rho}(x)$, $x \in \mathbb{R}^2$ and where, at any fixed time $t = \tau$, the function $\phi$ is computed by solving the following $\tau$-parametrized eikonal equation

$$s(\rho(\tau, x))\,|\nabla\phi(\tau, x)| = 1, \qquad x \in \Omega \setminus \Gamma \tag{4.36}$$

with boundary conditions $\phi(\tau, x) = 0$, $x \in \Gamma$ (in addition to suitable boundary conditions on $\partial\Omega$). The coupling between (4.35) and (4.36) is obtained by means of (4.34).

Setting the problem in the context of minimum time problems (see Sect. 4.4.3), the model has a clear physical meaning: Pedestrians move with some velocity $v$, its modulus $s(\rho)$ being dependent on the density, while its direction being optimally computed in a such a way it follows the minimum time path to the target. In turn, the minimum time problem is solved at any time $t = \tau$ by assuming that the speed in the whole domain is given by $s(\rho(\tau, x))$, $x \in \Omega$. Note that the use of the (parametrized) eikonal equation falls in the category described in (4.30) rather than (4.32). In this way, the model guarantees that pedestrians will choose their paths in the domain in a optimal manner with respect to the instantaneous walking cost information, that is, the pedestrian distribution *at the time*.

### 4.4.5 *Hoogendoorn and Bovy's Macroscopic Model*

The Hoogendoorn and Bovy's macroscopic model describes pedestrians with even more rational capabilities with respect to those described by the Hughes' model. Indeed, it is assumed that pedestrians forecast with no error the behavior of the others and choose their paths in a optimal manner with respect to the *complete*

walking cost information, that is, the pedestrian distribution *at any time*. The final behavior of the crowd represents an equilibrium for the system, in the sense that pedestrians cannot improve their choice of the path (further minimizing some given cost functional) by unilaterally changing their path choice (cf. the Nash equilibrium found by the mean field game models described in Sect. 4.4.6).

To avoid introducing new variables and notations, we present here a minimum-time version of the model, which is a direct generalization of the Hughes' model (see bibliographical notes for details). Referring to the notations of Sects. 4.4.3–4.4.4, and defining

$$v'[\rho](t,\, x,\, u) := \begin{pmatrix} 1 \\ s(\rho(t,\, x))u \end{pmatrix}, \qquad u \in B_1(0) \tag{4.37}$$

(cf. (4.31)), the system of equations to be solved is

$$\begin{cases} \dfrac{\partial \rho}{\partial t} + \nabla \cdot (\rho v[\rho, \phi]) = 0, & t > 0, \quad x \in \Omega \qquad \text{(4.38a)} \\ \max\limits_{u \in B_1(0)} \{-v'[\rho](t,\, x,\, u) \cdot \nabla_{t,x} \phi(t,\, x)\} = 1, & (t,\, x) \in (\mathbb{R}_+ \times \Omega) \setminus \Gamma' \qquad \text{(4.38b)} \end{cases}$$

with initial conditions $\rho(0, x) = \bar{\rho}(x)$ and boundary condition $\phi(t,\, x) = 0$ for $(x,\, t) \in \Gamma'$. The equation is solved iteratively in the following way:

1. The domain $\Omega$ is assumed to be completely empty ($\rho \equiv 0$). Function $s$ in (4.33) is computed, then function $v'$ in (4.37) is computed. Equation (4.38b) is solved for $\phi$.
2. Equation (4.38a) is solved for any $t > 0$, with $v$ defined as in (4.34), and $w[\phi]$ assumed to be given. An updated $\rho$ is computed.
3. Functions $s$ and $v'$ are evaluated with the updated $\rho$ and (4.38b) is solved again.
4. The procedure is iterated until a stationary solution for $\rho$ is found.

In this case the use of the eikonal equation falls in the category described in (4.32) rather than (4.30). Indeed the pedestrian velocity $v$ is now computed taking into account the future changes of the speed $s$, which, in turn, depend on the future pedestrian distribution $\rho$, and then on the pedestrian velocity $v$ itself.

See Sect. 4.4.6 for a similar approach based on the theory of mean field games.

### *4.4.6 Mean Field Game Models*

The mean field game approach assumes pedestrians to be rational and have rational expectations. Individuals anticipate the crowd evolution first, then evaluate their cost function. Next, they deduce their strategy (feedback control). Finally, the mass evolves according to these strategies. At the optimum the mass evolution has to coincide with the one which has been anticipated, according to the rational

expectations assumption. The crowd strategy is then a Nash equilibrium. This forward-backward approach is conceptually similar to the Hoogendoorn and Bovy's macroscopic model described in Sect. 4.4.5. There, (4.38a) is the forward equation and (4.38b) is the backward equation.

The mean field game setting has some analogies with the multiscale model discussed in this book. It has a microscopic foundation as a $N$-player differential game, but the crowd is treated as a density in the limit game when $N \to \infty$.

In the following we restrict the discussion to the continuum of players setting ($N = \infty$), presenting the equations of the mean field game system whose solutions are mean-field equilibria. The two-dimensional first order stochastic dynamics of a single pedestrian located at some generic point $x \in \mathbb{R}^2$ is

$$\begin{cases} dX_t = U_t\, dt + \sigma dW_t, \quad t \in [0,\, T] \\ X_0 = x \end{cases} \tag{4.39}$$

where $\sigma > 0$ is a parameter, $T$ is the final time, $W_t$ is the two-dimensional Brownian motion, $U \in \mathscr{U}$ is the control variable, and $\mathscr{U}$ is the set of admissible controls. Let us denote by $X_t^{U,x}$ the solution of (4.39) and by $\rho$ the macroscopic density distribution. For any $x$ and $t \le T$, the value function is defined by

$$\phi(t,\, x) = \inf_{U \in \mathscr{U}} \mathbb{E}\left[ \int_t^T L\left(s,\, X_s^{U,x},\, U_s,\, \rho(s,\, X_s^{U,x})\right) ds \right],$$

where $\mathbb{E}[\cdot]$ is the expected value. Here $L$ is the cost function (the terminal cost is assumed to be 0 for simplicity) which depends on time, trajectory, control and density distribution along the trajectory. Note that a single microscopic pedestrian is able to anticipate the crowd distribution and then evaluates the mass she encounters during her trip $X_s$.

Then, the Hamiltonian $H$ of the problem is defined, as usual, as the Legendre transform of $L$,

$$H(t,\, x,\, p,\, \rho) := \sup_{q \in \mathbb{R}^2} \{p \cdot q - L(t,\, x,\, q,\, \rho)\}, \qquad p \in \mathbb{R}^2,$$

and the mean field game system is

$$\begin{cases} \dfrac{\partial \rho}{\partial t} - \dfrac{\sigma^2}{2} \triangle \rho + \nabla \cdot \left( \rho \dfrac{\partial H}{\partial p}(t,\, x,\, \nabla \phi,\, \rho) \right) = 0 \\ \dfrac{\partial \phi}{\partial t} + \dfrac{\sigma^2}{2} \triangle \phi + H(t,\, x,\, \nabla \phi,\, \rho) = 0 \end{cases} \tag{4.40}$$

with initial and terminal conditions $\rho(0, x) = \bar{\rho}(x)$ and $\phi(T,\, x) = 0$.

The first equation in (4.40) describes the mass evolution equation of the system. Its solution is the distribution of pedestrians transported according to individuals'

optimal velocity field (forward in time). The second equation in (4.40) is a Hamilton-Jacobi-Bellman equation for the adjoint variable $\phi$. It basically gives the optimal strategy obtained by a feedback reasoning (backward in time).

### 4.4.7 Playing with Rationality

Other models for rational pedestrians can be obtained from the ones described in the previous sections.

A simplified version of the Hughes' model, named *dynamic continuum model with memory effect*, can be obtained by a full decoupling of Eqs. (4.35) and (4.36). First, the domain is assumed to be empty, so that $\rho \equiv 0$ and the speed $s$ is constant. Then the eikonal equation is solved, in order to compute the minimum-time trajectories to the target. Finally, the conservation law is solved for any $t > 0$ keeping $\phi$ frozen. In this way, the initially-optimal path does not change in time, thus resulting in the end to be nonoptimal. Nevertheless, theoretical and numerical investigation is simpler, and the method is expected to be accurate for low densities.

Interestingly, the Hughes' model and the Hoogendoorn and Bovy's macroscopic model can be *hybridized*, giving rise to a *family of models* indexed by a parameter $M \in [0, +\infty)$. For $M = 0$ one recovers the Hughes' model, while for $M \to \infty$ one recovers the Hoogendoorn and Bovy's model (in its minimum-time version presented in Sect. 4.4.5). The idea behind the model is that pedestrians do have predictive capabilities but limited in time, extending only up to a time $M$ in the future. As in the Hughes' model, at any fixed time $t = \tau$, an offline procedure is run, which returns the optimal velocity field at time $\tau$. But, as in the Hoogendoorn and Bovy's model, we assume not only that pedestrians are aware of the current distribution of the density $\rho(\tau, \cdot)$ on $\Omega$, but also that they can forecast the evolution of $\rho$, in this case until time $\tau + M$. Then, one ends up again with a coupled forward-backward system similar to (4.38a)–(4.38b), to be solved at any time $t = \tau$.

## 4.5 Bibliographical Notes

Although the research in pedestrian modeling is relatively young, the literature in this field is already large. This is probably due to the fact that many models are inspired by the vehicular traffic literature, which has been deeply investigated for decades. Some reviews are already available, see Bellomo and Dogbé [16], Duives et al. [67], Helbing [83], Ho and Wong [93], and Papadimitriou et al. [137]. See also the comprehensive papers by Bellomo and Bellouquid [14], Bellomo et al. [17], and the special issue [40].

In the following, we just point out some selected references which represent milestones in the field and/or are of particular interest for this book.

Section 4.1.1 The *magnetic force model* was introduced in 1979 in the very pioneer five-part paper by Okazaki [130–132], Okazaki and Matsushita [133], and Okazaki and Yamamoto [134]. Note that the original Japanese text is followed by a long summary in English, and that the paper is available online. The paper presents a number of numerical experiments which are still nowadays under investigation: Crossing flows of pedestrians (individuals and groups), passing pedestrians, pedestrians negotiating blind corners, pedestrians at intersections, flows at bottleneck, obstacle avoidance, wall-pedestrian interactions, evacuation from complex environments as a train station or a classroom (either or not guided by signals), and others.

The *social force model* was "officially" introduced by Helbing and Molnár [88] in 1995, even if same ideas appeared some years before, see, e.g., Helbing [81]. Modeling of panic conditions is studied in Helbing et al. [85]. The paper by Helbing and Vicsek [90] points out that the exact expression of the repulsion force is not really important for the emergence of self-organizing effects. This is confirmed by the fact that several models catch self-organization, even if they handle the repulsion among pedestrians in rather different ways.

The *centrifugal force model* was introduced by Yu et al. [174] in 2005. A generalization to non point-like pedestrians can be found in Chraibi et al. [37]. There, it is proposed a more detailed description by modelling pedestrians as ellipses with velocity-dependent semi-axes. A general discussion about advantages and drawbacks of force models can be found in Chraibi et al. [36], see also Köster et al. [112].

Section 4.1.2 The *Maury and Venel's model* was introduced in [122] in 2007 (see [123] for a reference in English). The macroscopic counterpart of the same model is described in Sect. 4.2.4.

Section 4.1.3 The literature for *Cellular Automata models* is huge. We point out the papers by Blue and Adler [19–21], and, among others, Burstedde et al. [30] and Kirchner and Schadschneider [109]. In Burger et al. [29] it is derived a macroscopic model passing to a continuous limit from the microscopic Cellular Automaton described by Kirchner and Schadschneider [109].

Section 4.1.4 For *discrete choice models* we referred primarily to the paper by Antonini et al. [8].

Section 4.2 Regarding *macroscopic models* in general, it is useful to mention first some milestone models for vehicular traffic flow, which served as a basis for two-dimensional generalizations. The Lighthill-Whitham-Richards model was proposed independently by Lighthill and Whitham [118] in 1955 and Richards [151] in 1956. The Payne-Whitham model was proposed independently by Payne [138] in 1971 and Whitham [170] in 1974. In 1995, the paper by Daganzo [55] pointed out some important drawbacks of second order models, healed later by, e.g., Aw and Rascle [10] in 2000 and Zhang [175] in 2002.

With regards to *macroscopic models for pedestrian flow*, Helbing [82] in 1992 wrote fluid-dynamic equations taking inspiration from the Boltzmann-like gas-kinetic approach by Henderson [91]. He avoided some unrealistic assumptions,

such as the conservation of momentum and energy, thereby obtaining a theory specifically focused on pedestrians.

Section 4.2.1 Literature regarding *fundamental diagrams* is huge, especially for vehicular traffic. Functions reported in Section 4.2.1 are discussed in the papers by Bellomo and Dogbé [15, 16], and by Coscia and Canavesio [43]. Recently, they have been used by Hartmann and von Sivers [80] with a *variable maximum speed*, which acts as a parameter structuring internally the crowd. Regarding specifically the experimental literature for pedestrian flow, we mention, among others, the papers by Daamen and Hoogendoorn [53], Seyfried et al. [158], Helbing et al. [87], Venuti and Bruno [162], and Schadschneider and Seyfried [156], where several experiments and comparisons are performed.

Section 4.2.2 The *Coscia and Canavesio's model* was introduced in [43] in 2008. The paper presents also several combinations of existing models. The idea of the *fictitious density* was introduced by De Angelis in [57].

Section 4.2.3 The *Colombo and Rosini's model* was first introduced in [41] in 2005. A more complete study is presented in 2009 by the same authors [42] and then further expanded in the book by Rosini [153]. The paper by Helbing et al. [87] confirmed experimentally the particular shape of the fundamental diagram.

Section 4.2.4 The *Maury et al.'s model* was introduced in [120] in 2010. One year later, Maury et al. [121] extensively compared this model with its microscopic counterpart (see Sect. 4.1.2). In both papers it is pointed out that the two models can have different bahavior in particular situations. In [121] the authors proposed an interesting nonstandard micro-macro approach for the numerical solution of the equation with the projection operator.

Section 4.2.5 *Nonlocal models* were introduced by several authors. The model (4.11)–(4.12) was investigated by Colombo et al. [38] in 2012 from the theoretical and numerical point of view. The choice described in (4.13) is used, for example, by Cristiani et al. [48] in 2011 and by Bruno et al. [26] in a civil-engineering-oriented context. It is inspired by the biological literature for swarms, flocks, schools, or herds. We refer to Mogilner et al. [124] and references therein for an accurate investigation of the nature of mutual interactions that lead to clustering, uniform spacing, and self-avoidance of the agents. The delocalization technique described in (4.14) is used by Piccoli and Tosin [144, 145], and by Bruno et al. [27]. Colombo et al. [39] study a nonlocal model in the framework of a control problem, aiming at finding initial conditions for the density such that it remains under a given threshold for all times.

Section 4.2.6 The *Bellomo and Dogbé's model* was introduced in [15] in 2008. Equation (4.17) with the closure relation (4.18) first appeared in 2006 in the paper by Al-nasur and Kachroo [3], together with its derivation from a microscopic follow-the-leader model and a finite volume approximation. Jiang et al. [106] introduced in 2010 a two-dimensional generalization of the Payne-Whitham macroscopic model coupled with the eikonal equation for the path choice strategy. Further references for second order fluid dynamic models are the papers by Bellomo and Bellouquid [14], Bellomo and Dogbé [16], and Bellomo

et al. [17]. A numerical approach for solving Eqs. (4.7a), (4.7b) complemented with Eq. (4.15) can be found in Dogbé [63].

Section 4.3 Concerning *mesoscopic models* in general, at present there are actually few contributions in the literature dedicated to crowds. Kinetic approaches seem to be much more developed for problems of swarm dynamics, see e.g., Carrillo et al. [33] and Ha and Tadmor [78]. Probably the very first attempt to describe crowd dynamics from a kinetic point of view is due to Henderson [91] in 1974, who points out some analogies between crowds and molecular systems of classical gas dynamics. Then, he postulates that in some circumstances conservation laws of mass, momentum, and kinetic energy can be applied to human flow and then that the Boltzmann transport equation is applicable. See also the more recent paper by Hoogendoorn and Bovy [94].

Section 4.3.1 The *Dogbé's model* was proposed in [65] in 2012.

Section 4.3.2 The *Bellomo and Bellouquid's model* was introduced in [14] in 2011. Notice that the effect of the microscopic granularity is taken into account only in the distribution of the velocity, while the other variable identifying the microstate of pedestrians, namely the position, is left continuous. Recently, a fully-discrete-state kinetic approach to the modeling of stochastically interacting agents has been proposed by Fermo and Tosin [70, 71] for vehicular traffic, in order to take into account also the impact of the granular spatial distribution of vehicles on the global traffic flow.

Section 4.4.1 The *Arechavaleta et al.'s model* was introduced in [9] in 2008. This model was designed using laboratory experiments. An inverse problem approach was used to determine the cost function which would generate the observed trajectories as optimal ones. The same approach was also followed in the recent paper by Chitour et al. [35].

Section 4.4.2 The *Hoogendoorn and Bovy's microscopic model* was introduced in [95] in 2003.

Section 4.4.3 With regards to the *eikonal equation* and Hamilton-Jacobi-Bellman equations in the framework of minimum time and optimal control problems, a comprehensive discussion can be found in the book by Bardi and Capuzzo Dolcetta [13]. The interested reader is also referred to Cristiani [45]. For numerical aspects we refer to the recent book by Falcone and Ferretti [69]. For the issue of reconstructing optimal controls and optimal trajectories, using the gradient of the viscosity solution to the Hamilton-Jacobi-Bellman equation, we refer to the book by Bressan and Piccoli [25] and to Piccoli and Sussmann [143].

Section 4.4.4 The *Hughes' model* was (very) briefly introduced in [101] in 2000 and then detailed by the same author in [102] in 2002. The interpretation of the model in terms of minimum time problem was pointed out by Huang et al. [100] in 2009, who also propose a numerical method to solve the associated equations. The one-dimensional version of the model was theoretically investigated by Di Francesco et al. [62], Amadori and Di Francesco [4], El-Khatib et al. [68], and Goatin and Mimault [73]. A second order version of a Hughes-like model was proposed by Twarogowska et al. [161].

Section 4.4.5 The *Hoogendoorn and Bovy's macroscopic model* was introduced in 2004 in the notable paper [96]. See also the preliminary paper [97]. In its original version, the optimal control problem is based on the finite-horizon formulation. The minimum-time version of such problem was proposed by Cristiani et al. [50] for a nonlocal model which is not based on fundamental diagrams.

Section 4.4.6 The *mean field game* approach for the study of crowd motion was investigated by Dogbé [64] in 2010 and by Lachapelle and Wolfram [115] in 2011 (see also the Ph.D. thesis by Lachapelle [114]). We refer to the long paper by Guéant et al. [77] and references therein for an overview of mean field game theory and its applications. Recently, Burger et al. [28] proposed a mean field game model specifically conceived for evacuation problems, in the spirit of the Hughes' model.

Section 4.4.7 The *dynamic continuum model with memory effect* was investigated by Xia et al. [173]. The *hybrid model* was proposed by Cristiani et al. [50], together with a classification of crowd models on the basis of their rationality degree. In addition, the authors solve a challenging shape optimization problem which consists in controlling the environment in such a way that the normal behavior is as close as possible to the rational one.

# Chapter 5
# Multiscale Modeling by Time-Evolving Measures

**Abstract** This chapter is devoted to a multiscale approach to the modeling of crowd dynamics, which is the core topic of the book. We begin by presenting, in Sect. 5.1, a general measure-based modeling framework suitable to include the basic features of pedestrian kinematics at any scale. Specifically, we assume that pedestrian motion results from the interplay between the individual will to follow a preferred travel program and the necessity to face the rest of the crowd. We discuss in Sect. 5.2 how to properly model these behavioral aspects. In Sect. 5.3 we show how discrete (microscopic) and continuous (macroscopic) models can be obtained in the proposed framework, before focusing, in Sect. 5.4, on multiscale modeling issues. We also propose a detailed dimensional analysis, which highlights the role of a few significant parameters, and a numerical scheme for the approximate solution of the equations. The scheme is obtained in two steps in Sect. 5.5. First we derive a discrete-in-time model; next we discretize the space variable as well, obtaining an algorithm (cf. Appendix B) which can be implemented on a computer to produce simulations (cf. Chap. 2). Finally, in Sect. 5.6 we extend the previous modeling structures to the case of two interacting crowds.

## 5.1 Conservation Laws by Time-Evolving Measures

The key idea of the multiscale approach is to describe the distribution of pedestrians in space through their mass, represented by an *abstract measure*. By measure we intend a mapping which associates to (some) subsets of the physical space $\mathbb{R}^d$ a (nonnegative) real number. The reader can find in Appendix A an introduction to the mathematical measure theory, and to its jargon, which we extensively use in what follows.

*Remark 5.1.* Although in this chapter we refer exclusively to human crowds, the modeling structures we present are suitable for application to a variety of other systems of mobile interacting agents, as discussed in Sect. 1.4.2. Therefore, the

E. Cristiani et al., *Multiscale Modeling of Pedestrian Dynamics*, MS&A 12,
DOI 10.1007/978-3-319-06620-2_5,

modeling framework is presented for a generic dimension $d$ of the physical space, which in most practical applications will be 1, 2, or 3.

We model the mass of a crowd at time $t \geq 0$ as a Radon positive measure $\mu_t$ defined on the Borel $\sigma$-algebra $\mathscr{B}(\mathbb{R}^d)$. For every measurable subset $E$ of $\mathbb{R}^d$, i.e., $E \in \mathscr{B}(\mathbb{R}^d)$, the number $\mu_t(E) \geq 0$ represents the mass of pedestrians contained in $E$ at time $t$. It is worth noticing that these are very general assumptions: In principle, the only real assumption on $\mu_t$ at this stage is $\sigma$-additivity, which directly translates the principle of additivity of the mass.

*Remark 5.2.* Like in the rest of the book, we will use the subscript $t$ to indicate that a certain measure depends on (or is parameterized by) time. In particular, this notation will *not* denote the partial derivative with respect to $t$, for which we will write instead $\frac{\partial}{\partial t}$.

Together with the $\sigma$-additivity principle, we will apply the *principle of conservation of mass*, stating that the mass of a set $E$ can vary in time only because of inflow or outflow of mass from the boundary $\partial E$. In an Eulerian frame of reference, this is expressed by the equation

$$\frac{\partial \mu_t}{\partial t} + \nabla \cdot (\mu_t v) = 0, \tag{5.1}$$

where $v : [0, +\infty) \times \mathbb{R}^d \to \mathbb{R}^d$, $v = v(t, x)$, is the velocity field which transports the mass. For the moment, we regard it as a generic function, ultimately depending on space and time. However, the way in which such a dependence is implemented may involve (and, in fact, in our model it will, cf. Sect. 5.2) the measure $\mu_t$ itself.

We recall that choosing an Eulerian point of view means referring the space coordinate $x$ to the current configuration of the system and looking at what happens in the geometrical point $x$ as the system evolves. Therefore, quantities computed in $x$ do not always refer to the same particle of the system as time goes by, but rather to the particle which is flowing through $x$ at the current time instant (namely, a different particle from time to time). We anticipate that in Sect. 5.5, with reference to discrete-in-time models, we will see how the conservation law (5.1) can be stated in a Lagrangian frame.

Derivatives as they appear in (5.1) are only formal and must be correctly understood in the functional sense of measures. For this, we consider each term of (5.1) as a distribution acting on a test function $\phi \in C_c^\infty(\mathbb{R}^d)$, so that for a.e. $t$ we have

$$\frac{d}{dt} \int_{\mathbb{R}^d} \phi(x)\, d\mu_t(x) = \int_{\mathbb{R}^d} v(t, x) \cdot \nabla \phi(x)\, d\mu_t(x), \tag{5.2}$$

where integration-by-parts has been used at the right-hand side, along with the compactness of the support of $\phi$ which drops the boundary term.

A family of time-evolving measures $\{\mu_t\}_{t>0}$ is then said to be a *weak solution* (or a solution in the sense of measures) to (5.1) if the mapping

$$t \mapsto \int_{\mathbb{R}^d} \phi(x)\, d\mu_t(x)$$

is absolutely continuous and satisfies (5.2) for all $\phi \in C_c^\infty(\mathbb{R}^d)$ and a.e. $t$. In particular, by integrating (5.2) between any two times $0 \le t_1 \le t_2$, the latter statement means that $\mu_t$ satisfies

$$\int_{\mathbb{R}^d} \phi(x)\, d\mu_{t_2}(x) = \int_{\mathbb{R}^d} \phi(x)\, d\mu_{t_1}(x) + \int_{t_1}^{t_2} \int_{\mathbb{R}^d} v(t,\, x) \cdot \nabla\phi(x)\, d\mu_t(x)\, dt \quad (5.3)$$

for all $\phi \in C_c^\infty(\mathbb{R}^d)$.

From (5.3) we can check that the modeling framework just depicted actually accounts for mass conservation. Assume indeed that there is a compact measurable set $\Omega \in \mathscr{B}(\mathbb{R}^d)$ such that $\mathrm{supp}(\mu_t) \subset \Omega$ for all $t \in [0,\, t_2]$ and choose a test function $\phi$ with $\phi \equiv 1$ in $\Omega$. Thus

$$\int_{t_1}^{t_2} \int_{\mathbb{R}^d} v(t,\, x) \cdot \nabla\phi(x)\, d\mu_t(x)\, dt = \int_{t_1}^{t_2} \int_{\Omega} v(t,\, x) \cdot \nabla\phi(x)\, d\mu_t(x)\, dt = 0$$

for all $t \in [t_1,\, t_2]$ because $\mu_t$ is zero in $\mathbb{R}^d \setminus \Omega$ and $\phi$ is constant in $\Omega$. But then (5.3) implies $\mu_{t_1}(\Omega) = \mu_{t_2}(\Omega)$, hence if no mass flows out of $\Omega$ the measure of the latter is conserved in time. The above computations also suggest that the double integral at the right-hand side of (5.3) accounts for the variation of the mass of measurable sets due to incoming/outgoing flux.

We defer to Chap. 6 a detailed theory of existence of weak solutions to (5.1). In this chapter we focus instead on modeling aspects, noting that (5.1) provides the spatiotemporal evolution of the measure $\mu_t$ as long as the velocity $v$ is specified. The forthcoming section is thus devoted to constructing $v$ from the reasonings about pedestrian behavior developed in the first part of the book. In particular, (5.1) will result in a self-consistent model for $\mu_t$ by expressing $v$ in terms of $\mu_t$ itself, hence our approach will give rise to first order modeling structures (see Remark 4.1 for a discussion about first vs second order models).

## 5.2 Velocity from Planning and Interactions

We assume that the velocity at time $t$ depends on the space $x$ and on the measure $\mu_t$ as

$$\begin{aligned} v(t,\, x) &= v[\mu_t](x) \\ &= v_{\mathrm{d}}(x) + v_{\mathrm{i}}[\mu_t](x), \end{aligned} \quad (5.4)$$

where the square brackets denote functional relationship with $\mu_t$. Notice that in (5.4) it is tacitly assumed that $v$ depends on time through $\mu_t$ only, i.e., that the system we are dealing with is autonomous.

Equation (5.4) decomposes the velocity into two terms detailed in what follows.

### 5.2.1 Desired Velocity

The function $v_\mathrm{d} : \mathbb{R}^d \to \mathbb{R}^d$ is the *desired velocity*, i.e., the velocity that pedestrians would set to reach their destination if they did not experience mutual interactions (see Sect. 1.1.1). In the simplest case it is a constant field, whereas in more complicated situations it accounts for the presence of possible obstacles to be bypassed. In the modeling framework described below, we assume that pedestrians already know from previous experiences the environment in which they move, hence the desired velocity is set a priori on the basis of the geometry of the walking area only. For this reason, the field $v_\mathrm{d}$ is time-independent. We assume $v_\mathrm{d}$ be a *conservative velocity field*, i.e. $v_\mathrm{d}$ is derived as the (possibly normalized) gradient of a scalar potential $u$:

$$v_\mathrm{d} = \nabla u \qquad \text{or} \qquad v_\mathrm{d} = \frac{\nabla u}{|\nabla u|}, \tag{5.5}$$

satisfying Laplace's equation in the spatial domain $\Omega \subset \mathbb{R}^d$ of the problem:

$$\Delta u = 0 \quad \text{in } \Omega. \tag{5.6}$$

Suitable boundary conditions on $\partial\Omega$ have to be joined to this equation in order for $v_\mathrm{d}$ to point toward pedestrian destinations while bypassing obstacles and avoiding perimeter walls. For instance, one can prescribe Dirichlet boundary conditions such that $u = 1$ on those portions of $\partial\Omega$ coinciding with pedestrian targets (e.g., exits) and $u = 0$ on the remaining parts of $\partial\Omega$. In such a way, owing to the maximum principle for elliptic equations, it results $0 \le u \le 1$ a.e. in $\Omega$, thus $\nabla u$ flows from the minimum $u = 0$ to the maximum $u = 1$ and one gets a desired velocity field actually pointing smoothly toward pedestrian destinations. The idea underlying this choice is to mimic a simplified dynamics of a fluid entering the domain and then flowing out through the exits.

Obstacles can be managed in a similar way, setting $u = 0$ on their boundaries. Alternatively, at the obstacle boundaries one might replace the Dirichlet condition with the Neumann one $\nabla u \cdot \hat{n} = 0$, where $\hat{n}$ is the outward normal unit vector. According to (5.5), this amounts to setting to zero the normal component of $v_\mathrm{d}$ at the obstacle walls. If along the perimeter walls one still prescribes the Dirichlet condition $u = 0$, then again the maximum principle asserts that $u$ ranges essentially between 0 and 1 in $\Omega$, so that the direction of $\nabla u$ is the convenient one for $v_\mathrm{d}$ as discussed before.

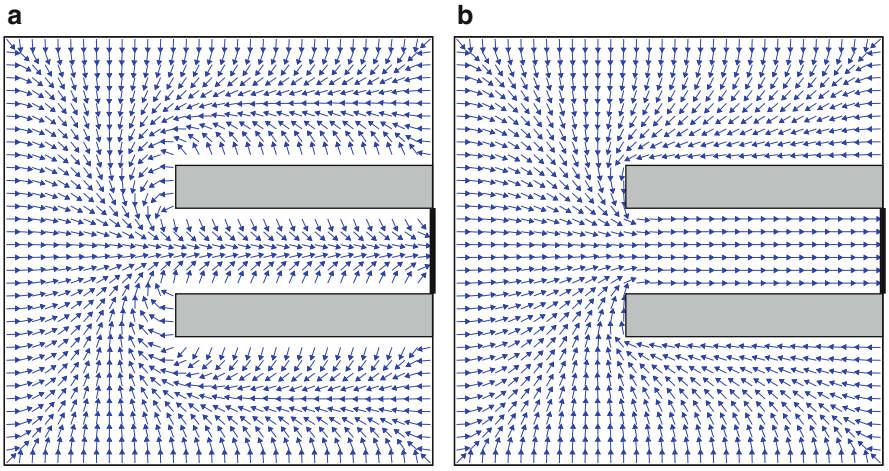


**Fig. 5.1** Desired velocity field $v_{\mathrm{d}}$ computed in a square domain with two obstacles using (5.5)–(5.6) supplemented by (**a**) Dirichlet and (**b**) Neumann boundary conditions at the obstacle walls. The target of walkers is the *thick black* portion of the right vertical edge of the domain, where a unit potential is imposed

Choosing either set of boundary conditions affects, often in a non-negligible manner, the topological properties of the resulting field $v_{\mathrm{d}}$ and the corresponding pedestrian dynamics as well. Figure 5.1 shows an example of desired velocity field generated with Dirichlet (Fig. 5.1a) and Neumann (Fig. 5.1b) boundary conditions at the obstacles. In the former case, pedestrians experience a repulsion from the obstacle walls, whereas, in the latter case, they are allowed to slide tangentially to the obstacle edges. As a result, a different access to the available space is induced. Therefore, the selection of boundary conditions is a real modeling task, which requires a careful consideration of the pedestrian behavior to be described.

### 5.2.2 *Interaction Velocity*

The function $v_{\mathrm{i}}[\mu_t] : \mathbb{R}^d \to \mathbb{R}^d$ is the *interaction velocity*, that is, the correction that pedestrians make to their desired velocity in consequence of the interactions. The *non-locality* of the interactions is introduced in this framework by deriving $v_{\mathrm{i}}[\mu_t]$ from a synthesis of the information on the crowd distribution around each pedestrian. Specifically, we assume

$$v_{\mathrm{i}}[\mu_t](x) = \int_{\mathbb{R}^d \setminus \{x\}} f(|y-x|) g(\alpha_{xy}) \frac{y-x}{|y-x|} \, d\mu_t(y), \tag{5.7}$$

where:

- $f : \mathbb{R}_+ \to \mathbb{R}$ is a function describing the interaction strength felt by the walker in $x$ according to the distance from her neighbors. If $\mathrm{supp}(f) = [0,\ R]$ for some $R > 0$, then a neighborhood is defined for the point $x$ in which the integral is actually computed, coinciding with the ball $B_R(x)$.
- $\alpha_{xy} \in [-\pi,\ \pi]$ is the angle between the vectors $y - x$ and $v_{\mathrm{d}}(x)$, that is, the angle under which a point $y$ is seen from $x$ with respect to the desired direction of motion.
- $g : [-\pi,\ \pi] \to [0,\ 1]$ is a function which reproduces the angular focus of the walker in $x$.

Integration with respect to $\mu_t$ accounts for the mass that the walkers see, considering that two fundamental attitudes characterize their behavior, cf. Sect. 1.1.1:

- *Repulsion*, i.e., the tendency to avoid collisions and crowded areas.
- *Attraction*, i.e., the tendency, under some circumstances, to keep contact with other group mates (e.g., groups of tourists in guided tours, groups of people sharing specific relationships such as families or parties).

The following prototypes can be suggested for the repulsion strength $f$:

$$f(z) = \begin{cases} -\dfrac{F_r}{z} & \text{if } 0 \le z \le R_r \\ 0 & \text{otherwise} \end{cases} \quad \text{for repulsion}$$
$$f(z) = \begin{cases} F_a z & \text{if } 0 \le z \le R_a \\ 0 & \text{otherwise} \end{cases} \quad \text{for attraction,} \tag{5.8}$$

where $F_r,\ F_a > 0$ are interaction parameters, and $R_r,\ R_a > 0$ are repulsion and attraction radii: Pedestrians are sensitive (i.e., they are repulsed or attracted) to the crowd mass closer than the given radius. These forms of $f$ translate the basic idea that repulsion and attraction are inversely and directly proportional, respectively, to the distance separating the interacting pedestrians. If repulsion and attraction are simultaneously active, then $v_{\mathrm{i}}[\mu_t]$ is given by the sum of two integrals of the form (5.7), one for either expression of $f$.

The function $g$ carries instead the *anisotropy* of the interactions, which essentially consists in that pedestrians cannot see all around them and are not equally sensitive to external stimuli coming from different directions. If $\bar{\alpha} \in [0,\ \pi]$ is the maximum sensitivity angular width, a prototype for $g$ is

$$g(\alpha) = \begin{cases} 1 & \text{if } -\bar{\alpha} \le \alpha \le \bar{\alpha} \\ 0 & \text{otherwise} \end{cases} \quad \text{for } \alpha \in [-\pi,\ \pi]. \tag{5.9}$$

By differentiating $\bar{\alpha}_r$, $\bar{\alpha}_c$ for repulsion and attraction, respectively, it is also possible to distinguish between different anisotropies due to the different nature of the two kinds of interaction, cf. Sect. 1.1.1.

*Remark 5.3.* The model for the velocity field considered here does not make use of the Fundamental Diagram, see Sect. 4.2.1. The dependence of the speed on the crowd density is handled directly by formula (5.7).

*Remark 5.4.* Suitable conditions on $f$, $g$ must be guaranteed in order for the integral in (5.7) to be well defined, usually integrability and/or continuity conditions. We refrain from entering here these issues, which will be extensively dealt with in Chap. 6. However, we stress that, in this respect, (5.8), (5.9) have to be regarded as prototypic examples, which catch some physiology but need proper adjustments in order to match analytical requirements. For instance, one may cut off the singularity producing an infinite repulsion at $z = 0$ by modifying the first expression in (5.8) as

$$f(z) = \begin{cases} -\dfrac{F_r}{\epsilon} & \text{if } 0 \le z \le \epsilon \\ -\dfrac{F_r}{z} & \text{if } \epsilon < z \le R_r \\ 0 & \text{otherwise} \end{cases}$$

where $0 < \epsilon < R_r$ is a parameter. On the other hand, the function (5.9) can be duly mollified about $\alpha = \pm\bar{\alpha}$ as

$$g(\alpha) = \begin{cases} e^{-\frac{\eta\alpha^2}{\bar{\alpha}^2-\alpha^2}} & \text{if } -\bar{\alpha} < \alpha < \bar{\alpha} \\ 0 & \text{otherwise} \end{cases}$$

where $\eta > 0$ is a parameter, which enables one to account also for the visual fading that usually occurs laterally in the visual field when approaching the maximum angular width.

If, as in the previous examples, $\mathrm{supp}(f)$ is compact and $g$ is an even function, then the domain of integration in (5.7) is actually a bounded subset $\mathscr{S}_R(x)$ of the ball $B_R(x)$ called *sensory region* or *neighborhood of interaction* of the point $x$. Confining our attention to the two-dimensional case ($d = 2$), $\mathscr{S}_R(x)$ is more precisely a sector of $B_R(x)$ with angular width $2\bar{\alpha}$ (cf. Fig. 5.2), coinciding with the whole ball for $\bar{\alpha} = \pi$ (isotropic interactions). When $\bar{\alpha} < \pi$ (anisotropic interactions), the orientation of $\mathscr{S}_R(x)$ must instead be specified. From the definition of the angle of interaction $\alpha_{xy}$, the reader can easily verify that, in practice, $\mathscr{S}_R(x)$ is symmetric with respect to the direction individuated by $v_\mathrm{d}(x)$. Hence we can provide the explicit definition:

$$\mathscr{S}_R(x) = \left\{ y \in \mathbb{R}^2 \,:\, |y - x| \le R,\ \frac{(y-x)\cdot v_\mathrm{d}(x)}{|y-x|\cdot|v_\mathrm{d}(x)|} \ge \cos\bar{\alpha} \right\}, \tag{5.10}$$

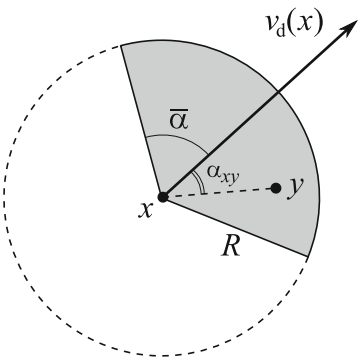


**Fig. 5.2** The interaction neighborhood $\mathscr{S}_R(x)$ (*gray set*) with radius $R$ and angular width $2\bar{\alpha}$, oriented according to the desired velocity $v_d(x)$

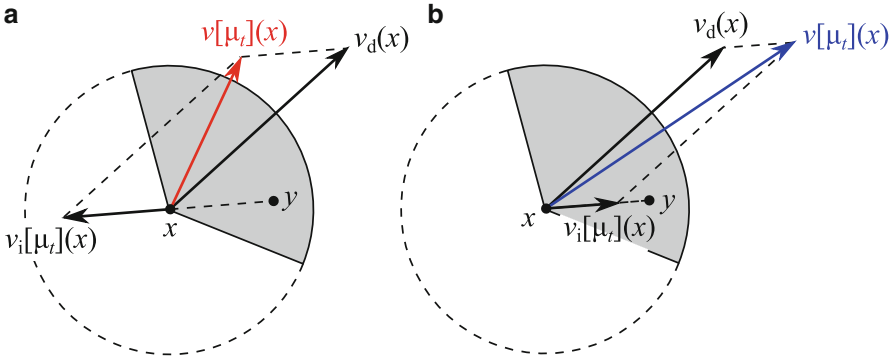


**Fig. 5.3** The total velocity $v[\mu_t]$ of the test pedestrian in $x$ computed for (**a**) repulsion and (**b**) attraction in the sample case of an interaction with one field pedestrian in $y$

the dot between two vectors standing for the Euclidean inner product. In the following we drop the subscript $R$ from the notation $\mathscr{S}_R(x)$ if not explicitly requested by the context. Notice that the vector $v_d(x)$ is used to define the direction of the anisotropy in $x$. From the point of view of pedestrians, this means distinguishing what is ahead and what is behind.

With reference to (5.7), it is useful to introduce a specific nomenclature for the individual in $x$, who undergoes the interactions, and pedestrians distributed in the points $y$ of the neighborhood $\mathscr{S}(x)$, who cause the interactions. Mimicking the terminology adopted in the kinetic theory for active particles, in the sequel we will call them *test pedestrian* and *field pedestrians*, respectively. Figure 5.3 represents the computation of the interactions between test and field pedestrians as the vector sum of the desired and the interaction velocities.

### 5.2.3 Metric and Topological Interactions

As discussed in Sect. 1.1.1, a further classification of pedestrian interactions, complementary to the distinction between repulsion and attraction, consists in characterizing them as *metric* or *topological*.

An interaction is *metric* if the radius $R$ of the corresponding neighborhood of interaction is set on the basis of a fixed maximal distance at which pedestrians feel comfortable to interact with other walkers. Consequently, the test pedestrian will interact with all field pedestrians comprised in $\mathscr{S}_R(x)$, no matter how many they are.

Conversely, an interaction is *topological* if the radius $R$ is tuned by the test pedestrian in such a way that her neighborhood $\mathscr{S}_R(x)$ encompasses a predefined mass of field pedestrians she agrees to interact with. If $\mathscr{M} > 0$ is such a mass of field pedestrians, $R$ is in particular the smallest radius necessary for finding at least the mass $\mathscr{M}$ in the interaction neighborhood:

$$R = \min\{r > 0 : \mu_t(\mathscr{S}_r(x)) \geq \mathscr{M}\}, \tag{5.11}$$

where $\{\mathscr{S}_r(x)\}_{r>0}$ is a family of sets defined as in (5.10). Notice that $R$ becomes now a function of $x$ and indirectly also of $t$ through the functional dependence on the measure $\mu_t$: $R = R[\mu_t](x)$.

*Remark 5.5.* In (5.11) we prefer the condition $\mu_t(\mathscr{S}_r(x)) \geq \mathscr{M}$ to the perhaps more intuitive one $\mu_t(\mathscr{S}_r(x)) = \mathscr{M}$ because in the latter case existence of the minimum might fail. For instance, this can happen, depending on the value of $\mathscr{M}$, if $\mu_t$ has some atoms, two or more of which at the same distance from $x$.

It is plain that, for particular choices of $\mathscr{M}$, the above definition may allow $R \to \infty$. In order to rule this possibility out, a topological interaction with *metric cutoff* can be devised, in which the radius topologically determined via (5.11) cannot however exceed a predefined maximal threshold $\bar{R} > 0$:

$$R = \min\{\min\{r > 0 : \mu_t(\mathscr{S}_r(x)) \geq \mathscr{M}\}, \bar{R}\}. \tag{5.12}$$

This choice, physically more meaningful, means that the test pedestrian might not be affected by very far field pedestrians e.g., because she cannot see them at all.

As we have seen in Chaps. 1 and 2, repulsion can be regarded as a metric interaction while attraction as a topological one, possibly with metric cutoff. Thus, in (5.8) the radius $R_r$ is a model parameter, whereas the radius $R_a$ should be computed by means of either (5.11) or (5.12).

## 5.3 Recovering Single-Scale Models

The framework consisting of (5.1), (5.4) is suitable to obtain, as particular cases, classical spatially discrete and continuous models, that, in analogy with the literature reviewed in Chap. 4, will be also referred to as *microscopic* and *macroscopic*,

respectively. In this section we discuss the procedure for their individual derivation, then in the subsequent section we exploit the tools offered by the measure-theoretic setting in order to merge these concepts into a unique *multiscale* model, in which the discrete and the continuous dynamics coexist.

### 5.3.1 Microscopic Models

Microscopic models aim at catching the evolution of single pedestrians, hence they are based on a discrete-in-space structure of the mass $\mu_t$. From the measure-theoretic point of view, this corresponds to assuming that the measure $\mu_t$ is *atomic* and that the whole mass is concentrated in a finite number of points, understood as the spatial positions of pedestrians.

Let us consider a population of $N$ pedestrians, whose positions at time $t$ are denoted by $\{X^k(t),\, k = 1, \dots, N\}$. Let us also denote by $\{x^k(t),\, k = 1, \dots, N\}$ the geometric points on which the pedestrian mass is concentrated, i.e. the *atoms* of the measure $\mu_t$. In this case, the mass of a set $E \in \mathscr{B}(\mathbb{R}^d)$ is the number of pedestrians contained in $E$:

$$\mu_t(E) = \mathrm{card}\{x^k(t) \in E\},$$

hence $\mu_t$ is the counting measure. We represent it as a sum of Dirac masses, each centered in one of the $x^k(t)$'s:

$$\mu_t = \sum_{k=1}^{N} \delta_{x^k(t)}. \tag{5.13}$$

Plugging this in (5.2) with $v(t,\, x) = v[\mu_t](x)$ gives

$$\frac{d}{dt} \sum_{k=1}^{N} \phi(x^k(t)) = \sum_{k=1}^{N} v[\mu_t](x^k(t)) \cdot \nabla\phi(x^k(t)), \tag{5.14}$$

whence, taking the time derivative at the left-hand side and rearranging the terms,

$$\sum_{k=1}^{N} \left[\dot{x}^k(t) - v[\mu_t](x^k(t))\right] \cdot \nabla\phi(x^k(t)) = 0.$$

The arbitrariness of the test function $\phi$ implies

$$\dot{x}^k(t) = v[\mu_t](x^k(t)), \qquad k = 1, \dots, N, \tag{5.15}$$

therefore the microscopic model specializes in an autonomous dynamical system of $N$ coupled ordinary differential equations for the $x^k(t)$'s, the coupling being realized by the measure $\mu_t$ in the velocity field. In particular, the right-hand side of (5.15) reads

$$v[\mu_t](x^k(t)) = v_{\mathrm{d}}(x^k(t)) + \sum_{\substack{h=1,\dots,N \\ x^h(t)\neq x^k(t)}} f(|x^h(t)-x^k(t)|)g(\alpha_{x^k(t)x^h(t)})\frac{x^h(t)-x^k(t)}{|x^h(t)-x^k(t)|}, \tag{5.16}$$

where the second term at the right-hand side is nothing but $v_{\mathrm{i}}[\mu_t](x^k(t))$ computed from (5.7) with the measure (5.13).

*Remark 5.6.* We point out that, with the function $f$ given by (5.8), the statement $x^h(t) \neq x^k(t)$ in the above formula can be converted into the milder one $h \neq k$. Indeed one can prove that if the $x^k(t)$'s are initially all distinct they remain distinct at all successive times $t > 0$.

*Remark 5.7.* In the following we will drop the distinction between the points $x^k(t)$ and $X^k(t)$, which is basically conceptual, and we will denote both the atoms of the measure $\mu_t$ and the agents' positions by $X^k(t)$. In this way (5.15) assumes the classical form of a first order differential model, see, for example, (4.5).

### 5.3.2 Macroscopic Models

Macroscopic models describe the average distribution of the crowd rather than looking at individual pedestrians, therefore they rely on a continuous-in-space structure of the mass $\mu_t$. Technically, they are based on the assumption that *the matter is continuous*, which means that there is proportionality between the mass and the volume of an infinitesimal reference volume $dx$. This translates, in measure-theoretic terms, as the measure $\mu_t$ being absolutely continuous with respect to the $d$-dimensional Lebesgue measure $\mathscr{L}^d$. Under this hypothesis, Radon-Nikodym's Theorem asserts that there exists a function $\rho(t,\cdot) \in L^1_{\mathrm{loc}}(\mathbb{R}^d)$ such that

$$\rho(t,x) = \lim_{r\to 0+} \frac{\mu_t(B_r(x))}{\mathscr{L}^d(B_r(x))} \quad \text{for a.e. } x \in \mathbb{R}^d,$$

called the *density* of $\mu_t$ with respect to $\mathscr{L}^d$. In our context $\rho(t,x)$ represents the density of pedestrians at time $t$ in the point $x$. Notice that $\rho(t,x) \geq 0$ because $\mu_t$ is, by assumption, a positive measure.

Using $\rho$ we have

$$\mu_t = \rho(t,\cdot)\mathscr{L}^d, \tag{5.17}$$

hence the mass conservation equation (5.2) with $v = v[\rho]$ rewrites as

$$\frac{d}{dt}\int_{\mathbb{R}^d} \phi(x)\rho(t,\,x)\,dx = \int_{\mathbb{R}^d} v[\rho](t,\,x)\cdot\nabla\phi(x)\rho(t,\,x)\,dx, \tag{5.18}$$

namely a weak form of the continuity equation

$$\frac{\partial\rho}{\partial t} + \nabla\cdot(\rho v[\rho]) = 0. \tag{5.19}$$

In particular, the velocity is computed from (5.7) with the measure (5.17):

$$v[\rho](t,\,x) = v_{\mathrm{d}}(x) + \int_{\mathbb{R}^d} f(|y-x|)g(\alpha_{xy})\frac{y-x}{|y-x|}\rho(t,\,y)\,dy, \tag{5.20}$$

hence the relationship between $v$ and $\rho$ is a functional dependence formally more elaborated than the pointwise dependence carried by fundamental diagrams in nonlinear hyperbolic conservation laws. On the other hand, this integral formulation is expected to have a smoothing effect on the solutions of the model.

## 5.4 Multiscale Model

After reobtaining classical microscopic and macroscopic models, now we indicate how to specialize the modeling framework in order to account simultaneously for discrete and continuous kinematic effects in the spatiotemporal evolution of crowds. In particular, we will derive a full range of representation scales, the microscopic and the macroscopic ones being the two endpoints. This will provide a multiscale description of crowds, allowing one, in particular, to include the effect of granularity in the continuous flow.

From the measure-theoretic point of view, we *interpolate* the discrete and continuous measures (5.13), (5.17), after renaming them as

$$m_t = \sum_{k=1}^{N}\delta_{X^k(t)}, \qquad M_t = \rho(t,\,\cdot)\mathscr{L}^d, \tag{5.21}$$

where the letters $m$, $M$ evoke the microscopic and the macroscopic scale, respectively. Specifically, the multiscale mass $\mu_t$ has the following form:

$$\mu_t = \theta m_t + (1-\theta)M_t, \tag{5.22}$$

the parameter $\theta \in [0,\,1]$ weighting the coupling between the two scales. Notice that $\theta = 0$ corresponding to a purely continuous model, whereas $\theta = 1$ corresponds to a purely discrete one.

Plugging the measure (5.22) in the mass conservation equation (5.2), with $v(t,\,x) = v[\mu_t](x)$, we get

$$\frac{d}{dt}\left(\theta\sum_{k=1}^{N}\phi(X^k(t)) + (1-\theta)\int_{\mathbb{R}^d}\phi(x)\rho(t,\,x)\,dx\right) =$$
$$\theta\sum_{k=1}^{N} v[\mu_t](X^k(t))\cdot\nabla\phi(X^k(t)) + (1-\theta)\int_{\mathbb{R}^d} v[\mu_t](x)\cdot\nabla\phi(x)\rho(t,\,x)\,dx, \tag{5.23}$$

formally an interpolation of (5.14), (5.18).

In strong form, the multiscale model can be thought of as convex linear combination, with coefficients $\theta$ and $1-\theta$, of the following equations:

$$\begin{cases} \dot{X}^k(t) = v[\mu_t](X^k(t)), \quad k = 1,\,\dots,\,N, \\ \dfrac{\partial\rho}{\partial t} + \nabla\cdot(\rho v[\mu_t]) = 0, \end{cases} \tag{5.24}$$

coupled by the transport velocity $v[\mu_t]$, which reads now

$$v[\mu_t](x) = v_{\mathrm{d}}(x) + \theta\sum_{\substack{k=1,\,\dots,\,N\\ X^k(t)\neq x}} f(|X^k(t)-x|)g(\alpha_{xX^k(t)})\frac{X^k(t)-x}{|X^k(t)-x|}$$
$$+ (1-\theta)\int_{\mathbb{R}^d} f(|y-x|)g(\alpha_{xy})\frac{y-x}{|y-x|}\rho(t,\,y)\,dy, \tag{5.25}$$

hence it coincides neither with the one of the fully discrete model, cf. (5.16), nor with the one of the fully continuous model, cf. (5.20). Rather, it comprises both discrete and continuous contributions to the interaction of the test pedestrian with field pedestrians.

Assume that the position $x$ of the test pedestrian coincides with one of the atoms of $\mu_t$, say $x = X^k(t)$. Then

$$v_{\mathrm{i}}[\mu_t](X^k(t)) = \theta\sum_{\substack{h=1,\,\dots,\,N\\ X^h(t)\neq X^k(t)}} f(|X^h(t)-X^k(t)|)g(\alpha_{X^k(t)X^h(t)})\frac{X^h(t)-X^k(t)}{|X^h(t)-X^k(t)|}$$
$$+ (1-\theta)\int_{\mathbb{R}^d} f(|y-X^k(t)|)g(\alpha_{X^k(t)y})\frac{y-X^k(t)}{|y-X^k(t)|}\rho(t,\,y)\,dy \tag{5.26}$$

hence the interaction velocity of the test pedestrian does not only depend on other discrete atoms of $\mu_t$ contained in her neighborhood of interaction (like in a purely

microscopic model) but also on the density distributed therein. In particular, the term

$$(1-\theta)\int_{\mathbb{R}^d} f(|y-X^k(t)|)g(\alpha_{X^k(t)y})\frac{y-X^k(t)}{|y-X^k(t)|}\rho(t,\,y)\,dy$$

is the continuous contribution to the discrete dynamics. Conversely, if the position of the test pedestrian does not coincide with any atom of $\mu_t$, then her interaction velocity does not only depend on the density distributed in her neighborhood of interaction (like in a purely macroscopic model) but also on the atoms of $\mu_t$ therein. Indeed, the term

$$\theta\sum_{\substack{k=1,\dots,N\\ X^k(t)\neq x}} f(|X^k(t)-x|)g(\alpha_{xX^k(t)})\frac{X^k(t)-x}{|X^k(t)-x|}$$

expresses in this case the discrete contribution to the continuous dynamics.

*Remark 5.8.* It is worth spending a few more words about the relationship between the discrete and the continuous scales in this multiscale coupling, especially when $\theta$ takes one of its extreme values.

According to (5.22), (5.23), for $\theta = 0$ or $\theta = 1$ the model is entirely formulated at one scale only, in the sense that neither the mass $\mu_t$ nor the evolution equation includes the other scale. For instance, for $\theta = 0$ the model is fully continuous and coincides with the macroscopic one described in Sect. 5.3. However, temporarily neglecting (5.23), we see from (5.26) that it is still possible to compute an interaction velocity for the points $X^k(t)$, determined uniquely by the density $\rho$:

$$v_{\mathrm{i}}[\rho(t,\,\cdot)](X^k(t)) = \int_{\mathbb{R}^d} f(|y-X^k(t)|)g(\alpha_{X^k(t)y})\frac{y-X^k(t)}{|y-X^k(t)|}\rho(t,\,y)\,dy.$$

Consequently, we can define a velocity for the $X^k(t)$'s as $v[\rho(t,\,\cdot)](X^k(t)) = v_{\mathrm{d}}(X^k(t)) + v_{\mathrm{i}}[\rho(t,\,\cdot)](X^k(t))$ and use it in (5.15). This way, we recover the classical method for tracking the trajectories of Lagrangian particles flowing passively in an Eulerian continuous medium, whose motion is known from independent calculations.

By far less classical is the situation for $\theta = 1$, when the model is fully discrete and coincides with the microscopic one described in Sect. 5.3. Equation (5.25) shows that it is still possible to compute a transport velocity for the distribution $\rho$, determined uniquely by the atoms $X^k(t)$'s:

$$v[\{X^k(t)\}_k](x) = v_{\mathrm{d}}(x) + \sum_{\substack{k=1,\dots,N\\ X^k(t)\neq x}} f(|X^k(t)-x|)g(\alpha_{xX^k(t)})\frac{X^k(t)-x}{|X^k(t)-x|}. \quad (5.27)$$

Using this in (5.19) we can compute a posteriori the spatiotemporal evolution of $\rho$ driven by the atoms $X^k(t)$'s.

For examples of a discrete dynamics ruled by a continuous one, and vice versa, we refer the reader to the numerical experiment on the shape of a crowd discussed in Sect. 2.2.

### *Dimensional Analysis and Scaling*

The multiscale coupling requires, as a major point, to scale correctly the discrete and continuous kinematic contributions. This issue leads ultimately to a dimensional analysis of the presented equations, that we will carry out by switching to the non-dimensional form of the model. For this, we preliminarily observe that the main quantities involved in the equations have the following dimensions:

- $[t]$ = time
- $[x]$ = length
- $[v] = [v_\mathrm{d}] = [v_\mathrm{i}]$ = length/time
- $[f]$ = length/(time $\times$ pedestrians)
- $[\mu_t]$ = pedestrians
- $[\rho]$ = pedestrians/length$^d$

where "pedestrians" is actually a dimensionless unit. Additionally, $g$ and $\theta$ are dimensionless. We let $L$, $V$, $\hat{\rho}$ be characteristic values of length, speed, and density, respectively. They are used to define the following non-dimensional variables and functions:

$$\begin{aligned}
&x^* = \frac{x}{L}, \quad t^* = \frac{V}{L}t, \\
&v_\mathrm{d}^*(x^*) = \frac{1}{V}v_\mathrm{d}(Lx^*), \quad v_\mathrm{i}^*[\mu_{t^*}^*](x^*) = \frac{1}{V}v_\mathrm{i}[\mu_{\frac{L}{V}t^*}](Lx^*), \\
&f^*(z^*) = \frac{1}{V}f(Lz^*), \\
&\rho^*(t^*, x^*) = \frac{1}{\hat{\rho}}\rho\left(\frac{L}{V}t^*, Lx^*\right), \quad X^{k,*}(t^*) = \frac{1}{L}X^k\left(\tfrac{L}{V}t^*\right).
\end{aligned} \tag{5.28}$$

In more detail, the infinitesimal non-dimensional mass measure $d\mu_{t^*}^*$ is given by

$$\begin{aligned}
d\mu_{t^*}^*(x^*) &= d\mu_{\frac{L}{V}t^*}(Lx^*) \\
&= \theta\sum_{k=1}^{N} d\,\delta_{LX^{k,*}(t^*)}(Lx^*) + (1-\theta)\hat{\rho}\rho^*(t^*, x^*)\,L^d\,dx^*
\end{aligned}$$

$$= \theta \sum_{k=1}^{N} d\delta_{X^{k,*}(t^*)}(x^*) + (1-\theta)\Lambda\rho^*(t^*, x^*)\, dx^*$$
$$= \theta\, dm^*_{t^*}(x^*) + (1-\theta)\Lambda\, dM^*_{t^*}(x^*)$$

where we have set

$$\Lambda := \hat{\rho} L^d \tag{5.29}$$

and we have recognized the dimensionless discrete and continuous masses:

$$m^*_{t^*} = \sum_{k=1}^{N} \delta_{X^{k,*}(t^*)}, \quad dM^*_{t^*}(x^*) = \rho^*(t^*, x^*)\, dx^*.$$

We notice that the coefficient $\Lambda$ has unit $[\Lambda]$ = pedestrians, therefore it is a non-dimensional number fixing the scaling between the discrete and the continuous mass. It says how many atoms a unit density in the infinitesimal reference volume $dx^*$ corresponds to, in average.

It is worth stressing that

$$\mu^*_{t^*} = \theta m^*_{t^*} + (1-\theta)\Lambda M^*_{t^*} \tag{5.30}$$

can be properly read as the interpolation between the discrete and the continuous masses only if $m^*_{t^*}(\mathbb{R}^d)$ and $M^*_{t^*}(\mathbb{R}^d)$ are, up to scaling, the *same* mass, i.e., provided $m^*_{t^*}(\mathbb{R}^d) = \Lambda M^*_{t^*}(\mathbb{R}^d)$. Since the multiscale model is based on mass conservation, and furthermore, as we will see in Chap. 6, the discrete and continuous masses are individually conserved in time, this requirement can be fulfilled by choosing the scaling parameter $\Lambda$ as

$$\Lambda = \frac{m^*_0(\mathbb{R}^d)}{M^*_0(\mathbb{R}^d)} = \frac{N}{M^*_0(\mathbb{R}^d)}, \tag{5.31}$$

$m^*_0(\mathbb{R}^d)$, $M^*_0(\mathbb{R}^d)$ being the initial discrete and continuous masses, respectively.

*Remark 5.9.* We will henceforth always refer to the non-dimensional form of the equations, omitting however the asterisks on the non-dimensional variables for brevity. Using (5.28), (5.29) the reader can convince herself that, in practice, all formulas written in Sect. 5.4 before this dimensional analysis remain formally the same, provided all quantities are understood as dimensionless and $\rho$ is replaced by $\Lambda\rho$ in the expressions of the interaction velocity.

## 5.5 Multiscale Numerical Scheme

In this section we propose a scheme for the numerical approximation of the multiscale model. A detailed analysis of convergence and error estimates will be proposed in Chap. 6. Here we focus instead on the formal derivation of the scheme from the measure-theoretic structures presented in the previous sections.

The construction of the scheme is organized in two steps. First we discretize the time variable, obtaining a discrete-in-time model in which a sequence of measures is recursively generated via a transport of mass at discrete time instants. Next, in order to approximate the continuous part of the mass, we discretize also the space variable, ending up with an iterative formula that can be implemented on a computer following the lines of the pseudo-code reported in Appendix B.

### *5.5.1 Discrete-in-Time Model*

Let us consider a finite time interval $[0,\ T]$, where $T > 0$ is some final time, and let us introduce over it the lattice

$$0 = t_0 < t_1 < \cdots < t_n < \cdots < t_{N_T} = T$$

with (possibly adaptive) time steps $\Delta t_n = t_{n+1} - t_n$, $n = 0, \ldots, N_T - 1$. Denoting $\mu_n := \mu_{t_n}$, and analogously $v_n(\cdot) := v(t_n, \cdot)$, if we collocate (5.3) between the points $t_n$ and $t_{n+1}$ we find

$$\begin{aligned}\int_{\mathbb{R}^d} \phi(x)\, d\mu_{n+1}(x) - \int_{\mathbb{R}^d} \phi(x)\, d\mu_n(x) &= \int_{t_n}^{t_{n+1}} \int_{\mathbb{R}^d} v(t,\, x) \cdot \nabla\phi(x)\, d\mu_t(x)\, dt \\ &= \Delta t_n \int_{\mathbb{R}^d} v_n(x) \cdot \nabla\phi(x) d\mu_n(x) + o(\Delta t_n),\end{aligned}$$

whence

$$\int_{\mathbb{R}^d} \phi(x)\, d\mu_{n+1}(x) = \int_{\mathbb{R}^d} (\phi(x) + \Delta t_n\, v_n(x) \cdot \nabla\phi(x))\, d\mu_n(x) + o(\Delta t_n).$$

To go on, let us explicitly assume that $\mu_n(\mathbb{R}^d) < +\infty$ and that $v_n$ is uniformly bounded. As we will see in Chap. 6, this is precisely the case with the velocity field (5.4), provided singularities in the interaction strength $f$ are cut off. Then Taylor's expansion gives $\phi(x) + \Delta t_n\, v_n(x) \cdot \nabla\phi(x) = \phi(x + \Delta t_n\, v_n(x)) + o(\Delta t_n)$, thus the previous calculation can be continued as

$$\int_{\mathbb{R}^d} \phi(x)\, d\mu_{n+1}(x) = \int_{\mathbb{R}^d} \phi(x + \Delta t_n\, v_n(x))\, d\mu_n(x) + o(\Delta t_n).$$

In order to obtain a computable equation, we must disregard the error term $o(\Delta t_n)$ at the right-hand side while still enforcing equality with the left-hand side. This way we slightly depart from the original equation and arrive at

$$\int_{\mathbb{R}^d} \phi(x)\, d\mu_{n+1}(x) = \int_{\mathbb{R}^d} \phi(\gamma_n(x))\, d\mu_n(x), \tag{5.32}$$

where we have defined the *flow map* $\gamma_n : \mathbb{R}^d \to \mathbb{R}^d$,

$$\gamma_n(x) := x + v_n(x)\Delta t_n.$$

Notice that, under the assumption $\mu_n(\mathbb{R}^d) < +\infty$ for all $n$, (5.32) does not only make sense for $\phi \in C_c^\infty(\mathbb{R}^d)$ but actually for every bounded and Borel test function. In particular, choosing $\phi = \mathbb{1}_E$ for some measurable set $E$ and observing that $\mathbb{1}_E(\gamma_n(x)) = \mathbb{1}_{\gamma_n^{-1}(E)}(x)$ we obtain

$$\mu_{n+1}(E) = \mu_n(\gamma_n^{-1}(E)), \quad \forall\, E \in \mathscr{B}(\mathbb{R}^d), \tag{5.33}$$

meaning that the measure $\mu_{n+1}$ is the *push forward* of $\mu_n$ via the flow map $\gamma_n$, also written $\mu_{n+1} = \gamma_n \# \mu_n$ (cf. Appendix A). In conclusion, if $\bar{\mu}$ is some prescribed initial condition, we have obtained the discrete-in-time model

$$\begin{cases} \mu_{n+1} = \gamma_n \# \mu_n, \quad n = 0, \ldots, N_T - 1 \\ \mu_0 = \bar{\mu}, \end{cases}$$

which recursively generates a sequence of measures $\{\mu_n\}_{n=1}^{N_T}$ approximating the mapping $t \mapsto \mu_t$ which solves (5.1).

*Remark 5.10.* The push forward $\mu_{n+1} = \gamma_n \# \mu_n$ expresses a conservative transport of mass under a Lagrangian point of view during each time step. Indeed, the space coordinate is referred to the starting configuration at time $t_n$, and the particle occupying the position $x$ is followed to its new position $\gamma_n(x)$ at the next time $t_{n+1}$.

In the multiscale framework, the measure $\mu_n$ has the structure

$$\mu_n = \theta m_n + (1 - \theta)\Lambda M_n,$$

where $m_n$, $M_n$ are the corresponding time discretization of the discrete and continuous masses $m_t$, $M_t$, respectively. Then the linearity of the push forward operator $\#\cdot$ entails

$$\mu_{n+1} = \theta(\gamma_n \# m_n) + (1 - \theta)\Lambda(\gamma_n \# M_n). \tag{5.34}$$

Let us examine in particular the first term at the right-hand side. If we represent $m_n$ as $m_n = \sum_{k=1}^N \delta_{X_n^k}$ with $X_n^k := X_{t_n}^k$, then we get $\gamma_n \# m_n = \sum_{k=1}^N \gamma_n \# \delta_{X_n^k}$. But the

measure $\gamma_n \# \delta_{X_n^k}$ is such that, for all $E \in \mathscr{B}(\mathbb{R}^d)$,

$$(\gamma_n \# \delta_{X_n^k})(E) = \delta_{X_n^k}(\gamma_n^{-1}(E)) = \begin{cases} 1 & \text{if } X_n^k \in \gamma_n^{-1}(E) \Leftrightarrow \gamma_n(X_n^k) \in E \\ 0 & \text{otherwise,} \end{cases}$$

hence it coincides actually with the measure $\delta_{\gamma_n(X_n^k)}$. It follows that

$$\gamma_n \# m_n = \sum_{k=1}^{N} \delta_{\gamma_n(X_n^k)}$$

is the discrete part $m_{n+1}$ of the mass $\mu_{n+1}$, the atoms of $\mu_n$ being transported in one time step to the new points

$$X_{n+1}^k := \gamma_n(X_n^k) = X_n^k + v[\mu_n](X_n^k)\Delta t_n, \tag{5.35}$$

where we have specified $v_n = v[\mu_n]$ in the expression of $\gamma_n$. Equation (5.35) corresponds to discretizing (5.15) in time by a classical explicit Euler scheme.

### 5.5.2 *Spatial Approximation*

In Chap. 6 we will prove that, under some reasonable assumptions on the flow map, $\gamma_n \# M_n$ in (5.34) is, as expected, the continuous part $M_{n+1}$ of the mass $\mu_{n+1}$. For the moment we simply trust this and study how to approximate it via a suitable spatial discretization. We address the latter in the abstract on the whole space $\mathbb{R}^d$, also in view of the forthcoming theoretical analysis.

*Remark 5.11.* Coherently with the previous notations, we denote by $\rho_n$ the density at time $t_n$. In addition, space-approximate quantities will be indicated by the symbol $\tilde{}$ over the quantities.

We partition $\mathbb{R}^d$ in pairwise disjoint $d$-dimensional cells $E_i \in \mathscr{B}(\mathbb{R}^d)$, where $i = (i_1, \ldots, i_d) \in \mathbb{Z}^d$ is a multi-index. In the simplest case, which we will focus on in the following, the $E_i$'s are cubic cells with characteristic edge size $\Delta x > 0$, centered at $x_i = i\Delta x$ (see Fig. 5.4):

$$E_i = \bigtimes_{\ell=1}^{d} \left[ i_\ell - \frac{1}{2}, i_\ell + \frac{1}{2} \right) \Delta x.$$

More generally, however, the $E_i$'s may have different shape and/or size from one another if different spatial resolution is required in different areas of the domain.

We approximate $\rho_n$ on the spatial mesh $\{E_i\}_{i \in \mathbb{Z}^d}$ by a *piecewise constant* function $\tilde{\rho}_n$, i.e.

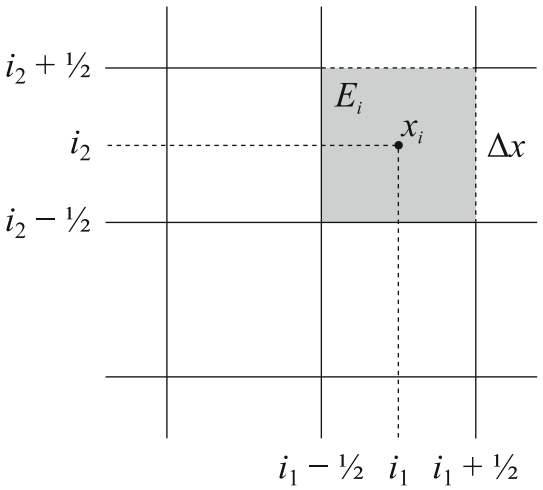


**Fig. 5.4** Portion of a mesh in $\mathbb{R}^2$ with square-shaped cells

$$\tilde{\rho}_n(x) = \sum_{i \in \mathbb{Z}^d} \rho_n^i \mathbb{1}_{E_i}(x),$$

where $\rho_n^i$ is the value of the density in the center of the cell $E_i$ at time $t_n$.

Consequently, the measure $M_n$ is approximated by the piecewise constant measure $d\tilde{M}_n = \tilde{\rho}_n \, d\mathscr{L}^d$, which entails for $\mu_n$ the approximation $\tilde{\mu}_n = \theta m_n + (1-\theta)\Lambda \tilde{M}_n$.

Analogously, we approximate the velocity $v[\mu_n]$ by a piecewise constant field

$$\tilde{v}[\tilde{\mu}_n](x) = \sum_{i \in \mathbb{Z}^d} v[\tilde{\mu}_n](x_i) \mathbb{1}_{E_i}(x),$$

where

$$v[\tilde{\mu}_n](x_i) = v_{\mathrm{d}}(x_i) + \theta \sum_{\substack{k=1,\dots,N \\ X_n^k \neq x_i}} f(|X_n^k - x_i|) g(\alpha_{x_i X_n^k}) \frac{X_n^k - x_i}{|X_n^k - x_i|}$$

$$+ (1-\theta)\Lambda \sum_{j \in \mathbb{Z}^d} \rho_n^j \int_{E_j} f(|y - x_i|) g(\alpha_{x_i y}) \frac{y - x_i}{|y - x_i|} \, dy. \tag{5.36}$$

The integral on $E_j$ can be further approximated by suitable quadrature formulas. Due to the compactness of the supports of $f$ and $g$, its computation actually involves only the elements of the spatial mesh having a nonempty intersection with the interaction neighborhood $\mathscr{S}(x_i)$ of the point $x_i$.

The discretization of the velocity gives rise to a corresponding discretization of the flow map:

$$\tilde{\gamma}_n(x) = x + \tilde{v}[\tilde{\mu}_n](x)\Delta t_n,$$

which turns out to be a piecewise translation because $\tilde{v}[\tilde{\mu}_n]$ is constant, by construction, in each cell.

Now we prepare for advancing to the next time $t_{n+1}$ by enforcing a piecewise constant approximation $\tilde{M}_{n+1}$ of $M_{n+1}$, i.e., we look for $d\,\tilde{M}_{n+1} = \tilde{\rho}_{n+1}\,dx$. The unknowns to be determined are therefore the coefficients $\{\rho^i_{n+1}\}_{i\in\mathbb{Z}^d}$. In order to make the step, we mimic the formula $M_{n+1} = \gamma_n \# M_n$ by imposing the push forward of $\tilde{M}_n$ via the flow map $\tilde{\gamma}_n$:

$$\tilde{M}_{n+1}(E) = \tilde{M}_n(\tilde{\gamma}_n^{-1}(E)), \quad \forall\, E \in \mathscr{B}(\mathbb{R}^d).$$

In particular, choosing $E = E_i$ yields

$$\begin{aligned}\Delta x^d \rho^i_{n+1} &= \int_{\tilde{\gamma}_n^{-1}(E_i)} \tilde{\rho}_n(x)\,dx = \sum_{j\in\mathbb{Z}^d} \int_{\tilde{\gamma}_n^{-1}(E_i)\cap E_j} \tilde{\rho}_n(x)\,dx \\ &= \sum_{j\in\mathbb{Z}^d} \rho^j_n \mathscr{L}^d(\tilde{\gamma}_n^{-1}(E_i)\cap E_j),\end{aligned}$$

with $\Delta x^d = \mathscr{L}^d(E_i)$. Invoking the invariance of Lebesgue measure under translations (see Fig. 5.5) we obtain $\mathscr{L}^d(\tilde{\gamma}_n^{-1}(E_i)\cap E_j) = \mathscr{L}^d(E_i \cap \tilde{\gamma}_n(E_j))$, whence finally

$$\rho^i_{n+1} = \frac{1}{\Delta x^d} \sum_{j\in\mathbb{Z}^d} \rho^j_n \mathscr{L}^d(E_i \cap \tilde{\gamma}_n(E_j)). \tag{5.37}$$

This equation provides an explicit scheme for computing the coefficients of $\tilde{\rho}_{n+1}$ from those of $\tilde{\rho}_n$. Notice, in particular, that the set $\tilde{\gamma}_n(E_j)$ is simply obtained by translation as $E_j + v[\tilde{\mu}_n](x_j)\Delta t_n$, thus it is much easier to construct than the inverse image $\tilde{\gamma}_n^{-1}(E_i)$.

In order to advance in time the atoms of $\tilde{\mu}_n$, we apply (5.35) complemented with the spatial discretization of the density. In practice, we enforce the relationship:

$$X^k_{n+1} = X^k_n + v[\tilde{\mu}_n](X^k_n)\Delta t_n \tag{5.38}$$

with

$$\begin{aligned}v[\tilde{\mu}_n](X^k_n) = v_{\mathrm{d}}(X^k_n) &+ \theta \sum_{\substack{h=1,\dots,N \\ X^h_n \neq X^k_n}} f(|X^h_n - X^k_n|)\, g(\alpha_{X^k_n X^h_n}) \frac{X^h_n - X^k_n}{|X^h_n - X^k_n|} \\ &+ (1-\theta)\Lambda \sum_{i\in\mathbb{Z}^d} \rho^i_n \int_{E_i} f(|y - X^k_n|)\, g(\alpha_{X^k_n y}) \frac{y - X^k_n}{|y - X^k_n|}\,dy.\end{aligned} \tag{5.39}$$

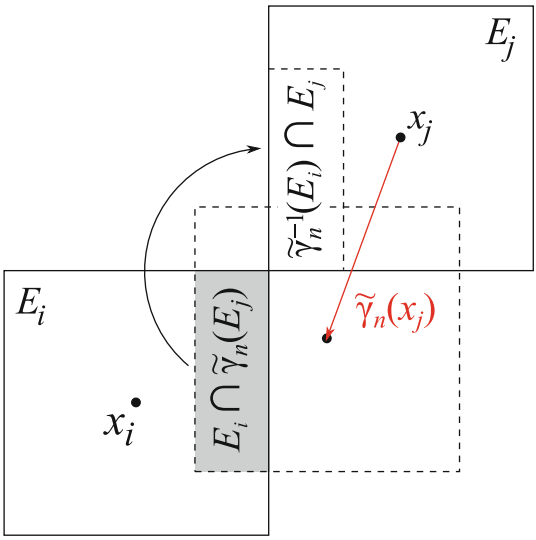


**Fig. 5.5** Pictorial representation of the action of the mapping $\tilde{\gamma}_n$ on the mesh cells. Notice that $E_i \cap \tilde{\gamma}_n(E_j)$ and $\tilde{\gamma}_n^{-1}(E_i) \cap E_j$ are not the same set, but they have the same volume because of the invariance of Lebesgue measure under translations

Again, the integral on $E_i$ can be approximated by classical quadrature formulas, taking into account that it has actually to be computed only for those cells intersecting the interaction neighborhood $\mathscr{S}(X_n^k)$.

To sum up, the multiscale numerical scheme we have presented is a time-explicit scheme, which enables one to compute $\{X_{n+1}^k\}_{k=1}^N$, $\{\rho_{n+1}^i\}_{i\in\mathbb{Z}^d}$ at time $t_{n+1}$ from the corresponding quantities at the previous time $t_n$. To this purpose, (5.37), (5.38) must be applied, supplemented by the velocity fields (5.36), (5.39), respectively.

### 5.5.3 The Algorithm

We end this section by discussing how a computational algorithm, stemming from the above multiscale numerical scheme, can be conceptually organized. The line of thought exposed here will directly result in the pseudo-code reported in Appendix B.

The algorithm is structured in a discrete and a continuous part. The former handles the evolution of the atoms of $\mu_n$, updating a vector which stores the values $X_n^k$. The latter manages instead the evolution of the density, updating at every time step the values $\rho_n^i$ in the cells of the spatial mesh. The two models evolve by means of the same velocity field $\tilde{v}[\tilde{\mu}_n]$, which has to be defined both at the atoms' positions $\{X_n^k\}_{k=1}^N$ (for the discrete part) and at the centers $\{x_i\}_{i\in\mathbb{Z}^d}$ of the mesh cells (for the continuous part).

Let us introduce the following superscripts:

- *Micro*: Quantities defined at points $X_n^k$.
- *Macro*: Quantities defined at points $x_i$.
- *Micro-for-micro*: Quantities pertaining to the discrete (microscopic) part of the algorithm, computed at points $X_n^k$.

- *Micro-for-macro*: Quantities pertaining to the discrete (microscopic) part of the algorithm, computed at points $x_i$.
- *Macro-for-micro*: Quantities pertaining to the continuous (macroscopic) part of the algorithm, computed at points $X_n^k$.
- *Macro-for-macro*: Quantities pertaining to the continuous (macroscopic) part of the algorithm, computed at points $x_i$.

The algorithm consists of the following steps.

1. *Initialization*. Fix the number $N$ of atoms of the mass, define their initial positions $\{X^k(0)\}_{k=1}^N$, and compute the values $\rho_0^i$ of the initial density according to a local average of the discrete mass, taking the scaling (5.31) into account. More precisely, we suggest to set:

$$\rho_0^i = \frac{m_0(B_\xi(x_i))}{\Lambda \mathscr{L}^d(B_\xi(x_i))},$$

where $m_0$ is the discrete mass at the initial time and $B_\xi(x_i)$ the ball centered in the center of the cell $E_i$ with radius $\xi > 0$. The latter is tuned depending on the positions $X^k(0)$ of the atoms, in such a way that the relation $\Lambda = m_0(\mathbb{R}^d)/\tilde{M}_0(\mathbb{R}^d)$ be approximately satisfied ($\tilde{M}_0$ being the approximate macroscopic mass at the initial time). It is worth pointing out that if one replaces $B_\xi(x_i)$ with the cell $E_i$ itself then the measures $m_0$, $\tilde{M}_0$ satisfy the scaling (5.31) exactly. However, averaging on a neighborhood slightly larger than a single grid cell is essential in order to have a density really distributed in space rather than clustered in mesh cells.
2. *Discrete part*. At time $t_n$, compute the first sum at the right-hand side of (5.39) for each $k = 1, \ldots, N$, obtaining

$$v_{\mathrm{i}}^{\text{micro-for-micro},k} := v_{\mathrm{i}}[m_n](X_n^k).$$

Then compute the first sum at the right-hand side of (5.36) for each $i \in \mathbb{Z}^d$ to get

$$v_{\mathrm{i}}^{\text{micro-for-macro},i} := v_{\mathrm{i}}[m_n](x_i),$$

which will be shared with the continuous part of the algorithm.
3. *Continuous part*. At time $t_n$, evaluate the integrals at the right-hand side of (5.36) for each $i \in \mathbb{Z}^d$, which gives

$$v_{\mathrm{i}}^{\text{macro-for-macro},i} := v_{\mathrm{i}}[\tilde{M}_n](x_i).$$

For instance, a zeroth-order quadrature formula can be used:

$$\int_{E_j} f(|y - x_i|) g(\alpha_{x_i y}) \frac{y - x_i}{|y - x_i|}\, dy \approx f(|x_j - x_i|) g(\alpha_{x_i x_j}) \frac{x_j - x_i}{|x_j - x_i|} \Delta x^d$$

for all $j \neq i$ such that $E_j \cap \mathscr{S}(x_i) \neq \emptyset$. Similarly, evaluate the integrals at the right-hand side of (5.39) for each $k = 1, \ldots, N$ to find

$$v_{\mathrm{i}}^{\text{macro-for-micro},k} := v_{\mathrm{i}}[\tilde{M}_n](X_n^k),$$

which will be shared with the discrete part of the algorithm.

4. *Desired velocity*. If the desired velocity is given analytically, the computation of

$$v_{\mathrm{d}}^{\text{micro},k} := v_{\mathrm{d}}(X_n^k), \qquad v_{\mathrm{d}}^{\text{macro},i} := v_{\mathrm{d}}(x_i)$$

for each $k = 1, \ldots, N$ and each $i \in \mathbb{Z}^d$ is straightforward. If instead $v_{\mathrm{d}}$ is known only at discrete points, then $v_{\mathrm{d}}^{\text{micro},k}$, $v_{\mathrm{d}}^{\text{macro},i}$ have to be computed by interpolation. This is, for instance, the case of the desired velocity obtained from (5.5), as Laplace's equation (5.6) is likely to be solved by an approximate numerical procedure. Since we are assuming that all continuous quantities are piecewise constant, the coherent choice is a zeroth-order interpolation.

5. *Total velocity*. Assemble the previous pieces of the velocity as

$$\begin{aligned} v^{\text{micro},k} &:= v[\tilde{\mu}_n](X_n^k) \\ &= v_{\mathrm{d}}^{\text{micro},k} + \theta v_{\mathrm{i}}^{\text{micro-for-micro},k} + (1-\theta)\Lambda v_{\mathrm{i}}^{\text{macro-for-micro},k}, \end{aligned}$$

and analogously

$$\begin{aligned} v^{\text{macro},i} &:= v[\tilde{\mu}_n](x_i) \\ &= v_{\mathrm{d}}^{\text{macro},i} + \theta v_{\mathrm{i}}^{\text{micro-for-macro},i} + (1-\theta)\Lambda v_{\mathrm{i}}^{\text{macro-for-macro},i}. \end{aligned}$$

6. *Computation of the time step*. Apply the following CFL condition:

$$\Delta t_n \max_{i \in \mathbb{Z}^d} |v^{\text{macro},i}| = \Delta x \tag{5.40}$$

for computing the time step needed to advance to the next time $t_{n+1}$. As we will see in Chap. 6, condition (5.40) is actually *not* necessary for the stability of the algorithm (like e.g., in the numerical approximation of hyperbolic conservation laws), but it is useful for accuracy and simplicity of implementation. On the one hand, it guarantees that the push forward operated by the approximate flow map $\tilde{\gamma}_n$ does not generate spurious singularities in $\tilde{\mu}_n$ besides the atoms $X_n^k$. On the other hand, it makes it sufficient in (5.37) to consider, for each $i \in \mathbb{Z}^d$, only the cells $E_j$ adjacent to $E_i$, as intersections $E_i \cap \gamma_n(E_j)$ involving farther cells $E_j$ are empty. In fact, condition (5.40) implies that the maximum displacement of a cell $E_j$ produced by the mapping $\tilde{\gamma}_n$ is at most $\Delta x$.

7. *Advancing in time*. Update $\rho_n^i$, $X_n^k$ to $\rho_{n+1}^i$, $X_{n+1}^k$, respectively, by means of (5.37), (5.38), using $v^{\text{macro},i}$, $v^{\text{micro},k}$, and the time step $\Delta t_n$ previously determined.

## 5.6 Two-Population Models

The measure-based model has been described so far with reference to a single crowd. However, some numerical experiments in Chap. 2 pointed out that many interesting applications, especially concerned with self-organization issues, imply the interaction between two groups of walkers, see, e.g., Fig. 2.16. In order to address such problems, it is necessary to further develop the modeling structures presented in this chapter, so as to account for cross-interactions occurring between different pedestrian populations. For the sake of simplicity, we will consider in the sequel the case of two populations only. Generalization of the forthcoming discussion to more than two populations is mainly a technical matter, involving more elaborated notations and, after all, not really fundamental for applicative purposes.

Let $p \in \{1, 2\}$ be the population index, and $q$ its conjugate index denoting the other population (i.e., $q = 2$ when $p = 1$ and $q = 1$ when $p = 2$). Either population is represented by its mass measure $\mu_t^p$, satisfying the continuity equation:

$$\frac{\partial \mu_t^p}{\partial t} + \nabla \cdot (\mu_t^p v^p[\mu_t^p, \mu_t^q]) = 0. \tag{5.41}$$

Notice that now the velocity of the $p$th population depends also on the mass of the $q$th population. This translates the influence of the latter on the dynamics of the former. In more detail, the proposed expression of $v^p$ is as follows:

$$v^p[\mu_t^p, \mu_t^q](x) = v_{\mathrm{d}}^p(x) + (1 - \Theta^p)v_{\mathrm{i}}^p[\mu_t^p](x) + \Theta^p v_{\mathrm{i}}^{pq}[\mu_t^q](x), \tag{5.42}$$

where

- $v_{\mathrm{d}}^p$ is the desired velocity of population $p$, obviously unaffected by population $q$ as it refers to the ideal situation in which pedestrians do not experience mutual interactions.
- $v_{\mathrm{i}}^p[\mu_t^p]$ is the usual interaction velocity internal to population $p$, i.e., the correction that the test pedestrian of population $p$ makes to her desired velocity due to the presence of field pedestrians of her own population. Hence $v_{\mathrm{i}}^p$ depends on $\mu_t^p$ only, and is expressed as

$$v_{\mathrm{i}}^p[\mu_t^p](x) = \int_{\mathbb{R}^d \setminus \{x\}} f^p(|y - x|) g^p(\alpha_{xy}) \frac{y - x}{|y - x|} \, d\mu_t^p(y). \tag{5.43}$$

  In this context, we refer to $v_{\mathrm{i}}^p[\mu_t^p]$ as the *self-interaction velocity*.
- $v_{\mathrm{i}}^{pq}[\mu_t^q]$ is the *cross-interaction velocity*, i.e., the correction to $v_{\mathrm{d}}^p$ stemming from the interactions that the test pedestrian of population $p$ experiences with surrounding field pedestrians of population $q$. Therefore it depends on the mass $\mu_t^q$, and is expressed as:

$$v_{\mathrm{i}}^{pq}[\mu_t^q](x) = \int_{\mathbb{R}^d \setminus \{x\}} f^{pq}(|y - x|) g^{pq}(\alpha_{xy}) \frac{y - x}{|y - x|} \, d\mu_t^q(y). \tag{5.44}$$

If $\mathrm{supp}(f^p) \neq \mathrm{supp}(f^{pq})$ or $\mathrm{supp}(g^p) \neq \mathrm{supp}(g^{pq})$, then the self-interaction neighborhood $\mathscr{S}^p(x)$ is different from the cross-interaction neighborhood $\mathscr{S}^{pq}(x)$ because of either a different radius or a different angular width. For instance, in case of crossing flows (cf. Sect. 2.5) the interaction with opposite walkers may require more promptness, hence a larger radius, than interactions with group mates.

- $\Theta^p \in [0,\, 1]$ is a parameter weighting the contribution of cross-interactions with respect to self-interactions in the dynamics of population $p$. Notice that if $\Theta^p = 0$ then population $p$ is totally insensitive to population $q$, and from (5.41) to (5.44) one recovers the model discussed in the previous sections of this chapter for a single crowd. Conversely, if $\Theta^p = 1$ then pedestrians of population $p$ do not interact among each other, the only important interactions being those with pedestrians of population $q$. Finally, with $0 < \Theta^p < 1$ a coupling between self- and cross-dynamics is realized.

By detailing the multiscale structure of the measures $\mu_t^p$, $\mu_t^q$ in (5.42), the total interaction velocity for population $p$ takes the form of a combination of self- and cross- discrete and continuous contributions:

$$
\begin{aligned}
v_{\mathrm{i}}^p[\mu_t^p,\, \mu_t^q](x) = {} & (1-\Theta^p)\theta^p \underbrace{\sum_{\substack{k=1,\dots,N^p \\ X^{k,p}(t)\neq x}} f^p(|X^{k,p}(t)-x|)\, g^p(\alpha_{x X^{k,p}(t)})\, \frac{X^{k,p}(t)-x}{|X^{k,p}(t)-x|}}_{\text{interaction with microscopic pedestrians of the \textbf{same} population}} \\
& + (1-\Theta^p)(1-\theta^p)\Lambda^p \underbrace{\int_{\mathbb{R}^d} f^p(|y-x|)\, g^p(\alpha_{xy})\, \frac{y-x}{|y-x|}\, \rho^p(t,\, y)\, dy}_{\text{interaction with the macroscopic density of the \textbf{same} population}} \\
& + \Theta^p\theta^q \underbrace{\sum_{\substack{k=1,\dots,N^q \\ X^{k,q}(t)\neq x}} f^{pq}(|X^{k,q}(t)-x|)\, g^{pq}(\alpha_{x X^{k,q}(t)})\, \frac{X^{k,q}(t)-x}{|X^{k,q}(t)-x|}}_{\text{interaction with microscopic pedestrians of the \textbf{other} population}} \\
& + \Theta^p(1-\theta^q)\Lambda^q \underbrace{\int_{\mathbb{R}^d} f^{pq}(|y-x|)\, g^{pq}(\alpha_{xy})\, \frac{y-x}{|y-x|}\, \rho^q(t,\, y)\, dy}_{\text{interaction with the macroscopic density of the \textbf{other} population}},
\end{aligned}
$$

where, with obvious meaning of the symbols, $N^p$, $N^q$ denote the number of microscopic pedestrians in populations $p$ and $q$, respectively (and similarly for the densities $\rho^p$, $\rho^q$), whereas $\{X^{k,p}(t)\}_{k=1}^{N^p}$, $\{X^{k,q}(t)\}_{k=1}^{N^q}$ are their positions. Each of the four terms at the right-hand side can be further split in two if $f^p$, $g^p$ or $f^{pq}$, $g^{pq}$ contain both repulsion and attraction effects.

As far as the multiscale representation is concerned, we observe that, in principle, either population has its own parameters $\theta^p$ and $\Lambda^p$. This framework enables thus one to account for different scalings within the two interacting crowds, see Fig. 2.23.

## 5.7 Bibliographical Notes

Sections 5.1–5.3 The measure-based modeling techniques for pedestrian flows have been introduced in Cristiani et al. [47], Piccoli and Tosin [144,145] inspired by [31,32].

Sections 5.4 and 5.5 Measure-based techniques have been specialized to multiscale issues, from the point of view of both modeling and numerical implementation, in Cristiani et al. [48]. References to other possible ways of understanding multiscale approaches in the mathematical modeling literature can be found in the bibliographical notes of Chap. 1.

Section 5.6 Measure-based equations for two interacting crowds are simulated in Cristiani et al. [48] and detailed here for the first time. A systematic existence and uniqueness theory of weak measure solutions for systems of PDEs with two populations is developed by Di Francesco and Fagioli [61], see also Piccoli and Rossi [141].

# Chapter 6
# Basic Theory of Measure-Based Models

**Abstract** This chapter is devoted to the mathematical foundations of the model introduced in Chap. 5. Contents go continuously back and forth between modeling and analysis, however with a more formal approach than that used in the previous chapter. The first three sections, from Sects. 6.1 to 6.3, discuss how the measure-based model can be derived from a particle description of pedestrians, thereby formalizing the link between individualities and collectivity which is at the basis of most of the complexity of crowd behaviors. In addition, in the light of such a derivation they propose a probabilistic reading of the measure-based model, which turns out to be particularly meaningful for applications. The central part of the chapter, encompassing Sects. 6.4–6.7, is concerned with the basic theory of well-posedness and numerical approximation of measure-valued Cauchy problems for first order models based on conservation laws, also in a multiscale perspective. Minimal generic assumptions are stated in order to achieve proofs, to be regarded possibly also as guidelines in the modeling approach. Finally, Sect. 6.8 resumes the discussion about the crowd model presented in Chap. 5 studying under which conditions it is in the scope of the theory set forth in the preceding sections.

## 6.1 Phenomenological Model with Perception

In order to motivate phenomenologically the model with measures, cf. (5.1), we start from a model at the *scale of the individuals* (probably the most natural one at which a crowd can be physically observed and described), which tries to incorporate the concept of *human perception*.

Let $X = X(t) \in \mathbb{R}^d$ be the position in space of a generic virtual pedestrian, that we will henceforth call *test pedestrian*, at time $t \geq 0$. Once an initial position $X(0) = \bar{x} \in \mathbb{R}^d$ is picked the mapping $t \mapsto X(t, \bar{x})$ denotes the trajectory of the particular pedestrian starting from $\bar{x}$ at the initial time. Resting on the phenomenology implemented in Sect. 5.2, we consider that pedestrians regulate their velocity on the basis of a local preferred path (desired velocity $v_{\mathrm{d}}$) and of the

E. Cristiani et al., *Multiscale Modeling of Pedestrian Dynamics*, MS&A 12,
DOI 10.1007/978-3-319-06620-2_6,

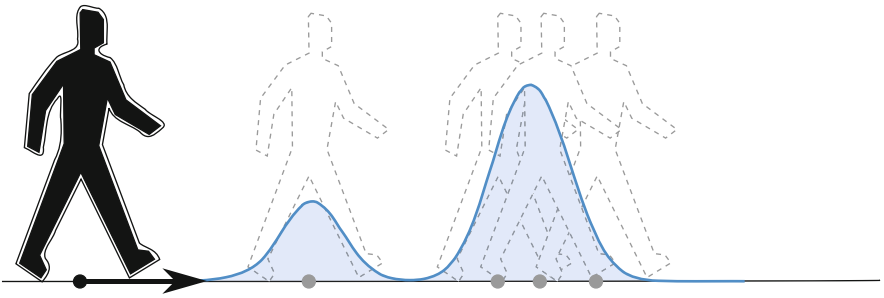

**Fig. 6.1** Human perception can cause pedestrians to react to the gross space occupancy in front of them, seen as a density distribution, rather than to single individuals, or to a mix of the twos

interactions they experience with other surrounding walkers (interaction velocity $v_\mathrm{i}$). The key point is that we further assume that microscopic interactions are mediated by the *perception* that each individual has of the surrounding crowd distribution. In particular, such a perception need not be "internal" to the microscopic scale.[1] For instance, the most common case is when pedestrians react to the gross space occupancy in front of them, without considering other walkers individually, pretty much in the spirit of Fig. 6.1. This can be modeled by assuming that the interaction velocity of the test pedestrian stems from a scanning of the *mass* $\mu_t$ distributed in her interaction neighborhood $\mathscr{S}(X)$, deferring to the spatial structure of the measure to translate the kind of perception activated by the individual $X$:

$$v_\mathrm{i} = \int_{\mathscr{S}(X)} K(X, y)\, d\mu_t(y).$$

Here, $K : \mathbb{R}^d \times \mathbb{R}^d \to \mathbb{R}^d$ is an *interaction kernel* (to be possibly modeled by means of the functions $f$, $g$ as indicated in (5.7)) which accounts for single interaction instances between the test pedestrian and the (infinitesimal) mass $d\mu_t$ she perceives in the point $y \in \mathscr{S}(X)$. The velocity $v_\mathrm{i}$ can also include additional terms related to the interaction of the test pedestrian with the environment (e.g., walls and obstacles), similarly to the microscopic force models described in Sect. 4.1.1. Alternatively, this interaction can be described in terms of appropriate boundary conditions.

An evolution equation for $X$ can then be proposed in the following form:

$$\dot{X} = v_\mathrm{d}(X) + \int_{\mathscr{S}(X)} K(X, y)\, d\mu_t(y). \tag{6.1}$$

[1] Cf. the mean field models discussed in Sect. 4.4.6, which assume that microscopic pedestrians are able to see the local macroscopic density and to use this information for assessing their optimal trajectories.

If perception is individual-by-individual (i.e., pointwise) then the measure $\mu_t$ should be chosen as the counting one:

$$\mu_t = \sum_{k=1}^{N} \delta_{x^k(t)}, \tag{6.2}$$

where $\{x^k(t)\}_{k=1}^N$ are the atoms where the mass of, say, $N$ walkers forming the crowd is concentrated at time $t$. Plugging this into (6.1) specializes the phenomenological model as:

$$\dot{X} = v_{\mathrm{d}}(X) + \sum_{\substack{k=1 \\ x^k \in \mathscr{S}(X)}}^{N} K(X, x^k).$$

Conversely, if perception is addressed to the crowd ahead as a whole then the measure $\mu_t$ should be chosen as an absolutely continuous one:

$$d\mu_t(y) = \rho(t, y)\, dy,$$

$\rho : [0, +\infty) \times \mathbb{R}^d \to [0, +\infty)$ being the space density of the crowd at time $t$. Hence the phenomenological model (6.1) takes the form:

$$\dot{X} = v_{\mathrm{d}}(X) + \int_{\mathscr{S}(X)} K(X, y)\rho(t, y)\, dy.$$

*Remark 6.1.* In order to better understand the relationship between the variable $X$ and the measure $\mu$, we can establish the following heuristic proportion:

$$X : \mu = \text{individuality} : \text{collectivity}.$$

$X$ models a generic representative individual within the collective distribution $\mu$ of walkers. In particular, (6.1) captures the point of view of the test pedestrian immersed in the crowd, who cannot be aware of, and consequently cannot voluntarily produce, collective behaviors because her perception of other group mates is limited to her interaction neighborhood $\mathscr{S}(X)$. For this reason collective behaviors are usually described as *spontaneous*, *emergent*, *self-organized*. They can be observed from a point of view external to the crowd, such as the one provided by the measure $\mu$. This motivates the search for a model for $\mu$ consistent with (6.1), which will be the object of the next sections.

## 6.2 From the Phenomenological to a Mathematical-Physical Model

The phenomenological model (6.1) involves two state variables, $X$ and $\mu$, so far correlated only at a conceptual, but not yet formal, level. A formal link can be established via the following argument: The crowd mass $\mu$, regardless of its specific spatial structure, is a *material quantity* for pedestrians, i.e., it has to move coherently with the motion of walkers. Indeed, it is the latter who generate the mass itself. This implies that $\mu$ is transported by $X$, so that, given a mass distribution $\mu_0$ at the initial time, we can set, for all successive times $t > 0$,

$$\mu_t = X(t)\#\mu_0, \tag{6.3}$$

which means

$$\mu_t(E) = \mu_0(X(t)^{-1}(E)) = \mu_0(\{X(0) \in \mathbb{R}^d : X(t) \in E\})$$

for every measurable set $E \subseteq \mathbb{R}^d$. In particular, $\{X(0) \in \mathbb{R}^d : X(t) \in E\}$ has to be understood as the set of all possible initial positions whence the test pedestrian can start in order to be in the set $E$ at time $t > 0$.

From (6.1) to (6.3) it is possible to derive formally an equation for the measure $\mu_t$. For this, we technically regard the mapping $t \mapsto \mu_t$ as a curve in the space of distributions, i.e., the dual space of $C_c^\infty(\mathbb{R}^d)$. Then, after picking a test function $\phi \in C_c^\infty(\mathbb{R}^d)$, we compute the time derivative of $\mu_t$ as:

$$\begin{aligned}
\frac{d}{dt}\langle \mu_t, \phi\rangle &= \frac{d}{dt}\int_{\mathbb{R}^d} \phi \, d\mu_t = \frac{d}{dt}\int_{\mathbb{R}^d} \phi(X)\, d\mu_0 = \int_{\mathbb{R}^d} \nabla\phi(X)\cdot \dot{X}\, d\mu_0 \\
&= \int_{\mathbb{R}^d} \nabla\phi(X)\cdot\left(v_{\mathrm{d}}(X) + \int_{\mathscr{S}(X)} K(X,\, y)\, d\mu_t(y)\right) d\mu_0 \\
&= \int_{\mathbb{R}^d} \nabla\phi\cdot\left(v_{\mathrm{d}} + \int_{\mathscr{S}(\cdot)} K(\cdot,\, y)\, d\mu_t(y)\right) d\mu_t,
\end{aligned} \tag{6.4}$$

where $\langle\cdot,\,\cdot\rangle$ denotes the duality pairing in $C_c^\infty(\mathbb{R}^d)$. After defining

$$v[\mu_t](x) := v_{\mathrm{d}}(x) + \int_{\mathscr{S}(x)} K(x,\, y)\, d\mu_t(y), \tag{6.5}$$

we recognize in (6.4) a weak form of the equation

$$\frac{\partial \mu_t}{\partial t} + \nabla\cdot(\mu_t v[\mu_t]) = 0, \tag{6.6}$$

i.e., exactly Eq. (5.1) which in Chap. 5 was directly postulated a priori out of phenomenological arguments.

## 6.3 Probabilistic Interpretation

By carefully inspecting the previous two sections it turns out that, despite (6.3), the quantitative characterization of $\mu$ as precisely the mass of the crowd has not been fully established yet. In fact, for the moment $\mu$ can be in principle *any* measure transported by $X$, which simply plays a role in determining the way the test pedestrian interacts with the rest of the crowd. The goal of this section is to fill such a gap by proposing a suitably new reading of $\mu$, which both enriches the modeling perspective and is technically useful for the next qualitative analysis.

Let us consider $N$ variables $X^1, X^2, \ldots, X^N$ modeling the positions in time of the various walkers composing the crowd. Any of them is actually a particular instance of the test pedestrian, therefore the trajectories $t \mapsto X^k(t)$ are technically obtained as

$$X^k(t) = X(t, \bar{x}^k), \qquad k = 1, \ldots, N, \tag{6.7}$$

where $\bar{x}^k$ is the initial position of the $k$-th walker.

Assume now that the $\bar{x}^k$'s are not deterministically known. In fact, very often a statistical estimate of the starting configuration of the crowd in an area of interest is the only reasonable information on which to ground predictions at future times. Thus the $\bar{x}^k$'s have to be regarded as random variables, which for the sake of simplicity we consider independent and identically distributed. Let $\nu_0$ be a probability measure on $\mathbb{R}^d$ representing their law:

$$\begin{aligned} &\nu_0(\mathbb{R}^d) = 1 \\ &\nu_0(E) = \text{Prob}(\bar{x}^k \in E), \quad \forall\, E \subseteq \mathbb{R}^d \text{ measurable.} \end{aligned}$$

If we think of the initial mass $\mu_0$ as proportional to the probability of finding pedestrians in certain areas of the space domain, we further have:

$$\mu_0 = N\nu_0, \tag{6.8}$$

in such a way that the total initial mass coincides with the total number of pedestrians, $\mu_0(\mathbb{R}^d) = N$.

Owing to (6.7) the uncertainty in the initial positions is transported at all future times, thereby inducing a probability distribution also on the variables $X^k(t), t > 0$:

$$\begin{aligned} \text{Prob}(X^k(t) \in E) &= \text{Prob}(X(t, \bar{x}^k) \in E) \\ &= \text{Prob}(\bar{x}^k \in X(t)^{-1}(E)) \\ &= \nu_0(X(t)^{-1}(E)) = (X(t)\#\nu_0)(E), \quad \forall\, E \subseteq \mathbb{R}^d \text{ measurable,} \end{aligned}$$

whence we see that the (common) law of the $X^k(t)$'s is the measure $\nu_t := X(t)\#\nu_0$. Recalling (6.3) and (6.8), this further implies $\mu_t = N\nu_t$.

Given the proportionality just stated between $\mu_t$ and $\nu_t$, an evolution equation for the latter can be derived straightforwardly from (6.6):

$$\frac{\partial \nu_t}{\partial t} + \nabla \cdot (\nu_t v[\nu_t]) = 0, \tag{6.9}$$

where by $v[\nu_t]$ we mean

$$v[\nu_t](x) = v_{\mathrm{d}}(x) + N \int_{\mathscr{S}(x)} K(x, y)\, d\nu_t(y). \tag{6.10}$$

Now it remains to show that this discussion does indeed legitimate the initial heuristic interpretation of $\mu$ as the crowd mass. For this, let us introduce the random variable $Y_E(t)$ which counts the number of pedestrians contained in a measurable set $E \subseteq \mathbb{R}^d$ at time $t$:

$$Y_E(t) = \sum_{k=1}^{N} \mathbb{1}_E(X^k(t)). \tag{6.11}$$

Its expectation can be computed through the law $\nu_t$ of the $X^k(t)$'s as:

$$\mathbb{E}[Y_E(t)] = \sum_{k=1}^{N} \mathbb{E}\left[\mathbb{1}_E(X^k(t))\right] = N \int_{\mathbb{R}^d} \mathbb{1}_E\, d\nu_t = N\nu_t(E) = \mu_t(E).$$

Therefore, $\mu_t$ is ultimately the crowd mass in the sense of the average number of pedestrians occupying a given spatial area at time $t$. This is a kind of physical information at the *macroscale* stemming from a collective look at the crowd at the *mesoscale* (see Sect. 8.1 for a deeper discussion about this issue).

## 6.4 Uniqueness and Continuous Dependence of the Solution

We now consider the initial-value problem for (6.9):

$$\begin{cases} \dfrac{\partial \nu_t}{\partial t} + \nabla \cdot (\nu_t v[\nu_t]) = 0, & t \in (0, T], \quad x \in \mathbb{R}^d \\ \nu_0 = \bar{\nu}, & x \in \mathbb{R}^d, \end{cases} \tag{6.12}$$

where $\bar{\nu}$ is a prescribed initial probability measure in $\mathbb{R}^d$ and $T > 0$ a certain final time, and prove uniqueness of the solution and its continuous dependence on the

initial datum. Clearly, this will straightforwardly imply analogous properties for the solution $\mu_t$ to (6.6). However, working with probabilities is more convenient because one can exploit a well consolidated theoretical background, whose essential elements are recalled in Appendix A.

To begin with, we report the precise sense in which it will be useful to understand the concept of solution to (6.12).

**Definition 6.1.** We say that $\nu_\bullet \in C([0,\,T];\,\mathscr{P}_1\mathbb{R}^d)$ is a (weak) solution to Problem (6.12) if it satisfies:

$$\int_{\mathbb{R}^d} \phi\, d\nu_t = \int_{\mathbb{R}^d} \phi\, d\bar{\nu} + \int_0^t \int_{\mathbb{R}^d} \nabla\phi \cdot v[\nu_s]\, d\nu_s\, ds \tag{6.13}$$

for all $\phi \in C_c^\infty(\mathbb{R}^d)$ and all $t \in [0,\,T]$.

Notice that, in practice, the weak formulation (6.13) of Problem (6.12) is obtained by integrating (6.4) in time after rescaling $\mu_t$ to $\nu_t$.

Using (6.13) we can formally check that

$$\nu_t = \gamma(t)\#\bar{\nu}, \qquad t \in (0,\,T] \tag{6.14}$$

is a representation formula of the solution provided $\gamma : [0,\,T] \times \mathbb{R}^d \to \mathbb{R}^d$, called the *flow map*, satisfies:

$$\begin{cases} \dfrac{\partial\gamma(t,\,x)}{\partial t} = v[\nu_t](\gamma(t,\,x)), & t \in (0,\,T], \quad x \in \mathbb{R}^d \\ \gamma(0,\,x) = x, & x \in \mathbb{R}^d. \end{cases} \tag{6.15}$$

In fact, using (6.14) and (6.15) in (6.13) we discover

$$\begin{aligned} \int_{\mathbb{R}^d} \phi(\gamma(t))\, d\bar{\nu} &= \int_{\mathbb{R}^d} \phi\, d\bar{\nu} + \int_0^t \int_{\mathbb{R}^d} \nabla\phi(\gamma(s)) \cdot \frac{\partial\gamma(s)}{\partial s}\, d\bar{\nu}\, ds \\ &= \int_{\mathbb{R}^d} \phi\, d\bar{\nu} + \int_0^t \int_{\mathbb{R}^d} \frac{\partial}{\partial s}\phi(\gamma(s))\, d\bar{\nu}\, ds \\ &= \int_{\mathbb{R}^d} \phi\, d\bar{\nu} + \int_{\mathbb{R}^d} [\phi(\gamma(t)) - \phi(\gamma(0))]\, d\bar{\nu}, \end{aligned}$$

which is clearly seen to be an identity upon considering that $\gamma$ is the identity map at $t = 0$.

Next, we state a basic assumption on the velocity field concerning its dependence on the space variable and the measure. We actually do not enter the details of the explicit expression of $v$ because this is not necessary for the development of a general qualitative theory. However, in Sect. 6.8 we will come back to the structure (6.10) and discuss the consequences of the general theory on the construction of particular models.

**Assumption 6.1 (Lipschitz continuity of $v$).** *There exists a constant* $\mathrm{Lip}(v) > 0$ *such that*

$$|v[\nu_2](x_2) - v[\nu_1](x_1)| \leq \mathrm{Lip}(v)\,(|x_2 - x_1| + W_1(\nu_1, \nu_2))$$

*for all* $x_1, x_2 \in \mathbb{R}^d$ *and all* $\nu_1, \nu_2 \in \mathscr{P}_1\mathbb{R}^d$.

Here $W_1(\cdot,\cdot)$ is the Wasserstein metric in the space $\mathscr{P}_1\mathbb{R}^d$ of probability measures in $\mathbb{R}^d$ with finite first moment, see Appendix A for details.

An immediate consequence of Assumption 6.1 is:

**Lemma 6.1.** *(i) For a given* $\nu_\bullet \in C([0,T];\mathscr{P}_1\mathbb{R}^d)$ *the flow map defined by (6.15) satisfies:*

$$|\gamma(t, x_2) - \gamma(t, x_1)| \leq \mathscr{C}\,|x_2 - x_1|$$

*for a suitable constant* $\mathscr{C} > 0$ *independent of* $\nu_\bullet$, $x_1$, $x_2$.

*(ii) Let* $\nu_{1,\bullet}, \nu_{2,\bullet} \in C([0,T];\mathscr{P}_1\mathbb{R}^d)$ *be given and let* $\gamma^{\nu_1}$, $\gamma^{\nu_2}$ *be the corresponding flow maps generated by (6.15). Then there exists a constant* $\mathscr{C} > 0$, *independent of both* $\nu_{1,\bullet}$ *and* $\nu_{2,\bullet}$, *such that*

$$|\gamma^{\nu_2}(t, x) - \gamma^{\nu_1}(t, x)| \leq \mathscr{C} \int_0^t W_1(\nu_{1,s}, \nu_{2,s})\,ds$$

*for all* $x \in \mathbb{R}^d$.

*Proof.* From (6.15) it follows $\gamma(t, x) = x + \int_0^t v[\nu_s](\gamma(s, x))\,ds$, hence:

(i) $$|\gamma(t, x_2) - \gamma(t, x_1)| \leq |x_2 - x_1| + \int_0^t |v[\nu_s](\gamma(s, x_2)) - v[\nu_s](\gamma(s, x_1))|\,ds$$
$$\leq |x_2 - x_1| + \mathrm{Lip}(v) \int_0^t |\gamma(s, x_2) - \gamma(s, x_1)|\,ds,$$

whence invoking Gronwall's inequality yields:

$$|\gamma(t, x_2) - \gamma(t, x_1)| \leq (1 + \mathrm{Lip}(v)t \exp \mathrm{Lip}(v)t)\,|x_2 - x_1|$$

and the thesis follows by bounding $t$ from above at the right-hand side by $T$.

(ii) $$\gamma^{\nu_2}(t, x) - \gamma^{\nu_1}(t, x) = \int_0^t \{v[\nu_{2,s}](\gamma^{\nu_2}(s, x)) - v[\nu_{1,s}](\gamma^{\nu_2}(s, x))\}\,ds$$
$$+ \int_0^t \{v[\nu_{1,s}](\gamma^{\nu_2}(s, x)) - v[\nu_{1,s}](\gamma^{\nu_1}(s, x))\}\,ds$$

thus

$$|\gamma^{\nu_2}(t,\,x)-\gamma^{\nu_1}(t,\,x)|\le \mathrm{Lip}(v)\left(\int_0^t W_1\,(\nu_{1,s},\,\nu_{2,s})\,ds + \int_0^t |\gamma^{\nu_2}(s,\,x)-\gamma^{\nu_1}(s,\,x)|\,ds\right)$$

and Gronwall's inequality says

$$|\gamma^{\nu_2}(t,\,x)-\gamma^{\nu_1}(t,\,x)|\le \mathrm{Lip}(v)\exp\mathrm{Lip}(v)t\int_0^t W_1\,(\nu_{1,s},\,\nu_{2,s})\,ds.$$

Owing to the lemma above, we are in a position to prove the main result of this section:

**Theorem 6.1.** *Let $\nu_{1,\bullet},\,\nu_{2,\bullet}\in C([0,\,T];\,\mathscr{P}_1\mathbb{R}^d)$ be two solutions to Problem (6.12) corresponding to initial data $\bar\nu_1,\,\bar\nu_2\in\mathscr{P}_1\mathbb{R}^d$. Under Assumption 6.1 there exists a constant $\mathscr{C}>0$, independent of $\bar\nu_1,\,\bar\nu_2$, such that*

$$W_1\,(\nu_{1,t},\,\nu_{2,t})\le \mathscr{C}W_1\,(\bar\nu_1,\,\bar\nu_2),\qquad \forall\, t\in[0,\,T]. \tag{6.16}$$

Estimate (6.16) gives the continuous dependence of the solutions to Problem (6.12) on the initial data. For $\bar\nu_1=\bar\nu_2$ it also gives uniqueness.

*Proof.* Let $\varphi\in\mathrm{Lip}_1(\mathbb{R}^d)$, then

$$\begin{aligned}\int_{\mathbb{R}^d}\varphi\,d(\nu_{2,t}-\nu_{1,t}) &= \int_{\mathbb{R}^d}\varphi(\gamma^{\nu_2}(t))\,d\bar\nu_2-\int_{\mathbb{R}^d}\varphi(\gamma^{\nu_1}(t))\,d\bar\nu_1\\ &= \int_{\mathbb{R}^d}(\varphi(\gamma^{\nu_2}(t))-\varphi(\gamma^{\nu_1}(t)))\,d\bar\nu_2+\int_{\mathbb{R}^d}\varphi(\gamma^{\nu_1}(t))\,d(\bar\nu_2-\bar\nu_1).\end{aligned}$$

Since both $\varphi$ and $\gamma^{\nu_1}(t)$ are Lipschitz continuous in $x$ so is $\varphi\circ\gamma^{\nu_1}(t)$, therefore we can bound from above the second term at the right-hand side by $W_1\,(\bar\nu_1,\,\bar\nu_2)$. As far as the first term is concerned, we first use the Lipschitz continuity of $\varphi$ and then Lemma 6.1 along with $\bar\nu_2(\mathbb{R}^d)=1$ to get:

$$\le\mathscr{C}\left(\int_0^t W_1\,(\nu_{1,s},\,\nu_{2,s})\,ds+W_1\,(\bar\nu_1,\,\bar\nu_2)\right).$$

Finally, taking the supremum of both sides over $\varphi$ we obtain

$$W_1\,(\nu_{1,t},\,\nu_{2,t})\le\mathscr{C}\left(\int_0^t W_1\,(\nu_{1,s},\,\nu_{2,s})\,ds+W_1\,(\bar\nu_1,\,\bar\nu_2)\right),$$

whence the thesis follows once again by Gronwall's inequality.

## 6.5 Existence of the Solution

Far more laborious is the proof of existence of solutions to Problem (6.12), of which we will outline here the main ideas without reporting all detailed calculations. The interested reader is referred to the bibliographical notes at the end of this chapter for a list of references addressing thoroughly the missing technical aspects.

In order to proceed further, we need to formulate additional assumptions on the velocity field:

**Assumption 6.2 (Boundedness and mild linearity of $v$).**

*(i) There exists a constant $V_{\max} > 0$ such that*

$$|v[\nu](x)| \leq V_{\max}$$

*for all $x \in \mathbb{R}^d$ and all $\nu \in \mathscr{P}_1\mathbb{R}^d$.*

*(ii) For any $a \in [0, 1]$ and any pair of measures $\nu_1, \nu_2 \in \mathscr{P}_1\mathbb{R}^d$ it results*

$$v[a\nu_1 + (1-a)\nu_2] = av[\nu_1] + (1-a)v[\nu_2].$$

We call Assumption 6.2(ii) *mild linearity* because it imposes the linearity of the mapping $\nu \mapsto v[\nu]$ for *convex* linear combinations only. As a matter of fact, it is not strictly needed for proving the existence of solutions, nevertheless it has the merit of allowing for a proof which does not require a sophisticated technical background in optimal transport. Additionally, as we will see in Sect. 6.8, it is not a nuisance as far as the application of the theory to reasonable models of crowd dynamics is concerned.

**Theorem 6.2.** *Under Assumptions 6.1 and 6.2, together with the further requirement $\bar{\nu} \in \mathbb{R}^d$, there exists a solution to Problem (6.12) in the sense of Definition 6.1.*

*Proof.* * The main idea is to start from a family of discrete-in-time versions, hereafter labeled by an index $k \in \mathbb{N}$, of the representation formula (6.14). These are constructed by introducing in the interval $[0, T]$ a lattice $\{t_n^k\}_{n=0}^{N_k}$ of uniformly spaced points, such that $t_0^k = 0$, $t_{N_k}^k = T$, $t_{n+1}^k - t_n^k = \Delta t_k$, and then computing in $\mathscr{P}_1\mathbb{R}^d$:

$$\begin{cases} \nu_{n+1}^k = \gamma_n^k \# \nu_n^k \\ \nu_0^k = \bar{\nu}, \end{cases} \qquad \gamma_n^k(x) = x + v[\nu_n^k](x)\Delta t_k, \tag{6.17}$$

*Skip on first reading.

where $\nu_n^k$ is shorthand for $\nu_{t_n^k}^k$. The index $k$ identifies the level of refinement of the lattice. In particular, for $k \to \infty$ we assume that $\Delta t_k \to 0$, however in such a way that $N_k \Delta t_k = T$ for all $k$.

By means of a piecewise linear interpolation in time, we construct the following measure-valued curve $t \mapsto \lambda_t^k$ in the space $C([0,\, T];\, \mathscr{P}_1\mathbb{R}^d)$:

$$\lambda_t^k = \sum_{n=0}^{N_k-1} \left[ \left( 1 - \frac{t - t_n^k}{\Delta t_k} \right) \nu_n^k + \frac{t - t_n^k}{\Delta t_k} \nu_{n+1}^k \right] \mathbb{1}_{[t_n^k,\, t_{n+1}^k]}(t), \tag{6.18}$$

which then we want to use for:

(i) Showing that the sequence $\{\lambda_\bullet^k\}_{k\geq 0}$ converges to some $\nu_\bullet \in C([0,\, T];\, \mathscr{P}_1\mathbb{R}^d)$ when $\Delta t_k \to 0$ (i.e., $k \to \infty$).
(ii) Showing that $\nu_\bullet$ is a weak solution to Problem 6.12 in the sense of Definition 6.1.

## *Step (i)*

The crucial estimates are:

- That first and second order moments of the $\nu_n^k$'s are uniformly bounded with respect to both $n$ and $k$:

$$\sup_{k\geq 0} \sup_{1\leq n\leq N_k} \int_{\mathbb{R}^d} |x|^p \, d\nu_n^k(x) < +\infty, \qquad p = 1,\, 2, \tag{6.19}$$

  which can be proved by induction from (6.17) using also the hypothesis $\bar{\nu} \in \mathbb{R}^d$.
- That the curves $t \mapsto \lambda_t^k$ are Lipschitz continuous uniformly in $k$:

$$W_1\left(\lambda_s^k,\, \lambda_t^k\right) \leq V_{\max} |t - s|, \qquad \forall\, s,\, t \in [0,\, T], \tag{6.20}$$

  which can be proved by first showing from (6.17) that $W_1\left(\nu_n^k\, \nu_{n+1}^k\right) \leq V_{\max} \Delta t_k$ for all $n$ (notice that here the uniform boundedness of $v$ comes into play) and then using the interpolation (6.18).
- That first and second order moments of $\lambda_t^k$ are uniformly bounded with respect to both $t$ and $k$:

$$\sup_{k\geq 0} \sup_{t\in[0,\, T]} \int_{\mathbb{R}^d} |x|^p \, d\lambda_t^k(x) < +\infty, \qquad p = 1,\, 2, \tag{6.21}$$

  which follows immediately by interpolation from (6.19).

Owing to them we can show that the sequence $\{\lambda_\bullet^k\}_{k\geq 0}$ is relatively compact in $C([0,\,T];\,\mathscr{P}_1\mathbb{R}^d)$, hence that it converges (upon passing to subsequences, but we continue to label the convergent subsequence by $k$ for brevity): $\lambda_\bullet^k \to \nu_\bullet$ for $k \to \infty$, namely

$$\lim_{k\to\infty} \sup_{t\in[0,\,T]} W_1\left(\lambda_t^k,\,\nu_t\right) = 0. \tag{6.22}$$

Particularly, we rely on Ascoli-Arzelà's compactness criterion, which says that such a relative compactness can be proved through the equicontinuity of $\{\lambda_\bullet^k\}_{k\geq 0}$ and the relative compactness of $\{\lambda_t^k\}_{k\geq 0}$ in $\mathscr{P}_1\mathbb{R}^d$ for any fixed $t \in [0,\,T]$.

- Equicontinuity follows straightforwardly from (6.20), thanks to the fact that the constant $V_{\max}$ does not depend on $k$.
- Relative compactness of $\{\lambda_t^k\}_{k\geq 0}$ in $\mathscr{P}_1\mathbb{R}^d$ is equivalent to its tightness and uniform integrability of first order moments.
  - A sufficient condition for tightness is the existence of a function $f : \mathbb{R}^d \to [0,\,+\infty]$, with compact sub-levels, such that

$$\sup_{k\geq 0} \int_{\mathbb{R}^d} f\, d\lambda_t^k < +\infty.$$

    Estimate (6.21) shows that we can take $f(x) = |x|$.
  - A sufficient condition for the uniform integrability of first order moments is that there exists $p > 1$ such that

$$\sup_{k\geq 0} \int_{\mathbb{R}^d} |x|^p\, d\lambda_t^k(x) < +\infty.$$

    Again, estimate (6.21) shows that this actually holds for $p = 2$.

### *Step (ii)*

We now proceed by inserting (6.18) into (6.13) to find, after some algebraic manipulations:

$$\frac{d}{dt}\int_{\mathbb{R}^d} \phi\, d\lambda_t^k - \int_{\mathbb{R}^d} \nabla\phi\cdot v[\lambda_t^k]\, d\lambda_t^k = \sum_{n=0}^{N_k-1} \left\{ \frac{\Delta t_k}{2} \int_{\mathbb{R}^d} D^2\phi(\bar{x}) v[\nu_n^k]\cdot v[\nu_n^k]\, d\nu_n^k \right.$$
$$\left. - \frac{t-t_n^k}{\Delta t_k} \int_{\mathbb{R}^d} \nabla\phi\cdot v[\nu_n^k]\, d(\nu_{n+1}^k - \nu_n^k) \right.$$

$$
\begin{aligned}
&- \left(\frac{t-t_n^k}{\Delta t_k}\right)^2 \int_{\mathbb{R}^d} \nabla\phi \cdot (v[\nu_{n+1}^k] - v[\nu_n^k])\, d\nu_{n+1}^k \\
&+ \left(\frac{t-t_n^k}{\Delta t_k}\right)^2 \int_{\mathbb{R}^d} \nabla\phi \cdot (v[\nu_{n+1}^k] - v[\nu_n^k])\, d\nu_n^k \Bigg\} \\
&\times \mathbb{1}_{[t_n^k,\, t_{n+1}^k]}(t),
\end{aligned}
$$

where $D^2\phi$ is the Hessian of $\phi$ and $\bar{x}$ is a point of the segment connecting $x$ and $x + v[\nu_n^k]\Delta t_k$ (they come from the Taylor expansion of $\phi(\gamma_n^k(x))$, after using the push forward (6.17) for converting integrals with respect to $\nu_{n+1}^k$ into integrals with respect to $\nu_n^k$). This step is where one uses specifically Assumption 6.2(ii) with $a = \frac{t-t_n^k}{\Delta t_k}$.

By invoking the estimates obtained in step 6.5 we further get:

$$
\begin{aligned}
&\left| \int_0^t \left( \frac{d}{ds} \int_{\mathbb{R}^d} \phi\, d\lambda_s^k - \int_{\mathbb{R}^d} \nabla\phi \cdot v[\lambda_s^k]\, d\lambda_s^k \right) ds \right| \\
&\qquad \le \int_0^t \left| \frac{d}{ds} \int_{\mathbb{R}^d} \phi\, d\lambda_s^k - \int_{\mathbb{R}^d} \nabla\phi \cdot v[\lambda_s^k]\, d\lambda_s^k \right| ds \le \mathscr{C}\Delta t_k,
\end{aligned}
$$

therefore, by performing the time integration at the left-hand side (with $\lambda_0^k = \nu_0^k \equiv \bar{\nu}$ by construction, cf. (6.17), (6.18)),

$$
\lim_{k\to\infty} \left| \int_{\mathbb{R}^d} \phi\, d\lambda_t^k - \int_{\mathbb{R}^d} \phi\, d\bar{\nu} - \int_0^t \int_{\mathbb{R}^d} \nabla\phi \cdot v[\lambda_s^k]\, d\lambda_s^k\, ds \right| = 0.
$$

In order to conclude the proof, it remains to show that

$$
\lim_{k\to\infty} \int_{\mathbb{R}^d} \phi\, d\lambda_t^k = \int_{\mathbb{R}^d} \phi\, d\nu_t, \qquad \lim_{k\to\infty} \int_0^t \int_{\mathbb{R}^d} \nabla\phi \cdot v[\lambda_s^k]\, d\lambda_s^k = \int_0^t \int_{\mathbb{R}^d} \nabla\phi \cdot v[\nu_s]\, d\nu_s
$$

for all $t \in (0, T]$. This is done easily via (6.22). In particular, in the second case one can use that the limit commutes with the time integral owing to dominated convergence (in fact $\left|\int_{\mathbb{R}^d} \nabla\phi \cdot v[\lambda_s^k]\, d\lambda_s^k\right| \le V_{\max}\|\nabla\phi\|_\infty$).

The requirement that $\bar{\nu} \in \mathbb{R}^d$ has been technically necessary in step 6.5 for obtaining the uniform integrability of first order moments of the $\lambda_t^k$'s. As such, it cannot be strictly motivated by appealing to modeling reasons. Nevertheless, it is worth pointing out that it is naturally satisfied in most real world applications, where one reasonably deals with initial conditions with compact support (indeed, a crowd spread in the whole space $\mathbb{R}^d$ would not make much sense). If this is the case, then $\mathrm{supp}(\bar{\nu})$ is contained in a ball $B_R(0)$ centered at the origin and with large enough radius $R > 0$, so that:

$$\int_{\mathbb{R}^d} |x|^p \, d\bar{\nu}(x) = \int_{\mathrm{supp}(\bar{\nu})} |x|^p \, d\bar{\nu}(x) \leq R^p.$$

Hence, $\bar{\nu}$ has actually finite moments of any order $p \geq 0$.

## 6.6 Approximation of the Solution

We now reconsider the numerical scheme (5.37) presented in Chap. 5 and show that it indeed approximates the solution to Problem (6.12). Actually, for technical purposes we will need here a notation slightly different from that introduced in the previous chapter. Therefore, in order to fix the ideas we begin by briefly reviewing the procedure which leads to the scheme.

First, one obtains from Problem (6.12) the discrete-in-time version (6.17), which actually corresponds to a time-explicit Euler approximation of (6.12). Secondly, one approximates $\nu_n^k$ by a piecewise constant absolutely continuous measure:

$$\tilde{\nu}_n^k = \tilde{\rho}_n^k \mathscr{L}^d, \qquad \tilde{\rho}_n^k(x) = \sum_{i \in \mathbb{Z}^d} \rho_{n,i}^k \mathbb{1}_{E_i^k}(x), \tag{6.23}$$

where $\{E_i^k\}_{i \in \mathbb{Z}^d}$ is a pairwise disjoint partition of $\mathbb{R}^d$, that for simplicity we will assume formed by hypercubes of size length $\Delta x_k > 0$, thus $\mathscr{L}^d(E_i^k) = \Delta x_k^d$ all $i$, with $\Delta x_k \to 0$ for $k \to \infty$. Notice that we are using the index $k$ to label the level of refinement of both the time and space lattice, whose grid steps are $\Delta t_k$ and $\Delta x_k$, respectively.

Next, one approximates also the velocity $v[\nu_n^k]$ by a spatially piecewise constant vector field:

$$\tilde{v}_n^k(x) = \sum_{i \in \mathbb{Z}^d} v[\tilde{\nu}_n^k](x_i^k) \mathbb{1}_{E_i^k}(x),$$

$x_j^k$ being any point of the cell $E_j^k$, for instance its center. In practice, in each space cell the velocity is computed by means of the true analytical expression of $v$ but using the approximate measure (6.23) in place of $\nu_n^k$. Consequently, also the flow map $\gamma_n^k$ is approximated as

$$\tilde{\gamma}_n^k(x) = x + \tilde{v}_n^k(x) \Delta t_k,$$

which in each cell acts as a rigid translation directed along the vector $v[\tilde{\nu}_n^k](x_j^k)\Delta t_k$.

Finally, one imposes that two successive measures $\tilde{\nu}_n^k$, $\tilde{\nu}_{n+1}^k$ are linked by a push forward over the grid cells guided by the mapping $\tilde{\gamma}_n^k$:

$$\tilde{\nu}_{n+1}^k(E_i^k) = (\tilde{\gamma}_n^k \# \tilde{\nu}_n^k)(E_i^k) = \tilde{\nu}_n^k((\tilde{\gamma}_n^k)^{-1}(E_i^k)), \qquad \forall\, i \in \mathbb{Z}^d, \tag{6.24}$$

which, after substituting the previous expressions of $\tilde{\nu}_n^k$, $\tilde{\nu}_{n+1}^k$, $\tilde{\gamma}_n^k$, gives rise to:

$$\rho_{n+1,i}^k = \frac{1}{\Delta x_k^d} \sum_{j \in \mathbb{Z}^d} \rho_{n,j}^k \mathscr{L}^d((\tilde{\gamma}_n^k)^{-1}(E_i^k) \cap E_j^k), \qquad i \in \mathbb{Z}^d. \tag{6.25}$$

*Remark 6.2.* Equivalence between (5.37) and (6.25) is readily established by observing that

$$\mathscr{L}^d((\tilde{\gamma}_n^k)^{-1}(E_i^k) \cap E_j^k) = \mathscr{L}^d(E_i^k \cap \tilde{\gamma}_n^k(E_j^k)),$$

in fact:

$$\begin{aligned}\mathscr{L}^d((\tilde{\gamma}_n^k)^{-1}(E_i^k) \cap E_j^k) &= \int_{E_j^k} \mathbb{1}_{E_i^k}(\tilde{\gamma}_n^k(x))\,dx = \int_{E_j^k} \mathbb{1}_{E_i^k}(x + v[\tilde{\nu}_n^k](x_j^k)\Delta t_k)\,dx \\ &= \int_{E_j^k + v[\tilde{\nu}_n^k](x_j^k)\Delta t_k} \mathbb{1}_{E_i^k}(y)\,dy = \int_{\tilde{\gamma}_n^k(E_j^k)} \mathbb{1}_{E_i^k}(y)\,dy \\ &= \mathscr{L}^d(E_i^k \cap \tilde{\gamma}_n^k(E_j^k)).\end{aligned}$$

Formula (5.37) is more convenient for computational purposes because it dispenses one from the computation of the inverse images of grid cells. In contrast, formula (6.25) is more convenient for analytical purposes, therefore we will invariably refer to it throughout this section.

*Remark 6.3.* Before going any further it is worth pausing a bit over two points.

First, in Chap. 5 we used the letter $\rho$ to denote the *mass* density, i.e., the density of the mass measure $\mu$. Conversely, in this section we are using $\rho$ to denote a *probability* density, namely the density of the probability measure $\nu$. Such a slight abuse of notation is justified by the fact that, owing to the discussion set forth in Sect. 6.3, the two densities are actually the same up to the scaling factor $N$. Hence the numerical scheme (6.25) is in turn the same in either case.

Secondly, in Chap. 5 we presented the numerical scheme (5.37) for approximating only the continuous part of the mass measure $\mu$, whereas here we have reintroduced it for approximating the whole probability measure $\nu$. We anticipate that we will indeed be able to prove the convergence of the numerical solution (6.23) to the weak solution of Problem (6.12) regardless of the spatial structure of the latter. Nevertheless, this theoretical result is true in the limit $\Delta t_k, \Delta x_k \to 0$. In practice, when one is forced to keep finite time and space steps, the approximation provided by (6.23)–(6.25) is much more reliable if the approximated measure is in turn absolutely continuous.

Some interesting elementary properties of the scheme (6.25) are:

- Preservation of the non-negativity of the solution,

$$\rho_{n,i}^k \geq 0, \ \forall\, i \in \mathbb{Z}^d \quad \Rightarrow \quad \rho_{n+1,i}^k \geq 0, \ \forall\, i \in \mathbb{Z}^d$$

and, by induction,

$$\rho^k_{0,i} \geq 0,\ \forall\, i \in \mathbb{Z}^d \quad \Rightarrow \quad \rho^k_{n,i} \geq 0,\ \forall\, i \in \mathbb{Z}^d,\ \forall\, n.$$

- Conservativeness,

$$\begin{aligned}\tilde{\nu}^k_{n+1}(\mathbb{R}^d) &= \int_{\mathbb{R}^d} \tilde{\rho}^k_{n+1}(x)\,dx = \sum_{i\in\mathbb{Z}^d} \rho^k_{n+1,i}\mathscr{L}^d(E^k_i)\\ &= \sum_{i\in\mathbb{Z}^d}\sum_{j\in\mathbb{Z}^d} \rho^k_{n,j}\mathscr{L}^d((\tilde{\gamma}^k_n)^{-1}(E^k_i)\cap E^k_j)\\ &= \sum_{j\in\mathbb{Z}^d} \rho^k_{n,j}\mathscr{L}^d((\tilde{\gamma}^k_n)^{-1}(\mathbb{R}^d)\cap E^k_j) =\\ &= \sum_{j\in\mathbb{Z}^d} \rho^k_{n,j}\mathscr{L}^d(E^k_j) = \int_{\mathbb{R}^d} \tilde{\rho}^k_n(x)\,dx = \tilde{\nu}^k_n(\mathbb{R}^d)\end{aligned}$$

and, by induction,

$$\tilde{\nu}^k_n(\mathbb{R}^d) = \tilde{\nu}^k_0(\mathbb{R}^d),\ \forall\, n.$$

They indicate that the numerical scheme is consistent with the main expected features of the exact solution $\nu_\bullet$. However, in order to achieve the proof of convergence some additional assumptions are needed.

**Assumption 6.3 (Discretization of the initial condition, mesh parameters).**

*(i) The initial coefficients $\{\rho^k_{0,i}\}_{i\in\mathbb{Z}^d}$ are obtained as*

$$\rho^k_{0,i} = \frac{\bar{\nu}(E^k_i)}{\Delta x_k^d},\ \forall\, i \in \mathbb{Z}^d,$$

*where $\bar{\nu}$ is the exact initial datum of Problem (6.12).*

*(ii) The time and space steps $\Delta t_k$, $\Delta x_k$ are such that*

$$\Delta x_k = o(\Delta t_k) \quad \textit{when} \quad k \to \infty.$$

*Equivalently, there exists a sequence $\{\beta_k\}_{k\geq 0} \subset \mathbb{R}_+$, with $\beta_k \to 0$ for $k \to \infty$, such that $\Delta x_k = \beta_k \Delta t_k$.*

In the same spirit as Sect. 6.5, we introduce now a piecewise linear time interpolation of the $\tilde{\nu}^k_n$'s in order to deal with time-continuous curves $t \mapsto \tilde{\lambda}^k_t$:

$$\tilde{\lambda}^k_t = \sum_{n=0}^{N_k-1} \left[\left(1 - \frac{t-t^k_n}{\Delta t_k}\right)\tilde{\nu}^k_n + \frac{t-t^k_n}{\Delta t_k}\tilde{\nu}^k_{n+1}\right] \mathbb{1}_{[t^k_n,\, t^k_{n+1}]}(t). \tag{6.26}$$

Again we assume that the time lattice is made of $N_k$ intervals of equal size $\Delta t_k$, such that $N_k \Delta t_k = T$ independently of $k$.

Equipped with all of this stuff, we can finally prove:

**Theorem 6.3.** *Under Assumptions 6.1, 6.2, and 6.3, with moreover $\bar{\nu} \in \mathscr{P}_1\mathbb{R}^d$, if $\{\tilde{\lambda}^k_\bullet\}_{k\geq 0}$ converges to some $\nu_\bullet$ in $C([0,\, T];\, \mathscr{P}_1\mathbb{R}^d)$ when $k \to \infty$ then $\nu_\bullet$ is a weak solution to Problem (6.12) in the sense of Definition 6.1.*

This result reminds of the Lax-Wendroff's Theorem about the convergence of conservative numerical schemes for hyperbolic conservation laws. In fact, the convergence of the approximating sequence $\{\tilde{\lambda}^k_\bullet\}_{k\geq 0}$ on finer and finer grids is taken as an assumption, and what is actually proved is that then its limit is a weak solution to Problem (6.12). Nevertheless, the theorem does not guarantee that the numerical solution constructed out of the scheme (6.25) does indeed converge to something. For this, see Proposition 6.1 at the end of the next proof.

*Proof.* * We organize the proof in two steps:

(i) First we establish some regularity estimates for the measures $\tilde{\nu}^k_n$ and consequently for the curves $t \mapsto \tilde{\lambda}^k_\bullet$.
(ii) Next we insert $\tilde{\lambda}^k_t$ into (6.13) and, using the previous estimates, pass to the limit $k \to \infty$.

## *Step (i)*

Relation (6.24) implies that the $\tilde{\nu}^k_n$'s satisfy

$$\int_{\mathbb{R}^d} s \, d\tilde{\nu}^k_{n+1} = \int_{\mathbb{R}^d} s(\tilde{\gamma}^k_n) \, d\tilde{\nu}^k_n \tag{6.27}$$

for all simple functions $s$ adapted to the spatial grid, i.e., piecewise constant functions of the form $s = \sum_{i\in\mathbb{Z}^d} \alpha_i \mathbb{1}_{E^k_i}$, $\alpha_i \in \mathbb{R}$. In general (6.27) does not hold for any $s$ (as it would if $\tilde{\nu}^k_{n+1}$ were the exact push forward of $\tilde{\nu}^k_n$ via $\tilde{\gamma}^k_n$), however it yields further the estimate

$$\left| \int_{\mathbb{R}^d} \varphi \, d\tilde{\nu}^k_{n+1} - \int_{\mathbb{R}^d} \varphi(\tilde{\gamma}^k_n) \, d\tilde{\nu}^k_n \right| \leq 2\,\mathrm{Lip}(\varphi)\sqrt{d}\,\Delta x_k \tag{6.28}$$

for all Lipschitz continuous $\varphi : \mathbb{R}^d \to \mathbb{R}$. With (6.28) one is in a position to check that the $\tilde{\nu}^k_n$'s have uniformly bounded first order moments with respect to both $n$ and $k$:

*Skip on first reading.

$$\sup_{k\geq 0}\sup_{1\leq n\leq N_k}\int_{\mathbb{R}^d}|x|\,d\tilde{\nu}_n^k(x)<+\infty$$

and, from this by interpolation, that the same is true also for the curves $t\mapsto\tilde{\lambda}_t^k$:

$$\sup_{k\geq 0}\sup_{t\in[0,\,T]}\int_{\mathbb{R}^d}|x|\,d\tilde{\lambda}_t^k(x)<+\infty.$$

This says, in particular, that $\tilde{\lambda}_t^k\in\mathscr{P}_1\mathbb{R}^d$ for all $t\in[0,\,T]$ and all $k\geq 0$ (the fact that $\tilde{\lambda}_t^k$ is a probability measure is obvious by interpolation from the conservativeness of the numerical scheme (6.25)).

Furthermore, from (6.28) choosing $\varphi\in\mathrm{Lip}_1(\mathbb{R}^d)$ it follows

$$W_1\left(\tilde{\nu}_n^k,\,\tilde{\nu}_{n+1}^k\right)\leq\left(V_{\max}+2\sqrt{d}\sup_{k\geq 0}\beta_k\right)\Delta t_k,$$

the $\beta_k$'s being the numbers appearing in Assumption 6.3(ii), whence also

$$W_1\left(\tilde{\lambda}_s^k,\,\tilde{\lambda}_t^k\right)\leq\left(V_{\max}+2\sqrt{d}\sup_{k\geq 0}\beta_k\right)(t-s),\tag{6.29}$$

thus in particular $\lambda_\bullet^k\in C([0,\,T];\,\mathscr{P}_1\mathbb{R}^d)$ all $k$.

### *Step (ii)*

Similarly to the proof of Theorem 6.2 we plug now (6.26) into (6.13) to discover, after some technical calculations (which again exploit Assumption 6.26.2):

$$\begin{aligned}\frac{d}{dt}\int_{\mathbb{R}^d}\phi\,d\tilde{\lambda}_t^k-\int_{\mathbb{R}^d}\nabla\phi\cdot v[\tilde{\lambda}_t^k]\,d\tilde{\lambda}_t^k=\frac{1}{\Delta t_k}\sum_{n=0}^{N_k-1}\left\{\int_{\mathbb{R}^d}\phi\,d\tilde{\nu}_{n+1}^k-\int_{\mathbb{R}^d}\phi(g_n^k)\,d\tilde{\nu}_n^k\right\}\\ \times\mathbb{1}_{[t_n^k,\,t_{n+1}^k]}(t)\\ +\sum_{n=0}^{N_k}\left\{\frac{\Delta t_k}{2}\int_{\mathbb{R}^d}(D^2\phi(\bar{x})v[\tilde{\nu}_n^k])\cdot v[\tilde{\nu}_n^k]\,d\tilde{\nu}_n^k\right.\\ -\frac{t-t_n^k}{\Delta t_k}\int_{\mathbb{R}^d}\nabla\phi\cdot v[\tilde{\nu}_n^k]\,d(\tilde{\nu}_{n+1}^k-\tilde{\nu}_n^k)\\ \left.+\left(\frac{t-t_n^k}{\Delta t_k}\right)^2\int_{\mathbb{R}^d}\nabla\phi\cdot(v[\tilde{\nu}_{n+1}^k]-v[\tilde{\nu}_n^k])\,d\tilde{\nu}_n^k\right.\end{aligned}$$

$$- \left( \frac{t - t_n^k}{\Delta t_k} \right)^2 \int_{\mathbb{R}^d} \nabla\phi \cdot (v[\tilde{\nu}_{n+1}^k] - v[\tilde{\nu}_n^k])\, d\,\tilde{\nu}_{n+1}^k \Bigg\}$$
$$\times \mathbb{1}_{[t_n^k, t_{n+1}^k]}(t).$$

The last four terms at the right-hand side are analogous to those appearing in the proof of Theorem 6.2. Owing to Assumption 6.1 and to the estimates obtained in the previous step (i), they can be collectively bounded from above by $\mathscr{C}\Delta t_k$.

Conversely, the first term at the right-hand side involves the function

$$g_n^k(x) := x + v[\tilde{\nu}_n^k](x)\Delta t_k,$$

i.e., the discrete-time flow map computed with respect to the space-approximate measure $\tilde{\nu}_n^k$ rather than to $\nu_n^k$, cf. (6.17). Notice that, compared to the approximate flow map $\tilde{\gamma}_n^k$, the mapping $g_n^k$ is in general not a piecewise translation over the grid cells. This term must be carefully estimated, also in view of the presence of the time step $\Delta t_k$ at the denominator. Adding and subtracting $\int_{\mathbb{R}^d} \varphi(\tilde{\gamma}_n^k)\, d\,\tilde{\nu}_n^k$ and invoking (6.28) to handle it, one ultimately sees that there exists $\mathscr{C} > 0$ such that

$$\left| \int_{\mathbb{R}^d} \varphi\, d\,\tilde{\nu}_{n+1}^k - \int_{\mathbb{R}^d} \varphi(g_n^k)\, d\,\tilde{\nu}_n^k \right| \le \mathscr{C}\,\mathrm{Lip}(\varphi)\sqrt{d}\,\Delta x_k$$

for all Lipschitz continuous functions $\varphi : \mathbb{R}^d \to \mathbb{R}$. Hence, taking in particular $\phi \in C_c^\infty(\mathbb{R}^d)$ gives

$$\frac{1}{\Delta t_k} \left| \int_{\mathbb{R}^d} \phi\, d\,\tilde{\nu}_{n+1}^k - \int_{\mathbb{R}^d} \phi(g_n^k)\, d\,\tilde{\nu}_n^k \right| \le \mathscr{C}\,\mathrm{Lip}(\varphi)\sqrt{d}\,\beta_k$$

and finally

$$\left| \frac{d}{dt} \int_{\mathbb{R}^d} \phi\, d\,\tilde{\lambda}_t^k - \int_{\mathbb{R}^d} \nabla\phi \cdot v[\tilde{\lambda}_t^k]\, d\,\tilde{\lambda}_t^k \right| \le \mathscr{C}(\beta_k + \Delta t_k).$$

Integrating in time from 0 to $t \le T$ we obtain

$$\left| \int_0^t \left( \frac{d}{ds} \int_{\mathbb{R}^d} \phi\, d\,\tilde{\lambda}_s^k - \int_{\mathbb{R}^d} \nabla\phi \cdot v[\tilde{\lambda}_s^k]\, d\,\tilde{\lambda}_s^k \right) ds \right|$$
$$\le \int_0^t \left| \frac{d}{ds} \int_{\mathbb{R}^d} \phi\, d\,\tilde{\lambda}_s^k - \int_{\mathbb{R}^d} \nabla\phi \cdot v[\tilde{\lambda}_s^k]\, d\,\tilde{\lambda}_s^k \right| ds \le \mathscr{C}T(\beta_k + \Delta t_k)$$

whence, by performing the integration at the left-hand side,

$$\lim_{k\to\infty} \left| \int_{\mathbb{R}^d} \phi\, d\,\tilde{\lambda}_t^k - \int_{\mathbb{R}^d} \phi\, d\,\tilde{\nu}_0^k - \int_0^t \int_{\mathbb{R}^d} \nabla\phi \cdot v[\tilde{\lambda}_s^k]\, d\,\tilde{\lambda}_s^k\, ds \right| = 0, \tag{6.30}$$

where we have used that $\tilde{\lambda}_0^k = \tilde{\nu}_0^k$ by interpolation, cf. (6.26).

Now, since by assumption $\{\tilde{\lambda}^k_\bullet\}_{k\geq 0}$ converges in $C([0,\,T];\,\mathscr{P}_1\mathbb{R}^d)$ to some $\nu_\bullet$, we have $\sup_{t\in[0,\,T]} W_1\left(\tilde{\lambda}^k_t,\,\nu_t\right)\to 0$ for $k\to\infty$. As seen in the proof of Theorem 6.2, this implies (up to subsequences)

$$\int_{\mathbb{R}^d}\phi\,d\tilde{\lambda}^k_t\to\int_{\mathbb{R}^d}\phi\,d\nu_t,\qquad \int_0^t\int_{\mathbb{R}^d}\nabla\phi\cdot v[\tilde{\lambda}^k_s]\,d\tilde{\lambda}^k_s\,ds\to\int_0^t\int_{\mathbb{R}^d}\nabla\phi\cdot v[\nu_s]\,d\nu_s\,ds$$

when $k\to\infty$. Therefore, from (6.30) it follows that such a $\nu_\bullet$ is a weak solution to Problem (6.12) provided we also have

$$\int_{\mathbb{R}^d}\phi\,d\tilde{\nu}^k_0\to\int_{\mathbb{R}^d}\phi\,d\bar{\nu}\qquad(k\to\infty).\tag{6.31}$$

But this holds due to the approximation of the initial datum prescribed by Assumption 6.3(i). In fact, for any $\varphi\in\mathrm{Lip}_1(\mathbb{R}^d)$ it results

$$\int_{\mathbb{R}^d}\varphi\,d\tilde{\nu}^k_0=\sum_{i\in\mathbb{Z}^d}\int_{E^k_i}\varphi(x)\frac{\bar{\nu}(E^k_i)}{\Delta x_k^d}\,dx=\sum_{i\in\mathbb{Z}^d}\left(\frac{1}{\Delta x_k^d}\int_{E^k_i}\varphi(x)\,dx\right)\bar{\nu}(E^k_i)=\int_{\mathbb{R}^d}s\,d\bar{\nu},$$

where $s=\sum_{i\in\mathbb{Z}^d}\alpha_i\,\mathbb{1}_{E^k_i}$ with $\alpha_i=\frac{1}{\Delta x_k^d}\int_{E^k_i}\varphi(x)\,dx$. Thus

$$\int_{\mathbb{R}^d}\varphi\,d(\bar{\nu}-\tilde{\nu}^k_0)=\int_{\mathbb{R}^d}(\varphi-s)\,d\bar{\nu}=\sum_{i\in\mathbb{Z}^d}\int_{E^k_i}(\varphi(x)-\alpha_i)\,d\bar{\nu}(x)$$

whence, considering that $|\varphi(x)-\alpha_i|\leq\frac{1}{\Delta x_k^d}\int_{E^k_i}|\varphi(x)-\varphi(y)|\,dy$, we obtain

$$\begin{aligned}&\leq\frac{1}{\Delta x_k^d}\sum_{i\in\mathbb{Z}^d}\int_{E^k_i}\int_{E^k_i}|x-y|\,dy\,d\bar{\nu}(x)\\&\leq\sqrt{d}\,\Delta x_k,\end{aligned}$$

which implies $W_1\left(\tilde{\nu}^k_0,\,\bar{\nu}\right)\to 0$ when $k\to\infty$, and this is enough for concluding (6.31).

As previously anticipated, the missing point of Theorem 6.3 is a criterion ensuring the convergence in $C([0,\,T];\,\mathscr{P}_1\mathbb{R}^d)$ of the (interpolated) sequence of approximate solutions $\{\tilde{\lambda}^k_\bullet\}_{k\geq 0}$. The gap is filled by the following proposition.

**Proposition 6.1.** *Let a bounded set $K\subset\mathbb{R}^d$ exist such that* $\mathrm{supp}(\tilde{\nu}^k_n)\subseteq K$ *for all* $0\leq n\leq N_k$ *and all* $k\geq 0$. *Then* $\{\tilde{\lambda}^k_\bullet\}_{k\geq 0}$ *converges in* $C([0,\,T];\,\mathscr{P}_1\mathbb{R}^d)$.

*Proof.* Due to the assumption on the supports of the $\tilde{\nu}^k_n$'s, it results $\mathrm{supp}(\tilde{\lambda}^k_t)\subseteq K$ for all $t\in[0,\,T]$ and all $k\geq 0$ as well. In addition, since $K$ is bounded, there exists $R>0$ so large that the ball $B_R(0)$ contains $K$, whence:

$$\int_{\mathbb{R}^d} |x|^p \, d\tilde{\lambda}_t^k(x) = \int_K |x|^p \, d\tilde{\lambda}_t^k(x) \leq R^p < +\infty, \qquad \forall\, p \geq 0.$$

Therefore the measures $\tilde{\lambda}_t^k$ have uniformly bounded moments of any order. Recalling the proof of Theorem 6.2, this implies that $\{\tilde{\lambda}_t^k\}_{k\geq 0}$ is relatively compact in $\mathscr{P}_1\mathbb{R}^d$ for any fixed $t \in [0, T]$. Moreover, estimate (6.29) implies that $\{\tilde{\lambda}_\bullet^k\}_{k\geq 0}$ is equicontinuous. Ascoli-Arzelà compactness criterion allows us to conclude that $\{\tilde{\lambda}_\bullet^k\}_{k\geq 0}$ is relatively compact in $C([0, T]; \mathscr{P}_1\mathbb{R}^d)$, and ultimately that it converges (up to subsequences).

The set $K$ mentioned in Proposition 6.1 is easily imagined to exist especially when the initial condition $\bar{v}$ has compact support, taking into account that (6.9) describes a transport with *finite* speed (cf. the simulations presented in Chap. 2).

## 6.7 Spatial Structure of the Solution

None of the theorems presented in the previous sections provides any information about the structure in space of the measure $v_t$ solving Problem (6.12). However, this is an important issue especially in view of the derivation of multiscale models, when one is interested in that a multiscale structure of the initial condition be preserved at all successive times.

Assume therefore that initially the probability measure associated with the crowd distribution is of the form

$$v_0 = \theta m_0 + (1 - \theta) M_0, \qquad \theta \in [0, 1],$$

where, with a slight abuse of notation with respect to (5.22), we have denoted by

$$m_0 = \frac{1}{N} \sum_{k=1}^{N} \delta_{x_0^k}, \qquad M_0 = \rho_0 \mathscr{L}^d$$

the discrete and continuous parts of $v_0$. (The symbols $m_0$, $M_0$ are the same as those used in Chap. 5 for the discrete and continuous parts of the mass measure, but since passing from the mass to the probability is only a matter of scaling we prefer to avoid an over-proliferation of new symbols.) According to the representation formula (6.14), and using the linearity of the push forward, the probability measure at successive times $t > 0$ is

$$v_t = \theta(\gamma(t)\#m_0) + (1 - \theta)(\gamma(t)\#M_0),$$

thus we can study separately the transport of the discrete and the continuous part.

The discrete part is the easy one, in fact for every measurable $E \in \mathscr{B}(\mathbb{R}^d)$ we see immediately that:

$$\begin{aligned} m_t(E) = (\gamma(t)\#m_0)(E) &= m_0(\gamma(t)^{-1}(E)) \\ &= \frac{1}{N}\sum_{k=1}^{N} \delta_{x_0^k}(\gamma(t)^{-1}(E)) \\ &= \frac{1}{N}\sum_{k=1}^{N} \delta_{\gamma(t,\, x_0^k)}(E), \end{aligned}$$

hence, up to defining $x^k(t) := \gamma(t,\, x_0^k)$, we obtain $m_t = \frac{1}{N}\sum_{k=1}^{N} \delta_{x^k(t)}$. In other words, the discrete part remains discrete at all times, its atoms being transported by the flow map $\gamma$.

The continuous part requires instead more care, for we have to ensure that the density does not concentrate over volumeless space structures (points, curves, surfaces, depending on the space dimension $d$) carrying a nonzero mass. As the next results demonstrate, this does not happen for all possible flow maps.

**Theorem 6.4.** *For every $t \in (0,\, T]$ let $\mathscr{C}_t > 0$ exist such that*

$$\mathscr{L}^d(\gamma(t)^{-1}(E)) \le \mathscr{C}_t \mathscr{L}^d(E), \qquad \forall\, E \in \mathscr{B}(\mathbb{R}^d). \tag{6.32}$$

*Then $M_t = \gamma(t)\#M_0$ is absolutely continuous with respect to $\mathscr{L}^d$ for all $t \in (0,\, T]$.*

*Proof.* Saying that $M_t$ is absolutely continuous with respect to $\mathscr{L}^d$ means that the measure $M_t$ of every Lebesgue-negligible measurable set vanishes.

Let $E \in \mathscr{B}(\mathbb{R}^d)$ be such that $\mathscr{L}^d(E) = 0$. Then $\mathscr{L}^d(\gamma(t)^{-1}(E)) = 0$ as well in view of (6.32), and furthermore $M_0(\gamma(t)^{-1}(E)) = 0$ because $M_0$ is absolutely continuous with respect to $\mathscr{L}^d$ by construction. But then $M_t(E) = M_0(\gamma(t)^{-1}(E)) = 0$ and the thesis is proved due to the arbitrariness of $E$.

Heuristically speaking, (6.32) says that the flow map does not shrink measurable sets too much (in the sense of their Lebesgue measure: Length, area, volume, or whatever). In fact, according to (6.32) the $\mathscr{L}^d$-measure of the "original" set $\gamma(t)^{-1}(E)$ can be controlled via the $\mathscr{L}^d$-measure of the set $E$ obtained after the transformation operated by $\gamma(t)$. The main point is how to check, in a reasonably simple way, the validity of property (6.32) for a given flow map. A sufficient answer, covering at least the case of smooth flow maps, is provided by the following result.

**Proposition 6.2.** *Let $\gamma(t) : \mathbb{R}^d \to \mathbb{R}^d$ be a diffeomorphism with Lipschitz constant "sufficiently" small, i.e., precisely:*

$$\mathrm{Lip}(\gamma(t)) < \frac{1}{\mathrm{Lip}(v)T}. \tag{6.33}$$

*Then $\gamma(t)$ satisfies* (6.32)*.*

*Proof.* First notice that for all $x_1,\ x_2$ we have

$$\begin{aligned}|\gamma(t,\,x_2)-\gamma(t,\,x_1)| &= \left|x_2-x_1+\int_0^t \{v[\nu_s](\gamma(s,\,x_2))-v[\nu_s](\gamma(s,\,x_1))\}\,ds\right| \\ &\geq |x_2-x_1|-\int_0^t |v[\nu_s](\gamma(s,\,x_2))-v[\nu_s](\gamma(s,\,x_1))|\,ds \\ &\geq |x_2-x_1|-\mathrm{Lip}(v)\int_0^t |\gamma(s,\,x_2)-\gamma(s,\,x_1)|\,ds \\ &\geq (1-\mathrm{Lip}(\gamma(t))\,\mathrm{Lip}(v)T)\,|x_2-x_1|\,,\end{aligned}$$

where $1-\mathrm{Lip}(\gamma(t))\,\mathrm{Lip}(v)T>0$ in view of (6.33).

Set now $\mathscr{C}:=1-\mathrm{Lip}(\gamma(t))\,\mathrm{Lip}(v)T$ for brevity. For all $x_1\neq x_2$ it results

$$\frac{|\gamma(t,\,x_2)-\gamma(t,\,x_1)|}{|x_2-x_1|}\geq\mathscr{C}.$$

Let $J_{\gamma(t)}(x_1)$ be the Jacobian matrix of $\gamma(t)$ in the point $x_1$ and let $\lambda$ be one of its eigenvalues with associated eigenvector, say, $u$ (i.e., $J_{\gamma(t)}(x_1)u=\lambda u$). We choose $x_2=x_1+hu$, $h>0$, and compute:

$$\mathscr{C}\leq\lim_{h\to0^+}\frac{|\gamma(t,\,x_1+hu)-\gamma(t,\,x_1)|}{h\,|u|}=\lim_{h\to0^+}\frac{h\left|J_{\gamma(t)}(x_1)u\right|}{h\,|u|}=|\lambda|\,.$$

Due to the arbitrariness of $x_1$ and $\lambda$, we conclude that the above inequality holds for all eigenvalues of $J_{\gamma(t)}$ in any point of $\mathbb{R}^d$, whence $\left|\det J_{\gamma(t)}\right|\geq\mathscr{C}^d$ and in turn $|\det J_{\gamma(t)^{-1}}|\leq\mathscr{C}^{-d}$.

Finally, for all $E\in\mathscr{B}(\mathbb{R}^d)$ it results:

$$\mathscr{L}^d(\gamma(t)^{-1}(E))=\int_{\gamma(t)^{-1}(E)}dx\overset{z:=\gamma(t)(x)}{=}\int_E\left|\det J_{\gamma(t)^{-1}}(z)\right|\,dz\leq\frac{1}{\mathscr{C}^d}\mathscr{L}^d(E),$$

therefore (6.32) is satisfied with $\mathscr{C}_t=(1-\mathrm{Lip}(\gamma(t))\,\mathrm{Lip}(v)T)^{-d}$.

*Remark 6.4.* By carefully inspecting the proof of Lemma 6.1 we discover that the Lipschitz constant in space of $\gamma(t)$ can be estimated uniformly in $t\in[0,\,T]$ as

$$\mathrm{Lip}(\gamma(t))\leq1+\mathrm{Lip}(v)Te^{\mathrm{Lip}(v)T},$$

thus (6.33) can be reduced to a condition on the product $a:=\mathrm{Lip}(v)T$. In particular, (6.33) is certainly fulfilled if $1+a\exp a<\frac{1}{a}$, which allows for $a\in(0,\,\bar{a})$ with $\bar{a}\in(0.527,\,0.528)$.

## 6.8 Study of Pedestrian Velocity Models

Assumptions 6.1 and 6.2 provide a set of general properties required to the transport velocity in order for the theory of well-posedness (cf. Theorems 6.1 and 6.2) and numerical approximation (cf. Theorem 6.3) to follow. Notice indeed that Assumption 6.3, which is actually also needed for Theorem 6.3, is not concerned with the structure of the pedestrian velocity field. The aim of this section is to resume the specific velocity model elaborated in Chap. 5 for discussing the conditions under which it complies with the aforesaid assumptions. This can provide useful guidelines for constructing models which are both realistic and mathematically robust.

We will henceforth consider the compact form of $v$ given by (6.10), which we rewrite for a generic measure $\nu \in \mathscr{P}_1\mathbb{R}^d$ as

$$v[\nu](x) = v_{\mathrm{d}}(x) + N \int_{\mathbb{R}^d} k(y-x)\eta_{\mathscr{S}(x)}(y)\, d\nu(y), \tag{6.34}$$

where:

- In accordance with Chap. 5, we assume that interactions depend on the *relative position* of the walkers, so that the interaction kernel $K$ can be expressed by means of a function $k : \mathbb{R}^d \to \mathbb{R}^d$ as

  $$K(x,\, y) = k(y-x).$$

  It is worth pointing out that, in spite of the apparent more generality provided by a generic kernel $K$, this choice is actually the most meaningful for applications. In fact it ensures the so-called *frame indifference* (known also as *frame invariance* or *objectivity*), namely the fact that the qualitative and quantitative description of interactions does not change under rigid transformations of the reference frame (i.e., changes of observer).
- We account in the integrand, rather than in the integration domain, for the interaction neighborhood $\mathscr{S}(x)$ by means of a *cut-off function* $\eta_{\mathscr{S}(x)} : \mathbb{R}^d \to \mathbb{R}_+$ such that $\eta_{\mathscr{S}(x)}(y) = 0$ for all $y \notin \mathscr{S}(x)$. Ideally, we would like to have $\eta_{\mathscr{S}(x)} = \mathbb{1}_{\mathscr{S}(x)}$ but, as we will see in a moment, we actually need to slightly mollify the indicator function in order to meet the required regularity of the velocity.

Next we formulate the following assumptions:

**Assumption 6.4 (Properties of the velocity as in (6.34)).**

*(i)* $v_{\mathrm{d}}$ *is Lipschitz continuous and bounded in* $\mathbb{R}^d$*, i.e., there exist constants* $\mathrm{Lip}(v_{\mathrm{d}})$, $V_{\mathrm{d}} > 0$ *such that*

$$|v_{\mathrm{d}}(x_2) - v_{\mathrm{d}}(x_1)| \le \mathrm{Lip}(v_{\mathrm{d}})\, |x_2 - x_1|\,, \ \forall\, x_1,\, x_2 \in \mathbb{R}^d,$$
$$|v_{\mathrm{d}}(x)| \le V_{\mathrm{d}}, \ \forall\, x \in \mathbb{R}^d.$$

*(ii)* *There exists* $R > 0$ *such that, for each* $x \in \mathbb{R}^d$, *the interaction neighborhood* $\mathscr{S}(x) \subseteq B_R(x)$ *is measurable and isometric to a reference neighborhood* $\mathscr{S}(0) \subseteq B_R(0)$.

*(iii)* $k : \mathbb{R}^d \to \mathbb{R}^d$ *is Lipschitz continuous in* $B_R(0)$, *i.e., there exists* $\mathrm{Lip}(k) > 0$ *such that*

$$|k(z_2) - k(z_1)| \leq \mathrm{Lip}(k)\,|z_2 - z_1|\,, \quad \forall\, z_1,\, z_2 \in B_R(0).$$

*(iv)* $\eta_E$ *is Lipschitz continuous and bounded between* 0 *and* 1, *i.e.,*

$$\begin{aligned} &|\eta_E(x_2) - \eta_E(x_1)| \leq \mathrm{Lip}(\eta_E)\,|x_2 - x_1|\,, \\ &0 \leq \eta_E(x) \leq 1, \end{aligned} \qquad \forall\, x,\, x_1,\, x_2 \in \mathbb{R}^d,\ \forall\, E \in \mathscr{B}(\mathbb{R}^d).$$

*Remark 6.5.* A comment on Assumption 6.4(ii) is in order. Saying that $\mathscr{S}(x)$ is isometric to $\mathscr{S}(0)$ means that there is a rigid transformation $\xi_x : \mathbb{R}^d \to \mathbb{R}^d$, parameterized by $x \in \mathbb{R}^d$, which maps $\mathscr{S}(0)$ onto $\mathscr{S}(x)$, i.e., $\xi_x(\mathscr{S}(0)) = \mathscr{S}(x)$. Specifically, $\xi_x$ has the form

$$\xi_x(z) = \mathscr{R}_x z + x, \tag{6.35}$$

where $\mathscr{R}_x \in \mathbb{R}^{d\times d}$ is a rotation matrix possibly depending on the point $x$. Consequently, the following relation holds true:

$$\eta_{\mathscr{S}(x)}(y) = \eta_{\mathscr{S}(0)}(z) \quad \text{for} \quad y = \xi_x(z). \tag{6.36}$$

Assumption 6.4 is actually all we need in order to apply the previous results of well-posedness and numerical approximation to our measure-based crowd model. In the sequel we will confine ourselves to the two-dimensional case ($d = 2$), which covers virtually all of the realistic settings relevant for applications. Remarkably, we will deal with an interaction neighborhood with *arbitrary* shape.

Upon making the change of variables $y = \xi_x(z)$ in the integral (6.34), and recalling (6.35), (6.36), we rewrite the velocity in the form

$$v[\nu](x) = v_{\mathrm{d}}(x) + N \int_{\mathbb{R}^2} k(\mathscr{R}_x z)\eta_{\mathscr{S}(0)}(z)\, d(\xi_x^{-1}\#\nu)(z). \tag{6.37}$$

Then the rotation matrix appears explicitly in the argument of the interaction kernel $k$. A preliminary study of some of its properties is necessary for preparing the next calculations.

In two space dimensions, a simple representation of $\mathscr{R}_x$ can be given:

$$\mathscr{R}_x = \begin{pmatrix} \cos\vartheta_x & -\sin\vartheta_x \\ \sin\vartheta_x & \cos\vartheta_x \end{pmatrix},$$

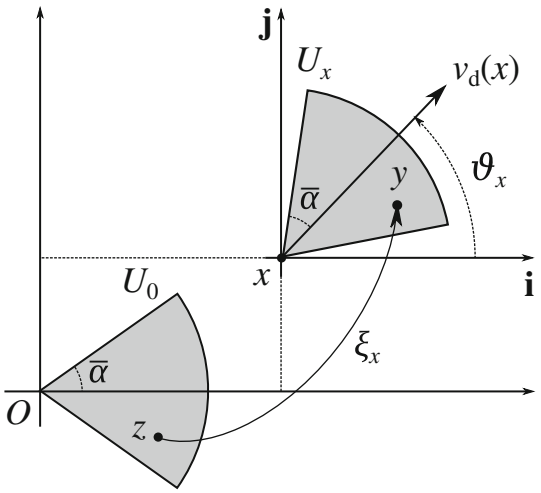


**Fig. 6.2** The relation between the interaction neighborhood $\mathscr{S}(x)$ (here supposed to be a circular sector for pictorial purposes only) and the reference one $\mathscr{S}(0)$ through the mapping $\xi_x$. Notice in particular the definition of the rotation angle $\vartheta_x$

$\vartheta_x \in [0, 2\pi)$ being the angle of rotation which determines the local orientation of the interaction neighborhood. More precisely, bearing in mind the prototypical definition of $\mathscr{S}(x)$ given by (5.10), it can be identified with the angle formed by the desired velocity $v_d(x)$ with respect to a fixed reference direction, for instance the horizontal one associated with the unit vector $\mathbf{i}$. It must not be confused with the angular width $2\bar{\alpha}$ of the interaction neighborhood introduced in Chap. 5 (see Figs. 5.2 and 6.2), which is instead a parameter carrying a precise modeling meaning. Assuming for simplicity that $v_d$ has constant unit modulus, we can write:

$$\cos\vartheta_x = v_d(x)\cdot\mathbf{i}, \qquad \sin\vartheta_x = (v_d(x)\times\mathbf{i})\cdot\mathbf{k}. \tag{6.38}$$

In the second formula, $v_d(x)$ and $\mathbf{i}$ are thought of as embedded into $\mathbb{R}^3$, with $\times$ denoting vector product and $\mathbf{k}$ the unit vector orthogonal to the plane of $v_d(x)$ and $\mathbf{i}$. If $v_d$ has not constant unit modulus then (6.38) still holds with $v_d(x)$ replaced by $v_d(x)/|v_d(x)|$, which is a Lipschitz continuous field (as required by Assumption 6.4(i)) provided $|v_d|$ is uniformly bounded away from zero.

The technical properties of the rotation matrix $\mathscr{R}_x$ we will need in the sequel are expressed by the following couple of lemmas.

**Lemma 6.2.** *The mapping $z \mapsto k(\mathscr{R}_x z)\eta_{\mathscr{S}(0)}(z)$ is Lipschitz continuous in $\mathbb{R}^2$ for all fixed $x$ with Lipschitz constant independent of $x$.*

*Proof.* In order to study the expression

$$e(z_1, z_2) := \left|k(\mathscr{R}_x z_2)\eta_{\mathscr{S}(0)}(z_2) - k(\mathscr{R}_x z_1)\eta_{\mathscr{S}(0)}(z_1)\right|, \quad z_1, z_2 \in \mathbb{R}^2$$

it is convenient to distinguish three cases.

(i) If $z_1,\, z_2 \in \mathscr{S}(0)$ we have

$$\begin{aligned} e(z_1,\, z_2) &\le \left|k(\mathscr{R}_x z_2)\eta_{\mathscr{S}(0)}(z_2) - k(\mathscr{R}_x z_2)\eta_{\mathscr{S}(0)}(z_1)\right| \\ &\quad + \left|k(\mathscr{R}_x z_2)\eta_{\mathscr{S}(0)}(z_1) - k(\mathscr{R}_x z_1)\eta_{\mathscr{S}(0)}(z_1)\right| \\ &\le \left(\max_{z\in B_R(0)} |k(z)|\,\mathrm{Lip}(\eta_{\mathscr{S}(0)}) + \mathrm{Lip}(k)\right)|z_2 - z_1|\,, \end{aligned}$$

where we have used that:

- $k$ is bounded in $B_R(0) \supseteq \mathscr{S}(0)$ due to Assumption 6.4(iii).
- $\mathscr{R}_x$ sends $B_R(0)$ into itself.
- $\mathscr{R}_x$ is an isometry, hence $|\mathscr{R}_x(z_2 - z_1)| = |z_2 - z_1|$.

(ii) If $z_1 \notin \mathscr{S}(0)$ and $z_2 \in \mathscr{S}(0)$ (or vice versa) then $e(z_1, z_2) = \left|k(\mathscr{R}_x z_2)\eta_{\mathscr{S}(0)}(z_2)\right|$. Let $z_r := rz_1 + (1-r)z_2$, $r \in [0,\, 1]$, be a point of the segment connecting $z_1$ to $z_2$ and pick $\bar r$ such that $z_{\bar r} \in \partial\mathscr{S}(0)$. Since by continuity $\eta_{\mathscr{S}(0)}(z_{\bar r}) = 0$, we have, mimicking the calculations of the previous point:

$$\begin{aligned} e(z_1,\, z_2) &= \left|k(\mathscr{R}_x z_2)\eta_{\mathscr{S}(0)}(z_2) - k(\mathscr{R}_x z_{\bar r})\eta_{\mathscr{S}(0)}(z_{\bar r})\right| \\ &\le \left(\max_{z\in B_R(0)} |k(z)|\,\mathrm{Lip}(\eta_{\mathscr{S}(0)}) + \mathrm{Lip}(k)\right)|z_2 - z_{\bar r}|\,. \end{aligned}$$

On the other hand, $|z_2 - z_{\bar r}| = \bar r\,|z_2 - z_1| \le |z_2 - z_1|$.

(iii) Finally, if $z_1,\, z_2 \notin \mathscr{S}(0)$ then $e(z_1,\, z_2) = 0 \le |z_2 - z_1|$.

**Lemma 6.3.** *For all $x_1,\, x_2,\, z \in \mathbb{R}^2$ it results*

$$|(\mathscr{R}_{x_2} - \mathscr{R}_{x_1})z| \le \sqrt{2}\,\mathrm{Lip}(v_\mathrm{d})\,|x_2 - x_1|\,|z|\,.$$

*The same holds with $\mathscr{R}_{x_1}$, $\mathscr{R}_{x_2}$ replaced by $\mathscr{R}_{x_1}^{-1}$, $\mathscr{R}_{x_2}^{-1}$.*

*Proof.* A direct computation shows that

$$|(\mathscr{R}_{x_2} - \mathscr{R}_{x_1})z| = \sqrt{(\cos\vartheta_{x_2} - \cos\vartheta_{x_1})^2 + (\sin\vartheta_{x_2} - \sin\vartheta_{x_1})^2}\,|z|\,,$$

and the same is true also using inverse matrices. In addition,

$$\begin{aligned} |\cos\vartheta_{x_2} - \cos\vartheta_{x_1}| &= |(v_\mathrm{d}(x_2) - v_\mathrm{d}(x_1))\cdot\mathbf{i}| \le |v_\mathrm{d}(x_2) - v_\mathrm{d}(x_1)|\,, \\ |\sin\vartheta_{x_2} - \sin\vartheta_{x_1}| &= |\{(v_\mathrm{d}(x_2) - v_\mathrm{d}(x_1)) \times \mathbf{i}\}\cdot\mathbf{k}| \le |v_\mathrm{d}(x_2) - v_\mathrm{d}(x_1)|\,, \end{aligned}$$

hence the thesis follows from the Lipschitz continuity of $v_\mathrm{d}$ claimed by Assumption 6.4(i).

We are finally in a position to prove, as desired, that the velocity (6.34), or equivalently (6.37), fulfills Assumptions 6.1 and 6.2, and yields therefore a mathematically robust model of pedestrian motion.

**Theorem 6.5.** *Let Assumption 6.4 hold and assume* $d = 2$. *Then the velocity field* (6.34) *complies with Assumptions 6.1 and 6.2.*

*Proof.* We check one by one the properties stated by Assumptions 6.1 and 6.2. Specifically, we start from the latter which is more immediate. We will invariably refer to the expression (6.37) of the velocity field throughout the proof.

(i) Uniform boundedness follows straightforwardly from the boundedness of $v_\mathrm{d}$ and of $k$ in $B_R(0)$:

$$|v[\nu](x)| \le V_\mathrm{d} + N \max_{z\in B_R(0)} |k(z)| =: V_{\max}, \quad \forall\, x \in \mathbb{R}^2,\ \forall\, \nu \in \mathbb{R}^2,$$

where the constant $V_\mathrm{d}$ has been defined in Assumption 6.4.

(ii) Also mild linearity with respect to the probability measure is straightforward. For all $a \in [0,\ 1]$ and all $\nu_1,\ \nu_2 \in \mathbb{R}^2$ it results indeed, owing to the linearity of the push forward:

$$\begin{aligned} v[a\nu_1 + (1-a)\nu_2](x) &= v_\mathrm{d}(x) \\ &\quad + N \int_{\mathbb{R}^2} k(\mathscr{R}_x z)\eta_{\mathscr{S}(0)}(z)\, d(a\xi_x^{-1}\#\nu_1 + (1-a)\xi_x^{-1}\#\nu_2)(z) \\ &= a v_\mathrm{d}(x) + (1-a)v_\mathrm{d}(x) \\ &\quad + aN \int_{\mathbb{R}^2} k(\mathscr{R}_x z)\eta_{\mathscr{S}(0)}(z)\, d(\xi_x^{-1}\#\nu_1)(z) \\ &\quad + (1-a)N \int_{\mathbb{R}^2} k(\mathscr{R}_x z)\eta_{\mathscr{S}(0)}(z)\, d(\xi_x^{-1}\#\nu_2)(z) \\ &= a v[\nu_1](x) + (1-a)v[\nu_2](x). \end{aligned}$$

(iii) Lipschitz continuity with respect to the probability measure requires to study, for arbitrary $\nu_1,\ \nu_2 \in \mathbb{R}^2$ and fixed $x \in \mathbb{R}^2$, the following expression:

$$|v[\nu_2](x) - v[\nu_1](x)| = N \left| \int_{\mathbb{R}^2} k(\mathscr{R}_x z)\eta_{\mathscr{S}(0)}(z)\, d(\xi_x^{-1}\#\nu_2 - \xi_x^{-1}\#\nu_1)(z) \right|$$

which, in view of Lemma 6.2, can be estimated by means of a suitable constant $\mathscr{C} > 0$ as

$$\begin{aligned} &\le \mathscr{C} W_1\left(\xi_x^{-1}\#\nu_1,\ \xi_x^{-1}\#\nu_2\right) \\ &= \mathscr{C} \sup_{\varphi\in \mathrm{Lip}_1(\mathbb{R}^2)} \int_{\mathbb{R}^2} \varphi(\xi_x^{-1})\, d(\nu_2 - \nu_1) \\ &= \mathscr{C} W_1\left(\nu_1,\ \nu_2\right). \end{aligned}$$

To justify the last equality above, notice that $\xi_x^{-1}(y) = \mathscr{R}_x^{-1}(y-x)$ belongs to $\mathrm{Lip}_1(\mathbb{R}^2)$, hence when $\varphi$ varies in $\mathrm{Lip}_1(\mathbb{R}^2)$ the function $\varphi \circ \xi_x^{-1}$ spans in turn the whole space $\mathrm{Lip}_1(\mathbb{R}^2)$.

(iv) Lipschitz continuity with respect to $x$ is instead more delicate, because it involves directly the rotation matrix $\mathscr{R}_x$. Let $x_1, x_2 \in \mathbb{R}^2$ and fix $\nu \in \mathbb{R}^2$, then

$$\begin{aligned}
|v[\nu](x_2) - v[\nu](x_1)| &\le |v_{\mathrm{d}}(x_2) - v_{\mathrm{d}}(x_1)| \\
&\quad + N \left| \int_{\mathbb{R}^2} k(\mathscr{R}_{x_2} z)\eta_{\mathscr{S}(0)}(z)\, d(\xi_{x_2}^{-1}\#\nu)(z) \right. \\
&\quad \left. - \int_{\mathbb{R}^2} k(\mathscr{R}_{x_1} z)\eta_{\mathscr{S}(0)}(z)\, d(\xi_{x_1}^{-1}\#\nu)(z) \right| \\
&\le \mathrm{Lip}(v_{\mathrm{d}})\, |x_2 - x_1| \\
&\quad + N \int_{\mathbb{R}^2} |k(\mathscr{R}_{x_2} z) - k(\mathscr{R}_{x_1} z)|\, \eta_{\mathscr{S}(0)}(z)\, d(\xi_{x_2}^{-1}\#\nu)(z) \\
&\quad + N \left| \int_{\mathbb{R}^2} k(\mathscr{R}_{x_1} z)\eta_{\mathscr{S}(0)}(z)\, d(\xi_{x_2}^{-1}\#\nu - \xi_{x_1}^{-1}\#\nu)(z) \right| .
\end{aligned} \tag{6.39}$$

In the first integral at the right-hand side of (6.39) we can assume $z \in \mathscr{S}(0)$, for otherwise $\eta_{\mathscr{S}(0)}(z) = 0$. Hence $|z| \le R$ and moreover $\mathscr{R}_x z \in B_R(0)$ for all $x \in \mathbb{R}^2$. Lipschitz continuity of $k$ in that ball, along with Lemma 6.3, implies

$$\begin{aligned}
|k(\mathscr{R}_{x_2} z) - k(\mathscr{R}_{x_1} z)| &\le \mathrm{Lip}(k)\, |(\mathscr{R}_{x_1} - \mathscr{R}_{x_2})z| \\
&\le \sqrt{2}\, \mathrm{Lip}(k)\, \mathrm{Lip}(v_{\mathrm{d}}) R\, |x_2 - x_1| ,
\end{aligned}$$

whence

$$\begin{aligned}
&N \int_{\mathbb{R}^2} |k(\mathscr{R}_{x_2} z) - k(\mathscr{R}_{x_1} z)|\, \eta_{\mathscr{S}(0)}(z)\, d(\xi_{x_2}^{-1}\#\nu)(z) \\
&\quad \le N \int_{\mathscr{S}(0)} |k(\mathscr{R}_{x_2} z) - k(\mathscr{R}_{x_1} z)|\, d(\xi_{x_2}^{-1}\#\nu)(z) \\
&\quad \le N \sqrt{2}\, \mathrm{Lip}(k)\, \mathrm{Lip}(v_{\mathrm{d}}) R\, |x_2 - x_1| ,
\end{aligned} \tag{6.40}$$

having observed that $(\xi_{x_2}^{-1}\#\nu)(\mathscr{S}(0)) = \nu(\mathscr{S}(x_2)) \le 1$.

As far as the second integral at the right-hand side of (6.39) is concerned, we have:

$$N \left| \int_{\mathbb{R}^2} k(\mathscr{R}_{x_1} z) \eta_{\mathscr{S}(0)}(z)\, d(\xi_{x_2}^{-1} \# \nu - \xi_{x_1}^{-1} \# \nu)(z) \right|$$

$$\leq N \int_{\mathscr{S}(x_1) \cup \mathscr{S}(x_2)} \left| k(\mathscr{R}_{x_1} \xi_{x_2}^{-1}(y)) \eta_{\mathscr{S}(0)}(\xi_{x_2}^{-1}(y)) \right.$$

$$\left. - k(\mathscr{R}_{x_1} \xi_{x_1}^{-1}(y)) \eta_{\mathscr{S}(0)}(\xi_{x_1}^{-1}(y)) \right| d\nu(y). \tag{6.41}$$

Notice that we can confine ourselves to $y \in \mathscr{S}(x_1) \cup \mathscr{S}(x_2)$ for otherwise $\eta_{\mathscr{S}(0)}(\xi_{x_i}^{-1}(y)) = \eta_{\mathscr{S}(x_i)}(y) = 0$ for both $i = 1, 2$. We distinguish two cases:

(a) $|x_2 - x_1| > 2R$.
In this case $\mathscr{S}(x_1) \cap \mathscr{S}(x_2) = \emptyset$ because the balls $B_R(x_1)$, $B_R(x_2)$ are disjoint. Thus:

$$(6.41) = N \int_{\mathscr{S}(x_1)} \left| k(\mathscr{R}_{x_1} \xi_{x_1}^{-1}(y)) \right| \eta_{\mathscr{S}(x_1)}(y)\, d\nu(y)$$

$$+ N \int_{\mathscr{S}(x_2)} \left| k(\mathscr{R}_{x_1} \xi_{x_2}^{-1}(y)) \right| \eta_{\mathscr{S}(x_2)}(y)\, d\nu(y).$$

For all $y \in \mathscr{S}(x_i)$, $i = 1, 2$, it results $\xi_{x_i}^{-1}(y) \in \mathscr{S}(0) \subset B_R(0)$, hence $\mathscr{R}_{x_1} \xi_{x_i}^{-1}(y) \in B_R(0)$ and we can use the boundedness of $k$ in that ball to get

$$\leq N \max_{z \in B_R(0)} |k(z)| \left( \int_{\mathscr{S}(x_1)} \eta_{\mathscr{S}(x_1)}(y)\, d\nu(y) + \int_{\mathscr{S}(x_2)} \eta_{\mathscr{S}(x_2)}(y)\, d\nu(y) \right)$$

$$\leq N \max_{z \in B_R(0)} |k(z)|\, \nu(\mathscr{S}(x_1) \cup \mathscr{S}(x_2))$$

$$\leq N \max_{z \in B_R(0)} |k(z)|\,.$$

But $1 < \frac{|x_2 - x_1|}{2R}$, therefore we conclude

$$(6.41) \leq \frac{N}{2R} \max_{z \in B_R(0)} |k(z)|\, |x_2 - x_1|\,. \tag{6.42}$$

(b) $|x_2 - x_1| \leq 2R$.
In this case the neighborhoods $\mathscr{S}(x_1)$, $\mathscr{S}(x_2)$ need not be disjoint, however we can resort to Lemma 6.2 to find $\mathscr{C} > 0$ such that:

$$(6.41) \leq \mathscr{C} N \int_{\mathscr{S}(x_1) \cup \mathscr{S}(x_2)} \left| \xi_{x_2}^{-1}(y) - \xi_{x_1}^{-1}(y) \right| d\nu(y)$$

$$= \mathscr{C} N \int_{\mathscr{S}(x_1) \cup \mathscr{S}(x_2)} \left| \mathscr{R}_{x_2}^{-1}(y - x_2) - \mathscr{R}_{x_1}^{-1}(y - x_1) \right| d\nu(y)$$

$$= \mathscr{C} N \int_{\mathscr{S}(x_1)\cup\mathscr{S}(x_2)} \left| (\mathscr{R}_{x_2}^{-1} - \mathscr{R}_{x_1}^{-1})(y - x_1) + \mathscr{R}_{x_2}^{-1}(x_2 - x_1) \right| \, dv(y)$$

and further, thanks to Lemma 6.3 and to the fact that $\mathscr{R}_{x_2}^{-1}$ is an isometry,

$$\leq \mathscr{C} \left( \int_{\mathscr{S}(x_1)\cup\mathscr{S}(x_2)} |y - x_1| \, dv(y) + v(\mathscr{S}(x_1) \cup \mathscr{S}(x_2)) \right) |x_2 - x_1| \,,$$

where we have collected in $\mathscr{C}$ all further constants.

Let us examine the term with the integral. If $y \in \mathscr{S}(x_1)$ then $|y - x_1| \leq R$ whereas if $y \in \mathscr{S}(x_2)$ then $|y - x_1| \leq |y - x_2| + |x_2 - x_1| \leq 3R$. Finally, $|y - x_1| \leq 3R$ for all $y \in \mathscr{S}(x_1) \cup \mathscr{S}(x_2)$, which ultimately yields

$$(6.41) \leq \mathscr{C} \, |x_2 - x_1| \,. \tag{6.43}$$

In conclusion, from (6.42) and (6.43) we deduce that there exists a constant $\mathscr{C} > 0$ such that (6.41) $\leq \mathscr{C} \, |x_2 - x_1|$ for all $x_1, \, x_2 \in \mathbb{R}^2$. This, together with the estimate (6.40), completes the proof of Lipschitz continuity of the mapping $x \mapsto v[v](x)$.

*Remark 6.6 (Higher dimension).* For $d > 2$ additional technicalities arise, due to a more complex structure of the rotation matrix. Nevertheless, in the special case that the desired velocity is constant in $x$, it is straightforward to extend the results to any spatial dimension. In fact, the rotation matrix being independent of $x$, Theorem 6.5 can be proved without using Lemma 6.3, which is the only point where we use the explicit representation of the matrix. Models with constant desired velocity have been recently proposed for swarm dynamics problems and for *rendez-vous* algorithms.

*Remark 6.7 (Zero desired velocity).* When the desired velocity is zero the orientation of the neighborhood of interaction cannot be defined by (6.38). However, this issue can be solved by replacing $v_\mathrm{d}$ in (6.38) with any other Lipschitz continuous unit vector field e.g., a nonzero constant one, with the only purpose of defining a rotation angle. This problem does not arise if the desired velocity is zero but the interaction neighborhood $\mathscr{S}(x)$ coincides with the whole ball $B_R(x)$.

## 6.9 Bibliographical Notes

Sections 6.5 and 6.6 All missing technical details of the proofs of Theorems 6.2 and 6.3 can be found in Tosin and Frasca [160]. Further estimates on the error produced by the spatial approximation of the discrete-in-time model (6.17) can be found in Piccoli and Tosin [145].

Section 6.7 Properties analogous to those stated by Theorem 6.4 and Proposition 6.2 but for the solution to the discrete-in-time model (6.17), plus additional estimates on the density in the absolutely continuous case, are reported in Cristiani et al. [48] and in Piccoli and Tosin [145].

Section 6.8 Models of swarm and *rendez-vous* dynamics which can be recast in the framework (6.9)–(6.10) have been proposed in Cristiani et al. [46] and in Canuto et al. [31, 32], respectively. In these models the agents feature a constant desired velocity, therefore, according to Remark 6.6, the conclusions of Theorem 6.5 hold also in spatial dimensions greater than 2 (for instance, $d = 3$ in the case of swarms).

# Chapter 7
# Evolution in Measure Spaces with Wasserstein Distance

**Abstract** In this chapter, we provide a fairly general mathematical setting for the nonlinear transport equation analyzed in Chap. 6 (namely Eqs. (5.1) and (6.6)). More precisely, we study the evolution of solutions in measures spaces endowed with the Wasserstein distance and its generalizations. Moreover, we illustrate the connections between the Wasserstein distance, the transport equation and optimal transportation problems in the sense of Monge-Kantorovich. We also deal with numerical schemes for the transport equation in measure spaces and prove convergence of a Lagrangian scheme to the unique solution, when the discretization parameters approach zero. Convergence of an Eulerian scheme is then achieved under more strict hypotheses. Both schemes are discretizations of the push-forward formula defined by the transport equation as in Chap. 6. As a by-product, we obtain existence and uniqueness of the solution under general assumptions. All the results of convergence are proved with respect to the Wasserstein distance. We first show that the total variation distance is not natural for such equations, since we lose uniqueness of the solution. Then transport equations with sources are considered. In this case the solution does not conserve its total mass, thus we can not directly use the classical Wasserstein distance. For this we introduce a generalized Wasserstein distance, which allows mass creation/destruction and has interest in itself as distance among measures with different total mass.

## 7.1 The Homogeneous Nonlinear Evolution Equation

We first focus on a homogeneous nonlinear transport equation of the type:

$$\begin{cases} \dfrac{\partial \mu}{\partial t} + \nabla \cdot (\mu v[\mu]) = 0 \\ \mu_{|_{t=0}} = \mu_0. \end{cases} \tag{7.1}$$

E. Cristiani et al., *Multiscale Modeling of Pedestrian Dynamics*, MS&A 12,
DOI 10.1007/978-3-319-06620-2_7,

Notice that this is the same as Eqs. (5.1) and (6.6) respectively. Solutions will be considered in the space $\mathscr{P}_p(\mathbb{R}^d)$ $(1 \le p < +\infty)$ of probability measures with finite $p$-moment, that is such that $\int |x|^p \, d\mu$ is finite. However, all results extend to the case when $\mu$ is not necessarily a probability measure but has finite mass.

Let us indicate by $\mathscr{P}_c(\mathbb{R}^d)$ the space of probability measures with compact support. Sometimes we will restrict our presentation to this space.

We always assume the following hypotheses on Eq. (7.1):

**Assumption 7.1.** *The function*

$$v[\mu] : \begin{cases} \mathscr{P}_p(\mathbb{R}^d) \to C^1(\mathbb{R}^d) \cap L^\infty(\mathbb{R}^d) \\ \mu \qquad\quad \mapsto v[\mu] \end{cases}$$

*satisfies:*

*(i) $v[\mu]$ is uniformly Lipschitz and uniformly bounded w.r.t. $\mu$, i.e., there exist $L$, $M$ such that for all $\mu \in \mathscr{P}_p(\mathbb{R}^d)$, $x,\ y \in \mathbb{R}^d$*

$$|v[\mu](x) - v[\mu](y)| \le L\,|x - y| \qquad |v[\mu](x)| \le M.$$

*(ii) $v$ is a Lipschitz function, i.e., there exists $K$ such that*

$$\|v[\mu] - v[\nu]\|_{C^0} \le K W_p\,(\mu,\ \nu)\,.$$

The main result of this chapter for (7.1) will be the following:

**Theorem 7.1.** *Under Assumption 7.1, it holds*

*(i) There exists a unique weak solution to (7.1).*
*(ii) Lagrangian schemes derived by discretization of the push-forward formula provide sequences of approximate solutions converging to the unique solution.*
*(iii) Eulerian schemes provide sequences of approximate solutions converging to the unique solution, under additional assumptions on the discretization parameters.*

Before proving Theorem 7.1 we show how the Wasserstein setting is the correct one, as opposed to the distance associated to the total variation norm, and illustrate connections between the Wasserstein distance and the transport equation (7.1). Then in Sect. 7.2 we will prove existence and uniqueness of solutions by proving convergence of a semi-discrete Lagrangian scheme. Finally, in Sect. 7.3 we will deal with the convergence of discrete Lagrangian and Eulerian schemes.

## *Wasserstein vs. Total Variation Distance ($L^1$ Distance)*

The vector space $\mathscr{M}$ generated by probability measures is the space of all finite signed measures $\mu$, i.e. such that $\mu = \mu_+ - \mu_-$ with $\mu_\pm$ finite. We equip this space with the total variation norm given by:

$$\|\mu\|_{TV} = \inf\{\mu_+(\mathbb{R}^d) + \mu_-(\mathbb{R}^d) : \mu = \mu_+ - \mu_-, \mu_\pm \text{ finite positive measure}\}.$$

This norm defines a distance among finite measures by setting:

$$d_{TV}(\mu, \nu) = \|\mu - \nu\|_{TV}.$$

Notice that if $\mu$ and $\nu$ are absolutely continuous w.r.t. Lebesgue measure, then this coincides with the $L^1$ distance. Indeed, by Radon-Nikodym Theorem we can write $d\mu = f_\mu d\lambda$, $d\nu = f_\nu d\lambda$, where $\lambda$ denotes the Lebesgue measure and get:

$$\|\mu - \nu\|_1 := \int \left| f_\mu(x) - f_\nu(x) \right| \, d\lambda.$$

For simplicity we will indicate the total variation norm by $|\cdot|$.

The aim of this section is to show that the Wasserstein distance is more natural than the total variation or $L^1$ distance in order to study the evolution equation (7.1). Our aim is to exhibit examples showing how the Wasserstein distance captures more correctly the natural concept of distance among pedestrian distribution in a given area and also gives rise to a more complete theoretical framework.

**Modeling.** Let us start with the modeling aspects. Observe that the Wasserstein metric is more adapted than $L^1$ distance to measure if two pedestrian populations are close or far. Indeed, take three different measures as in Fig. 7.1, and call $\mu_i$ the measure centered in $x_i$, for $i = 0, 1, 2$. It is easy to prove that

$$W_1(\mu_i, \mu_j) = |x_i - x_j| \quad \text{while} \quad \|\mu_i - \mu_j\|_1 = 2 \ \text{ for } i \neq j.$$

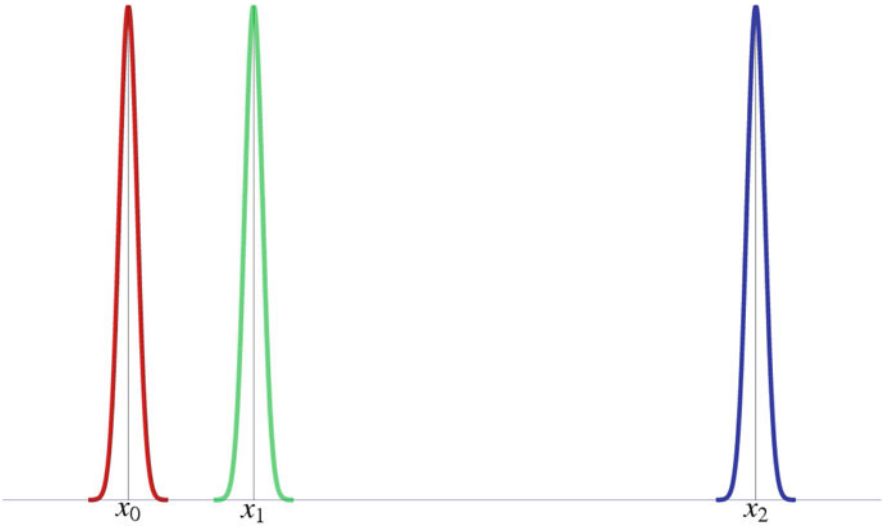


**Fig. 7.1** Difference between Wasserstein and $L^1$ distances

In particular, the $L^1$ distance between the measures $\mu_0$ and $\mu_1$ is identical to the distance between $\mu_0$ and $\mu_2$. This is not natural with respect to our perception of distance between pedestrian crowds, that is better modeled by Wasserstein distance.

As shown in Chaps. 4–6, the interaction velocity is often defined by convolution with a certain kernel. Then two measures that are close with respect to $W_1$ but far with respect to the $L^1$ distance give velocity fields that are close. For example, define $\mu_\epsilon := \frac{1}{2\epsilon}\mathbb{1}_{(-\epsilon,\epsilon)}$ and observe that $\mu_\epsilon$ and $\mu_{2\epsilon}$ are close for small $\epsilon$ with respect to $W_1$, but not with respect to the $L^1$ distance.

On the other hand, if the velocity $v = v[\mu]$ is defined by the value of $\mu$ at a point (provided a good definition of this quantity), i.e., $v[\mu](x) := f(\mu(x))$ for a certain $f$, then the same example provides a completely different result. For $f(\mu(x)) = \mu(x)$, we get $v[\mu_\epsilon](0) = 2v[\mu_{2\epsilon}](0)$ and thus the velocities are far, even if the measures are close with respect to $W_1$.

**Uniqueness and non-uniqueness of solutions.** Replacing the Wasserstein distance with the total variation distance in Assumption 7.1, one loses uniqueness of solutions to (7.1). To show this, consider the alternative assumption:

**Assumption 7.2.** *The function*

$$v[\mu] : \begin{cases} \mathscr{P}_p(\mathbb{R}^d) \to C^1(\mathbb{R}^d) \cap L^\infty(\mathbb{R}^d) \\ \mu \quad\quad \mapsto v[\mu] \end{cases}$$

*satisfies:*

*(i)* $v[\mu]$ *is uniformly Lipschitz and uniformly bounded w.r.t.* $\mu$*, i.e., there exist* $L$*,* $M$ *such that for all* $\mu \in \mathscr{P}_p(\mathbb{R}^d)$*,* $x,\ y \in \mathbb{R}^d$*,*

$$|v[\mu](x) - v[\mu](y)| \le L\,|x-y|\,, \qquad |v[\mu](x)| \le M.$$

*(ii)* $v$ *is a Lipschitz function w.r.t. the total variation distance, i.e., there exists* $K$ *such that*

$$\|v[\mu] - v[\nu]\|_{C^0} \le K\,|\mu - \nu|.$$

We now define a function $v$ satisfying Assumption 7.2 and a measure $\mu_0$ such that there exist two distinct solutions to (7.1). The main idea is to use non-uniqueness of solutions to the Cauchy problem $\dot{x} = \sqrt{x}$, $x(0) = 0$.

We set the dimension of the space $d = 2$, the final time $T = 1$ and define a one-parameter family of measures $\nu_t \in \mathscr{P}_c(\mathbb{R}^d)$, $t \in [0, 1]$, as shown in Fig. 7.2 (dimensions are not respected). More precisely, $\nu_t$ is defined as follows. First define a sequence of squares $Q_t^i$, all with sides parallel to axes $x$ and $y$, with base length $s_i := 4^{-i}$ and such that the upper side is on the line $y = 1 + t^2$. Moreover, the square $Q_t^0$ has the left side on the $y$-axis and, for $i > 0$, the left side of the square $Q_t^i$ is contained in the right side of the square $Q_t^{i-1}$. Then we set

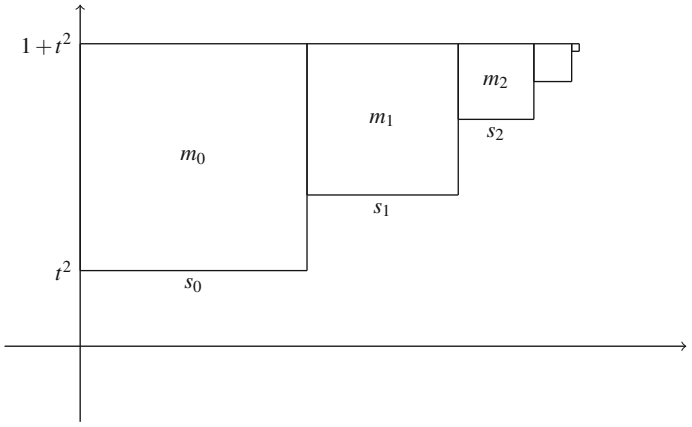


**Fig. 7.2** Assumption 7.2 does not guarantee uniqueness of the solution

$$\nu_t := \sum_{i=0}^{\infty} m_i \mathbb{1}_{Q_t^i} \lambda,$$

where $m_i = \frac{1}{2}8^i$ and $\lambda$ is the Lebesgue measure. It is evident that $\nu_t$ is positive and absolutely continuous with respect to the Lebesgue measure. Moreover, $\nu_t$ has bounded support, contained in a rectangle of sides $s_0$ and $\sum_{i=0}^{\infty} s_i = \frac{4}{3}$. We also have that $\nu_t(\mathbb{R}^d) = \sum_{i=0}^{\infty} m_i s_i^2 = 1$.

Now define $v[\nu_t] := (0, 2t)$. We first prove that $v$ satisfies Assumption 7.2 for the family of measures $\nu_t$. We then extend $v$ to the whole space $\mathscr{P}_p(\mathbb{R}^d)$ so as to still satisfy Assumption 7.2. For each $t \geq 0$, $v[\nu_t]$ is a constant vector field, thus it is uniformly Lipschitz with $L = 0$ and uniformly bounded with $M = 2T = 2$. We now prove that $v$ is Lipschitz with respect to the $L^1$ distance on the family $\nu_t$. For this, let $t, s \in [0, 1]$ and assume $t > s$ with no loss of generality. Then, for all $x \in \mathbb{R}^d$ we have $|v[\nu_t](x) - v[\nu_s](x)| = 2(t - s)$. Now take $n$ such that $s_n < t^2 - s^2 \leq s_{n-1}$. Remark that such a $s_n$ always exists, since $s_n \searrow 0$. Then, for all $i \geq n$ the squares $Q_t^i$ and $Q_s^i$ are disjoint. Moreover, the squares $Q_t^i$ and $Q_s^j$ are always disjoint for $j \neq i$. As a consequence,

$$|\nu_t - \nu_s| \geq \sum_{i=n}^{\infty} 2\nu_t(Q_t^i) = \sum_{i=n}^{\infty} 2m_i s_i^2 = 2 \cdot 2^{-n} = 2^{-n+1},$$

hence

$$\|v[\nu_t] - v[\nu_s]\|_{C^0} = 2(t - s) \leq 2\sqrt{t^2 - s^2} \leq 2\sqrt{s_{n-1}} = 2 \cdot 2^{1-n} \leq 2\,|\nu_t - \nu_s|.$$

Now consider the rectangle $R := [0, \frac{4}{3}] \times [1, 2]$ and define the following functional:

$$\mathscr{F} : \begin{cases} \mathscr{P}_p(\mathbb{R}^d) \to [0, +\infty) \\ \mu \quad \mapsto F(\mu) := \mu(R). \end{cases}$$

Observe that $F$ is well defined and finite, since $F(\mu) \leq \mu(\mathbb{R}^2) = 1$. Moreover, $F(\nu_0) = 0$, $F(\nu_1) = 1$ and $F(\nu_t)$ is strictly increasing w.r.t. $t$, thus we can implicitly define the function $f : [0, 1] \mapsto \mathbb{R}$ by setting:

$$f(F(\nu_t)) := 2t.$$

We now prove that $f$ is a Lipschitz continuous function. Notice that

$$\frac{|f(\xi_2) - f(\xi_1)|}{|\xi_2 - \xi_1|} = \frac{2\,|t_2 - t_1|}{|F(\nu_{t_2}) - F(\nu_{t_1})|},$$

where $t_i$ is the unique value such that $F(\nu_{t_i}) = \xi_i$. First assume $s_{n+1} \leq t_1^2 < t_2^2 \leq s_n$ for some $n$. All squares $Q^i_{t_k}$, with $i \geq n+1$ and $k = 1, 2$, are completely contained in $R$, since $1 + t_k^2 - s_m \geq 1$. On the other side, the intersection of $R$ with $Q^i_{t_k}$, with $i \leq n$ and $k = 1, 2$, is given by the rectangle of horizontal side $s_i$ and vertical side $t_k^2$. Therefore:

$$|F(\nu_{t_2}) - F(\nu_{t_1})| = \left| \sum_{i=0}^{n} \nu_{t_2}(Q^i_{t_2} \cap R) - \sum_{i=0}^{n} \nu_{t_1}(Q^i_{t_1} \cap R) \right| = \sum_{i=0}^{n} m_i s_i t_2^2 - \sum_{i=0}^{n} m_i s_i t_1^2$$

$$= |t_2 - t_1| \cdot |t_1 + t_2| \sum_{i=0}^{n} m_i s_i \geq \frac{1}{2} |t_2 - t_1|,$$

and thus one gets

$$\frac{|f(\xi_2) - f(\xi_1)|}{|\xi_2 - \xi_1|} \leq \frac{2\,|t_2 - t_1|}{2^{-1}\,|t_2 - t_1|} = 4,$$

for $\xi_1, \xi_2$ satisfying $s_{n+1} \leq t_1^2 < t_2^2 \leq s_n$ for some $n \in \mathbb{N}$. Since the Lipschitz constant 4 does not depend on $n$, we can easily pass to the general case via the triangular inequality. One can observe that the Lipschitz continuity is also verified in 0, since $f$ is continuous and the Lipschitz constant 4 for $\xi > 0$ does not depend on $\xi$ itself.

We now define $v[\mu](x) := (0, f(F(\mu)))$ (thus, by construction, we have $v[\nu_t](x) = (0, 2t)$) and show that $v$ satisfies Assumption 7.2. The only non-straightforward point is to prove that $v$ is Lipschitz with respect to the total

variation distance. For this, take two distinct measures $\mu, \nu$. If $F(\mu) = F(\nu)$, then $\|v[\mu] - v[\nu]\|_{C^0} = 0 < |\mu - \nu|$. Otherwise:

$$|\mu - \nu| \geq |\mathbb{1}_R \mu - \mathbb{1}_R \nu| \geq |F(\mu) - F(\nu)|,$$

thus

$$\frac{\|v[\mu] - v[\nu]\|_{C^0}}{|\mu - \nu|} \leq \frac{|f(F(\mu)) - f(F(\nu))|}{|F(\mu) - F(\nu)|}.$$

Hence $v$ is uniformly Lipschitz, since $f$ is Lipschitz.

Now consider the Cauchy problem (7.1) with $\mu_0 = \nu_0$. Since $v[\nu_0] = (0, 0)$, setting $\mu_t = \nu_0$, for all $t \in [0, 1]$, we get a first solution to the Cauchy problem (7.1). A second solution is obtained by setting $\mu_t = \nu_t$. Indeed, consider the non-autonomous vector field $w(t, x) := (0, 2t)$, generating the flow $\Phi_t^w(x, y) = (x, y + t^2)$. Then $\Phi_t^w \# \nu_0 = \nu_t$, thus $\nu_t$ satisfies (7.1) with $v[\nu_t] = (0, 2t)$.

It is easy to observe that $v$ does not satisfy Assumption 7.1, for any $p \geq 1$. Indeed, $W_p(\nu_t, \nu_s) = t^2 - s^2$, thus it is impossible to find a finite $K'$ such that, for all $t, s$, it holds

$$\|v[\nu_t] - v[\nu_s]\|_{C^0} = 2(t - s) \leq K'(t^2 - s^2) = K' W_p(\nu_t, \nu_s).$$

## 7.2 Transport Equation, Optimal Transportation, and the Wasserstein Distance

In this section we provide further relationships between the transport equation (7.1) and the Wasserstein distance. Moreover, we show how the Wasserstein distance arises naturally in connection with optimal transportation problems.

Given two probability measures $\mu, \nu$, one can ask if there exists a measurable map $\gamma$ such that $\gamma \# \mu = \nu$. Moreover, defining the cost $\int c(x, \gamma(x))\, d\mu$, with $c : \mathbb{R}^d \times \mathbb{R}^d \mapsto [0, \infty)$, one can look for the $\gamma$ with minimal cost. A standard choice for the function $c$ is $c(x, y) = |x - y|^p$ with $p \geq 1$ and one considers the cost:

$$I[\gamma] = \left( \int_{\mathbb{R}^d} |\gamma(x) - x|^p \, d\mu \right)^{1/p}.$$

This optimization problem is called the optimal transportation problem and was first proposed by Monge in 1781.

If $\mu$ and $\nu$ are absolutely continuous with respect to the Lebesgue measure, then an optimal $\gamma$ always exists. However, this does not hold true in the general case, because a $\gamma$ that sends $\mu$ to $\nu$ may not exist. For example if $\mu = \delta_1$, and $\nu = \frac{1}{2}\delta_0 + \frac{1}{2}\delta_2$ (on the real line), then there exists no $\gamma$ such that $\nu = \gamma \# \mu$. This is due to the

fact that $\gamma$ cannot split the mass placed in 1 for $\mu$ into two separate masses placed in 0 and 2. Moreover, one can exhibit cases in which there exist minimizing sequences $\gamma_n$, which admit limits that are not maps.

For such reasons, one generalizes the problem to the following setting. Given a probability measure $\pi$ on $\mathbb{R}^d \times \mathbb{R}^d$, one can interpret it as a method to transfer a measure $\mu$ on $\mathbb{R}^d$ to another measure $\nu$ on $\mathbb{R}^d$ as follows: each infinitesimal mass on a location $x$ is sent to a location $y$ with a probability given by $\pi(x, y)$. Formally, $\mu$ is sent to $\nu$ if the following properties hold:

$$\int_{\mathbb{R}^d} d\pi(x, \cdot) = d\mu(x), \qquad \int_{\mathbb{R}^d} d\pi(\cdot, y) = d\nu(y). \tag{7.2}$$

Such a $\pi$ is called a transference plan from $\mu$ to $\nu$. A condition equivalent to (7.2) is that, for all $f, g \in C_c^\infty(\mathbb{R}^d)$ it holds $\int_{\mathbb{R}^d \times \mathbb{R}^d} (f(x) + g(y))\, d\pi(x, y) = \int_{\mathbb{R}^d} f(x)\, d\mu(x) + \int_{\mathbb{R}^d} g(y)\, d\nu(y)$. Then, one can define a cost for $\pi$ as follows

$$J[\pi] := \left( \int_{\mathbb{R}^d \times \mathbb{R}^d} |x - y|^p \, d\pi(x, y) \right)^{1/p},$$

and look for a minimizer of $J$. This problem is called the Monge-Kantorovich problem. This problem induces a definition of distance between two measures, which is named the Wasserstein distance:

$$W_p(\mu, \nu) = \inf_{\pi \in \Gamma(\mu,\nu)} J[\pi], \tag{7.3}$$

where $\Gamma(\mu, \nu)$ is the set of transference plans from $\mu$ to $\nu$. Notice that we can easily extend the definition of $W_p$ to measures with the same finite mass.

It is important to observe that this problem is a generalization of the Monge problem. Indeed, given a $\gamma$ sending $\mu$ to $\nu$, one can define a transference plan by setting $\pi = (\mathrm{Id} \times \gamma)\#\mu$, i.e., $d\pi(x, y) = d\mu(x) \otimes \delta_{y=\gamma(x)}$. It also holds $J[\mathrm{Id} \times \gamma] = I[\gamma]$. The main advantages of this approach are the following: first, the existence of at least one $\pi$ satisfying (7.2) is easy to check, since one can choose $\pi(A \times B) = \mu(A)\nu(B)$, i.e., the mass from $\mu$ is proportionally split to $\nu$. Moreover, a minimizer of $J$ always exists for $\mu, \nu \in \mathscr{P}_p(\mathbb{R}^d)$.

For later use we recall the Kantorovich-Rubinstein duality formula:

$$W_1(\mu, \nu) = \sup \left\{ \int_{\mathbb{R}^d} \psi \, d(\mu - \nu) \,:\, \psi \text{ is Lipschitz with } \mathrm{Lip}(\psi) \le 1 \right\}, \tag{7.4}$$

where $\mathrm{Lip}(\psi) = \sup_{x \neq y} \frac{|\psi(x) - \psi(y)|}{\|x - y\|}$ denotes the Lipschitz constant of $\psi$.

An interesting property is that the distance can be estimated by dividing the measures in different parts, i.e.,

$$W_p^p(\mu_1 + \mu_2, \nu_1 + \nu_2) \le W_p^p(\mu_1, \nu_1) + W_p^p(\mu_2, \nu_2). \tag{7.5}$$

This formula makes sense for positive measures $\mu_i, \nu_i$ such that $\mu_i(\mathbb{R}^d) = \nu_i(\mathbb{R}^d)$. We give two corollaries of this result, that we use in the following. Given $\mu$,$\nu$ sharing a common mass $\eta$, we have

$$W_p(\mu, \nu) = W_p(\mu - \eta, \nu - \eta). \tag{7.6}$$

Moreover, $W_p$ distances are "ordered", in the sense that

$$p_1 \le p_2 \quad \Rightarrow \quad W_{p_1}(\mu, \nu) \le W_{p_2}(\mu, \nu). \tag{7.7}$$

This has a direct consequence in our context. Take a function $v$ satisfying Assumption 7.1 for a certain $p_1$ with constants $L$, $M$, $K$. Then $v$ satisfies Assumption 7.1 for all $p > p_1$ and the same constants $L$, $M$, $K$. The converse is not true, since we only have that, given $\Omega$ bounded metric space, it holds

$$p_1 \ge p_2 \quad \Rightarrow \quad W_{p_1}(\mu, \nu) \le W_{p_2}^{p_2/p_1}(\mu, \nu)\, \mathrm{diam}(\Omega)^{1-p_2/p_1}.$$

Thus, for $p < p_1$ we only have Hölder continuity. In particular, the strongest condition in Assumption 7.1 is for $p = 1$.

Given a semigroup of diffeomorphisms $\gamma_t$, one can define a time-dependent push-forward $\mu_t = \gamma_t \# \mu$. The generated trajectory, in the space of measures, is connected to the solution of a corresponding transport equation, more precisely:

**Theorem 7.2.** *Let $(\gamma_t)_{t\in[0,T]}$ be a locally Lipschitz in time family of diffeomorphisms of $\mathbb{R}^d$, with $\gamma_0 = \mathrm{Id}$. Let $v = v(t, x)$ be the velocity field associated with the trajectories of $\gamma_t$. Given $\mu_0 \in \mathscr{P}_c(\mathbb{R}^d)$, if $\mu_t := \gamma_t \# \mu_0$, then $\mu = \mu_{[0,T]}$ is the unique solution of the linear transport equation*

$$\begin{cases} \dfrac{\partial \mu}{\partial t} + \nabla \cdot (\mu v) = 0 \\ \mu_{|_{t=0}} = \mu_0 \end{cases} \tag{7.8}$$

*in $C([0, T], \mathscr{P}_c(\mathbb{R}^d))$, where $\mathscr{P}_c(\mathbb{R}^d)$ is endowed with the weak topology.*

The solution to the previous equation is to be intended in the weak sense, i.e., for all functions $f \in C_c^\infty([0, T] \times \mathbb{R}^d)$, it holds $\int_{[0,T]\times\mathbb{R}^d} (\partial_t f + \nabla f \cdot v)\, d\mu_t\, dt = 0$.

A typical example of an application of Theorem 7.2 is the case in which $v$ is a given Lipschitz vector field, and $\gamma_t = \Phi_t^v$ is the flow of $v$. We recall that $\Phi_t^v(x_0)$ is the value at time $t$ of the unique solution to

$$\begin{cases} \dot{x} = v(x) \\ x(0) = x_0. \end{cases}$$

Then the velocity field associated to $\gamma_t$ is exactly $v$. One can easily pass to time-dependent vector fields $v_t$, assuming that they generate a flow. This is also true

when $v$ is measurable with respect to time, uniformly Lipschitz in $x$ and uniformly bounded. In this context, both approaches (push-forward of measures and transport equations) are equivalent.

*Remark 7.1.* Our problem does not fit exactly into the hypotheses of Theorem 7.2, since we endow $\mathscr{P}_c(\mathbb{R}^d)$ with the $W_p$ metric, and the corresponding topology, instead of weak topology. Nevertheless, observe that we always deal with a compactly supported measure $\mu_0$, and that the velocity is bounded. Hence, all $\mu_t$ have compact support, contained in $\text{supp}(\mu_0) + B_{Mt}(0)$. Then we can change the metric of $\mathbb{R}^d$ outside the support of the $\mu_t$ to have $\mathbb{R}^d$ bounded. In this context, $W_p$ metrizes the weak convergence, thus the weak topology coincides with the $W_p$ topology on $\mathscr{P}_c(\mathbb{R}^d)$.

### 7.2.1 Wasserstein Distance Under the Action of Flows

In this section, we prove estimates of the distance $W_p$ under the action of flows $\Phi_t^v(\cdot)$, where $v$ is a bounded and Lipschitz vector field.

**Proposition 7.1.** *Let $v$ be an autonomous vector field, Lipschitz with constant $L$ and bounded. Let $\mu,\ \nu \in \mathscr{P}_c(\mathbb{R}^d)$ be two probability measures. Then*

$$W_p\left(\Phi_t^v\#\mu,\ \Phi_t^v\#\nu\right) \leq e^{Lt} W_p\left(\mu,\ \nu\right) \tag{7.9}$$

*and*

$$W_p\left(\mu,\ \Phi_t^v\#\mu\right) \leq \|v\|_{C^0} t. \tag{7.10}$$

*Proof.* We start with the first estimate (7.9). Let $\pi$ be the transference plan realizing $W_p\left(\mu,\ \nu\right)$. Observe that $\Phi^t$ is a diffeomorphism of the space $\mathbb{R}^d$, then $\Phi_t^v \times \Phi_t^v$ is a diffeomorphism of the space $\mathbb{R}^d \times \mathbb{R}^d$. Since $\pi$ is a probability density on $\mathbb{R}^d \times \mathbb{R}^d$, one can define $\pi' := (\Phi_t^v \times \Phi_t^v)\#\pi$, another probability density on $\mathbb{R}^d \times \mathbb{R}^d$. It is easy to prove that $\pi'$ is indeed a transference plan between $\Phi_t^v\#\mu$ and $\Phi_t^v\#\nu$. Then we can use this transference plan $\pi'$ to estimate $W_p\left(\Phi_t^v\#\mu,\ \Phi_t^v\#\nu\right)$. This gives

$$\begin{aligned} W_p^p(\Phi^t\#\mu,\ \Phi^t\#\nu) &\leq |\mu|^p \int |x-y|^p \ d\pi'(x,\ y) = |\mu|^p \int |\Phi_t^v(x) - \Phi_t^v(y)|^p \ d\pi(x,\ y) \\ &\leq |\mu|^p \int e^{Lpt}\, |x-y|^p \ d\pi(x,\ y) = e^{Lpt} W_p^p(\mu,\ \nu), \end{aligned}$$

where we used the definition of the push-forward in the first equality and the Gronwall lemma in the second inequality. Therefore (7.9) is proved.

To prove the second inequality, define the transference plan $\pi$ such that $d\pi(x, y) = d\mu(x) \otimes \delta_{y=\Phi^t(x)}$ on $\mathbb{R}^d \times \mathbb{R}^d$. Observe that it is a transference plan between $\mu$ and $\Phi_t^v \# \mu$, thus

$$W_p^p(\mu, \Phi_t^v \# \mu) \leq \int |x - y|^p \, d\pi(x, y) = \int \left|x - \Phi^t(x)\right|^p \, d\mu(x)$$
$$\leq \int (\|v\|_{C^0} t)^p \, d\mu(x) = \|v\|_{C^0}{}^p t^p.$$

We now turn our attention to an estimate in which the flows are given by two distinct vector fields. With a proof similar to that of the first inequality of Proposition 7.1, we get the following:

**Proposition 7.2.** *Let $v$, $w$ be two vector fields, both Lipschitz with constant $L$ and bounded. Let $\mu, \nu \in \mathscr{P}_c(\mathbb{R}^d)$ be two probability measures. Then*

$$W_p\left(\Phi_t^v \# \mu, \Phi_t^w \# \nu\right) \leq e^{Lt} W_p(\mu, \nu) + \frac{e^{Lt} - 1}{L} \|v - w\|_{C^0}. \tag{7.11}$$

*Remark 7.2.* These results can be generalized to non-autonomous vector fields $w_t, v_t$, if they generate smooth flows. This is the case if they are measurable with respect to time and uniformly bounded and Lipschitz with respect to space. In this case, in Proposition 7.2 we have to replace $\|v - w\|_{C^0}$ with $\sup_t \|v_t - w_t\|_{C^0}$.

*Remark 7.3.* These results can be easily adapted to positive measures that are not probability measures but have finite mass, i.e., $\mu(\mathbb{R}^d) = C \neq 1$. In this case, we have

$$W_p\left(\Phi_t^v \# \mu, \Phi_t^w \# \nu\right) \leq e^{Lt} W_p(\mu, \nu) + \mu(\mathbb{R}^d) \frac{e^{Lt} - 1}{L} \|v - w\|_{C^0}.$$

### 7.2.2 Existence and Uniqueness of Solutions

In this section we introduce a semi-discrete in time Lagrangian scheme to solve (7.1). The limit of this scheme, when the discretization parameter tends to zero, is indeed a solution.

We first precisely define the semi-discrete in time Lagrangian scheme, that defines a Cauchy sequence in $C([0, T], \mathscr{P}_p(\mathbb{R}^d))$, endowed with the distance:

$$d(\mu, \nu) = \sup_{t \in [0, T]} W_p(\mu_t, \nu_t). \tag{7.12}$$

The idea of the scheme is the following: divide the time interval $[0,\ T]$ in intervals $[j\Delta t,\ (j\ +\ 1)\Delta t]$. For each interval, compute the velocity at the initial time $v_{j\Delta t}\ =\ v[\mu_{j\Delta t}]$ and use it as a constant on the whole interval, i.e., compute $\mu_t = \Phi^{v_{j\Delta t}}_{(t-j\Delta t)}\#\mu_{j\Delta t}$.

**Scheme 1** Lagrangian, semi-discrete in time, exact velocity
**initialization:**

- Fix a time discretization parameter $\Delta t$;
- Fix a starting measure $\mu_0$;
- $i \leftarrow 0$;

**while** $i\Delta t \le T$ **do**
  Set $v_{i\Delta t} := v[\mu_{i\Delta t}]$ on the interval $[i\Delta t,\ (i\ +\ 1)\Delta t]$;
  Compute the corresponding flow $\Phi_t^{v_{i\Delta t}}$;
  Set $\mu_t := \Phi_t^{v_{i\Delta t}}\#\mu_{i\Delta t}$ for $t \in [i\Delta t,\ (i\ +\ 1)\Delta t]$;
  $i \leftarrow i\ +\ 1$;
**end**

Fix an integer $k\ >\ 0$ and divide $[0,\ T]$ in $2^k$ intervals, i.e., choose $\Delta t\ =\ \frac{T}{2^k}$. Call $\mu_t^k$ the solution of this numerical scheme. For the convergence of the sequence $\{\mu^k_{[0,\ T]}\}_{k\in\mathbb{N}}$ in $C([0,\ T],\ \mathscr{P}_p(\mathbb{R}^d))$, we have the following result:

**Proposition 7.3.** *Let $v$ satisfy Assumption 7.1, and $\mu_0$ be given. Let $\mu^k = \mu^k_{[0,\ T]}$ be constructed by **Scheme 1** with $\Delta t = \frac{T}{2^k}$. Then the sequence $\{\mu^k_{[0,\ T]}\}_{k\in\mathbb{N}}$ is a Cauchy sequence in $C([0,\ T],\mathscr{P}_p(\mathbb{R}^d))$. The limit $\bar{\mu}\ =\ \lim_k \mu^k$ exists and is a solution to (7.1).*

The proof is similar to that of Theorem 6.2, thus we omit it. Moreover, we have:

**Proposition 7.4.** *Let $v$ satisfy Assumption 7.1, and $\mu_0$ be given. Let $\mu = \mu_{[0,\ T]}$ be the solution of (7.1), and $\mu^k$ the approximation of $\mu$ computed using **Scheme 1** with $\Delta t = \frac{T}{2^k}$. Then, for $\Delta t$ sufficiently small, it holds*

$$d(\mu,\ \mu^k) \le KM\frac{e^{4T(L+K)}-1}{L+K}\Delta t. \tag{7.13}$$

## 7.3 Lagrangian and Eulerian Numerical Schemes

In this section we consider two other schemes for (7.1). We prove that all these schemes converge to the solution of (7.1), whose existence and uniqueness have just been proved. **Scheme L** is a Lagrangian scheme discrete in space and time, while **scheme E** is a discrete Eulerian scheme.

We start this section by introducing the spatial discretization. Fix a space discretization parameter $\Delta x > 0$ and discretize the space $\mathbb{R}^d$, dividing it using a grid of hypercubes with side $\Delta x$. For simplicity, from now on we will use the notation for grids in $\mathbb{R}^2$, calling each hypercube simply "square". We denote the grid with the symbol $\boxplus$. Given a measure $\mu$, we denote the discretized measure (with an abuse of notation) with the symbol $\boxplus[\mu]$, computed as follows: given a square $\square$ in the grid $\boxplus$, we define $\boxplus[\mu]$ on this square to be constant and with the same mass as $\mu$ on the square. More precisely, we have

$$\boxplus : \begin{cases} \mathscr{P}_p(\mathbb{R}^d) \to \mathscr{P}_p(\mathbb{R}^d) \\ \mu \quad \mapsto \boxplus[\mu] := \displaystyle\sum_{\square \in \boxplus} \frac{\mu(\square)}{\Delta x^d} \cdot \end{cases}$$

This choice clearly permits to preserve the total measure, i.e., $\mu(\mathbb{R}^d) = \boxplus[\mu](\mathbb{R}^d)$.

We now estimate $W_p\left(\mu, \boxplus[\mu]\right)$ using a map $\gamma$ that redistributes the mass inside each square $\square$ only. Remark that $\gamma$ is not optimal in general. We have $W_p^p(\mu, \boxplus[\mu]) \leq \int_{\mathbb{R}^d} |\gamma(x) - x|^p \, d\mu(x) \leq \sqrt{d}^p \Delta x^p$, i.e.,

$$W_p\left(\mu, \boxplus[\mu]\right) \leq \sqrt{d}\,\Delta x. \tag{7.14}$$

The same idea can be used to estimate $W_p\left(\mu, \boxplus[\mu]\right)$ when $\mu$ is a positive measure with mass $\mu(\mathbb{R}^d) = C \neq 1$. We have:

$$W_p\left(\mu, \boxplus[\mu]\right) \leq \mu(\mathbb{R}^d)^{1/p}\sqrt{d}\,\Delta x. \tag{7.15}$$

### 7.3.1 Discrete Lagrangian Scheme with Velocity of Centers

In this section we introduce the Lagrangian scheme. We indicate with $\mu_t^L$ the function computed via this scheme. Fix a space discretization parameter $\Delta x$ and a time discretization $\Delta t$. We perform a first approximation $\mu_0^L$ of the initial data $\mu_0$ in space, that is $\mu^L := \boxplus[\mu_0]$. Given a square of the grid $\square_0$, we denote the center of this square as $x_{\square_0}$ and $v(\square_0)$ to indicate the velocity $v[\mu_0^L](x_{\square_0})$, i.e., the vector field $v[\mu_0^L]$ evaluated at the center of the square. This can be seen as the approximation of the vector field $v[\mu_0^L]$ with a vector field that is piecewise-constant on the same grid. We then translate the square $\square_0$ by the vector $\Delta t\, v(\square_0)$. Then $\mu_{\Delta t}^L$ is defined as the sum of all the translated squares, i.e.,

$$\mu_{\Delta t}^L := \sum_{\square_0 \in \boxplus} \mu_0^L(\square_0) \frac{\mathbb{1}_{\square_{\Delta t}}}{\Delta x^d}.$$

Then we compute the translation $\square_{2\Delta t}$ of the square $\square_{\Delta t}$ using $v(\square_{\Delta t}) := v[\mu^L_{\Delta t}](x_{\square_{\Delta t}})$, i.e. the new velocity field evaluated at the center of the squares. The process is repeated up to time $T$.

**Scheme L** Lagrangian, discrete in space and time, velocity at centers
**initialization:**

- Fix space and time discretization parameters $\Delta x$, $\Delta t$, respectively;
- Fix a starting measure $\mu_0$;
- Set $\mu^L_0 := \boxplus[\mu_0]$;
- $i \leftarrow 0$;

**while** $i\Delta t \leq T$ **do**
  Set $x_{\square_{i\Delta t}}$ := center of the square $\square_{i\Delta t}$;
  Set $v(\square_{i\Delta t}) := v[\mu^L_{i\Delta t}](x_{\square_{i\Delta t}})$;
  Set $\square_t := \square_{i\Delta t} + (t - i\Delta t)v(\square_{i\Delta t})$;
  Set $\mu^L_t := \sum_{\square_0 \in \boxplus} \mu^L_{i\Delta t}(\square_0) \frac{\mathbb{1}_{\square_t}}{\Delta x^d}$ for $t \in [i\Delta t,\ (i+1)\Delta t]$;
  $i \leftarrow i + 1$;
**end**

One of the advantages of **Scheme L** is that the evolution of a square is still a square of the same dimension and with sides parallel to axes of $\mathbb{R}^d$. Hence the measure $\mu^L_t$ is always piecewise-constant. Remark instead that the grid is used at the beginning of the algorithm only, and that afterwards the squares do not belong to the grid. Moreover, the squares can overlap and follow different velocities, thus the evolution cannot be written globally as a solution of (7.1), since $v[\mu^L_t](x)$ is not uniquely determined. Another important feature of the scheme is that the value of the function inside each square does not change. Nevertheless, there is an interaction among all the squares, since the velocity of each square is given by the map $v[\mu_t]$. One can also observe that, if at time $l\Delta t$ two different squares have the same center, then they have the same dynamics from that moment on. This is possible, since the evolution of centers is not given by a flow (that would give existence and uniqueness), but by a discrete-time dynamics.

We now state a convergence result for this scheme.

**Proposition 7.5.** *Let $v$ satisfy Assumption 7.1, and $\mu_0$ be given. Let $\mu^L = \mu^L_{[0,T]}$ be computed using* ***Scheme L*** *with parameters $\Delta x$ and $\Delta t = \frac{T}{2^k}$. Let $\mu$ be the exact solution of (7.1). Then, for $\Delta t < \frac{\log(2)}{L}$, it holds*

$$d(\mu,\, \mu^L) \leq \sqrt{d}\left(2e^{\lceil T\max\{2L,\,8K\}\rceil} + 2L\frac{e^{KTe^{LT}} - 1}{K}\right)\Delta x + KM\frac{e^{4T(L+K)} - 1}{L+K}\Delta t,$$

*where* $\lceil\cdot\rceil$ *indicates the ceiling function. Thus, as* $\Delta x, \Delta t \to 0$, $\mu^L$ *converges weakly to* $\mu$ *in* $C([0, T], \mathscr{P}_c(\mathbb{R}^d))$.

*Remark 7.4.* The convergence of the Lagrangian schemes is not really surprising in the context of pedestrian modeling by using measures. Indeed, we approximate a set of discrete agents (the pedestrians) with a continuous measure. This is the passage from microscopic to macroscopic model. Then, the scheme is convergent for $\Delta x \to 0$, that means that we go back to a microscopic scale, i.e., the pedestrians.

One can improve this scheme by computing a more precise evolution of each square. For example, one can allow deformations of the axes, rotations and so on. This idea coincides with the idea of computing the vector field $v$ for each square as a certain approximation of the original $v$. For our scheme, we simply evaluate $v$ at the center, i.e., we perform a Taylor expansion of order 0. Improvements of this kind certainly result in better convergence rates but need a more complicated implementation.

### 7.3.2 Eulerian Scheme

In this section we present a last scheme to compute numerically the solutions of (7.1). We indicate the solution of the scheme as $\mu_t^E$. We call it Eulerian, since we are interested in the evolution of the value $\mu_t(P)$ at a point $P$ not changing in time. Instead, the previous schemes were Lagrangian, since we were interested in the spatial evolution of a point $x$, i.e., its trajectory $x(t)$. This was particularly clear in the previous scheme, in which we fixed a starting square $\square_0$ and studied its evolution in time $\square_t$.

Fix a space discretization parameter $\Delta x > 0$ and a time discretization $\Delta t$. We perform a first approximation $\mu_0^E$ of the initial datum $\mu_0$ in space, that is $\mu_0^E := \boxplus[\mu_0]$. Take a square of the grid $\square \in \boxplus$. We denote the center of this square as $x_\square$ and $v_t(\square)$ to indicate the velocity $v[\mu_t^E](x_\square)$, i.e., the vector field $v[\mu_t^E]$ evaluated at the center of the square. We compute the evolution of the square $\square$ as its translation of the vector $\Delta t v_0(\square)$, i.e., $\square + \Delta t v_0(\square)$. We define $\tilde{\mu}_{\Delta t}$ as the sum of all the translated squares, i.e., $\tilde{\mu}_{\Delta t} := \sum_{\square \in \boxplus} \mu_0^E(\square) \frac{\mathbb{1}_{\square + \Delta t v_0(\square)}}{\Delta x^d}$. For the moment, this coincides with **Scheme 4**. The difference is that we define $\mu_{\Delta t}^E$ as the approximation of $\tilde{\mu}_{\Delta t}$ computing the mean values on the starting grid, i.e., $\mu_{\Delta t}^E = \boxplus[\tilde{\mu}_{\Delta t}]$. We then repeat the same idea "evolution + mean values" starting from $\mu_{\Delta t}^E$ and continue until reaching $T$.

**Scheme E** Eulerian, discrete in space and time, velocity at centers
**initialization:**

- Fix space and time discretization parameters $\Delta x$, $\Delta t$, respectively;
- Fix a starting measure $\mu_0$;
- Set $\mu_0^E := \boxplus[\mu_0]$;
- $i \leftarrow 0$;

**while** $i\Delta t \leq T$ **do**
  Set $x_\square :=$ center of the square $\square$;
  Set $v_{i\Delta t}(\square) := v[\mu^E_{i\Delta t}](x_\square)$;
  Set $\tilde{\mu}_{(i+1)\Delta t} := \sum_{\square\in\boxplus} \mu^E_{i\Delta t}(\square)\frac{\mathbb{1}_{\square+\Delta t v_{i\Delta t}(\square)}}{\Delta x^d}$;
  Define the approximate solution $\mu^E_{(i+1)\Delta t} := \boxplus[\tilde{\mu}_{(i+1)\Delta t}]$;
  $i \leftarrow i+1$;
**end**

We now prove that the scheme is convergent. First observe that $\mu^E$ is defined for times $j\Delta t$ only, thus the distance $d(\mu, \mu^E)$ is not defined by Eq. (7.12). Nevertheless, we redefine it with a slight abuse of notation

$$d(\mu, \mu^E) := \sup\{W_p\left(\mu_t, \mu_t^E\right) \text{ for } t \in [0, T] : \mu_t^E \text{ is defined}\}.$$

We have the following result.

**Proposition 7.6.** *Let $v$ satisfy Assumption 7.1, and $\mu_0$ be given. Let $\mu^E$ be computed using **Scheme E** with parameters $\Delta x$ and $\Delta t = \frac{T}{2^k}$. Let $\mu$ be the exact solution of (7.1). Then $d(\mu, \mu^E) \leq d(\mu, \mu^L) + d(\mu^L, \mu^E)$ and we have:*

- *For $p > 1$:*

$$d(\mu^L, \mu^E) \leq \frac{(2^{1-1/p}\Delta t L + 1)e^{TK}\sqrt{d}}{2^{1-1/p}-1} 2^{(1-1/p)\frac{T}{\Delta t}}\Delta x. \tag{7.16}$$

  *For $\Delta t \to 0$ and $\lim_{\Delta x, \Delta t\to 0} 2^{(1-1/p)\frac{T}{\Delta t}}\Delta x = 0$, $\mu^E$ converges weakly to $\mu$.*
- *For $p = 1$:*

$$d(\mu^L, \mu^E) \leq \frac{\sqrt{d}(\Delta t L + 1)(e^{TK}-1)}{K} \cdot \frac{\Delta x}{\Delta t}. \tag{7.17}$$

  *For $\Delta t \to 0$ and $\lim_{\Delta x, \Delta t\to 0} \frac{\Delta x}{\Delta t} = 0$, $\mu^E$ converges weakly to $\mu$.*

*Remark 7.5.* It is interesting to observe that, if $\lim_{\Delta x, \Delta t\to 0} 2^{(1-1/p)\frac{T}{\Delta t}}\Delta x = 0$ is satisfied for a certain $p_1$, then it is satisfied for all $p_2 < p_1$. Moreover,

$\lim_{\Delta x,\,\Delta t\to 0} \frac{\Delta x}{\Delta t} = 0$, i.e., the condition for $p_2 = 1$ is satisfied as well. This is a direct consequence of the fact that Assumption 7.1 becomes stronger for decreasing $p$, thus the corresponding condition for convergence of the scheme can be weaker.

## 7.4 Interaction Velocities for Pedestrians

We now want to analyze interaction velocities for pedestrian models. More precisely, we focus on models of the type (6.34) and argue when such models do satisfy the assumptions for existence of the corresponding transport equation (7.1).

From now on, we focus on the velocity field defined by interactions with other pedestrians. A simple model is the following: take a kernel $\eta : \mathbb{R}^d \mapsto [0, +\infty)$, set

$$x^* := \frac{\int_{\mathbb{R}^d} y\, \eta(x-y)\, d\mu(y)}{\int_{\mathbb{R}^d} \eta(x-y)\, d\mu(y)},$$

that is the center of mass of the crowd with respect to the kernel $\eta$, and define

$$v[\mu](x) := (x - x^*) f\left(\int_{\mathbb{R}^d} \eta(x-y)\, d\mu(y)\right), \tag{7.18}$$

where $f$ is a non-decreasing weight function. Observe that (7.18) is not defined for $\int_{\mathbb{R}^d} \eta(x-y)\, d\mu(y) = 0$. In this case, we simply define $v[\mu](x) = 0$. This choice does not change the dynamics, since an area without mass undergoes no change in time.

We now study two particular cases of velocity (7.18). The first is given by $f(x) \equiv 1$, while the second is given by $f(x) = x^\alpha$ with $\alpha \geq 1$. We prove that in the first case $v$ does not satisfy Assumption 7.1, while in the second it does.

Let $f(x) \equiv 1$. Given a kernel $\eta$ that is not identically 0, we find a family of measures $\mu_t$ such that $v[\mu]$ is not even a continuous vector field with respect to $\mu_t$ in the Wasserstein space. The idea is explained in Fig. 7.3.

Let $R$ be such that $\mathrm{supp}(\eta) \subset B_R(0)$. Since $\eta$ is continuous, we have that the set $A := \{\eta > 0\}$ is open. It is always possible to choose $r$ sufficiently small to have $A \setminus \overline{B_r(0)}$ nonempty. Since it is open, we can always choose a point $\tilde{x}$ in this set, and $\epsilon > 0$ sufficiently small to have $B_\epsilon(\tilde{x}) \subset A \setminus B_r(0)$. Clearly, if $y \in B_\epsilon(\tilde{x})$ then $|y| \geq r > 0$. Finally, choose a compact set $C$ of nonzero Lebesgue measure outside the ball $B_R(0)$, and let $s$ be the maximum distance between elements of $B_\epsilon(\tilde{x})$ and $C$, i.e., $s = \sup\{|x-y| : x \in B_\epsilon(\tilde{x}),\ y \in C\}$. Clearly it holds $s < \infty$.

Now define the family $\mu_t$ of measures by

$$\mu_t := \left(t \frac{\mathbb{1}_{B_\epsilon(\tilde{x})}}{\lambda(B_\epsilon(\tilde{x}))} + (1-t)\frac{\mathbb{1}_C}{\lambda(C)}\right)\lambda,$$

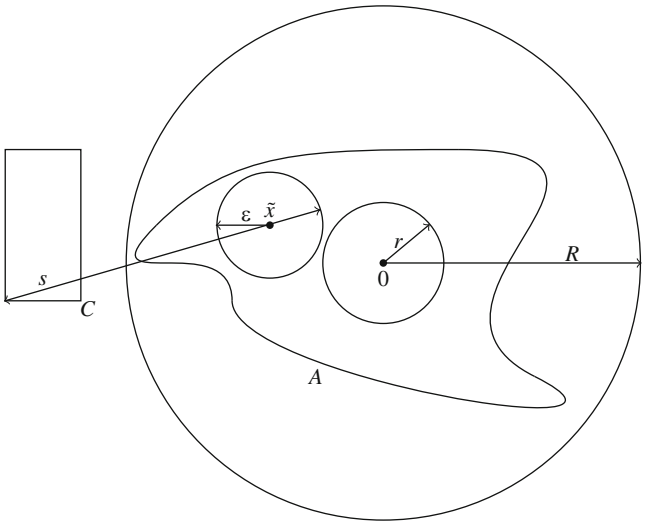


**Fig. 7.3** The convolution kernel does not satisfy Assumption 7.1 for $f \equiv 1$

where $\lambda$ is the Lebesgue measure. Observe that $v[\mu_0](0) = 0$, since $\int_{\mathbb{R}^d} \eta(-y)\, d\mu_0(y) = \frac{1}{\lambda(C)} \int_C 0\, d\lambda(y) = 0$. Now observe that, for $t > 0$, we have $\int_{\mathbb{R}^d} \eta(-y)\, d\mu_t(y) > 0$, hence

$$|v[\mu_t](0)| = \left| \frac{\int_{\mathbb{R}^d} y\eta(-y)\, d\mu_t(y)}{\int_{\mathbb{R}^d} \eta(-y)\, d\mu_t(y)} \right| = \left| \frac{\frac{t}{\lambda(B_\epsilon(\tilde{x}))} \int_{B_\epsilon(\tilde{x})} y\eta(-y)\, d\lambda(y)}{\frac{t}{\lambda(B_\epsilon(\tilde{x}))} \int_{B_\epsilon(\tilde{x})} \eta(-y)\, d\lambda(y)} \right|$$
$$\geq \frac{\inf\{|y| \,:\, y \in B_\epsilon(\tilde{x})\} \int_{B_\epsilon(\tilde{x})} \eta(-y)\, d\lambda(y)}{\int_{B_\epsilon(\tilde{x})} \eta(-y)\, d\lambda(y)} \geq r.$$

As a consequence, $v[\mu_t](0)$ is not continuous with respect to the parameter $t$. We now show that $\mu_t$ is continuous with respect to $t$ in 0, i.e., $\lim_{t\to 0} W_p(\mu_0, \mu_t) = 0$. Fix a time $t$ and consider the measure $\nu_t$ shared by $\mu_0$ and $\mu_t$, that is exactly $\nu_t := (1-t)\frac{\mathbb{1}_C}{\lambda(C)}\lambda$. Thus, by (7.6), we have

$$W_p(\mu_0, \mu_t) = W_p(\mu_0 - \nu_t, \mu_t - \nu_t) = W_p\left(t\frac{\mathbb{1}_C}{\lambda(C)}\lambda,\, t\frac{\mathbb{1}_{B_\epsilon(\tilde{x})}}{\lambda(B_\epsilon(\tilde{x}))}\lambda\right).$$

Take the optimal map $\gamma$ between these measures, and observe that $|x - \gamma(x)| \leq s$. Thus $W_p(\mu_0, \mu_t) \leq s t^{1/p}$. Since $s$ and $\lambda(C)$ are finite and do not depend on $t$, then $W_p(\mu_0, \mu_t)$ is continuous at $t = 0$. Thus, $v[\mu_t](0)$ is not continuous with respect to the distance $W_p(\mu_0, \mu_t)$.

We now study the case $f(x) = x^\alpha$ with $\alpha \geq 1$.

**Proposition 7.7.** *Let $v = v[\mu]$ be defined by (7.18), with $\eta$ a positive, Lipschitz function with bounded support. Let $f(x) = x^\alpha$ with $\alpha \geq 1$. Then $v$ satisfies Assumption 7.1.*

*Proof.* Let $L$ be the Lipschitz constant of $\eta$, $M = \|\eta\|_\infty$ its maximal value and $R$ the radius of its bounded support, i.e. $\text{supp}(\eta) \subset B_R(0)$. Set $\phi(x) := \int_{\mathbb{R}^n} \eta(x - y)\, d\mu(y)$, then we can write

$$v[\mu](x) = x\phi(x)^\alpha - \frac{\int y\eta(x-y)\, d\mu(y)}{\phi(x)}\phi(x)^\alpha = \phi(x)^{\alpha-1} \int (x-y)\eta(x-y)\, d\mu(y).$$

Recall that $|\mu| = 1$, then we have $0 \leq \phi(x) \leq M$ and $|v[\mu](x)| \leq RM^\alpha$. Moreover:

$$|v[\mu](x) - v[\mu](z)| \leq M^{\alpha-1} \left| \int_{\mathbb{R}^n} \big((x-y)\eta(x-y) - (z-y)\eta(z-y)\big)\, d\mu(y) \right|.$$

Using the triangular inequality we can write:

$$\begin{aligned} |(x-y)\eta(x-y) - (z-y)\eta(z-y)| &\leq |(x-y)\eta(x-y) - (x-y)\eta(z-y)| \\ &\quad + |(x-y)\eta(z-y) - (z-y)\eta(z-y)| \\ &\leq (L|x-y| + M)\, |x-z|. \end{aligned}$$

Going back to the integral, since $|x - y| \leq R$ on the support of $\mu(y)$, we get:

$$\begin{aligned} |v[\mu](x) - v[\mu](z)| &\leq M^{\alpha-1}|x-z| \left( \int_{\mathbb{R}^n} (L|x-y| + M) d\mu(y) \right) \\ &\leq M^{\alpha-1}(LR + M)\, |x-z|. \end{aligned}$$

Finally we prove that $v$ is Lipschitz with respect to the $W_1$ distance. We have:

$$|v[\mu](x) - v[\nu](x)| \leq M^{\alpha-1} \left| \int_{\mathbb{R}^d} (x-y)\eta(x-y)\, d(\mu-\nu)(y) \right|.$$

We now show that $g(y) := (x - y)\eta(x - y)$ is a Lipschitz function. First write:

$$\begin{aligned} &|(x-y_1)\eta(x-y_1) - (x-y_2)\eta(x-y_2)| \leq \\ &|y_1 - y_2|\, |\eta(x-y_1)| + |(x-y_2)|\, |\eta(x-y_1) - \eta(x-y_2)|\,. \end{aligned}$$

Now if $|x - y_2| > R$ and $|x - y_1| > R$ then the second term vanishes because of the bound on the support of $\eta$. Otherwise, possibly changing $y_1$ with $y_2$ in the estimate, we can bound the first factor of the second term with $R$. Finally, we have:

$$|(x-y_1)\eta(x-y_1) - (x-y_2)\eta(x-y_2)| \leq M\ |y_1 - y_2| + R\ L\ |y_1 - y_2|\,.$$

Thus $\int_{\mathbb{R}^d}(x-y)\eta(x-y)\,d(\mu-\nu)(y) \leq (M+RL)W_1(\mu,\nu)$ via the Kantorovich-Rubinstein duality formula (7.4), hence $\|v[\mu]-v[\nu]\|_{C^0} \leq M^{\alpha-1}(M+RL)W_1(\mu,\nu)$.

## 7.5 Transport Equation with Source

In this section we deal with the case of transport equation with a source term:

$$\begin{cases} \dfrac{\partial \mu}{\partial t} + \nabla \cdot (\mu v[\mu]) = h[\mu] \\ \mu_{|_{t=0}} = \mu_0. \end{cases} \tag{7.19}$$

Unfortunately we cannot directly use the Wasserstein distance $W_p(\mu,\nu)$, since it is defined only if the two measures $\mu$, $\nu$ carry the same mass. Indeed, because of the presence of the source $h$, the mass of the measure $\mu_t$ varies in time, hence in general $W_p(\mu_t,\mu_s)$ is not defined for $t \neq s$. For this reason, we first define a generalized Wasserstein distance $W_p^{a,b}(\mu,\nu)$, combining the standard Wasserstein and total variation distances, see Sect. 7.6 below.

We look for solutions to (7.19) in the space of Borel measures with finite mass and compact support on $\mathbb{R}^d$, denoted with $\mathscr{M}_c$, that we endow with the generalized Wasserstein distance $W_p^{a,b}$. In this framework, we prove existence and uniqueness of the solution of (7.19) with $\mu_0 \in \mathscr{M}_c$ under the following assumption:

**Assumption 7.3.** *The function*

$$v[\mu] : \begin{cases} \mathscr{M}_c \to C^1(\mathbb{R}^d) \cap L^\infty(\mathbb{R}^d) \\ \mu \mapsto v[\mu] \end{cases}$$

*satisfies:*

- *$v[\mu]$ is uniformly Lipschitz and uniformly bounded w.r.t. $\mu$, i.e., there exist $L$, $M$ such that for all $\mu \in \mathscr{M}_c$, $x$, $y \in \mathbb{R}^d$,*

$$|v[\mu](x)-v[\mu](y)| \leq L|x-y| \qquad |v[\mu](x)| \leq M.$$

- *$v$ is a Lipschitz function, i.e., there exists $N$ such that*

$$\|v[\mu]-v[\nu]\|_{C^0} \leq NW_p^{a,b}(\mu,\nu).$$

*The function*

$$h[\mu] : \begin{cases} \mathscr{M}_c \to \mathscr{M}_c \\ \mu \mapsto h[\mu] \end{cases}$$

*satisfies:*

- *$h[\mu]$ has uniformly bounded mass and support w.r.t. $\mu$, i.e., there exist $P, R$ such that*

$$|h[\mu]| = |h[\mu](\mathbb{R}^d) \leq P, \qquad \text{supp}(h[\mu]) \subseteq B_R(0).$$

- *$h$ is a Lipschitz function, i.e., there exists $Q$ such that*

$$W_p^{a,b}(h[\mu],\, h[\nu]) \leq Q W_p^{a,b}(\mu,\, \nu).$$

*Remark 7.6.* Assumption 7.3 can be relaxed in standard ways. For example, the results still hold if we remove the uniform boundedness of $\nu$ on $\mathbb{R}^d$ and ask for uniform boundedness only at a point $x_0$.

## 7.6 Generalized Wasserstein Distance

In this section we define the generalized Wasserstein distance $W_p^{a,b}(\mu,\, \nu)$ and describe some of its useful properties.

We first give a rough description of the construction. Imagine to have three different admissible actions on $\mu,\, \nu$: either add/remove mass to $\mu$, add/remove mass to $\nu$, or transport mass from $\mu$ to $\nu$. The three techniques have their cost: adding/removing mass has a unitary cost $a$ (in both cases); transporting mass has the classic Monge-Kantorovich cost $J$, multiplied by a fixed constant $b$. The distance is the minimal cost of a mix of such techniques. We will show in the following that, depending on $\mu,\, \nu$, all mixes are possible: either remove all the mass of $\mu$ and $\nu$ (if they are very far), or transport the whole $\mu$ to $\nu$ (if they have the same mass and are close enough), or a mix of the two (for example when $\mu$ and $\nu$ are very close but with different masses). Instead, we will prove that adding mass is never optimal.

*Remark 7.7.* The fact that the unit cost of adding/removing mass is the same for the two terms $\mu,\, \nu$ is to ensure symmetry of $W_p^{a,b}$.

First we need additional pieces of notation: If $\tilde{\mu} \ll \mu$ and $\tilde{\mu}(A) \leq \mu(A)$ for all Borel sets, we write $\tilde{\mu} \leq \mu$. We now formally define the generalized Wasserstein distance.

**Definition 7.1.** Given $a,\, b \in (0,\, +\infty)$ and $p \geq 1$, the *generalized Wasserstein distance* between $\mu$ and $\nu$ is:

$$W_p^{a,b}(\mu,\, \nu) := \inf_{\substack{\tilde{\mu},\, \tilde{\nu} \in \mathscr{M}_c \\ |\tilde{\mu}| = |\tilde{\nu}|}} (a\, |\mu - \tilde{\mu}| + a\, |\nu - \tilde{\nu}| + b\, W_p\, (\tilde{\mu},\, \tilde{\nu})). \tag{7.20}$$

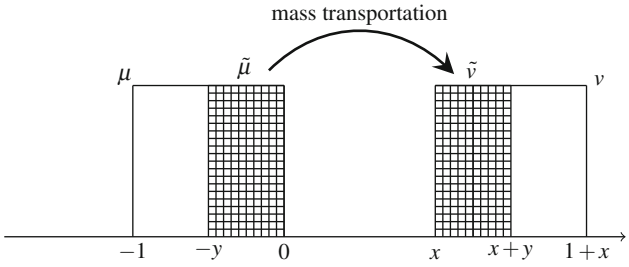


**Fig. 7.4** Choice of $\tilde{\mu}, \tilde{\nu}$ (*shaded*) for the computation of $W_p^{a,b}$

**Proposition 7.8.** *The operator $W_p^{a,b}$ is a distance. Moreover, one can restrict the computation in (7.20) to $\tilde{\mu} \le \mu$, $\tilde{\nu} \le \nu$ and the infimum is always attained.*

One interesting feature of this distance is that the total variation term $|\cdot|$ and the Wasserstein term $W_p$ have different degree of homogeneity with respect to translation in $\mathbb{R}^d$, thus the optimal strategy for $W_p^{a,b}$ varies when translating one measure. For example, compute $W_p^{a,b}(\delta_0, \delta_x)$ as a function of $x \ge 0$. We have $|\delta_0 - \delta_x| = 2$ and $W_p(\delta_0, \delta_x) = x$. Hence $W_p^{a,b}(\delta_0, \delta_x) = \min\{2a, bx\}$. If $2a < bx$, i.e., measures are "far", then the optimal strategy is to delete both masses $\delta_0$ and $\delta_x$, otherwise it is optimal to move $\delta_0$ to $\delta_x$ with a translation.

Another simple example permits us to show that optimal strategies can be either based on removing mass only (total variation strategy), or on transporting mass only ($W_p$ strategy), or on a mix of them. We give an example in Fig. 7.4. Take the measures $\mu, \nu$ on the real line with densities $\mu = \mathbb{1}_{[-1,0]}\mathscr{L}$, $\nu = \mathbb{1}_{[x,1+x]}\mathscr{L}$ with $x \ge 0$, where $\mathscr{L}$ is the Lebesgue measure. It is clear that the optimal strategy amounts to choosing $\tilde{\mu}, \tilde{\nu}$ with densities $\mathbb{1}_{[-y,0]}$, $\mathbb{1}_{[x,x+y]}$, respectively, for a certain parameter $y \in [0, 1]$. The total variation strategy is given by choosing $y = 0$, while the $W_p$ strategy is given by $y = 1$. We now prove that all values of $y$ can be optimal, depending on $x$ and the parameters $a, b, p$. We have $|\mu - \tilde{\mu}| = |\nu - \tilde{\nu}| = 1 - y$ and $W_p(\tilde{\mu}, \tilde{\nu}) = |y|^{1/p}(x + y)$. We choose for simplicity $a = b = p = 1$. Thus $W_p^{a,b}(\mu, \nu) = \min_{y\in[0,1]}(2 - 2y + xy + y^2)$. A simple computation shows that the minimum is attained for $y = \frac{2-x}{2}$ if $x \in [0, 2]$, and for $y = 0$ if $x \ge 2$. This clearly shows that if the measures are very close ($x = 0$), then the best strategy is the $W_p$ one (since $y = 1$), while for measures that are far ($x$ large) the best strategy is the total variation one. As stated above, varying $x \in [0, 2]$ one has mixed strategies.

We now state some simple properties of $W_p^{a,b}$.

**Proposition 7.9.** *The following properties hold:*

- $W_p^{a,b}(k\mu, k\nu) \le \max\{k^{1/p}, k\} W_p^{a,b}(\mu, \nu)$ *for* $k \ge 0$.
- $W_p^{a,b}(\mu_1 + \mu_2, \nu_1 + \nu_2) \le W_p^{a,b}(\mu_1, \nu_1) + W_p^{a,b}(\mu_2, \nu_2)$.
- $a\big||\mu| - |\nu|\big| \le W_p^{a,b}(\mu, \nu) \le a(|\mu| + |\nu|)$.

*Proof.* The first two properties follow from similar properties for $|\cdot|$ and $W_p$.

Concerning the third property, we first prove the first inequality. Choose $\tilde{\mu} \leq \mu$, $\tilde{\nu} \leq \nu$ realizing $W_p^{a,b}(\mu, \nu)$, then $|\mu - \tilde{\mu}| = |\mu| - |\tilde{\mu}|$, $|\nu - \tilde{\nu}| = |\nu| - |\tilde{\nu}|$ and $|\tilde{\mu}| = |\tilde{\nu}|$. Therefore $|\mu| - |\tilde{\mu}| = |\mu| - |\tilde{\nu}| \geq |\mu| - |\nu|$. Assuming, without loss of generality, that $|\mu| \geq |\nu|$, we get

$$W_p^{a,b}(\mu, \nu) \geq a\,|\mu - \tilde{\mu}| + a\,|\nu - \tilde{\nu}| \geq a(|\mu| - |\tilde{\mu}|) \geq a(|\mu| - |\nu|) = a\big|\,|\mu| - |\nu|\,\big|.$$

Now, if we choose $\tilde{\mu} = \tilde{\nu} = 0$ in the right-hand side of (7.20), we get $a(|\mu| + |\nu|)$. Since $W_p^{a,b}$ is the infimum on all $\tilde{\mu}$, $\tilde{\nu}$, also the second inequality is proved.

**Topology of the generalized Wasserstein distance.** We now show that $W_p^{a,b}$ metrizes the weak convergence topology for tight sequences. We also prove that $\mathbb{R}^d$ is complete with respect to $W_p^{a,b}$.

We first state a simple lemma showing that the optimal choices $\tilde{\mu}$, $\tilde{\nu}$, in the definition of the generalized Wasserstein distance, are close to one another in $\mathbb{R}^d$. Indeed, if we transfer too far masses between $\tilde{\mu}$ and $\tilde{\nu}$, then it is cheaper to remove such masses from both measures.

**Proposition 7.10.** *Let $\mu, \nu \in \mathscr{M}_c$ and $\tilde{\mu}$, $\tilde{\nu}$ realize $W_p^{a,b}(\mu, \nu)$. If $\tilde{\mu}$ has support contained in a compact set $K$, then the support of $\tilde{\nu}$ is contained in the compact set*

$$K^d := \bigcup_{x \in K} B_d(x) \tag{7.21}$$

*with $d = 2a/b$. Here, $B_r(x)$ denotes the closed ball of radius $r$ centered in $x$.*

*Similarly, let $\tilde{\mu}$, $\tilde{\nu}$ realize $W_p^{a,b}(\mu, \nu)$, and let $\pi$ be the transference plan realizing $W_p(\tilde{\mu}, \tilde{\nu})$. If $\mu' \leq \tilde{\mu}$ has support contained in a compact $K$, then the corresponding marginal $\nu'$, with respect to $\pi$, has support contained in $K^d$.*

A sequence $\{\mu_n\}$ of measures is called tight if for each $\epsilon > 0$ there exists a compact set $K_\epsilon \subset \mathbb{R}^d$ such that $\mu_n(\mathbb{R}^d \setminus K_\epsilon) < \epsilon$ for all $n$. The following convergence theorem states that $W_p^{a,b}$ metrizes the weak convergence for tight sequences.

**Theorem 7.3.** *Consider a sequence $\{\mu_n\} \subset \mathscr{M}_c$ and let $\mu \in \mathscr{M}_c$. Then*

$$W_p^{a,b}(\mu_n, \mu) \to 0 \quad \Leftrightarrow \quad \mu_n \rightharpoonup \mu \text{ and } \{\mu_n\} \text{ is tight},$$

*where $\rightharpoonup$ denotes weak convergence.*

We now prove the completeness of $\mathscr{M}_c$:

**Proposition 7.11.** *$\mathscr{M}_c$ is complete with respect to $W_p^{a,b}$.*

*Proof.* Consider a Cauchy sequence $\{\mu_n\}$ with respect to $W_p^{a,b}$. We first show that $\{\mu_n\}$ is tight. Fix $\delta > 0$ and let $N = N(\delta)$ be such that $W_p^{a,b}(\mu_n, \mu_{n+k}) < \delta$ for all $n \geq N$, $k \geq 0$. Denote by $\tilde{\mu}_k$, $\tilde{\nu}_k$ the measures realizing $W_p^{a,b}(\mu_N, \mu_{N+k})$ and

$\pi_k$ the transference plan realizing $W_p(\tilde{\mu}_k, \tilde{\nu}_k)$. Let $K_N$ be a compact set containing the support of $\mu_N$, then $\mathrm{supp}(\tilde{\mu}_k) \subset K_N$ for every $k \geq 0$ and, by Proposition 7.10, $\mathrm{supp}(\tilde{\nu}_k) \subset K_N^d$ for every $k \geq 0$. Since $a\,|\mu_{N+k} - \tilde{\nu}_k| \leq W_p^{a,b}(\mu_N, \mu_{N+k}) < \delta$, we get $\mu_{N+k}(\mathbb{R}^d \setminus K_N^d) \leq \tilde{\nu}_k(\mathbb{R}^d \setminus K_N^d) + |\mu_{N+k} - \tilde{\nu}_k| \leq \delta/a$. Now, given $\epsilon > 0$, let $\delta = a\epsilon$ then the compact set $K^\epsilon = K^d_{N(\delta)} = K^d_{N(a\epsilon)}$ satisfies the requirement for tightness of the sequence $\{\mu_{N(a\epsilon)+k}\}$, $k \geq 0$. Then also the sequence $\{\mu_n\}$ is tight. (Indeed for the finite sequence $\{\mu_1, \ldots, \mu_{N(a\epsilon)+k}\}$ tightness is obviously true.)

Now observe that $|\mu_n|$ is uniformly bounded, thus there exists a subsequence $\{\mu_{n_k}\} \rightharpoonup \mu^*$ for a certain $\mu^*$. Using Theorem 7.3, we have that $W_p^{a,b}(\mu_{n_k}, \mu^*) \to 0$, thus $W_p^{a,b}(\mu_n, \mu^*) \to 0$.

**Estimates under flow actions.** To study (7.19) in the setting of the generalized Wasserstein distance, we first estimate the evolution of $W_p^{a,b}$ under a flow action. Recall the estimates provided by Propositions 7.1 and 7.2 for the Wasserstein distance. Similar properties hold true for the generalized Wasserstein distance.

**Proposition 7.12.** *Given $v$, $w$ bounded and Lipschitz vector fields with Lipschitz constant $L$, the following holds:*

*(i)* $W_p^{a,b}(\Phi_t^v \# \mu, \Phi_t^v \# \nu) \leq e^{Lt} W_p^{a,b}(\mu, \nu)$.
*(ii)* $W_p^{a,b}(\mu, \Phi_t^v \# \mu) \leq t\,\|v\|_{C^0} \mu(\mathbb{R}^d)^{1/p}$.
*(iii)* $W_p^{a,b}(\Phi_t^v \# \mu, \Phi_t^w \# \nu) \leq e^{Lt} W_p^{a,b}(\mu, \nu) + \mu(\mathbb{R}^d)^{1/p} \frac{e^{Lt}-1}{L} \|v - w\|_{C^0}$.

## 7.7 Existence and Uniqueness of Solutions for the Transport Equation with Source

We now discuss the existence and uniqueness of the solution of (7.19), under Assumption 7.3. The key tool is the construction of a candidate solution by sample-and-hold. More precisely, the sample-and-hold method allows us to construct a sequence of functions in $C([0, T], \mathscr{M}_0^{ac})$ such that the limit exists and it is a solution of (7.19).

With no loss of generality, assume that $T = 1$ and define a sequence of approximate solutions $\mu^k$, $k \in \mathbb{N}$, as follows. Set $\Delta t := \frac{1}{2^k}$ and consider the decomposition of the time interval in $[0, \Delta t], [\Delta t, 2\Delta t], [2\Delta t, 3\Delta t], \ldots, [(2^k - 1)\Delta t, 2^k \Delta t]$. The construction is based on a Lagrangian scheme similar to that of Sect. 7.2. More precisely, define:

- $\mu_0^k := \mu_0$.
- $\mu^k_{(n+1)\Delta t} := \Phi_{\Delta t}^{v[\mu^k_{n\Delta t}]} \# \mu^k_{n\Delta t} + \Delta t h[\mu^k_{n\Delta t}]$.
- $\mu_t^k := \Phi_\tau^{v[\mu^k]_{n\Delta t}} \# \mu^k_{n\Delta t} + \tau h[\mu^k_{n\Delta t}]$ with $n$ the maximum integer such that $t - n\Delta t \geq 0$ and $\tau := t - n\Delta t$.

One can prove that, given $v$, $h$ satisfying Assumption 7.3, the sequence $\{\mu^k\}$ is a Cauchy sequence for the space $(C([0,\,1],\mathscr{M}_c),\,\mathscr{D})$, where

$$\mathscr{D}(\mu,\,\nu) := \sup_{t\in[0,\,1]} W_p^{a,b}(\mu_t,\,\nu_t).$$

Since $(\mathscr{M}_c,\,W_p^{a,b})$ is a complete space, then so is $(C([0,\,1],\mathscr{M}_c),\,\mathscr{D})$, thus the sequence $\mu^k$ admits a limit $\bar{\mu}_t := \lim_k \mu_t^k$. Since $\mu_0^k = \mu_0$ for all $k$, then $\bar{\mu}_0 = \mu_0$. For each $f \in C_c^\infty([0,\,1]\times\mathbb{R}^d)$, one can prove that

$$\int_0^1 \int_{\mathbb{R}^d} (\partial_t f + v[\bar{\mu}_t]\cdot\nabla f\, d\bar{\mu}_t + f\, dh[\bar{\mu}_t])\, dt = 0,$$

whence:

**Proposition 7.13.** *The measure $\bar{\mu}_t := \lim_k \mu_t^k$ is a weak solution to (7.19).*

We now prove the continuous dependence on the initial data of solutions to (7.19), thus also implying uniqueness of the solution.

**Theorem 7.4.** *Consider $v$, $h$ satisfying Assumption 7.3 and let $\mu_t$, $\nu_t$ be two solutions of (7.19) with initial data $\mu_0$, $\nu_0$, respectively. Then*

$$W_p^{a,b}(\mu_t,\,\nu_t) \le e^{t(L+Q)+N\int_0^t(\mu_0(\mathbb{R}^d)+\tau P)^{1/p}\,d\tau}\, W_p^{a,b}(\mu_0,\,\nu_0). \tag{7.22}$$

*In particular, under Assumption 7.3, the solution of (7.19) is unique.*

*Proof.* Define $w(t) := W_p^{a,b}(\mu_t,\,\nu_t)$. We first prove that $w$ is locally Lipschitz in time. For this, write:

$$\begin{aligned} w(t+s)-w(t) &= W_p^{a,b}(\mu_{t+s},\,\nu_{t+s}) - W_p^{a,b}(\mu_t,\,\nu_t)\\ &\le W_p^{a,b}(\mu_{t+s},\,\mu_t) + W_p^{a,b}(\mu_t,\,\nu_t) + W_p^{a,b}(\nu_t,\,\nu_{t+s}) - W_p^{a,b}(\mu_t,\,\nu_t)\\ &= W_p^{a,b}(\mu_{t+s},\,\mu_t) + W_p^{a,b}(\nu_t,\,\nu_{t+s}). \end{aligned}$$

It holds $\mu_{t+s} = \Phi_s^{v[\mu_t]}\#\mu_t + s\,h[\mu_t] + o(s)$. Then, by Proposition 7.12 and Assumption 7.3, we have:

$$\begin{aligned} W_p^{a,b}(\mu_{t+s},\,\mu_t) &\le W_p^{a,b}(\Phi_s^{v[\mu_t]}\#\mu_t,\,\nu_t) + s\,|h[\mu_t]| + o(s)\\ &\le s\,\|v\|_{C^0}\,\mu_t(\mathbb{R}^d)^{1/p} + s\,P + o(s)\\ &\le s\,\big(M\,[\mu_0(\mathbb{R}^d) + tP] + P\big) + o(s) \end{aligned}$$

where we used $\mu_t(\mathbb{R}^d) \le \mu_0(\mathbb{R}^d) + tP$. A similar estimate holds for $W_p^{a,b}(\nu_t,\,\nu_{t+s})$, thus we conclude by uniform (local in time) estimates of $o(s)$.

Now, again using Proposition 7.12 and Assumption 7.3, we can write:

$$\begin{aligned} w(t+s) &\le W_p^{a,b}(\Phi_s^{v[\mu_t]}\#\mu_t,\, \Phi_s^{v[\nu_t]}\#\nu_t) + s\,Q\,W_p^{a,b}(\mu_t,\,\nu_t) + o(s) \\ &\le (1+Ls+o(s))\,W_p^{a,b}(\mu_t,\,\nu_t) + \mu_t(\mathbb{R}^d)^{1/p}(s+o(s))\,N\,W_p^{a,b}(\mu_t,\,\nu_t) \\ &\quad + s\,Q\,W_p^{a,b}(\mu_t,\,\nu_t) + o(s) \\ &\le w(t)\left[1+s\big(L+N\,(\mu_0(\mathbb{R}^d)+tP)^{1/p}+Q\big)+o(s)\right], \end{aligned}$$

thus we get:

$$D^+w(t) = \limsup_{s\to 0+}\frac{w(t+s)-w(t)}{s} \le w(t)\,\big(L+N(\mu_0(\mathbb{R}^d)+tP)^{1/p}+Q\big).$$

By Gronwall inequality we get (7.22). The uniqueness of the solution of (7.19) is a direct consequence.

## 7.8 Bibliographical Notes

Section 7.1 The presented results, as well as the comparison between the $L^1$ and Wasserstein distance, are taken from Piccoli and Rossi [141]. For alternative distances to $W_p$ that the space $\mathscr{P}_c(\mathbb{R}^d)$ can be endowed with, a good reference is the book by Rachev [150].

Section 7.2 The general discussion on optimal transportation and the Wasserstein metric is inspired by the books by Villani [166, 167], which provide a complete account of recent results. The proofs of Propositions 7.1 and 7.2 are taken from Piccoli and Rossi [140], while the Lagrangian scheme is taken from Piccoli and Rossi [141]. The Eulerian scheme was first proposed by Piccoli and Tosin [144]. General results on the existence of solutions to 7.1 can be found in the paper by Ambrosio and Gangbo [5].

Section 7.2.2 All results are from Piccoli and Rossi [142].

Sections 7.3 and 7.4 All results are from Piccoli and Rossi [141].

Sections 7.5 and 7.6 All results are from Piccoli and Rossi [142].

# Chapter 8
# Generalizations of the Multiscale Approach

**Abstract** In this chapter we present some natural generalizations of the multiscale approach described in Chap. 5. In most of the cases, the following ideas are not yet fully developed. Nevertheless, they give some interesting directions for future research, from theoretical, numerical, and applied point of view.

## 8.1 Second Order Time-Evolving Measures

The measure-based crowd model introduced in Chap. 5, and deeply analyzed in Chap. 6, is a *first order* one. In fact, the microscopic state of the test pedestrian is fully characterized by her spatial position only, cf. Sect. 6.1. This causes the equation for the collective distribution, cf. (6.6), (6.9), to be a conservation law with the velocity expressed directly in terms of the pedestrian distribution itself, cf. (6.5), (6.10). However, as reviewed in Chap. 4, some important pedestrian models are based on the idea that walkers are (possibly nonstandard) Newtonian particles reacting also to inertial effects. It is therefore of some interest, also in a multiscale perspective, to extend the method of time-evolving measures to cases in which the microscopic state of the test pedestrian is described not only by the space position but also by the velocity.

### *8.1.1 Phenomenological Microscopic Model*

To accomplish the aforesaid program we follow a procedure inspired by the one presented in the first three sections of Chap. 6. Let $X(t)$, $V(t)$ be, respectively, the position and the velocity of the test pedestrian at time $t$ (see Sect. 6.1 for a precise characterization of the test pedestrian). Obviously, the following relation must hold true:

$$\dot{X} = V.$$

E. Cristiani et al., *Multiscale Modeling of Pedestrian Dynamics*, MS&A 12,
DOI 10.1007/978-3-319-06620-2_8,

The actual key point is that modeling is now done at the level of velocity variations, i.e., accelerations, therefore the phenomenological microscopic model should explain how $V$ changes in time. Mimicking the ideas proposed in Sects. 5.2 and 6.1, we assume that inertial effects are produced on the test pedestrian because of two mechanisms:

- A personal desire to maintain a certain walking program, which we model in terms of a *desired acceleration* depending on the current state of the test pedestrian: $a_{\mathrm{d}}(X, V)$. For instance, the desired acceleration may express a relaxation in time toward a desired velocity:

$$a_{\mathrm{d}}(X, V) = \frac{v_{\mathrm{d}}(X) - V}{\tau},$$

  $\tau > 0$ being the relaxation time.
- Interactions with the surrounding *collectivity*, which we model in terms of an *interaction acceleration* depending on the *perceived* distribution of the microstates of nearby pedestrians. Specifically, we express such a distribution via a measure $\nu_t$ on $\mathbb{R}^d \times \mathbb{R}^d$, such that $d\nu_t(x, v)$ is the (infinitesimal) probability of finding a walker in the space volume $dx$ centered at $x \in \mathbb{R}^d$ with a velocity comprised in the volume $dv$ centered at $v \in \mathbb{R}^d$. Since $\nu_t$ accounts for the joint distribution of the microscopic position and velocity of walkers, it provides a *mesoscopic* (or *kinetic*) representation of the crowd. The structure of $\nu_t$ over $(x, v) \in \mathbb{R}^d \times \mathbb{R}^d$ translates the perception of the test pedestrian. If $N$ pedestrians form the crowd, we write the interaction acceleration as:

$$a_{\mathrm{i}} = N \iint_{\mathscr{S}(X)\times\mathbb{R}^d} K(X, V, y, w)\, d\nu_t(y, w),$$

  where $\mathscr{S}(X)$ is the sensory region (interaction neighborhood) of the test pedestrian, cf. (5.10), and $K : (\mathbb{R}^d \times \mathbb{R}^d) \times (\mathbb{R}^d \times \mathbb{R}^d) \to \mathbb{R}^d$ is the *interaction kernel* accounting for single interaction instances, pretty much like in the spirit of the first order model of Chap. 6.

Setting $\dot{V} = a_{\mathrm{d}}(X, V) + a_{\mathrm{i}}$ we are finally left with the following phenomenological microscopic model:

$$\begin{cases} \dot{X} = V \\ \dot{V} = a_{\mathrm{d}}(X, V) + N \iint_{\mathscr{S}(X)\times\mathbb{R}^d} K(X, V, y, w)\, d\nu_t(y, w). \end{cases} \tag{8.1}$$

A pointwise, i.e., individual-by-individual, perception may be modeled by

$$\nu_t = \frac{1}{N} \sum_{k=1}^{N} \delta_{(x^k(t), v^k(t))},$$

where $\{(x^k(t),\, v^k(t))\}_{k=1}^N$ are the mechanical microstates of the $N$ walkers at time $t$ and the normalization coefficient $\frac{1}{N}$ is due to that $\nu_t$ has to be a probability measure. The phenomenological model specializes then as

$$\begin{cases} \dot{X} = V \\ \dot{V} = a_{\mathrm{d}}(X,\, V) + \displaystyle\sum_{\substack{k=1 \\ x^k \in \mathscr{S}(X)}}^{N} K(X,\, V,\, x^k,\, v^k). \end{cases}$$

Conversely, a perception addressed to the crowd ahead as a whole may be modeled by

$$d\nu_t(x,\, v) = f(t,\, x,\, v)\, dx\, dv,$$

where $f : [0, +\infty) \times \mathbb{R}^d \times \mathbb{R}^d \to [0, +\infty)$ is the probability density of the microstates at time $t$. Then the phenomenological model takes the form:

$$\begin{cases} \dot{X} = V \\ \dot{V} = a_{\mathrm{d}}(X,\, V) + N \displaystyle\int_{\mathbb{R}^d} \int_{\mathscr{S}(X)} K(X,\, V,\, y,\, w)\, f(t,\, y,\, w)\, dy\, dw. \end{cases}$$

### 8.1.2 Mathematical-Physical Model

The distribution of microstates is a *material quantity* for pedestrians, since it is generated by the latter themselves. Therefore it has to evolve in time across the state space $\mathbb{R}^d \times \mathbb{R}^d$ according to the crowd dynamics. Owing to this argument, we join to (8.1) the following equation:

$$\nu_t = (X,\, V)(t)\#\nu_0, \tag{8.2}$$

where $\nu_0$ is the initial distribution of microstates, which means

$$\nu_t(E) = \nu_0((X,\, V)(t)^{-1}(E)), \quad \forall\, E \subseteq \mathbb{R}^d \times \mathbb{R}^d \text{ measurable.}$$

In particular, the set appearing at the right-hand side is explicitly:

$$(X,\, V)(t)^{-1}(E) = \{(X(0),\, V(0)) \in \mathbb{R}^d \times \mathbb{R}^d \,:\, (X(t),\, V(t)) \in E\},$$

i.e., it is the set of all possible initial states which lead the test pedestrian in the subset of microstates $E$ at time $t > 0$.

The coupling of (8.1) and (8.2) enables us to obtain an evolution equation of the measure $\nu_t$. The procedure is similar to that used in Sect. 6.2: We pick a test

function $\phi \in C_c^\infty(\mathbb{R}^d \times \mathbb{R}^d)$, $\phi = \phi(x, v)$, and, thanks to (8.2), we compute the time derivative of $\nu_t$ pretty much in the spirit of Reynolds transport theorem:

$$\begin{aligned}\frac{d}{dt}\langle \nu_t, \phi\rangle &= \frac{d}{dt}\iint_{\mathbb{R}^d\times\mathbb{R}^d} \phi \, d\nu_t = \frac{d}{dt}\iint_{\mathbb{R}^d\times\mathbb{R}^d} \phi(X, V)\, d\nu_0 \\ &= \iint_{\mathbb{R}^d\times\mathbb{R}^d} \left\{\nabla_x\phi(X, V)\cdot\dot{X} + \nabla_v\phi(X, V)\cdot\dot{V}\right\} d\nu_0,\end{aligned}$$

where $\nabla_x$, $\nabla_v$ denote the gradient with respect to the variables $x$ and $v$, respectively. Then, invoking (8.1), we continue the calculation as:

$$\begin{aligned}&= \iint_{\mathbb{R}^d\times\mathbb{R}^d} \Bigg\{ \nabla_x\phi(X, V)\cdot V \\ &\quad + \nabla_v\phi(X, V)\cdot\left[a_{\mathrm{d}}(X, V) + N\iint_{\mathscr{S}(X)\times\mathbb{R}^d} K(X, V, y, w)\, d\nu_t(y, w)\right]\Bigg\} d\nu_0\end{aligned}$$

and finally we go back to $\nu_t$ using again (8.2):

$$= \iint_{\mathbb{R}^d\times\mathbb{R}^d} \left\{\nabla_x\phi\cdot v + \nabla_v\phi\cdot\left[a_{\mathrm{d}} + N\iint_{\mathscr{S}(\cdot)\times\mathbb{R}^d} K(\cdot, \cdot, y, w)\, d\nu_t(y, w)\right]\right\} d\nu_t. \tag{8.3}$$

After defining the Eulerian acceleration field

$$a[\nu_t](x, v) := a_{\mathrm{d}}(x, v) + N\iint_{\mathscr{S}(x)\times\mathbb{R}^d} K(x, v, y, w)\, d\nu_t(y, w), \tag{8.4}$$

we read (8.3) in distributional sense as

$$\frac{d}{dt}\langle \nu_t, \phi\rangle = \langle \nu_t, \nabla_x\phi\cdot v\rangle + \langle \nu_t, \nabla_v\phi\cdot a[\nu_t]\rangle, \tag{8.5}$$

whence, "integrating by parts" in $(x, v)$ at the right-hand side, we further say that $\nu_t$ satisfies formally the conservation law

$$\frac{\partial \nu_t}{\partial t} + v\cdot\nabla_x\nu_t + \nabla_v\cdot(a[\nu_t]\nu_t) = 0 \tag{8.6}$$

provided (8.3) holds for all test functions $\phi \in C_c^\infty(\mathbb{R}^d \times \mathbb{R}^d)$.

### 8.1.3 Mass and Momentum Equations

Equation (8.6) is in principle a sufficient model for studying the mesoscopic evolution of the crowd collectivity, also from a multiscale perception viewpoint. It is nonetheless useful to link $\nu_t$ to more tangible physical concepts, in the same spirit as in Sect. 6.3 we bridged the physical version of the model, based on the crowd mass, and its probabilistic interpretation. As we will see, in the present case we do not only need the concept of mass but also that of linear momentum in order to fully account, at a higher scale, for the dynamics described by (8.1), (8.6). For this reason, we say that the present model is a *second order* one.

To begin with, we consider $N$ specific instances of the test pedestrian which embody the walkers of the crowd. To this purpose, we introduce $N$ pairs of variables $(X^1, V^1), (X^2, V^2), \ldots, (X^N, V^N)$ modeling the microstates of the various individuals composing the crowd. Then we technically have:

$$(X^k(t), V^k(t)) = (X, V)(t) \circ (\bar{x}^k, \bar{v}^k), \qquad k = 1, \ldots, N,$$

where $\bar{x}^k, \bar{v}^k$ are the initial position and velocity, respectively, of the $k$-th walker. From (8.2), by understanding the $(\bar{x}^k, \bar{v}^k)$'s as independent and identically distributed and $\nu_0$ as their (common) law, it readily follows that $\nu_t$ is the law of $(X^k(t), V^k(t))$ for all $t > 0$, which is coherent with the interpretation we gave it when constructing the interaction acceleration $a_{\mathrm{i}}$ in the phenomenological model. Hence, again, the idea is that the uncertainty in the initial states of pedestrians is transported at future times and (8.6) tells us how.

From $\nu_t$ we obtain the law of the sole $X^k(t)$ as the first marginal, say $\tilde{\nu}_t$. Specifically, $\tilde{\nu}_t$ is the probability measure on $\mathbb{R}^d$ such that (see Appendix A, Sect. A.5):

$$\tilde{\nu}_t(E) = \nu_t(E \times \mathbb{R}^d), \qquad \forall\, E \subseteq \mathbb{R}^d \text{ measurable.}$$

Inspired by the conclusion of Sect. 6.3, we then define the *mass* of the crowd as the measure

$$\mu_t := N\tilde{\nu}_t, \tag{8.7}$$

which is such that $\mu_t(E) = \mathbb{E}[Y_E(t)]$ for all measurable $E \subseteq \mathbb{R}^d$, where $Y_E(t)$ is the same as in (6.11).

From $\nu_t$ we also extract a second useful information related to the variable $V^k(t)$. By disintegrating $\nu_t$ with respect to its first marginal $\tilde{\nu}_t$ (see again Appendix A, Sect. A.5) we obtain a new probability measure on the space of the velocity, parameterized by $x$, say $\hat{\nu}_t(\cdot|x)$, such that

$$\nu_t(dx\,dv) = \hat{\nu}_t(dv|x) \otimes \tilde{\nu}_t(dx). \tag{8.8}$$

In practice, $\hat{\nu}_t(\cdot|x)$ and $\tilde{\nu}_t$ allow $\nu_t$-integrals on $\mathbb{R}^d \times \mathbb{R}^d$ to be reduced to iterated integrals on $\mathbb{R}^d$. Recalling the conditioned probability theorem, it is useful to understand $\hat{\nu}_t(\cdot|x)$ as the probability distribution of $V^k(t)$ conditioned to the point $x$. As such, it can be used to compute the *average velocity* of the crowd, say $u(t, x)$, in the point $x$ at time $t$:

$$u(t, x) := \int_{\mathbb{R}^d} v \, d\hat{\nu}_t(v|x). \tag{8.9}$$

Equipped with all of this preliminary material, we can formally deduce from (8.6) two coupled partial differential equations for the evolution in time and space of the velocity-averaged quantities $\mu_t, u$.

#### 8.1.3.1 Mass Equation

In (8.5) we choose a test function $\phi = \phi_m(x, v) = \varphi(x)\psi_m(v)$, where $\varphi \in C_c^\infty(\mathbb{R}^d)$ is fixed while $\{\psi_m\}_{m\geq 1} \subset C_c^\infty(\mathbb{R}^d)$ is a sequence such that $0 \leq \psi_m \leq 1$ with uniformly bounded gradient in $\mathbb{R}^d$ for all $m$ and moreover such that $\psi_m \to 1$, $\nabla_v \psi_m \to 0$ pointwise in $\mathbb{R}^d$ as $m \to \infty$ (the existence of such a sequence is guaranteed by Urysohn's Lemma). Then using (8.8) we obtain:

$$\begin{aligned}\frac{d}{dt}\int_{\mathbb{R}^d} \varphi(x) \int_{\mathbb{R}^d} \psi_m(v) \, d\hat{\nu}_t(v|x) \, d\tilde{\nu}_t(x) = \int_{\mathbb{R}^d} \nabla_x \varphi(x) \int_{\mathbb{R}^d} v\psi_m(v) \, d\hat{\nu}_t(v|x) \, d\tilde{\nu}_t(x) \\ + \int_{\mathbb{R}^d} \varphi(x) \int_{\mathbb{R}^d} a[\nu_t](x, v) \cdot \nabla_v \psi_m(v) \, d\hat{\nu}_t(v|x) \, d\tilde{\nu}_t(x).\end{aligned}$$

By integrating further in time, then passing to the limit $m \to \infty$ by dominated convergence, and finally going back to the time derivative in the obtained result we get:

$$\frac{d}{dt}\int_{\mathbb{R}^d} \varphi(x)\hat{\nu}_t(\mathbb{R}^d|x) \, d\tilde{\nu}_t(x) = \int_{\mathbb{R}^d} \nabla_x \varphi(x) \cdot \left( \int_{\mathbb{R}^d} v \, d\hat{\nu}_t(v|x) \right) d\tilde{\nu}_t(x).$$

But $\hat{\nu}_t(\mathbb{R}^d|x) = 1$ for all $x$ because every $\hat{\nu}_t(\cdot|x)$ is a probability measure, while at the right-hand side we recognize the definition (8.9) of $u$. Hence:

$$\frac{d}{dt}\int_{\mathbb{R}^d} \varphi \, d\tilde{\nu}_t = \int_{\mathbb{R}^d} \nabla_x \varphi \cdot u \, d\tilde{\nu}_t,$$

which, up to multiplying by $N$ both sides and recalling (8.7), is a weak form of the *mass conservation equation*

$$\frac{\partial \mu_t}{\partial t} + \nabla \cdot (\mu_t u) = 0, \tag{8.10}$$

cf. (6.6). The difference with respect to (6.6) is that now the transport velocity does not appear directly in terms of $\mu_t$ itself. A second equation linking $\mu_t$ and $u$ is therefore needed, which, as previously anticipated, makes the resulting model a second order one.

### 8.1.3.2 Momentum Equation

The *linear momentum* of the crowd mass $\mu_t$ is the vector-valued measure $u\mu_t$, sometimes denoted $p$ or $q$ depending on the context, which is absolutely continuous with respect to $\mu_t$ with vector-valued density $u(t, \cdot)$. Its action against a test function $\varphi \in C_c^\infty(\mathbb{R}^d)$ is defined to be

$$\langle u\mu_t, \varphi \rangle = \int_{\mathbb{R}^d} \varphi(x) u(t, x)\, d\mu_t(x).$$

The second equation to be joined to (8.10) is one for the linear momentum, which indeed appears in (8.10) under the divergence operator. In order to obtain it, we start by multiplying formally (8.6) by $v$:

$$\frac{\partial}{\partial t}(v v_t) + v(v \cdot \nabla_x v_t) + v \nabla_v \cdot (a[v_t] v_t) = 0,$$

which in the proper distributional sense has to be understood as:

$$\frac{d}{dt}\langle v_t, v\phi \rangle = \langle v_t, (v \otimes v)\nabla_x \phi \rangle + \langle v_t, a[v_t] \nabla_v \cdot (v\phi) \rangle \tag{8.11}$$

for all test functions $\phi \in C_c^\infty(\mathbb{R}^d \times \mathbb{R}^d)$.

*Remark 8.1.* The first term at the right-hand side is worth a brief comment. Originally it appears at the left-hand side as $\langle v \cdot \nabla_x v_t, v\phi \rangle = \langle \nabla_x \cdot (v v_t), v\phi \rangle$, namely the distributional form of $v(v \cdot \nabla_x v_t)$. By the derivation rules of distributions it can be rewritten as $-\langle v v_t, v \cdot \nabla_x \phi \rangle = -\langle v_t, v(v \cdot \nabla_x \phi) \rangle$, thus the point is to see that $(v \otimes v)\nabla_x \phi = v(v \cdot \nabla_x \phi)$. This is actually immediate, after considering that $v \otimes v$ denotes the following matrix in $\mathbb{R}^{d \times d}$:

$$v \otimes v = \begin{pmatrix} v_1^2 & v_1 v_2 & \dots & v_1 v_d \\ v_2 v_1 & v_2^2 & \dots & v_2 v_d \\ \dots & \dots & \dots & \dots \\ v_d v_1 & v_d v_2 & \dots & v_d^2 \end{pmatrix},$$

where $v_1, v_2, \dots, v_d$ are the $d$ scalar components of $v$.

We now choose $\phi$ in (8.11) as $\phi(x, v) = \varphi(x)\psi_m(v)$, where $\varphi$, $\psi_m$ are as before, and, utilizing again (8.8), we compute:

$$\begin{aligned}\frac{d}{dt}\int_{\mathbb{R}^d}\varphi(x)\left(\int_{\mathbb{R}^d} v\psi_m(v)\,d\hat{\nu}_t(v|x)\right)d\tilde{\nu}_t(x)\\ =\int_{\mathbb{R}^d}\nabla_x\varphi(x)\left(\int_{\mathbb{R}^d}(v\otimes v)\psi_m(v)\,d\hat{\nu}_t(v|x)\right)d\tilde{\nu}_t(x)\\ +\int_{\mathbb{R}^d}\varphi(x)\left(d\int_{\mathbb{R}^d} a[\nu_t](x, v)\psi_m(v)\,d\hat{\nu}_t(v|x)\right)d\tilde{\nu}_t(x)\\ +\int_{\mathbb{R}^d}\varphi(x)\left(\int_{\mathbb{R}^d} a[\nu_t](x, v)(v\cdot\nabla_v\psi_m(v))\,d\hat{\nu}_t(v|x)\right)d\tilde{\nu}_t(x).\end{aligned}$$

Passing to the limit $m\to\infty$ as before by dominated convergence, we further discover:

$$\frac{d}{dt}\int_{\mathbb{R}^d}\varphi(x)u(t, x)\,d\tilde{\nu}_t(x)=\int_{\mathbb{R}^d}\nabla_x\varphi(x)\left(\int_{\mathbb{R}^d} v\otimes v\,d\hat{\nu}_t(v|x)\right)d\tilde{\nu}_t(x) \tag{8.12}$$

$$+\,d\int_{\mathbb{R}^d}\varphi(x)\left(\int_{\mathbb{R}^d} a[\nu_t](x, v)\,d\hat{\nu}_t(v|x)\right)d\tilde{\nu}_t(x). \tag{8.13}$$

Next we notice that

$$\int_{\mathbb{R}^d} v\otimes v\,d\hat{\nu}_t(v|x)=\int_{\mathbb{R}^d}(v-u(t, x))\otimes(v-u(t, x))\,d\hat{\nu}_t(v|x)+u(t, x)\otimes u(t, x).$$

Particularly, the tensor

$$\mathbb{T}(t, x):=\int_{\mathbb{R}^d}(v-u(t, x))\otimes(v-u(t, x))\,d\hat{\nu}_t(v|x) \tag{8.14}$$

accounts for the average quadratic variation of $V_t^k$ in the point $x$ (recall indeed that $u(t, x)$ is the expectation of $V_t^k$ in $x$). In classical Continuum Mechanics it is called the *stress tensor* as it expresses the internal stress of a continuum medium (such as, for instance, pressure and viscous effects in a fluid) generated by the thermal state of its composing particles. In our context, however, it is preferable to stay with the original statistical interpretation, since crowds can hardly be assimilated to a continuum in the classical mechanical sense. By further defining the *average acceleration* in the point $x$ at time $t$:

$$b(t, x):=d\int_{\mathbb{R}^d} a[\nu_t](x, v)\,d\hat{\nu}_t(v|x) \tag{8.15}$$

we finally rewrite (8.13) in the form:

$$\frac{d}{dt}\int_{\mathbb{R}^d}\varphi u\,d\tilde{\nu}_t=\int_{\mathbb{R}^d}\nabla_x\varphi(\mathbb{T}+u\otimes u)\,d\tilde{\nu}_t+\int_{\mathbb{R}^d}\varphi b\,d\tilde{\nu}_t,$$

whence, after multiplying both sides by $N$, we recognize a weak form of

$$\frac{\partial}{\partial t}(\mu_t u)+\nabla\cdot[\mu_t(u\otimes u+\mathbb{T})]=\mu_t b, \tag{8.16}$$

expressing the balance of linear momentum of the crowd.

The terms $\mathbb{T}$, $b$ are defined in terms of $u$ itself and of the phenomenological model of pedestrian acceleration set forth at the beginning. Nevertheless they cannot completely get rid of the knowledge of the crowd mesoscale, because they depend on $\nu_t$ both directly (cf. $a[\nu_t]$ in $b$) and through $\hat{\nu}_t(\cdot|x)$. In other words, the *averaged model* (8.10), (8.16):

$$\begin{cases}\dfrac{\partial\mu_t}{\partial t}+\nabla\cdot(\mu_t u)=0\\[2ex]\dfrac{\partial}{\partial t}(\mu_t u)+\nabla\cdot[\mu_t(u\otimes u+\mathbb{T})]=\mu_t b\end{cases} \tag{8.17}$$

is not fully self-consistent as it requires some information from a lower scale. This does not happen in the case of first order models discussed in Sects. 6.1–6.3 because there the relationship between the mesoscale (represented by $\nu_t$) and the macroscale (viz. the averaged scale represented by $\mu_t$) is simply a direct proportionality.

### 8.1.4 Monokinetic Solutions

Since (8.17) is numerically much more affordable than (8.6) (in fact the state space is reduced to $\mathbb{R}^d$ rather than $\mathbb{R}^d\times\mathbb{R}^d$), people generally tend to use it as a prototype for second order models. The modeling approach consists then in devising appropriate phenomenological closures of $\mathbb{T}$ and $b$ involving only $\mu_t$, $u$ so as to obtain a closed set of equations. This way the final model departs from the original phenomenological one (8.1), often in a hardly controllable way, and has therefore to be accepted *per se*.

A very special case of (8.17), which both uses the true expressions (8.14), (8.15) of $\mathbb{T}$, $b$ and gives rise to a closed averaged model, is that of the so-called *monokinetic solutions*. The basic assumption is that at every time $t$ the test pedestrian perceives deterministically in every point $x$ just the average velocity $u(t,\,x)$, according to an extremely synthetic process of evaluation and elaboration of the information to be retained for interactions. This idea can formalized by postulating:

$$\hat{\nu}_t(\cdot|x)=\delta_{u(t,\,x)},$$

which implies $\nu_t(dx\,dv) = \delta_{u(t,x)}(dv) \otimes \tilde{\nu}_t(dx)$, thus owing to (8.14) and to (8.4), (8.15):

$$\begin{cases} \mathbb{T} = 0 \\ b(t, x) = a_{\mathrm{d}}(x, u(t, x)) + \displaystyle\int_{\mathscr{S}(x)} K(x, u(t, x), y, u(t, x))\, d\mu_t(y). \end{cases}$$

Notice that $\mathbb{T} = 0$ is coherent with the assumed absence of fluctuations in the mesoscopic distribution of the velocity. Recalling the classical meaning of $\mathbb{T}$ as stress tensor, the monokinetic solutions are sometimes also called *pressureless solutions* by analogy with the terminology used in fluid dynamics.

## 8.2 Multidimensional Multiscale Coupling

In this section we show how the multiscale model presented in Chap. 5 can handle multiple-dimensional dynamics in the same framework. We consider the case in which the domain of computation has one or more dimensions much more relevant than the others. For example, a road is a two-dimensional domain such that its length is usually much more relevant than its width. In these cases, a macroscopic description can avoid the full dimensionality, being more interested in the motion along the leading dimensions. On the other hand, a microscopic description often needs a complete view of the domain, in order to catch small but important effects.

The measure-theoretic setting allows us to obtain easily and rigorously such a multiscale multidimensional coupling. It suffices to assume that the density $\rho = \rho(t, x_1, \ldots, x_d)$, do not actually depend on all the space variables. The mathematical model remains formally the same, but for the fact that the advection velocity $v$ in the equation for the density has to be projected onto the leading directions. For example, in two dimensions ($d = 2$), if the first dimension is dominating we assume

$$\frac{\partial \rho}{\partial x_2} = 0 \quad \Rightarrow \quad \rho = \rho(t, x_1)$$

and the multidimensional model reads (cf. (5.24)–(5.25)):

$$\begin{cases} \dot{X}^k(t) = v(t, X^k(t)) \\ \dfrac{\partial \rho}{\partial t} + \nabla \cdot (\rho v \cdot \mathbf{i}) = 0 \end{cases} \tag{8.18}$$

where $\mathbf{i} = (1, 0)$ is the unit vector in the leading direction. Notice that, thanks to the fact that $v$ is projected in one dimension after being computed as genuinely two-dimensional, multiscale interactions are automatically evaluated with the correct dimensionality. The microscopic two-dimensional points $X^k(t)$ perceive a spatially

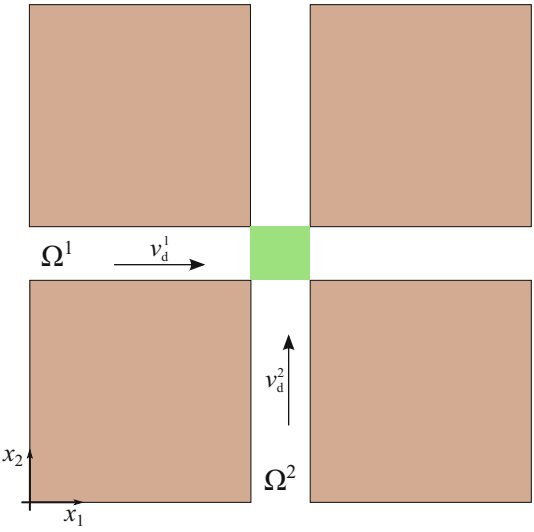


**Fig. 8.1** Two one-way roads with a junction (*green square*)

two-dimensional density, simply constant in the $x_2$-direction. On the other hand, the macroscopic one-dimensional density $\rho$ is affected only by the first component of the interactions with the mass points, which are however two-dimensional.

It is very important to note that this multidimensional approach avoids, at the macroscopic level, the imposition of boundary conditions along the (negligible) $x_2$-direction. Such an additional constraints would be quite artificial from the physical point of view and can massively affect the solution inside the domain, posing also some problems in the numerical approximation.

As a natural application, we consider the vehicular traffic flow on two orthogonal roads. At the macroscopic scale, the interest is mainly in the propagation of density waves along the road length, so that the roads are better described as a one-dimensional domains. On the other hand, near the junction it can be crucial to retain the detail of possible lateral displacements of single cars. Therefore, describing the road as a two-dimensional domain is required at the microscopic scale.

The computational domain $\Omega = \Omega_1 \cup \Omega_2$ is depicted in Fig. 8.1.

$\Omega_1$ is the horizontal road and $\Omega_2$ is the vertical road. Microscopic cars can freely move in the whole domain, while car densities are defined only in the middle line of the roads.

We can use the multipopulation version of the model introduced in Sect. 5.6. Here we have two populations, the first one continuously enters the domain from the left and flows in the horizontal direction, while the second one continuously enters the domain from the bottom and flows in the vertical direction. The density of the first population is $\rho^1 = \rho^1(t, x_1)$ and that of the second population is $\rho^2 = \rho^2(t, x_2)$. Coherently with the observation that cars are indeed anisotropic particles, we model the endogenous interaction neighborhood as the right half-ball in the road $\Omega^1$ and the upper half-ball in the road $\Omega^2$, for translating the fact that drivers normally look

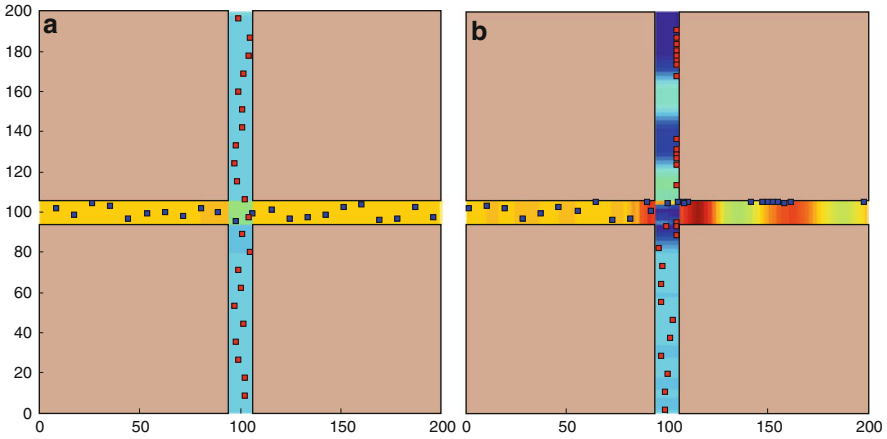


**Fig. 8.2** (**a**) Simulation with $\theta = 0$ (genuinely macroscopic dynamics). No particular effect is visible at the junction. (**b**) Simulation with $\theta = 0.7$ (multiscale dynamics). Traffic light effect beyond the junction is visible in both densities and microscopic cars

ahead only. Conversely, we model the exogenous interaction neighborhood as the intersection of the right and bottom half-balls in the road $\Omega^1$ and the upper and left half-balls in the road $\Omega^2$, for translating the fact that drivers look also in the direction of the incoming opposite flow of cars, especially at the junction.

In order to deal with the multidimensional domain, the numerical method presented in Sect. 5.5 is easily modified. The main difference here is that the equations for the densities are one-dimensional, therefore the two-dimensional quantities computed by the microscopic part of the algorithm have to be projected to scalar quantities before they can be used by the macroscopic part of the algorithm. For pictorial purposes, the one-dimensional densities $\rho^1(t, x_1)$ and $\rho^2(t, x_2)$ of the two populations are represented coloring the whole two-dimensional domain using the extended functions $\bar{\rho}^p(t, x_1, x_2) = \rho^p(t, x_p)$, $p = 1, 2$.

Results of the simulations with $\theta = 0$ (genuinely macroscopic dynamics) and $\theta = 0.7$ (multiscale dynamics) are reported in Fig. 8.2.

Let us stress that the junction under consideration is not regulated by any give-way rule nor by red-green traffic light cycles. If the macroscopic scale leads the dynamics of both point cars and densities, the traffic flow is quite uniformly and do not show any notable behavior at the junction. Instead, if the multiscale dynamics is active, a clear traffic light effect appears beyond the junction: By this we mean an oscillatory pattern which shows up since groups of cars from incoming roads occupy alternately the junction, giving rise to a sequence of density wave packets along the outgoing roads. This is due to the fact that interactions among point cars are much different from those among densities: More granularity expedites the break of symmetry and triggers the typical alternate occupation of the space also at the macroscopic scale.

We conclude stressing that this interesting result strongly depends on the multidimensional coupling. A fully two-dimensional approach gives much less clear outcomes on the densities, especially due to the boundary conditions to be imposed at the sides of the roads. Densities tend to accumulate at one side of the road (as microscopic cars do) making the traffic light effect less evident. The multidimensional coupling gives also a clear advantage in terms of computational time.

## 8.3 Space-Time-Dependent Multiscale Coupling

The parameter $\theta$, which determines the multiscale coupling, is assumed to be constant in (5.22). This implies that the contribution of the microscopic and macroscopic scales to the dynamics is the same everywhere in the domain $\Omega$. However, as a further model refinement, one may imagine situations in which their relative importance is actually different in different sub-domains. For instance, it might be important to retain the microscopic perceptive detail only where the shape of the domain is particularly complex, the dynamics is highly nonlinear, or many agents interact with each other. Conversely, where no complex dynamics are present, a gross continuous description may be the appropriate way for representing the actual agent perception.

This amounts to converting $\theta$ into a function of $x$, and possibly also of $t$, $\theta = \theta(t, x)$, which takes values in the interval $[0, 1]$. Nevertheless, if this modification is straightforwardly introduced in (5.22) then nontrivial technicalities arise in the resulting measure equation (5.1). In fact, in such a case one has to care about time and space derivatives of $\theta$, too, which ultimately cause the multiscale equation (5.23) to be no longer the formal linear combination of Eqs. (5.24) valid for the discrete and continuous components. This has also consequences on the numerical scheme, which cannot take advantage anymore of the separate transport of the two components as expressed by (5.34). Therefore a different strategy for introducing a variable multiscale coupling is preferable.

To this purpose we extend the modeling approach presented in Sects. 6.1–6.3 by differentiating between the mass *perceived* by the test agent and that *transported* by the agents on the whole. In practice, we rewrite (6.1)–(6.3) as:

$$\begin{cases} \dot{X} = v_{\mathrm{d}}(X) + \displaystyle\int_{\mathscr{S}(X)} K(X, y)\, d\lambda_t(y|X(t)) \\ \mu_t = X(t)\#\mu_0, \end{cases} \tag{8.19}$$

where, at time $t$, $X = X(t)$ is the position of the test pedestrian and $\lambda_t(\cdot|X(t))$ is the *perceived mass* in $X(t)$, whereas $\mu_t$ is the *transported mass*. In principle, $\lambda_t(\cdot|X(t))$ and $\mu_t$ are two different non-negative measures with the only requirement that:

$$\lambda_t(\mathbb{R}^d|X(t)) = \mu_t(\mathbb{R}^d) = N, \quad \forall\, t > 0,$$

$N$ being the total number of agents considered in the model. The conceptual difference between $\lambda_t(\cdot|X(t))$ and $\mu_t$ is that the former need not be, strictly speaking, a physical quantity, because it represents the mass *filtered* by the perception of the test agent. For this reason, it may not follow directly the movement of the individuals. Instead, the latter expresses genuinely the physical group mass, which is a material quantity transported by the agents.

Now assume that the test agent has a possibly multiscale perception $\theta(t,\, X)$ of the mass distributed in its interaction neighborhood $\mathscr{S}(X)$, so that the measure $\lambda_t(\cdot|X(t))$ can be given the following form:

$$\lambda_t(\cdot|X(t)) = \theta(t,\, X(t))m_t + (1 - \theta(t,\, X(t)))M_t,$$

where we used the same symbols $m_t$, $M_t$ for the discrete and continuous masses, respectively, like in (5.21). Hence the first equation in (8.19) becomes:

$$\begin{aligned}\dot{X} &= v_{\mathrm{d}}(X) + \theta(t,\, X) \sum_{\substack{k=1 \\ x^k \in \mathscr{S}(X)}}^{N} K(X,\, x^k) + (1 - \theta(t,\, X)) \int_{\mathscr{S}(X)} K(X,\, y)\rho(t,\, y)\, dy \\ &= v_{\mathrm{d}}(X) + \theta(t,\, X)v_{\mathrm{i}}[m_t](X) + (1 - \theta(t,\, X))v_{\mathrm{i}}[M_t](X). \end{aligned} \tag{8.20}$$

On the other hand, notice that both $m_t$ and $M_t$ can play, separately, the role of physical masses transported by the agents. Therefore, we can take either $\mu_t = m_t$ or $\mu_t = M_t$ in (8.19) and let them be transported by the flow field (8.20). By the same procedure described in Sect. 6.2 we get then:

$$\begin{cases} \dfrac{\partial m_t}{\partial t} + \nabla \cdot (m_t v[m_t,\, M_t]) = 0 \\ \dfrac{\partial M_t}{\partial t} + \nabla \cdot (M_t v[m_t,\, M_t]) = 0, \end{cases} \tag{8.21}$$

where

$$v[m_t,\, M_t](x) = v_{\mathrm{d}}(x) + \theta(t,\, x)v_{\mathrm{i}}[m_t](x) + (1 - \theta(t,\, x))v_{\mathrm{i}}[M_t](x) \tag{8.22}$$

is the transport field, which incorporates the non-constant multiscale coupling (compare (8.21)–(8.22) with (5.24)–(5.25)). Scaling $m_t$ and $M_t$ with respect to the total number $N$ of agents further yields the probabilistic interpretation of these equations, in the very same spirit as Sect. 6.3.

The framework (8.21)–(8.22) is suitable for the use of the analytical and numerical machinery set forth in the previous chapters. In fact, the discrete and continuous masses are transported separately by construction, being however coupled by the velocity field. The multiscale coupling parameter $\theta$, now variable in space and time, is used only where it is really needed, i.e., in the expression of the velocity for modeling the agent perception and their resulting interactions. This structure is

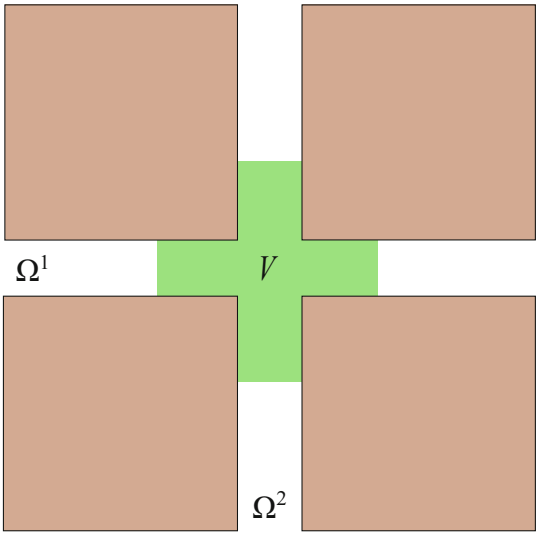


**Fig. 8.3** Computational domain partitioned in two regions: The microscopic scale leads the dynamics in the *green area* $V$, the macroscopic scale in the remaining region $(\Omega^1 \cup \Omega^2) \setminus V$

particularly convenient for implementing also quite elaborated modeling solutions, in which $\theta$ depends on $x$ and $t$ through the solution to (8.21). For instance, one may argue that the test agent perception is such that the lower the continuous mass distributed in its interaction neighborhood the stronger the effect of localized individualities, and vice versa. Two possible choices of $\theta$, actually not completely equivalent to one another despite appearances, which formalize this idea are:

$$\theta(t, x) = 1 - \frac{1}{N} M_t(\mathscr{S}(x)) \qquad \text{or} \qquad \theta(t, x) = \frac{1}{N} m_t(\mathscr{S}(x)),$$

to be plugged directly into (8.22).

In order to exemplify in practice the effect of a variable multiscale coupling, we refer again to the scenario described in Sect. 8.2 (see Fig. 8.1). We expect that a microscopic description is actually needed only at the junction, where granularity plays a major role in shaping the exogenous interactions between the crossing populations. Conversely, away from the junction, where only endogenous interactions occur, a purely macroscopic approach is able to catch all the details of the dynamics. In order to simulate this situation, we simply need to set a priori the space-dependence of $\theta$:

$$\theta(x) = \mathbb{1}_V(x) = \begin{cases} 1 & \text{if } x \in V \\ 0 & \text{if } x \in (\Omega^1 \cup \Omega^2) \setminus V, \end{cases} \tag{8.23}$$

where $V \subset \mathbb{R}^2$ is a neighborhood of the junction $\Omega^1 \cap \Omega^2$ (see Fig. 8.3). Figure 8.4a–c shows the outcome of the simulation.

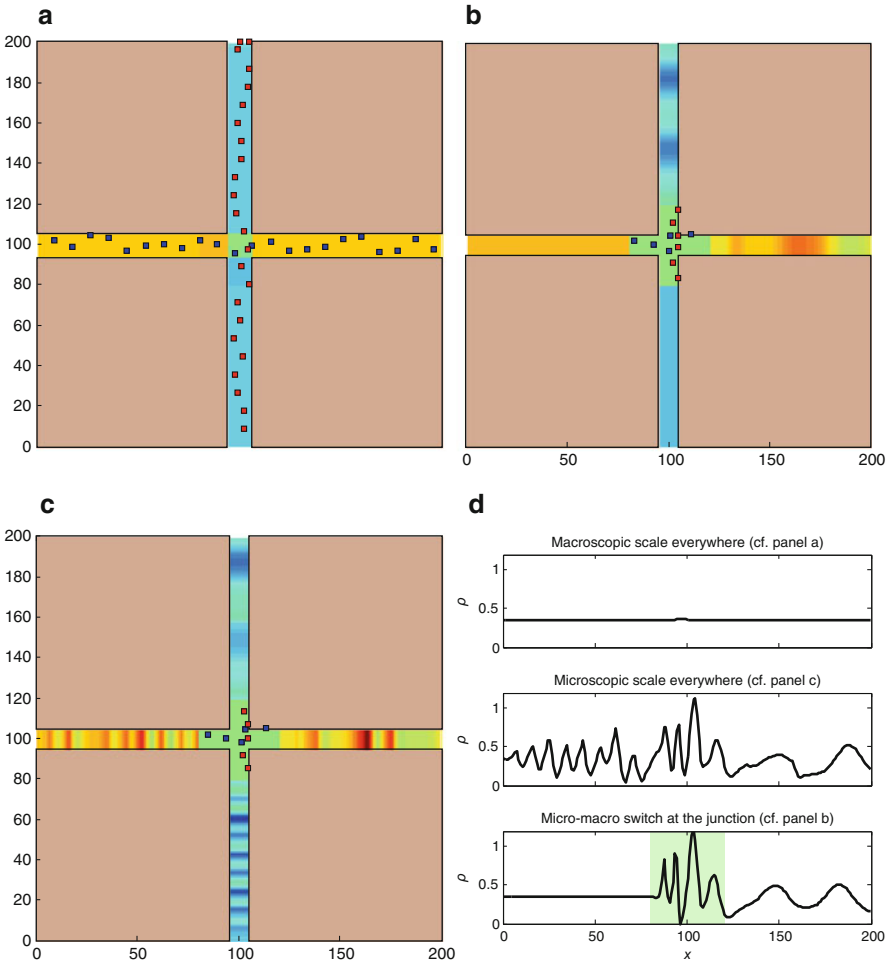


**Fig. 8.4** (**a**) $\theta(x) \equiv 0$. The macroscopic scale leads everywhere; (**b**) $\theta(x) = \mathbb{1}_V(x)$. The microscopic scale leads near the junction, the macroscopic scale elsewhere; (**c**) $\theta(x) \equiv 1$. The microscopic scale leads everywhere; (**d**) Car density along the vertical road with $\theta(x) \equiv 0$ (*top*), $\theta(x) \equiv 1$ (*middle*), and $\theta(x) = \mathbb{1}_V(x)$ (*bottom*)

We recall that *both scales are present everywhere and evolve at all times* (even if they are not always plotted), thus no transmission conditions are imposed at the interfaces of $V$. Comparing the results obtained with $\theta(x) \equiv 0$, $\theta(x) \equiv 1$, and $\theta(x) = \mathbb{1}_V(x)$, we see that the macroscopic approach is not able by itself to trigger a self-organizing alternate passage beyond the junction (Fig. 8.4a). By using a purely microscopic approach, the traffic light effect comes up at and beyond the junction (Fig. 8.4c). However, an annoying effect also appears before and, less visible, beyond the junction: Behind every point car (not shown) density accumulates,

due to strong interactions with Dirac delta's. Such an effect perturbs the density, especially where it should be ideally constant (e.g., before the junction). The space-dependent multiscale coupling triggers a self-organizing alternate passage at the junction, perfectly visible in terms of density waves, which persists also when the microscopic scale ceases its influence on the dynamics (Fig. 8.4b). This numerical experiment shows that self-organization can be obtained by adding granularity only at the junction rather than from the very beginning and motivates the use of the microscopic scale *only where it is really needed*.

To better quantify this qualitative discussion, we plotted in Fig. 8.4d the one-dimensional density along the vertical road $\Omega^2$. Fully macroscopic dynamics do not show any appreciable effect either at the junction or beyond it. Conversely, fully microscopic dynamics generate irregular waves beyond the junction, as well as a noisy density profile before it. Finally, mixed dynamics (fully microscopic near the junction, fully macroscopic elsewhere) produce a constant density before the junction and clear density wave packets beyond it.

## 8.4 More General ODE-PDE Coupling

As already anticipated in Sect. 2.1, the multiscale coupling discussed in Chap. 5 suggests a general method to couple a PDE and a system of ODEs modeling the same physical phenomenon. Indeed, once the measure $\mu$ is specialized in a sum of Dirac delta's and in an absolutely continuous measure, we simply get a system of ODEs (2.1) and a PDE (2.2) coupled by means of a common velocity field (2.3). In this section we show, by means of a specific example, how this coupling idea can be extended to a large class of equations and physical phenomena.

### *8.4.1 Coupling the Heat Equation and the Brownian Motion*

The goal of this section is to apply the multiscale coupling to a well-known example in mathematical physics and probability theory. Let us consider the following system of Stochastic Differential Equations (SDEs)

$$\begin{cases} dX_t^k = dW_t^k \\ X_0^k = 0 \end{cases} \qquad k = 1, \ldots, N, \tag{8.24}$$

where $W_t^k$ is the $d$-dimensional Brownian motion (standard Wiener process). The Fokker-Planck equation associated with the Brownian motion is the heat equation

$$\begin{cases} \dfrac{\partial u}{\partial t} - \dfrac{1}{2}\triangle u = 0, & t > 0,\ x \in \mathbb{R}^d \\ u(0,\ x) = \delta_0, & x \in \mathbb{R}^d, \end{cases} \tag{8.25}$$

where $\delta_0$ is the Dirac delta centered in 0. The solution $u$ to (8.25) describes the time evolution of the probability density function of each Brownian motion generated by (8.24), i.e.

$$\text{Prob}(X_t^k \in A) = \int_A u(t,\ x)\, dx, \qquad \forall\ A \subset \mathbb{R}^d, \quad k = 1,\ \ldots,\ N.$$

Defining the *macroscopic velocity field* $v_M$ as

$$v_M(t,\ x) := -\frac{\nabla u(t,\ x)}{2u(t,\ x)}, \tag{8.26}$$

(8.25) can be formally written as

$$\begin{cases} \dfrac{\partial u}{\partial t} + \nabla \cdot (u v_M) = 0, & t > 0,\ x \in \mathbb{R}^d \\ u(0,\ x) = \delta_0, & x \in \mathbb{R}^d. \end{cases} \tag{8.27}$$

The form (8.27) makes the velocity field $v_M$, which transports the probability density function, appear explicitly. On the microscopic side, let us write (8.24) as

$$\begin{cases} \dot{X}_t^k = \xi_t^k \\ X_0^k = 0 \end{cases} \qquad k = 1,\ \ldots,\ N, \tag{8.28}$$

where $\xi_t$ is the Gaussian white noise process. It is important to note that the velocities $\xi_t^k$, $k = 1,\ \ldots,\ N$ define a vector field only at the agent positions $X_t^k$, $k = 1,\ \ldots,\ N$. In order to make the macroscopic part of the system interact with the microscopic part, the latter should define a microscopic velocity field at every point $x$ of the space. This can be done by using the following natural definition for the *microscopic (stochastic) velocity field* $v_m$

$$v_m(t,\ x) := \begin{cases} \dfrac{1}{|J(t,\ x)|} \displaystyle\sum_{\ell \in J(t,\ x)} \xi_t^\ell, & \text{if } J(t,\ x) \neq \emptyset \\ 0, & \text{if } J(t,\ x) = \emptyset, \end{cases} \tag{8.29}$$

where

$$J(t,\ x) := \{k \in \{1,\ \ldots,\ N\} \ :\ X_t^k = x\}.$$

This definition differs from the analogous one given for pedestrians, cf. (5.27), since the concept of *test agent* is not invoked here. In fact, in the present context agents are not assumed to interact with each other.

Once the velocity field is defined at both scales, it is possible to define

$$v := \theta v_m + (1-\theta) v_M, \qquad \theta \in [0,\, 1]. \tag{8.30}$$

Since

$$\begin{aligned} 0 &= \frac{\partial u}{\partial t} + \nabla \cdot (uv) \\ &= \frac{\partial u}{\partial t} + \nabla \cdot \left( u\theta \frac{1}{|J|} \sum_{\ell \in J} \xi_t^\ell \right) + \nabla \cdot \left( u(1-\theta) \frac{-\nabla u}{2u} \right) \\ &= \frac{\partial u}{\partial t} + \theta \nabla \cdot \left( u \frac{1}{|J|} \sum_{\ell \in J} \xi_t^\ell \right) - \frac{1}{2}(1-\theta) \triangle u, \end{aligned}$$

the fully-coupled dynamics is

$$\begin{cases} dX_t^k = \theta\, dW_t^k + (1-\theta) \dfrac{-\nabla u(t,\, X_t^k)}{2u(t,\, X_t^k)} dt, \quad t > 0, \quad k = 1, \ldots, N & \text{(8.31a)} \\ \dfrac{\partial u}{\partial t} + \theta \nabla \cdot \left( u \dfrac{1}{|J|} \displaystyle\sum_{\ell \in J} \xi_t^\ell \right) - \dfrac{1}{2}(1-\theta) \triangle u = 0, \quad t > 0, \quad x \in \mathbb{R}^d & \text{(8.31b)} \end{cases}$$

with initial conditions $X_0^k = 0$, $k = 1, \ldots, N$, and $u(0, x) = \delta_0$. The system (8.31a)–(8.31b) couples a system of mixed ordinary-stochastic differential equations with a deterministic-stochastic advection-diffusion partial differential equation.

### 8.4.2 Numerical Approximation of the Coupled Equation

In the following we restrict the discussion to the dimension one ($d = 1$). The heat equation (8.25) can be solved analytically and we have

$$u(t,\, x) = \frac{1}{\sqrt{2\pi t}} e^{-\frac{x^2}{2t}}, \qquad v_M(t,\, x) := -\frac{\nabla u(t,\, x)}{2u(t,\, x)} = \frac{x}{2t}. \tag{8.32}$$

Let us introduce a structured space-time grid with spatial cell size $\Delta x$ and a time step $\Delta t$ like in Sect. 5.5. We denote space cells by $E_i = \left[x_i - \frac{\Delta x}{2},\, x_i + \frac{\Delta x}{2}\right)$, where

$x_i = i\Delta x$, and by $\phi_n^i$ the approximate value of a generic function $\phi(t, x)$ at $x = x_i$ and $t = t_n = n\Delta t$.

The numerical approximation of (8.31a)–(8.31b) is extremely hard. Let us approach it step by step. First of all, let us discretize (8.25) and (8.27). Equation (8.25) can be easily discretized by means of a first-order centered finite difference scheme

$$u_{n+1}^i = u_n^i + \frac{1}{2}\frac{\Delta t}{\Delta x^2}\left(u_n^{i+1} - 2u_n^i + u_n^{i-1}\right), \qquad n \in \mathbb{N},\ i \in \mathbb{Z}. \tag{8.33}$$

Equation (8.27) instead, although it is formally equivalent to (8.25), must be carefully approximated by a scheme which respects the directionality of the vector field $v_M$ (*assumed to be given*). To this end, let us define the flux

$$f[v_M] := uv_M.$$

The one-dimensional version of the scheme (5.37) reads as

$$u_{n+1}^i = u_n^i + \frac{\Delta t}{\Delta x}\Big(-L_n^i[f] + G_n^{i-}[f] + G_n^{i+}[f]\Big), \qquad n \in \mathbb{N},\ i \in \mathbb{Z}, \tag{8.34}$$

where the L(oss) term is given by

$$L_n^i[f] := |f_n^i|, \tag{8.35}$$

and the G(ain) terms are given by

$$G_n^{i-}[f] := \begin{cases} f_n^{i-1}, & \text{if } (v_M)_n^{i-1} \geq 0 \\ 0, & \text{if } (v_M)_n^{i-1} < 0, \end{cases} \qquad G_n^{i+}[f] := \begin{cases} -f_n^{i+1}, & \text{if } (v_M)_n^{i+1} \leq 0 \\ 0, & \text{if } (v_M)_n^{i+1} > 0. \end{cases} \tag{8.36}$$

Note that scheme (8.34) is nothing else than the classical *upwind* scheme for space-dependent velocities with nonconstant sign. To avoid to manage the initial datum $\delta_0$ at the discrete level, we set the initial time for the simulation at $t_0 = \frac{1}{2}$ and, consequently, the new initial datum at $u(t, x_0) = \frac{1}{\sqrt{2\pi t_0}} \exp -\frac{x^2}{2t_0}$. The computational domain is set at $[-10, 10]$.

Figure 8.5 shows the initial datum $u(t_0, x)$, the numerical solution $u_{\text{parab}}$ of (8.25) obtained by (8.33) at time $t = 5$, the exact macroscopic velocity field $v_M = -\frac{\nabla u}{2u} = \frac{x}{2t}$ in $[-10, 10]\times[t_0, 3]$, and the numerical solution $u_{\text{iperb}}$ of (8.27) obtained by (8.34) at time $t = 5$. It can be seen that the approximation of $u_{\text{iperb}}$ is slightly worse than that of $u_{\text{parab}}$, due to the different features of the numerical scheme.

Regarding the microscopic part, the Ito processes satisfying (8.24) can be approximated by using the weak Euler scheme

$$X_{n+1}^k = X_n^k + \Delta W_n^k, \qquad k = 1, \ldots, N \tag{8.37}$$

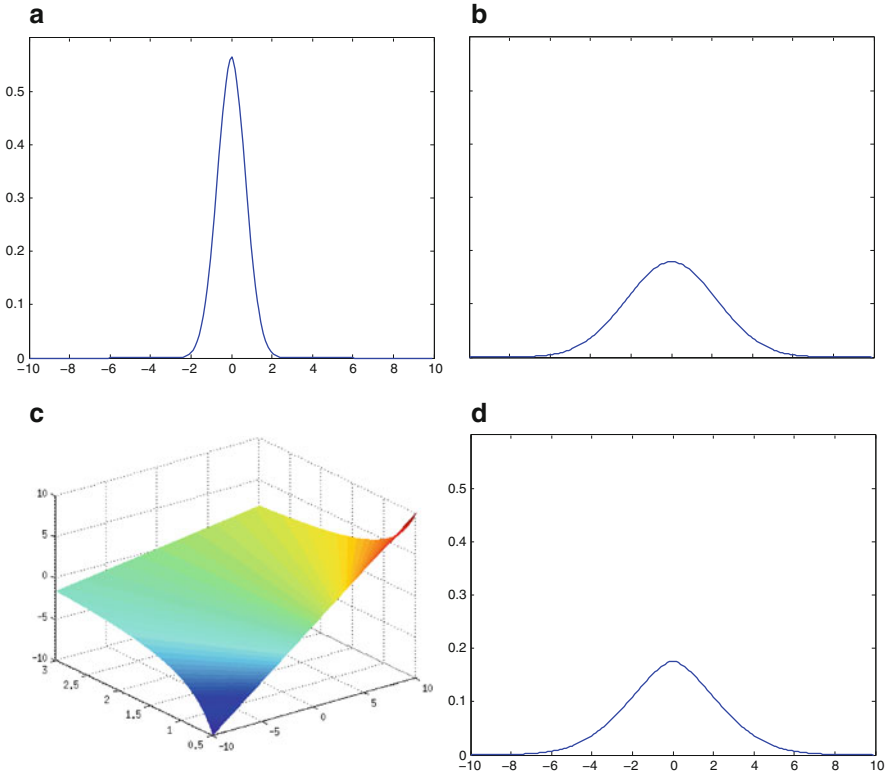


**Fig. 8.5** (**a**) Initial datum $u(t_0, x)$; (**b**) Function $u_{\text{parab}}(t = 5, x)$; (**c**) The velocity field $v_M = -\frac{\nabla u}{2u} = \frac{x}{2t}$; (**d**) Function $u_{\text{iperb}}(t = 5, x)$

where the random increments $\Delta W_n^k$'s are given by

$$\Delta W_n^k = \pm\sqrt{\Delta t}, \qquad \text{Prob}(W_n^k = \pm\sqrt{\Delta t}) = \frac{1}{2}. \tag{8.38}$$

The discrete velocity $\xi_n^k$ of the Brownian motion can be computed *a posteriori* as $\frac{\Delta W_n^k}{\Delta t}$ and then it is possible to define the discrete microscopic velocity as (cf. (8.29))

$$(v_m)_n^i := \begin{cases} \dfrac{1}{|J_n^i|} \displaystyle\sum_{\ell \in J_n^i} \frac{\Delta W_n^\ell}{\Delta t}, & \text{if } J_n^i \neq \emptyset \\ 0, & \text{if } J_n^i = \emptyset, \end{cases} \tag{8.39}$$

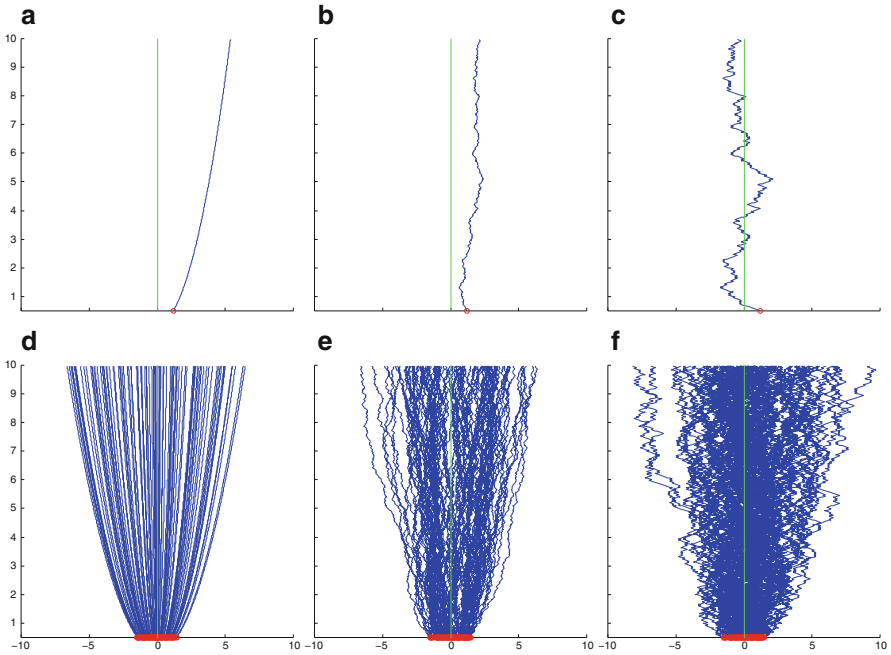


**Fig. 8.6** Trajectories of $N = 1$ particles (*first row*) and $N = 100$ particles (*second row*) in the plane $x$-$t$ for $x \in [-10, 10]$ and $t \in [t_0, 10]$. *Red circles* are the initial positions of the particles (a,d) $\theta = 0$ (macroscopic velocity is leading). (b,e) $\theta = 0.3$ (coupled velocity). (c,f) $\theta = 1$ (pure Brownian motion)

where

$$J_n^i := \{k \in \{1, \ldots, N\} : X_n^k \in E_i\}.$$

At time $t = t_0 = \frac{1}{2}$, we assume the microscopic agents $\{X_{t_0}^k\}_{k=1}^N$ to be randomly distributed in $\{x \in \mathbb{R} : |x| < r\}$ with $r = \frac{3}{2}$.

A preliminary coupling of the microscopic and macroscopic scale can be obtained by assuming that the solution $u$ to the heat equation (8.25) is known (see (8.32)), and then solving the equation for $X^k$ in (8.31a), discretized as follows:

$$X_{n+1}^k = X_n^k + \theta \Delta W_n^k + (1-\theta)\frac{X_n^k}{2t_n}\Delta t, \qquad k = 1, \ldots, N. \tag{8.40}$$

Figure 8.6 shows the solution of (8.40) for $\theta = 0$, $\theta = 0.3$ and $\theta = 1$ ($N = 1$ and $N = 100$ agents). Interestingly, the coupling works fine and the Brownian motion is regularized as expected, still preserving the overall statistical properties of the dynamics.

The numerical scheme for the fully-coupled system (8.31a)–(8.31b) can be obtained by means of the ingredients introduced above, ending up with the following discrete explicit system

$$\begin{cases} X_{n+1}^k = X_n^k + \theta \Delta W_n^k + (1-\theta)\Delta t \left(\dfrac{-1}{2u_n^j}\right)\left(\dfrac{u_n^{j+1} - u_n^{j-1}}{2\Delta x}\right) & \text{(8.41a)} \\ u_{n+1}^i = u_n^i + \theta \dfrac{\Delta t}{\Delta x}\big(-L_n^i[f] + G_n^{i-}[f] + G_n^{i+}[f]\big) + \\ \qquad\qquad (1-\theta)\dfrac{1}{2}\dfrac{\Delta t}{\Delta x^2}\big(u_n^{i+1} - 2u_n^i + u_n^{i-1}\big) & \text{(8.41b)} \end{cases}$$

where $L$ and $G$'s are defined in (8.35) and (8.36), respectively, $j$ is defined, for any $n$ and $k$, as the unique index such that $X_n^k \in E_j$ (we are assuming here a zeroth order interpolation for the values of $u$ not sitting on grid nodes), and $f = f[v_m]$ is defined, at grid nodes, as

$$f_n^i = u_n^i (v_m)_n^i, \qquad n \in \mathbb{N},\ i \in \mathbb{Z},$$

with $v_m$ as in (8.39).

The scheme (8.41a)–(8.41b) raises severe numerical issues. Three of them are in order: (i) Even if the initial time for the simulation is shifted to $t_0 = \frac{1}{2} > 0$, the function $u$ is very close to 0 (close to or below the machine precision) in some portion of the domain, see Fig. 8.5a. This makes the division by $u$ in (8.41a) to be a source of errors; (ii) The microscopic dynamics is very irregular and, consequently, the function $u$ becomes in short time quite irregular. This makes it almost impossible to compute $\nabla u$ in (8.41a) with a certain precision; (iii) Limiting our attention to the advection part of (8.41b), the hyperbolic CFL condition takes the nonstandard implicit form

$$\Delta t \max_{n,i} |(v_m(\Delta t))_n^i| \le \Delta x.$$

Indeed, the discrete microscopic velocity field $(v_m)_n^i$ depends on the choice of $\Delta t$, cf. (8.39). In particular, we have

$$\mathbb{E}\left[\max_{n,i} |(v_m(\Delta t))_n^i|\right] = \mathbb{E}\left[\frac{|\Delta W|}{\Delta t}\right] = \frac{1}{\sqrt{\Delta t}}.$$

Finally, the CFL condition can be explicitly written as

$$\sqrt{\Delta t} \le \Delta x \quad \text{or} \quad \Delta t \le \Delta x^2.$$

Figure 8.7 shows the result of the coupled dynamics (8.31a)–(8.31b) for $u$ at $t = 5$ with $\theta = 1$ and $N = 100$. Here the Brownian motion leads the dynamics,

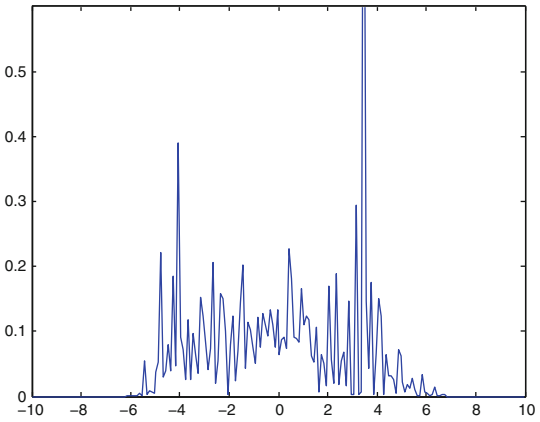


**Fig. 8.7** Solution $u(t = 5, x)$ of the system (8.31a)–(8.31b) with $\theta = 1$ and $N = 100$

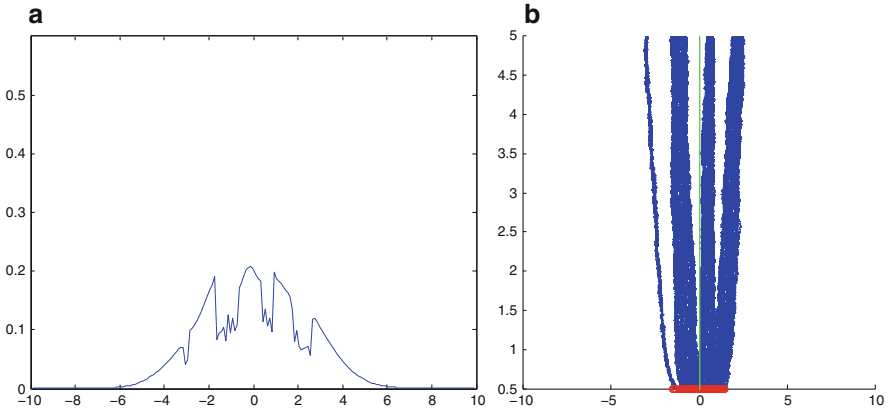


**Fig. 8.8** Solution of the system (8.31a)–(8.31b) with $\theta = 0.3$ and $N = 100$. (**a**) $u(t = 5, x)$; (**b**) Trajectories $X_t^k$ of the particles in the plane $x$-$t$ for $x \in [-10, 10]$ and $t \in [t_0, 5]$

making the macroscopic solution $u$ strongly irregular. It is interesting to note that the microscopic dynamics is able to "stretch" the Gaussian in the correct way. This is perfectly visible comparing Figs. 8.5d and 8.7: The support of the two solutions is approximately the same, i.e. $[-7, 7]$.

Figure 8.8 shows the result of the coupled dynamics (8.31a)–(8.31b) for $u$ and $X^k$ at $t = 5$ with $\theta = 0.3$ and $N = 100$. Here both scales contribute to the overall dynamics, making the result quite unpredictable. We observe a clustering effect in the microscopic particles, likely due to numerical issues rather than actual effects of scale interactions.

Similar results can be obtained analogously in two dimensions. Figure 8.9 shows the two-dimensional version of the simulation described in Fig. 8.6d–f.

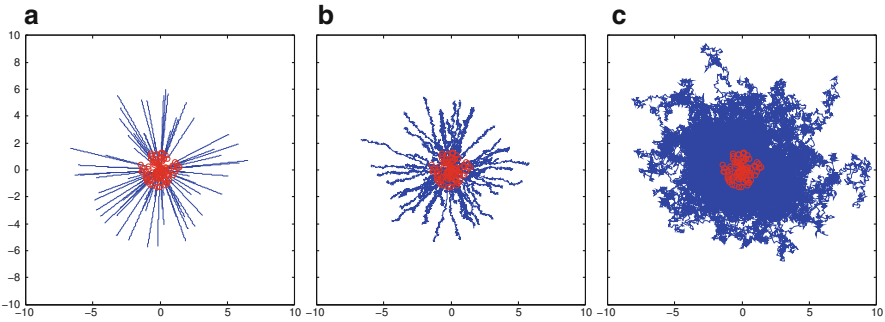


**Fig. 8.9** Trajectories of $N = 100$ particles in the plane $x$-$y$. *Red circles* are the initial positions of the particles. (**a**) $\theta = 0$ (macroscopic velocity is leading). (**b**) $\theta = 0.1$ (coupled velocity). (**c**) $\theta = 1$ (pure Brownian motion)

## 8.5 Conclusions

The example discussed above shows that the multiscale coupling described in Chap. 5 can be understood in a quite broad sense. Although the numerics is still far from being able to catch the full potentiality of the approach, new scenarios for a number of applications in different fields are disclosed. For example, the same ideas presented in this section can be adapted to describe, in a multiscale fashion, the wave-particle duality, replacing the heat equation by the Schrödinger equation.

## 8.6 Bibliographical Notes

Section 8.1 The results about second order time-evolving measures appear for the first time in this book.

Sections 8.2, 8.3 The results about multidimensional and space-time-dependent multiscale coupling can be found, in less detail, in Cristiani et al. [49].

Section 8.4 The coupling of the heat equation with the Brownian motion was first presented in Cristiani [44].

# Appendix A
# Basics of Measure and Probability Theory

**Abstract** This appendix collects sequentially some basic material about measure, probability, and transport theory. The goal is to provide readers with quick-access references to the more technical contents of the book, especially those used in Chaps. 6 and 7. On the other hand, the presented topics are by no means covered in an exhaustive manner: The appendix does indeed assume prior knowledge of real and functional analysis. Hints to more complete texts, at both undergraduate and graduate or research levels, are given in the final bibliographical notes.

## A.1 Measurable Spaces, Measures, and Measurable Functions

### *A.1.1 Sets and Operations with Sets*

Let us consider an *abstract set* $U$, i.e., a set with no special structure (either topological or metrical). We denote by $u$ a generic element of $U$ and we write $u \in U$ to mean that $u$ belongs to $U$, $u \notin U$ to mean that $u$ does not belong to $U$.

A *subset* of $U$ is another set whose elements belong also to $U$. We write $A \subseteq U$ to mean that $A$ is a subset of $U$:

$$A \subseteq U \quad \Leftrightarrow \quad u \in A \Rightarrow u \in U, \ \forall\, u \in A.$$

Notice that $A$ may coincide with the whole $U$. If it does not then $A$ is said to be a *proper* subset of $U$. When we want to stress that $A$ is a proper subset of $U$ we write $A \subset U$ or even $A \subsetneq U$.

Two subsets $A$, $B$ of $U$ are *equal* if and only if $A \subseteq B$ and $B \subseteq A$. In this case we write $A = B$.

We denote by $\emptyset$ the *empty set*, i.e., the set with no elements. The empty set is a subset of any other set.

E. Cristiani et al., *Multiscale Modeling of Pedestrian Dynamics*, MS&A 12,
DOI 10.1007/978-3-319-06620-2,

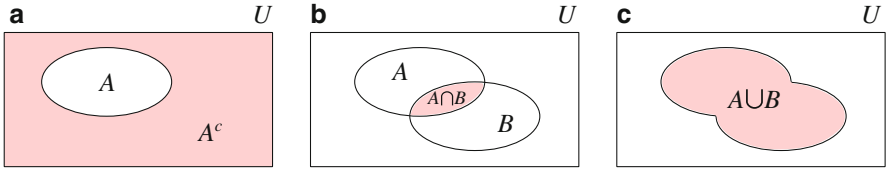


**Fig. A.1** Venn diagrams illustrating the basic set operations introduced in Definition A.1: (**a**) complement; (**b**) intersection; (**c**) union

The following logical operations can be defined among sets (cf. Fig. A.1).

**Definition A.1 (Operations with sets).** Let $A$, $B$ be two subsets of $U$. We define the following basic operations:

- *Complement*: The complement of $A$ (in $U$) is a set, denoted by $A^c$, whose elements are all and only those $u \in U$ which do *not* belong to $A$:

$$A^c := \{u \in U \ : \ u \notin A\}.$$

  Notice that $(A^c)^c = A$.
- *Intersection*: The intersection of $A$ and $B$ is a set, denoted by $A \cap B$, whose elements are all and only those $u \in U$ which belong to *both A and B*:

$$A \cap B := \{u \in U \ : \ u \in A \text{ and } u \in B\}.$$

  If $A \cap B = \emptyset$ then $A$ and $B$ are said to be *disjoint*. Notice that $A \cap A^c = \emptyset$, $A \cap \emptyset = \emptyset$, and $A \cap U = A$ for all $A \subseteq U$.
- *Union*: The union of $A$ and $B$ is a set, denoted by $A \cup B$, whose elements are all and only those $u \in U$ which belong to *at least one between A and B*:

$$A \cup B := \{u \in U \ : \ u \in A \text{ or } u \in B\}.$$

  Notice that $A \cup A^c = U$, $A \cup \emptyset = A$, and $A \cup U = U$ for all $A \subseteq U$.

### *A.1.2 σ-Algebras and Measurable Spaces*

We now consider *families of subsets* of $U$. In particular, we denote by $\mathfrak{M}$ any of such families. The interesting ones are those *stable* with respect to the logical operations introduced in Definition A.1, therefore we give the following definition:

**Definition A.2 ($\sigma$-algebra).** A family $\mathfrak{M}$ of subsets of $U$ is said to be a *$\sigma$-algebra* if the following three properties hold true:

(i) The empty set and the whole set $U$ belong to the family; That is:

$$\emptyset,\ U \in \mathfrak{M}.$$

(ii) The family is stable (or "closed") with respect to complementation; That is, whenever $A$ is an element of the family also $A^c$ is:

$$A \in \mathfrak{M} \ \Rightarrow\ A^c \in \mathfrak{M}.$$

(iii) The family is stable with respect to *countable* unions; That is, if $\{A_i\}_{i\in\mathbb{N}}$ is a countable collection of subsets of $U$, each belonging to $\mathfrak{M}$, then also their union belongs to $\mathfrak{M}$:

$$\{A_i\}_{i\in\mathbb{N}} \subseteq \mathfrak{M} \ \Rightarrow\ \bigcup_{i=1}^{\infty} A_i \in \mathfrak{M}.$$

*Remark A.1.* From Definition A.2 it follows that a $\sigma$-algebra is stable also with respect to:

- *Finite* unions, indeed if $\{A_i\}_{i=1}^N \subseteq \mathfrak{M}$ with $N < \infty$ then it is sufficient to take in Definition A.2(iii) $A_{N+1} = A_{N+2} = \cdots = \emptyset$ (which belong to $\mathfrak{M}$ owing to Definition A.2(i)) to see that $\cup_{i=1}^N A_i \in \mathfrak{M}$ as well.
- *Finite* and *countable intersections*, as it can be immediately checked by recalling *De Morgan's laws* $(\cap_i A_i)^c = \cup_i A_i^c$ and $(\cup_i A)^c = \cap_i A_i^c$, which hold for both finite and countable unions and intersections.

*Example A.1 (of $\sigma$-algebras).*

(i) For every abstract set $U$, the family $\mathfrak{M} = \{\emptyset, U\}$ is the minimal possible $\sigma$-algebra of subsets of $U$ (sometimes it is called the *trivial* $\sigma$-algebra).

(ii) For $A \subseteq U$, the family $\mathfrak{M} = \{\emptyset, A, A^c, U\}$ is called the $\sigma$-algebra *generated* by $A$. To stress this fact, it is often denoted by the symbol $\sigma(A)$ in place of $\mathfrak{M}$. It is the *smallest* $\sigma$-algebra of subsets of $U$ containing $A$, namely if $\mathfrak{M}'$ is any other $\sigma$-algebra such that $A \in \mathfrak{M}'$ then $\sigma(A) \subseteq \mathfrak{M}'$.

(iii) If $U$ is a *topological* space, i.e., such that *open sets* can be defined among its subsets, then the $\sigma$-algebra generated by the open sets is called the *Borel* $\sigma$-algebra and is usually denoted by $\mathscr{B}(U)$. Any element of $\mathscr{B}(U)$ is also called a *Borel set*. It is worth stressing that $\mathscr{B}(U)$ does *not* contain only open subsets of $U$: For instance, all closed subsets of $U$ are Borel sets as well, as they are complements of open sets.

**Definition A.3 (Measurable space).** Each element of a $\sigma$-algebra $\mathfrak{M}$ is called a *measurable set*. The pair $(U, \mathfrak{M})$ is called a *measurable space*.

### A.1.3 Measures

**Definition A.4 (Measure).** A real-valued positive *measure* $\mu$ on the measurable space $(U, \mathfrak{M})$ is a mapping $\mu : \mathfrak{M} \to \mathbb{R}_+$ which satisfies the following condition only, called $\sigma$*-additivity*:

- For every countable sequence $\{A_i\}_{i\in\mathbb{N}}$ of elements of $\mathfrak{M}$ *pairwise disjoint*, i.e., such that $A_i \cap A_j = \emptyset$ for all $i \neq j$, it results:

$$\mu\left(\bigcup_{i=1}^{\infty} A_i\right) = \sum_{i=1}^{\infty} \mu(A_i). \tag{A.1}$$

**Definition A.5 (Measure space).** The triple $(U, \mathfrak{M}, \mu)$ is called a *measure space*.

*Remark A.2.* Notice that the definition above is consistent, in fact $A_i \in \mathfrak{M}$ for all $i$ implies, owing to Definition A.2, $\cup_{i=1}^{\infty} A_i \in \mathfrak{M}$. Therefore this union still belongs to the domain of the measure $\mu$, hence the left-hand side of (A.1) is well defined.

*Example A.2 (of measures).*

(i) Let $U = \mathbb{R}^d$ and $\mathfrak{M} = \mathscr{B}(\mathbb{R}^d)$. In the "physical" measurable space $(\mathbb{R}^d, \mathscr{B}(\mathbb{R}^d))$ with the usual topology coming from the Euclidean metric $|\cdot|$, the $d$-dimensional *Lebesgue measure*, here denoted by $\mathscr{L}^d$, is the measure which assigns to every Borel set of the form $A = (a_1, b_1) \times (a_2, b_2) \times \cdots \times (a_d, b_d)$ the number

$$\mathscr{L}^d(A) = \prod_{i=1}^{d} (b_i - a_i)$$

called the *volume* of $A$.

(ii) In an abstract measurable space $(U, \mathfrak{M})$, the *Dirac measure* concentrated on a given point $u_0 \in U$ is the measure, usually denoted by $\delta_{u_0}$, such that:

$$\delta_{u_0}(A) = \begin{cases} 1 & \text{if } u_0 \in A \\ 0 & \text{otherwise,} \end{cases} \qquad \forall\, A \in \mathfrak{M}. \tag{A.2}$$

When $U$ is a topological space and one considers in it the Borel $\sigma$-algebra $\mathscr{B}(U)$ (cf. Example A.1(iii)), a measure $\mu$ on $(U, \mathscr{B}(U))$ is said to be *inner regular* if for all $B \in \mathscr{B}(U)$ the value $\mu(B)$ can be approximated with arbitrary precision by $\mu(K)$, where $K$ is a *compact* subset of $B$. That is:

$$\forall\, \epsilon > 0,\ \exists\, K \subseteq B \text{ compact} : |\mu(B) - \mu(K)| < \epsilon$$

or, equivalently,

$$\mu(B) = \sup_{\substack{K \subseteq B \\ \text{compact}}} \mu(K).$$

In addition, $\mu$ is said to be *locally finite* if every point $u$ of $U$ has a neighborhood of finite measure. Finally, $\mu$ is said to be a *Radon measure* if it is inner regular and locally finite.

Conversely, in an abstract (i.e., not necessarily topological) measurable space $(U, \mathfrak{M})$, a measure $\mu$ is said to be *$\sigma$-finite* if there exists a sequence $\{A_i\}_{i\in\mathbb{N}} \subseteq \mathfrak{M}$ such that $U = \cup_{i\in\mathbb{N}} A_i$ and $\mu(A_i) < +\infty$ each $i$. Notice that this does not imply that $U$ has in turn finite measure. When $\mu(U) < +\infty$, $\mu$ is said to be *finite*.

*Remark A.3.* Concerning the finiteness of a measure, we notice that if there exists $A \in \mathfrak{M}$ such that $\mu(A) < +\infty$ then it invariably results $\mu(\emptyset) = 0$. In fact, let us consider the sequence $\{A_i\}_{i\in\mathbb{N}} \subseteq \mathfrak{M}$ where $A_1 = A$ and $A_2 = A_3 = \cdots = \emptyset$; Then owing to (A.1) it results $\mu(A) = \mu(A) + \sum_{i=2}^{\infty} \mu(\emptyset)$, i.e. (using that $\mu(A)$ is finite, hence it can be dropped from both sides), $\sum_{i=2}^{\infty} \mu(\emptyset) = 0$. Since $\mu(\emptyset) \geq 0$, the only possibility is indeed $\mu(\emptyset) = 0$.

This also shows that $\sigma$-additivity implies the additivity of $\mu$ for finite unions. In fact, if $\{A_i\}_{i=1}^{N} \subseteq \mathfrak{M}$ with $N < \infty$ are pairwise disjoint then it is sufficient to take $A_{N+1} = A_{N+2} = \cdots = \emptyset$ in (A.1) to see that $\mu(\cup_{i=1}^{N} A_i) = \sum_{i=1}^{N} \mu(A_i)$.

*Remark A.4 (Sum of measures).* Generally, usual algebraic operations *cannot* be performed with measures. For instance, two measures $\mu_1$, $\mu_2$ on $(U, \mathfrak{M})$ cannot be multiplied, since the *mathematical object* $\mu_1 \cdot \mu_2$ is not defined (although it is of course defined the *number* $\mu_1(A)\mu_2(A)$ once a measurable set $A$ has been fixed, but this amounts to ordinary multiplication of real numbers).

However, measures can be *added* and *multiplied by a scalar*. In practice, *linear combinations* of measures are allowed and the result is still a measure in the sense of Definition A.4. In particular:

- $\mu = \mu_1 + \mu_2$ is the measure on $(U, \mathfrak{M})$ defined as

$$\mu(A) := \mu_1(A) + \mu_2(A), \quad \forall\, A \in \mathfrak{M}.$$

- For $a \in \mathbb{R}$, $\mu = a\mu_1$ is the measure on $(U, \mathfrak{M})$ defined as

$$\mu(A) := a\mu_1(A), \quad \forall\, A \in \mathfrak{M}.$$

When we say that $\mu = \mu_1 + \mu_2$ and $\mu = a\mu_1$ are measures in the sense of Definition A.4 we mean that the mapping $A \mapsto \mu(A)$ from $\mathfrak{M}$ to $\mathbb{R}_+$ is $\sigma$-additive. In contrast, the mapping $A \mapsto \mu_1(A)\mu_2(A)$ can of course be defined from $\mathfrak{M}$ to $\mathbb{R}_+$ but it is *not* $\sigma$-additive, hence it does not define a measure.

### A.1.4 Measurable Functions

Now we go from the abstract measure space $(U, \mathfrak{M}, \mu)$ to the "physical" measurable space $(\mathbb{R}^d, \mathscr{B}(\mathbb{R}^d))$, $d \geq 1$, with functions.

**Definition A.6 (Measurable function).** A function $f : U \to \mathbb{R}^d$ is said to be *measurable* if:

$$f^{-1}(B) \in \mathfrak{M}, \quad \forall\, B \in \mathscr{B}(\mathbb{R}^d).$$

We recall that $f^{-1}(B)$ is the subset of $U$, called the *inverse image* (or *pre-image*) of $B$ through $f$, defined as:

$$f^{-1}(B) := \{u \in U \ : \ f(u) \in B\}.$$

Roughly speaking, measurable functions are those functions which operate back and forth between the $\sigma$-algebras $\mathfrak{M}$ and $\mathscr{B}(\mathbb{R}^d)$. However, the precise definition makes use of the inverse images.

**Theorem A.1 (Operations with measurable functions).**

*(i)* Algebraic operations. *If $f$, $g$ are two measurable functions from $(U, \mathfrak{M})$ to $(\mathbb{R}^d, \mathscr{B}(\mathbb{R}^d))$ then also $f \pm g$, $fg$ are measurable. If $g(u) \neq 0$ for all $u \in U$ then $f/g$ is measurable as well.*

*(ii)* Composition. *If $f : (U, \mathfrak{M}) \to (\mathbb{R}^d, \mathscr{B}(\mathbb{R}^d))$, $g : (\mathbb{R}^d, \mathscr{B}(\mathbb{R}^d)) \to (\mathbb{R}^d, \mathscr{B}(\mathbb{R}^d))$ are measurable then so is $g \circ f : (U, \mathfrak{M}) \to (\mathbb{R}^d, \mathscr{B}(\mathbb{R}^d))$.*

*(iii)* Sequences. *If $\{f_i\}_{i \in \mathbb{N}}$ is a sequence of measurable functions from $(U, \mathfrak{M})$ to $(\mathbb{R}^d, \mathscr{B}(\mathbb{R}^d))$ then the following functions are measurable as well:*

$$\sup_{i \in \mathbb{N}} f_i(u), \quad \inf_{i \in \mathbb{N}} f_i(u), \quad \limsup_{i \to \infty} f_i(u), \quad \liminf_{i \to \infty} f_i(u).$$

*In addition, if $\lim_{i \to \infty} f_i(u)$ exists for all $u \in U$ then it is measurable as well.*

**Theorem A.2 (Measurable functions transport measures).** *Let $f : U \to \mathbb{R}^d$ be a measurable function from the measure space $(U, \mathfrak{M}, \mu)$ into the measurable space $(\mathbb{R}^d, \mathscr{B}(\mathbb{R}^d))$. Define the mapping $\nu : \mathscr{B}(\mathbb{R}^d) \to \mathbb{R}_+$ by setting:*

$$\nu(B) := \mu(f^{-1}(B)), \quad \forall\, B \in \mathscr{B}(\mathbb{R}^d). \tag{A.3}$$

*Then $\nu$ is a measure (in the sense of Definition A.4) on the measurable space $(\mathbb{R}^d, \mathscr{B}(\mathbb{R}^d))$.*

*Proof.* Proving the theorem is essentially a matter of checking that $\nu$ is $\sigma$-additive, cf. (A.1). Indeed, its non-negativity follows straightforwardly from the analogous property of $\mu$.

Let $\{B_i\}_{i\in\mathbb{N}} \subseteq \mathscr{B}(\mathbb{R}^d)$ a pairwise disjoint collection of Borel sets. The key point is that inverse images commute with set operations, thus e.g., $f^{-1}(\cup_{i\in\mathbb{N}} B_i) = \cup_{i\in\mathbb{N}} f^{-1}(B_i)$, and moreover that since the $B_i$'s are pairwise disjoint so are their inverse images through $f$. Then we write:

$$\begin{aligned}
\nu\left(\bigcup_{i=1}^{\infty} B_i\right) &= \mu\left(f^{-1}\left(\bigcup_{i=1}^{\infty} B_i\right)\right) && \text{(by definition of } \nu\text{, cf. (A.3))}\\
&= \mu\left(\bigcup_{i=1}^{\infty} f^{-1}(B_i)\right)\\
&= \sum_{i=1}^{\infty} \mu(f^{-1}(B_i)) && \text{(because } \mu \text{ is } \sigma\text{-additive)}\\
&= \sum_{i=1}^{\infty} \nu(B_i) && \text{(again by definition of } \nu\text{)}
\end{aligned}$$

and we are done.

Notice that in (A.3) the right-hand side is well defined because $f$ is measurable (hence $f^{-1}(B)$ belongs to the domain $\mathfrak{M}$ of $\mu$).

The measure $\nu$ is called the *image* of $\mu$ through $f$. It is often indicated by the notation

$$\nu = f\#\mu,$$

which is termed the *push forward* of $\mu$ (through $f$).

## A.2 Integration with Respect to an Abstract Measure

For the sake of notational simplicity, in this section we restrict ourselves to real-valued functions $f : U \to \mathbb{R}$, i.e., we set $d = 1$. However, the main ideas that we will discuss work in the same way also in higher dimensions up to reasoning componentwise.

We begin by defining the integral on the measure space $(U, \mathfrak{M}, \mu)$ of a very special class of functions.

A (real-valued) non-negative *simple function* $s$ is a measurable function $s : U \to \mathbb{R}_+$ which takes only a finite number, say $n$, of values. It can be represented as:

$$s(u) = \sum_{i=1}^{n} s_i \mathbb{1}_{A_i}(u), \tag{A.4}$$

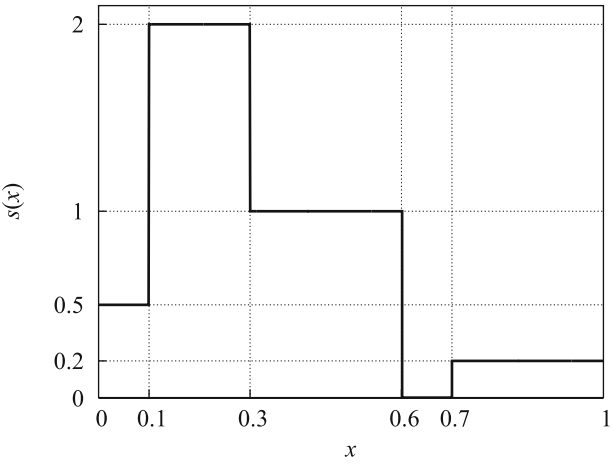


**Fig. A.2** Example of a simple function $s : \mathbb{R} \to \mathbb{R}$ taking $n = 5$ values in the interval [0, 1], particularly: $s_1 = 0.5$ in $A_1 = [0, 0.1)$, $s_2 = 2$ in $A_2 = [0.1, 0.3)$, $s_3 = 1$ in $A_3 = [0.3, 0.6)$, $s_4 = 0$ in $A_4 = [0.6, 0.7)$, and $s_5 = 0.2$ in $A_5 = [0.7, 1]$. *Solid vertical lines* are jump-type discontinuities plotted for visual reference

where (cf. Fig. A.2):

- $s_i \in \mathbb{R}_+$ is the $i$-th value taken by $s$.
- $A_i = \{u \in U : s(u) = s_i\}$ is the subset of $U$ on which $s$ takes the value $s_i$. In other words $A_i = s^{-1}(\{s_i\})$, therefore $A_i \in \mathfrak{M}$ all $i$ because $s$ is measurable[1].
- $\mathbb{1}_{A_i}$ is the characteristic function of the set $A_i$, such that $\mathbb{1}_{A_i}(u) = 1$ if $u \in A_i$, $\mathbb{1}_{A_i}(u) = 0$ if $u \notin A_i$.

**Definition A.7 (Integral of simple functions).** The *integral* of $s$ on $U$ with respect to the measure $\mu$ is the *real number*:

$$\int_U s \, d\mu := \sum_{i=1}^{n} s_i \mu(A_i). \tag{A.5}$$

This stuff is the building block for constructing the integral of more general functions. As a further intermediate step, we consider now a function $f$ which need not be simple but is still non-negative.

**Definition A.8 (Integral of non-negative functions).** The *integral* of a non-negative measurable function $f : U \to \mathbb{R}_+$ on $U$ with respect to the measure $\mu$ is the *real number* (or possibly $+\infty$):

[1] Actually, the function $s$ defined by (A.4) is measurable *if and only if* $A_i \in \mathfrak{M}$ for all $i = 1, \ldots, n$.

$$\int_U f\, d\mu := \sup\left\{ \int_U s\, d\mu \,:\, s \text{ simple and } 0 \le s \le f \right\}.$$

In practice, one approximates $f$ from below by simple functions and then takes the supremum of their integrals computed according to (A.5).

*Remark A.5 (Simple functions are dense).* In view of the procedure of approximation by simple functions implied by Definition A.8, it is useful to know that *simple functions are dense in the set of summable functions*.

We anticipate that *summable* functions are those for which $\int_U |f|\, d\mu < +\infty$ (notice that $|f|$ is a non-negative measurable function for every measurable $f$, hence its integral is constructed according to Definition A.8, see also Definition A.9 and Remark A.6 below).

In particular, the statement above holds in the sense of the pointwise convergence: If $f$ is measurable then there exists a nondecreasing sequence $\{s_i\}_{i\in\mathbb{N}}$ of simple functions such that:

- $0 \le s_1(u) \le s_2(u) \le \cdots \le f(u)$ for all $u \in U$.
- $s_i(u) \to f(u)$ when $i \to \infty$, $u \in U$.

One such sequence can be given explicitly. For all $i$ define the measurable sets:

$$A_{i,k} := f^{-1}\left((k2^{-i},\, (k+1)2^{-i})\right) \qquad (k = 0,\, 1,\, \ldots,\, 2^{2i} - 1),$$
$$B_i := f^{-1}\left((2^i,\, +\infty]\right),$$

then let:

$$s_i(u) := \sum_{k=0}^{2^{2i}-1} k2^{-i}\, \mathbb{1}_{A_{i,k}}(u) + 2^i\, \mathbb{1}_{B_i}(u), \tag{A.6}$$

see Fig. A.3.

Notice that we allow for functions possibly taking the value $+\infty$ (cf. the definition of the set $B_i$).

Finally, in order to deal with a generic measurable function $f : U \to \mathbb{R}$ taking both positive and negative values we introduce its *positive part* $f^+$ and *negative part* $f^-$, defined respectively as:

$$f^+ := \max\{0,\, f\}, \quad f^- := \max\{-f,\, 0\}.$$

Notice that both $f^+$ and $f^-$ are measurable and *non-negative*, regardless of the sign of $f$. Moreover, it is not difficult to see that the following relationship holds true:

$$f = f^+ - f^-. \tag{A.7}$$

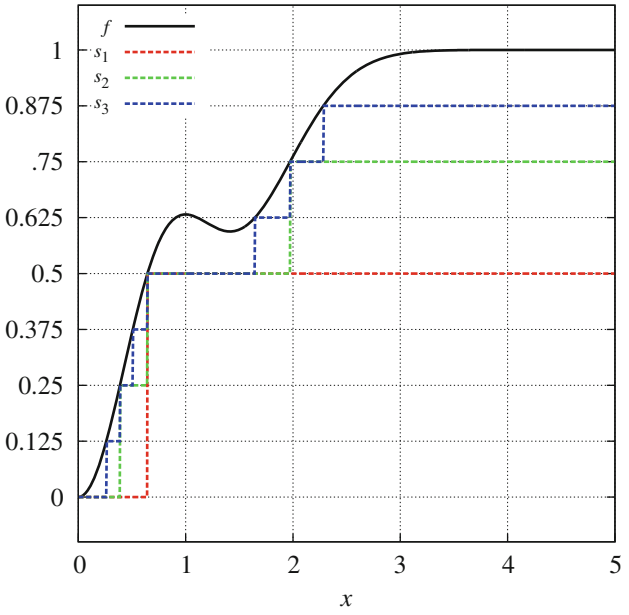


**Fig. A.3** Plot of the first three terms of the sequence of simple functions (A.6) which approximate $f(x) = 1 - (x^4 - x^2 + 1)e^{-x^2}$ (*solid black line*) in the interval $[0,\ 5]$

Thanks to Definition A.8 we are able to define the integrals on $U$ of $f^+$, $f^-$ with respect to $\mu$. Hence we use (A.7) in the obvious way to define the integral of $f$ as well.

**Definition A.9 (Integral of generic measurable functions).** The *integral* of a measurable function $f : U \to \mathbb{R}$ on $U$ with respect to the measure $\mu$ is the *real number* (or possibly $\infty$):

$$\int_U f \, d\mu := \int_U f^+ \, d\mu - \int_U f^- \, d\mu$$

provided at least one of the two terms at the right-hand side is finite so as to avoid the indeterminate form $\infty - \infty$.

If $\int_U f \, d\mu$ exists then $f$ is said to be *integrable* on $U$. If, in addition, $\int_U |f| \, d\mu < +\infty$ then $f$ is said to be *summable* on $U$.

*Remark A.6.* Since $|f| \geq 0$, its integral on $U$ with respect to $\mu$ can be constructed directly from Definition A.8. Alternatively, noting that $|f| = f^+ + f^-$, it results also:

$$\int_U |f| \, d\mu := \int_U f^+ \, d\mu + \int_U f^- \, d\mu.$$

If $\mu$ is *positive* then

$$\left| \int_U f \, d\mu \right| \leq \int_U |f| \, d\mu.$$

**Theorem A.3 (Linearity of the integral).** *Both mappings:*

$$f \mapsto \int_U f \, d\mu, \qquad \mu \mapsto \int_U f \, d\mu$$

*are linear, i.e.,*

$$\int_U (af + bg) \, d\mu = a \int_U f \, d\mu + b \int_U g \, d\mu$$
$$\int_U f \, d(a\mu_1 + b\mu_2) = a \int_U f \, d\mu_1 + b \int_U f \, d\mu_2$$

*for all* $a, b \in \mathbb{R}$*, all measurable functions* $f$*,* $g$*, and all measures* $\mu$*,* $\mu_1$*,* $\mu_2$*.*

The notion of integral set forth above is usually referred to as the *Lebesgue integral*, as opposed to the *Riemann integral* normally learned in undergraduate Calculus courses. The advantage of the former over the latter is that it offers more straightforward ways of interchanging the operations of limit and integration. This is extremely useful when we have a sequence of functions $\{f_i\}_{i \in \mathbb{N}}$, for each of which we have some information about the integral on $U$, and we want to infer something about the integral of their limit (which we might even not know explicitly).

When both Riemann and Lebesgue integrals exist for a function $f$ they coincide. However, there are functions which are not Riemann-integrable but are Lebesgue-integrable. One of such functions (actually, a very classical example) is the *Dirichlet's function* $f : \mathbb{R} \to \{0, 1\}$ defined as:

$$f(x) = \begin{cases} 1 & \text{if } x \in \mathbb{Q} \\ 0 & \text{otherwise,} \end{cases}$$

where $\mathbb{Q}$ is the set of rational numbers. Its Riemann integral on $\mathbb{R}$ with respect to the Lebesgue measure $\mathscr{L}$ does not exist while its Lebesgue integral is zero because $\mathscr{L}(\mathbb{Q}) = 0$ (compute it using (A.5)).

**Theorem A.4 (Convergence theorems for integrals).** *Let the* $f_i$*'s be measurable for all* $i = 1, 2, \ldots$

*(i)* Fatou's Lemma.

$$\int_U \left( \liminf_{i \to \infty} f_i \right) d\mu \leq \liminf_{i \to \infty} \int_U f_i \, d\mu.$$

*(ii)* Beppo Levi's Monotone Convergence Theorem. *If:*

*(a)* $0 \le f_1(u) \le f_2(u) \le \cdots \le \infty$ *for every* $u \in U$.
*(b) There exists* $f : U \to \mathbb{R}_+$ *such that* $f_i(u) \to f(u)$ *pointwise as* $i \to \infty$,

*then* $f$ *is measurable as well and:*

$$\int_U f \, d\mu = \lim_{i\to\infty} \int_U f_i \, d\mu.$$

*(iii)* Lebesgue's Dominated Convergence Theorem. *If:*

*(a) There exists* $f : U \to \mathbb{R}_+$ *such that* $f_i(u) \to f(u)$ *pointwise as* $i \to \infty$.
*(b) There exists a summable function* $g : U \to \mathbb{R}_+$ *such that* $|f_i(u)| \le g(u)$ *for every* $i = 1, 2, \ldots$ *and every* $u \in U$,

*then* $f$ *is summable and:*

$$\lim_{i\to\infty} \int_U |f - f_i| \, d\mu = 0 \quad \Rightarrow \quad \int_U f \, d\mu = \lim_{i\to\infty} \int_U f_i \, d\mu.$$

Another important property of the integral is that it behaves well with respect to the transport of measures as defined in (A.3).

**Theorem A.5 (Integrals depend only on the image measure).** *Let* $f : U \to \mathbb{R}$ *be a measurable function from* $(U, \mathfrak{M}, \mu)$ *to* $(\mathbb{R}, \mathscr{B}(\mathbb{R}), \nu)$, *where* $\nu = f\#\mu$. *Let* $g : \mathbb{R} \to \mathbb{R}$ *be another measurable function from* $(\mathbb{R}, \mathscr{B}(\mathbb{R}))$ *into itself. Then*

$$\int_U g \circ f \, d\mu = \int_{\mathbb{R}} g \, d(f\#\mu) = \int_{\mathbb{R}} g \, d\nu$$

*provided integrals exist (finite or infinite).*

## A.3 Decomposition of a Measure

Let $\mu$, $\nu$ be two positive measures on a measurable space $(U, \mathfrak{M})$.

**Definition A.10 (Support of a measure).** We say that $\mu$ is *concentrated* on a measurable set $E \in \mathfrak{M}$ if we have:

$$\mu(A) = \mu(A \cap E), \quad \forall\, A \in \mathfrak{M}.$$

If $U$ is a topological space then the smallest of such $E$ which is also closed is called the *support* of $\mu$, denoted $\mathrm{supp}(\mu)$.

**Definition A.11 (Absolutely continuous and singular measures).** We say that $\nu$ is *absolutely continuous* with respect to $\mu$, written

$$\nu \ll \mu,$$

if $\nu(A) = 0$ whenever $\mu(A) = 0$ ($A \in \mathfrak{M}$).

Conversely, we say that $\mu$, $\nu$ are *(mutually) singular*, written

$$\nu \perp \mu,$$

if they are concentrated on two disjoint measurable sets.

The interest in the concepts of absolute continuity and mutual singularity is that they are at the basis of a *representation theorem* of a measure once another measure has been fixed.

**Theorem A.6.** *Let $\mu$, $\nu$ be as above plus $\sigma$-finite.*

*(i)* Lebesgue's Decomposition Theorem. *There exists a unique pair of measures $\nu_a$, $\nu_s$ on $(U, \mathfrak{M})$ such that:*

$$\nu = \nu_a + \nu_s \quad \textit{with} \quad \nu_a \ll \mu, \quad \nu_s \perp \mu.$$

*If $\nu$ is positive and finite then so are $\nu_a$, $\nu_s$.*

*(ii)* Radon-Nikodym's Theorem. *There exists a unique non-negative function $f$, integrable on $U$ with respect to $\mu$, such that:*

$$\nu_a(A) = \int_A f \, d\mu, \quad \forall\, A \in \mathfrak{M}. \tag{A.8}$$

*The function $f$ is called the* density *of $\nu_a$ with respect to $\mu$.*

Formula (A.8) is often also written as $d\nu_a = f \, d\mu$ or even:

$$f = \frac{d\nu_a}{d\mu}.$$

Inspired by this writing, some call $f$ the *Radon-Nikodym derivative* of $\nu_a$ with respect to $\mu$. Owing to Radon-Nikodym Theorem, to say that a measure $\nu$ is absolutely continuous with respect to another measure $\mu$ means equivalently that $d\nu = f \, d\mu$ (i.e., $\nu \equiv \nu_a$, $\nu_s = 0$).

Concerning the singular part $\nu_s$, it is possible to prove that it has invariably the following form:

$$\nu_s = \nu_s^{\mathrm{pp}} + \nu_s^{\mathrm{C}},$$

where $\nu_s^{\mathrm{pp}}$ is the *pure point* part and $\nu_s^{\mathrm{C}}$ is the *Cantor part*. In particular, $\nu_s^{\mathrm{pp}}$ is a *discrete measure*, i.e., a measure concentrated on at most a countable set. If $U = \mathbb{R}^d$ and $\mu$ is the *Lebesgue measure* then $\nu_s^{\mathrm{pp}}$ is a collection of *point masses*, that is it can be written as (cf. (A.2)):

$$\nu_s^{\mathrm{pp}} = \sum_i \alpha_i \delta_{x_i},$$

where $\alpha_i \in \mathbb{R}$, $x_i \in \mathbb{R}^d$ each $i$ and the sum can be either finite or countably infinite.

## A.4 Probabilities

Abstract measure theory and probability theory speak, to a large extent, of similar issues but often with different terminologies. Each terminology is rooted in the history of the corresponding theory, and nowadays it would be impossible to unify them *de jure*. Here we simply try to establish the necessary linguistic parallelisms between the two theories.

### *A.4.1 Events, Operations with Events, and σ-Algebras*

In the language of probability, the abstract set $U$ is denoted by $\Omega$, its points by $\omega$, and it is called the *state space*. It is the set of all possible outcomes of a *random experiment*. Every subset $A$ of $\Omega$ is said to be an *event*, i.e., a property which can be observed to hold or not to hold after the random experiment is performed.

Given two events $A$, $B \subseteq \Omega$, the usual operations with sets take the following meanings:

- *Complementation*: $A^c$ is said to be the event *contrary* to $A$.
- *Intersection*: $A \cap B$ is said to be the event $A$ *and* $B$.
- *Union*: $A \cup B$ is said to be the event $A$ *or* $B$.

Moreover, $\Omega$ is also called the *sure event* and the empty set $\emptyset$ the *impossible event*. If two events $A$, $B$ are such that $A \cap B = \emptyset$ then they are said to be *incompatible*.

*Example A.3 (Tossing of two coins).* When tossing one coin the state space of the possible outcomes is $\Omega = \{\mathrm{h}, \mathrm{t}\}$ ("h" standing for *head* and "t" for *tail*). When tossing two coins, the new state space is the set of pairs $\Omega = \{(\mathrm{h}, \mathrm{h}), (\mathrm{h}, \mathrm{t}), (\mathrm{t}, \mathrm{h}), (\mathrm{t}, \mathrm{t})\}$. The event $A =$"The output of the first toss is head" can be identified with the subset $A = \{(\mathrm{h}, \mathrm{h}), (\mathrm{h}, \mathrm{t})\}$. The event $B =$"The output of the second toss is tail" is instead the set $B = \{(\mathrm{h}, \mathrm{t}), (\mathrm{t}, \mathrm{t})\}$. The event "The first toss gives head and the second one tail" is the set $A \cap B = \{(\mathrm{h}, \mathrm{t})\}$. The two events $A$, $B$ are not incompatible.

The notions of $\sigma$-algebra and of measurable space are the same as those seen in Sect. A.1.2. The only difference is that in probability theory one speaks, of course, of *families of events* rather than of subsets and usually denotes them by $\mathscr{F}$ rather than by $\mathfrak{M}$. In addition, once a $\sigma$-algebra $\mathscr{F}$ has been introduced, it is customary to understand the events as the measurable sets only, i.e., the elements of $\mathscr{F}$.

### A.4.2 Probability Measures

A *probability measure* on a measurable space $(\Omega, \mathscr{F})$ is a positive measure $P : \mathscr{F} \to \mathbb{R}_+$ like in Definition A.4 (up to the change of notation from $\mu$ to $P$) with the additional property that:

$$P(\Omega) = 1.$$

It follows that $0 \leq P(A) \leq 1$ for all $A \in \mathscr{F}$, i.e., the probability of any event is a number between 0 and 1 (this can be seen by considering that $\Omega = A \cup A^c$ and that $A$, $A^c$ are disjoint, hence $P(\Omega) = P(A) + P(A^c)$ but $P(A^c) \geq 0$ because $P$ is positive).

Any probability measure is thus a finite measure. In particular, this implies $P(\emptyset) = 0$, i.e., the probability of the impossible event is zero.

The triple $(\Omega, \mathscr{F}, P)$ is called a *probability space* (i.e., the probabilistic counterpart of a generic measure space).

### A.4.3 Random Variables

Random variables are nothing but *measurable functions* in the probabilistic language. Another difference is that they are usually denoted by $X$ rather than by $f$.

Therefore, after fixing the "physical" measurable space $(\mathbb{R}^d, \mathscr{B}(\mathbb{R}^d))$ as the destination space, a *random variable* $X : \Omega \to \mathbb{R}^d$ from the measurable space $(\Omega, \mathscr{F})$ into $(\mathbb{R}^d, \mathscr{B}(\mathbb{R}^d))$ is a mapping such that:

$$X^{-1}(B) \in \mathscr{F}, \quad \forall\, B \in \mathscr{B}(\mathbb{R}^d).$$

Notice that a random variable is *not* a "variable" in the classical analytical sense but indeed a function!

Random variables are mostly used for transporting probability measures. In particular, Theorem A.2 still holds with the function $f$ replaced by $X$ and the measure space $(U, \mathfrak{M}, \mu)$ by the probability space $(\Omega, \mathscr{F}, P)$. In addition, it is immediate to check that the image measure $\nu = X\#P$ is a probability on $\mathbb{R}^d$, i.e., $\nu(\mathbb{R}^d) = 1$. Such a $\nu$ is called the *law* of the random variable $X$.

If $B$ is any Borel set of $\mathbb{R}^d$, one may ask what is the probability that a random variable $X$ takes values in $B$. This actually corresponds to the event $A = \{\omega \in \Omega : X(\omega) \in B\} = X^{-1}(B) \in \mathscr{F}$, hence, owing to the push forward # linking $P$ and $\nu$, $P(A) = \nu(B)$. Therefore, if the law of $X$ is known, one can compute probabilities of events involving $X$ directly on the space of the values taken by $X$.

### A.4.4 Integrals of Random Variables

Since random variables are ultimately measurable functions, it is possible to introduce for them, too, the notion of (Lebesgue) integral on $\Omega$, which is constructed by following slavishly the procedure reviewed in Sect. A.2.

In this context we want to pause in particular over the consequences of Theorem A.5, which we restate here with the new "probabilistic" notation for the sake of convenience. Again, we confine our attention to *scalar* random variables, i.e., we set $d = 1$ for simplicity. In higher dimensions it is basically sufficient to argue componentwise.

**Theorem A.7 (cf. Theorem A.5).** *Let $X : \Omega \to \mathbb{R}$ be a random variable from $(\Omega, \mathscr{F}, P)$ to $(\mathbb{R}, \mathscr{B}(\mathbb{R}), \nu)$, where $\nu = X\#P$. Let $g : \mathbb{R} \to \mathbb{R}$ be another measurable function from $(\mathbb{R}, \mathscr{B}(\mathbb{R}))$ into itself. Then*

$$\int_\Omega g \circ X \, dP = \int_{\mathbb{R}} g \, d(X\#P) = \int_{\mathbb{R}} g \, d\nu \tag{A.9}$$

*provided integrals exist (finite or infinite).*

This theorem says that integrals on $\Omega$ can be computed as integrals on $\mathbb{R}$, i.e., on the space where $X$ takes its values. All one needs to know is again the law of $X$, namely the measure $\nu$. Notice that it is even not necessary to know the expression of $X$! For this reason, probabilistic models are usually constructed on the "physical" space by characterizing random variables through their laws. The state space $\Omega$, the original probability $P$, and the random variable $X$ itself are ignored in practice, they remain only at a conceptual level for grounding the theory.

If in (A.9) we take $g(x) = x$ we get:

$$\mathbb{E}[X] := \int_\Omega X(\omega) \, dP(\omega) = \int_{\mathbb{R}} x \, d\nu(x).$$

This number is called the *expectation* (or *expected value*, or *average*) of $X$. It is the *first statistic moment* of $X$.

Taking $g(x) = x^2$ we get instead the *second statistic moment* of $X$:

$$\mathbb{E}\left[X^2\right] := \int_\Omega X^2(\omega) \, dP(\omega) = \int_{\mathbb{R}} x^2 \, d\nu(x)$$

and

$$\mathrm{Var}[X] := \mathbb{E}\left[X^2\right] - \mathbb{E}\left[X\right]^2$$

is the *variance* of $X$. With a few algebraic manipulations it can also be written as

$$\mathrm{Var}[X] = \mathbb{E}\left[(X - \mathbb{E}\left[X\right])^2\right],$$

whence it can be seen that it is a non-negative quantity.

In general, the *p-th statistical moment* of $X$ is:

$$\mathbb{E}\left[X^p\right] := \int_\Omega X^p(\omega)\, dP(\omega) = \int_{\mathbb{R}} x^p\, d\nu(x).$$

When looking at the last integral, without reference to any random variable, this number is also called the *p-th moment of the measure* $\nu$.

## A.5 Product Spaces, Marginals, and Disintegration of a Measure

In this section we temporarily resume the notation of real measure theory for the sake of generality. Indeed it is a mainly technical fact that the measures involved are probabilities, the most important point being actually that they are finite. Everything can be restated for finite measures as well, up to a proper rescaling.

Let $(U, \mathfrak{M}_U)$, $(V, \mathfrak{M}_V)$ be two measurable spaces, $U$, $V$ being abstract sets. The *Cartesian product* of $U$ and $V$, denoted $U \times V$, is the set of *ordered* pairs of elements of $U$ and $V$:

$$U \times V := \{(u, v) \,:\, u \in U,\ v \in V\}.$$

We equip it with the $\sigma$-algebra $\mathfrak{M} := \sigma(\mathfrak{M}_U \otimes \mathfrak{M}_V)$, i.e., the one generated by Cartesian products of measurable subsets of $U$ and $V$, to form the new measurable space $(U \times V, \mathfrak{M})$. On the latter we introduce then a probability $\mu$, which induces the following two probabilities on $(U, \mathfrak{M}_U)$, $(V, \mathfrak{M}_V)$, respectively:

$$\begin{aligned} \tilde{\mu}_U(A) &:= \mu(A \times V), \qquad \forall\, A \in \mathfrak{M}_U \\ \tilde{\mu}_V(B) &:= \mu(U \times B), \qquad \forall\, B \in \mathfrak{M}_V. \end{aligned} \tag{A.10}$$

They are called the *marginals* of $\mu$ on $U$, $V$, respectively.

Another way to obtain marginals is by pushing $\mu$ forward properly. If

$$\begin{aligned} \pi_U &: U \times V \to U, \qquad \pi_U(u, v) := u, \\ \pi_V &: U \times V \to V, \qquad \pi_V(u, v) := v, \end{aligned}$$

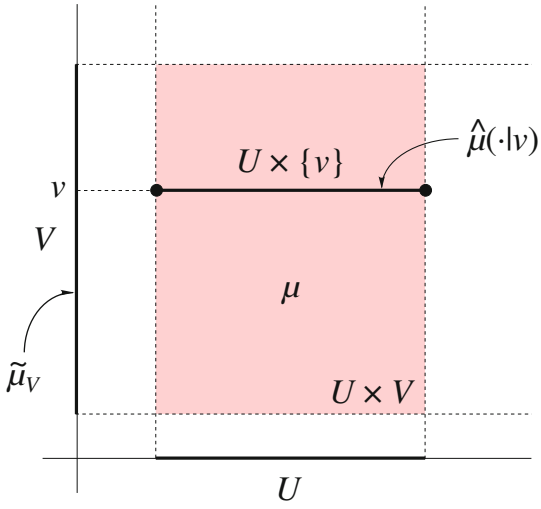


**Fig. A.4** Sketch of the main actors of Theorem A.8

are the *canonical projections* of $U \times V$ onto $U$ and $V$, respectively, then $\tilde{\mu}_U$, $\tilde{\mu}_V$ are also recovered as:

$$\tilde{\mu}_U = \pi_U \# \mu, \qquad \tilde{\mu}_V = \pi_V \# \mu.$$

When dealing with integrals over a product space, such as e.g.,

$$\iint_{U \times V} f(u, v)\, d\mu(u, v), \tag{A.11}$$

it is quite natural to ask whether they can be computed *iteratively*, i.e., by integrating first on $U$ (with $v$ fixed) and then finally on $V$ (or vice versa), by means of suitable probabilities "living" on $(U, \mathfrak{M}_U)$ and $(V, \mathfrak{M}_V)$. The answer is affirmative but the two probabilities to be used are in general *not* the marginals of $\mu$. Actually one of them can be a marginal while the other one is normally not the other marginal. The precise statement is provided by the following theorem (keep at hand also Fig. A.4):

**Theorem A.8 (Disintegration of a measure).** *In the setting above, consider the probability $\mu$ on $(U \times V, \mathfrak{M})$ and its marginal $\tilde{\mu}_V = \pi_V \# \mu$ on $(V, \mathfrak{M}_V)$. For $\tilde{\mu}_V$-almost every $v \in V$ (i.e., up to possibly some points $v$ forming a subset of $V$ of zero $\tilde{\mu}_V$ measure) there exists a unique probability measure $\hat{\mu}(\cdot|v)$ on $(U \times V, \mathfrak{M})$, parameterized by $v$, such that:*

- *For every $A \in \mathfrak{M}$ the mapping $v \mapsto \hat{\mu}(A|v)$ is measurable from $(V, \mathfrak{M}_V)$ to $(\mathbb{R}, \mathscr{B}(\mathbb{R}))$.*
- *The probability $\hat{\mu}(\cdot|v)$ is actually concentrated on the fiber $\pi_V^{-1}(\{v\}) = U \times \{v\}$, that is $\hat{\mu}(A|v) = \hat{\mu}(A \cap (U \times \{v\})|v)$ for every $A \in \mathfrak{M}$.*

- *For every Borel-measurable function* $f : (U \times V, \mathfrak{M}) \to (\mathbb{R}, \mathscr{B}(\mathbb{R}))$ *the integral* (A.11) *can be computed iteratively first on the fiber* $U \times \{v\}$ *with respect to* $\hat{\mu}(\cdot|v)$*, keeping* $v$ *fixed, and then on* $V$ *with respect to* $\tilde{\mu}_V$*:*

$$\iint_{U\times V} f(u,\, v)\, d\mu(u,\, v) = \int_V \left( \int_{U\times\{v\}} f(u,\, v)\, d\,\hat{\mu}(u|v) \right) d\,\tilde{\mu}_V(v). \tag{A.12}$$

It is worth noticing that each of the fibers $\pi_V^{-1}(\{v\}) = U \times \{v\}$ can be canonically identified with $U$ itself, thus $\hat{\mu}(\cdot|v)$ can be identified with a probability on $(U, \mathfrak{M}_U)$ for ($\tilde{\mu}_V$-almost) every $v \in V$. Consequently, (A.12) can also be read in the more intuitive form:

$$\iint_{U\times V} f(u,\, v)\, d\mu(u,\, v) = \int_V \left( \int_U f(u,\, v)\, d\,\hat{\mu}(u|v) \right) d\,\tilde{\mu}_V(v).$$

The disintegration of $\mu$ in $\hat{\mu}(\cdot|v)$ and $\tilde{\mu}_V$ is often written as

$$\mu(du\, dv) = \hat{\mu}(du\,|v) \otimes \tilde{\mu}_V(dv),$$

which recalls that the measure $\mu$ of the infinitesimal volume $du\, dv$ centered at $(u,\, v)$ in the product space $U \times V$ is evaluated by multiplying the measure $\hat{\mu}(\cdot|v)$ of $du \subset U$ along the $v$-fiber $U \times \{v\}$ and the marginal measure $\tilde{\mu}_V$ of $dv \subset V$. This idea is indeed at the basis of a well-known formula for computing the area or volume of subsets of $\mathbb{R}^2$, $\mathbb{R}^3$, respectively, as shown by the next example.

*Example A.4.* If, for $A \in \mathfrak{M}$, we take $f(u,\, v) = \mathbb{1}_A(u,\, v)$, the indicator function of $A$, then from (A.12) we discover:

$$\mu(A) = \int_V \hat{\mu}(A|v)\, d\,\tilde{\mu}_V(v) = \int_V \hat{\mu}(A \cap (U \times \{v\})|v)\, d\,\tilde{\mu}_V(v). \tag{A.13}$$

Let $U = V = [0,\, 1] \subset \mathbb{R}$ and $\mu = \mathscr{L}^2$ (the Lebesgue measure on $[0,\, 1] \times [0,\, 1]$, which we incidentally notice is there a probability). Then it can be seen that $\tilde{\mu}_V = \mathscr{L}$ (the Lebesgue measure on $[0,\, 1]$, in turn a probability) and moreover, using the more customary letter $y$ in place of $v$ for the variable of the vertical axis in the plane, that $\hat{\mu}(\cdot|y) = \mathscr{L}(\cdot \cap ([0,\, 1] \times \{y\}))$. Hence (A.13) becomes:

$$\mathscr{L}^2(A) = \int_0^1 \mathscr{L}(A \cap ([0,\, 1] \times \{y\}))\, dy,$$

namely the formula for computing the area of a two-dimensional set by integrating parallel to the horizontal axis (see Fig. A.5) normally learned in basic Calculus.

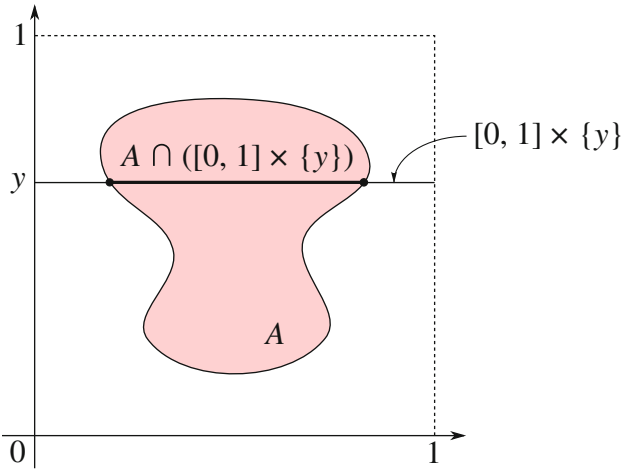


**Fig. A.5** The area of $A$ can be conceptually computed by "summing" the lengths of the segments obtained by cutting $A$ with *straight lines* parallel to the horizontal axis

## *Conditional Probability*

We now rephrase the discussion above in a markedly probabilistic spirit and draw some noticeable consequences.

Given two random variables $X, Y : (\Omega, \mathscr{F}, P) \to (\mathbb{R}^d, \mathscr{B}(\mathbb{R}^d))$, we construct the further random variable:

$$\begin{aligned} Z := (X, Y) : \Omega &\to \mathbb{R}^d \times \mathbb{R}^d \\ \omega &\mapsto (X(\omega), Y(\omega)), \end{aligned}$$

which takes values in the product space $\mathbb{R}^d \times \mathbb{R}^d$ (endowed with the Borel $\sigma$-algebra $\mathscr{B}(\mathbb{R}^d \times \mathbb{R}^d)$), and we denote by $\nu := Z\#P$ its law on $(\mathbb{R}^d \times \mathbb{R}^d, \mathscr{B}(\mathbb{R}^d \times \mathbb{R}^d))$.

First we claim that *the marginals of* $\nu$ *on* $(\mathbb{R}^d, \mathscr{B}(\mathbb{R}^d))$ *are the laws of* $X, Y$, respectively. To see this, let us consider for instance the marginal with respect to the second component of $Z$, which we call $\tilde{\nu}_Y$ (the reasoning for the first component is completely analogous). Then for all $A \in \mathscr{B}(\mathbb{R}^d)$ we have:

$$\begin{aligned} \tilde{\nu}_Y(A) &= \nu(\mathbb{R}^d \times A) && \text{(by (A.10))} \\ &= P(\{\omega \in \Omega \,:\, Z(\omega) \in \mathbb{R}^d \times A\}) && \text{(by definition of law of } Z) \\ &= P(\{\omega \in \Omega : X(\omega) \in \mathbb{R}^d\} \cap \{\omega \in \Omega : Y(\omega) \in A\}) && \text{(because } Z = (X, Y)) \\ &= P(\Omega \cap \{\omega \in \Omega \,:\, Y(\omega) \in A\}) && \text{(because } X \text{ is } \mathbb{R}^d\text{-valued}) \\ &= P(Y \in A). \end{aligned}$$

Second, by applying Theorem A.8 to $\nu$ we discover that there exists a probability measure $\hat{\nu}(\cdot|y)$ on $(\mathbb{R}^d \times \mathbb{R}^d, \mathscr{B}(\mathbb{R}^d \times \mathbb{R}^d))$, but actually concentrated on $\mathbb{R}^d \times \{y\}$, such that:

$$\nu(dx\,dy) = \hat{\nu}(dx\,|\,y) \otimes \tilde{\nu}_Y(dy), \tag{A.14}$$

hence:

$$\iint_{\mathbb{R}^d \times \mathbb{R}^d} f(x,\ y)\, d\nu(x,\ y) = \int_{\mathbb{R}^d} \left( \int_{\mathbb{R}^d} f(x,\ y)\, d\hat{\nu}(x|y) \right) d\tilde{\nu}_Y(y) \tag{A.15}$$

for all Borel-measurable function $f : \mathbb{R}^d \times \mathbb{R}^d \to \mathbb{R}$.

The measure $\hat{\nu}(\cdot|y)$ is called the *conditional law* of $X$ given $Y$ (or the law of $X$ *conditioned to* $Y$). The quantity:

$$\mathbb{E}[X|Y] := \int_{\mathbb{R}^d} x\, d\hat{\nu}(x|y)$$

is a function of $y$ called the *conditional expectation* of $X$ given $Y$. Remarkably:

$$\begin{aligned}
\mathbb{E}[\mathbb{E}[X|Y]] &= \int_{\mathbb{R}^d} \mathbb{E}[X|Y]\ d\tilde{\nu}_Y(y) \text{ (because } \mathbb{E}[X|Y] \text{ is a function of } Y, \text{ cf. (A.9))} \\
&= \int_{\mathbb{R}^d} \left( \int_{\mathbb{R}^d} x\, d\hat{\nu}(x|y) \right) d\tilde{\nu}_Y(y) \qquad \text{(by definition of } \mathbb{E}[X|Y]) \\
&= \iint_{\mathbb{R}^d \times \mathbb{R}^d} x\, d\nu(x,\ y) \qquad \text{(by (A.15))} \\
&= \int_{\mathbb{R}^d} \left( \int_{\mathbb{R}^d} x\, d\hat{\nu}(y|x) \right) d\tilde{\nu}_X(x) \quad \text{(by (A.14) interchanging } X \text{ and } Y) \\
&= \int_{\mathbb{R}^d} x\hat{\nu}(\mathbb{R}^d|x)\, d\tilde{\nu}_X(x) \\
&= \int_{\mathbb{R}^d} x\, d\tilde{\nu}_X(x) = \mathbb{E}[X] \qquad \text{(because } \hat{\nu}(\cdot|x) \text{ is a probability).}
\end{aligned}$$

## A.6 Wasserstein Distance in Probability Spaces

Starting from this section we will mostly forget about the abstract probability space $(\Omega, \mathscr{F}, P)$ and work directly with the "physical" probability space $(\mathbb{R}^d, \mathscr{B}(\mathbb{R}^d), \nu)$ without even invoking explicitly the random variable $X$ linking them.

For $p \geq 1$, let $\mathscr{P}_p(\mathbb{R}^d)$ be the space of probability measures $\nu$ on $\mathbb{R}^d$ with finite $p$-th moment, i.e.:

$$\int_{\mathbb{R}^d} |x|^p \, d\nu(x) < +\infty.$$

Notice that $\mathscr{P}_p(\mathbb{R}^d)$ is *not* a vector space, as for example the sum of two probability measures $\nu_1$, $\nu_2$ is not a probability measure (indeed $(\nu_1 + \nu_2)(\mathbb{R}^d) = \nu_1(\mathbb{R}^d) + \nu_2(\mathbb{R}^d) = 2 \neq 1$).

Nevertheless, it is possible to introduce a *distance* in $\mathscr{P}_p(\mathbb{R}^d)$, which measures "how far" two probabilities are from each other.

**Definition A.12 (Wasserstein distance).** The *p-th Wasserstein distance* in $\mathscr{P}_p(\mathbb{R}^d)$ is the mapping $W_p : \mathscr{P}_p(\mathbb{R}^d) \times \mathscr{P}_p(\mathbb{R}^d) \to \mathbb{R}_+$ defined as:

$$W_p(\nu_1, \nu_2) := \left( \inf_{\gamma \in \Gamma(\nu_1, \nu_2)} \iint_{\mathbb{R}^d \times \mathbb{R}^d} |y - x|^p \, d\gamma(x, y) \right)^{1/p}, \tag{A.16}$$

where $\Gamma(\nu_1, \nu_2)$ is the set of all probability measures on the measurable space $(\mathbb{R}^d \times \mathbb{R}^d, \mathscr{B}(\mathbb{R}^d \times \mathbb{R}^d))$ whose marginals are $\nu_1$, $\nu_2$.

In formula (A.16) of Definition A.12, any measure $\gamma \in \Gamma(\nu_1, \nu_2)$, i.e., with marginals $\nu_1$, $\nu_2$, is also called a *transference plan* between $\nu_1$ and $\nu_2$. The reason is that the double integral in (A.16) expresses the global *cost* for transferring the mass distribution carried by $\nu_1$ into the mass distribution carried by $\nu_2$. Specifically, the elementary cost needed for transferring the infinitesimal mass $d\nu_1(x)$ in $x$ to the infinitesimal mass $d\nu_2(y)$ in $y$ is expressed in terms of (the $p$-th power of) the distance $|y - x|$ between the origin and destination points. Aside from the $p$-th power, the Wasserstein distance $W_p$ is thus the optimal (i.e., minimum) of such costs.

For $p = 1$, the *first Wasserstein distance* in $\mathscr{P}_1(\mathbb{R}^d)$ is:

$$W_1(\nu_1, \nu_2) = \inf_{\gamma \in \Gamma(\nu_1, \nu_2)} \iint_{\mathbb{R}^d \times \mathbb{R}^d} |y - x| \, d\gamma(x, y).$$

Owing to the *Kantorovich-Rubinstein's duality*, an alternative sometimes more practical expression of $W_1$ is:

$$W_1(\nu_1, \nu_2) = \sup_{\varphi \in \mathrm{Lip}_1(\mathbb{R}^d)} \int_{\mathbb{R}^d} \varphi \, d(\nu_2 - \nu_1)$$

where:

$$\mathrm{Lip}_1(\mathbb{R}^d) := \{\varphi : \mathbb{R}^d \to \mathbb{R} \, : \, \varphi \text{ is Lipschitz continuous with } \mathrm{Lip}(\varphi) \leq 1\}.$$

The importance of Wasserstein distances is that they provide the spaces $\mathscr{P}_p(\mathbb{R}^d)$ with a useful functional structure. Indeed:

**Theorem A.9.** *For any $p \geq 1$ the Wasserstein distance $W_p$ introduced in Definition A.12 is a metric on $\mathscr{P}_p(\mathbb{R}^d)$, i.e., it satisfies the axioms of a metric.*

*In addition, $\mathscr{P}_p(\mathbb{R}^d)$ endowed with $W_p$ is a separable Banach space.*

## A.7 Measures as Distributions

An alternative approach to finite positive measures (hence, in particular, to probability measures) is from the side of *distributions*. Combined with the one presented in the previous sections, this point of view is a powerful tool for tackling measure-valued differential equations and their proper weak formulation. Within this perspective, we set our forthcoming discussion in the "physical" measurable space $(\mathbb{R}^d, \mathscr{B}(\mathbb{R}^d))$.

In Functional Analysis, distributions are defined as the elements of the dual space of $C_c^\infty(\mathbb{R}^d)$, where:

$$C_c^\infty(\mathbb{R}^d) := \{\phi : \mathbb{R}^d \to \mathbb{R} \,:\, \phi \in C^\infty(\mathbb{R}^d) \text{ with compact support}\}.$$

Functions belonging to $C_c^\infty(\mathbb{R}^d)$ are called *test functions*. The space of distributions is instead usually denoted by $\mathscr{D}'(\mathbb{R}^d)$. This notation comes from the fact that the space $C_c^\infty(\mathbb{R}^d)$ is sometimes also denoted by $\mathscr{D}(\mathbb{R}^d)$, thus $\mathscr{D}'$ would stand for its dual.

Any distribution $\Phi \in \mathscr{D}'(\mathbb{R}^d)$ is therefore a bounded linear functional on $C_c^\infty(\mathbb{R}^d)$. Its action on a test function $\phi$ is denoted by[2] $\langle \Phi, \phi \rangle$, called a *duality form*. Hence we have:

- $\langle \Phi, a\phi + b\psi \rangle = a\langle \Phi, \phi \rangle + b\langle \Phi, \psi \rangle$ for all $a, b \in \mathbb{R}$ and $\phi, \psi \in C_c^\infty(\mathbb{R}^d)$.
- $|\langle \Phi, \phi \rangle| \leq \mathscr{C}\|\phi\|_\infty$ for all $\phi \in C_c^\infty(\mathbb{R}^d)$, where $\mathscr{C}$ is a constant independent of $\phi$ and $\|\phi\|_\infty := \max_{x \in \mathbb{R}^d} |\phi(x)|$ is the $\infty$-norm of $\phi$ in $C_c^\infty(\mathbb{R}^d)$.

In addition, we say that a distribution (and, more in general, a linear functional) $\Phi$ is *positive* if

$$\phi(x) \geq 0 \quad \forall\, x \in \mathbb{R}^d \;\Rightarrow\; \langle \Phi, \phi \rangle \geq 0.$$

When $\Phi$ is a finite positive measure, say $\mu$, on $(\mathbb{R}^d, \mathscr{B}(\mathbb{R}^d))$ the duality pairing between $\mu$ and a test function $\phi$ is defined to be:

$$\langle \mu, \phi \rangle := \int_{\mathbb{R}^d} \phi \, d\mu. \tag{A.17}$$

[2] Other notations also frequently used are $\Phi(\phi)$ and $\Phi\phi$.

The mapping $\phi \mapsto \int_{\mathbb{R}^d} \phi \, d\mu$ is indeed a bounded linear functional on $C_c^\infty(\mathbb{R}^d)$. Linearity is obvious because the integral is linear with respect to the integrand, whereas boundedness follows from the finiteness of $\mu$: $|\langle \mu, \phi \rangle| \leq \mu(\mathbb{R}^d)\|\phi\|_\infty$.

Formula (A.17) is remarkable because it is the building block of an important theorem, which states that virtually "all" positive linear functionals can actually be represented by integrals with respect to a positive measure:

**Theorem A.10 (Riesz's Representation Theorem).** *Let $C_c(\mathbb{R}^d)$ be the space of continuous functions with compact support in $\mathbb{R}^d$ and let $\Phi$ be a positive linear functional on it. Then there exist a $\sigma$-algebra $\mathfrak{M}$, which contains $\mathscr{B}(\mathbb{R}^d)$, and a unique positive measure $\mu$ on $(\mathbb{R}^d, \mathfrak{M})$ such that:*

$$\langle \Phi, \phi \rangle = \int_{\mathbb{R}^d} \phi \, d\mu, \quad \forall \, \phi \in C_c(\mathbb{R}^d).$$

Notice that $C_c(\mathbb{R}^d)$ contains $C_c^\infty(\mathbb{R}^d)$ as a proper subset, hence not all positive distributions in $\mathscr{D}'(\mathbb{R}^d)$ are actually measures (because the dual of $C_c(\mathbb{R}^d)$, for which Riesz's Theorem holds, is smaller than $\mathscr{D}'(\mathbb{R}^d)$). However, those positive distributions whose action is well defined also on continuous (albeit not necessarily infinitely differentiable) functions compactly supported in $\mathbb{R}^d$ are indeed measures (but Riesz's Theorem does not say how to obtain in practice $\mu$ out of the knowledge of $\Phi$).

*Example A.5 (Dirac delta).* In Example A.2 we introduced the Dirac measure defined by (A.2). In view of (A.17), it makes sense to ask whether we can read it also as a distribution and, in such a case, how we can define its action on test functions. For this, we essentially need to be able to compute integrals with respect to the Dirac measure.

We begin by fixing a point $x_0 \in \mathbb{R}^d$ and denoting by $\delta_{x_0}$ the Dirac measure concentrated in $x_0$. Given a simple function $s$ like in (A.4) (with $U = \mathbb{R}^d$), we can assume that the $A_i$'s form a pairwise disjoint partition of $\mathbb{R}^d$ (up to possibly including among them a "big" set where $s$ is zero), so that there is exactly one of them, say $A_{i_0}$, which contains $x_0$. Then, according to (A.5), the integral of $s$ on $\mathbb{R}^d$ with respect to $\delta_{x_0}$ is:

$$\int_{\mathbb{R}^d} s \, d\delta_{x_0} = \sum_{i=1}^{n} s_i \delta_{x_0}(A_i) = s_{i_0} = s(x_0),$$

considering that $\delta_{x_0}(A_i) = 0$ for all $i \neq i_0$ and $\delta_{x_0}(A_{i_0}) = 1$.

Next, let $\phi \in C_c^\infty(\mathbb{R}^d)$ be a non-negative test function. We construct $\int_{\mathbb{R}^d} \phi \, d\delta_{x_0}$ on the basis of Definition A.8:

$$\int_{\mathbb{R}^d} \phi \, d\delta_{x_0} = \sup\{s(x_0) \, : \, s \text{ simple and } 0 \leq s \leq \phi\}. \tag{A.18}$$

Notice that $s(x_0) \leq \phi(x_0)$. However, simple functions being dense among summable functions[3] in terms of pointwise convergence (cf. Remark A.5), for every $\epsilon > 0$ there exists $s_\epsilon$, among the simple functions which approximate $\phi$ at the right-hand side of (A.18), such that $|\phi(x_0) - s_\epsilon(x_0)| < \epsilon$. Therefore the sought supremum cannot be strictly less than $\phi(x_0)$ and we conclude:

$$\int_{\mathbb{R}^d} \phi \, d\delta_{x_0} = \phi(x_0), \qquad \forall\, \phi \in C_c^\infty(\mathbb{R}^d),\ \phi \geq 0.$$

Finally, for a generic $\phi \in C_c^\infty(\mathbb{R}^d)$ we use Definition A.9 with positive and negative parts to discover:

$$\int_{\mathbb{R}^d} \phi \, d\delta_{x_0} = \int_{\mathbb{R}^d} \phi^+ \, d\delta_{x_0} - \int_{\mathbb{R}^d} \phi^- \, d\delta_{x_0} = \phi^+(x_0) - \phi^-(x_0) = \phi(x_0).$$

Ultimately, we can read the Dirac measure as a distribution according to (A.17), its action on test functions being defined as:

$$\langle \delta_{x_0}, \phi \rangle := \phi(x_0), \qquad \forall\, \phi \in C_c^\infty(\mathbb{R}^d).$$

The *distribution* $\delta_{x_0}$ is often called the *Dirac delta*.

## A.8 Bibliographical Notes

Sections A.1–A.3 and A.7 A very good reference for real (and complex) analysis issues related to measure theory is the book by Rudin [154].

Section A.4 A nice introduction to probability theory soundly grounded on measure theory can be found in the textbook by Jacod and Protter [105].

Sections A.5 and A.6 A technical reference for more general statements of the disintegration theorem (Theorem A.8), as well as for advanced topics in optimal transportation, is the book by Ambrosio et al. [6], see also the books by Villani [166, 167]. Notice that the Wasserstein metric measures the distance between *probability* measures or, in a broader sense, between finite measures carrying the *same* total mass. Nevertheless, in applications one can face problems involving measures with different total mass (especially if one cannot rely on the principle of conservation of mass). A technique to extend the notion of Wasserstein distance also to these cases is proposed by Piccoli and Rossi [142].

[3] Notice that any test function $\phi$ is certainly summable with respect to the Dirac measure (although at this stage we still do not know how its integral is defined) because it is bounded. In fact: $\int_{\mathbb{R}^d} |\phi| \, d\delta_{x_0} \leq \|\phi\|_\infty \delta_{x_0}(\mathbb{R}^d) = \|\phi\|_\infty < +\infty$.

# Appendix B
# Pseudo-code for the Multiscale Algorithm

**Abstract** This appendix reports a pseudo-code for the multiscale algorithm described in Chap. 5 and used to produce all of the simulations presented in Chaps. 2 and 8. The pseudo-code is structured in a main body, which keeps track of the temporal iterations, plus a few additional functions called by the main body, which perform specific tasks at each time iteration like computing the microscopic and macroscopic components of the total transport velocity and updating the numerical solution. This pseudo-code is intended as a support for the logical organization of a real machine-executable code to be implemented in one's own favorite programming language.

## B.1 Preliminaries

We present here a pseudo-code for the basic multiscale algorithm described in Chap. 5. Functions called from the main code are denoted by F1, F2, F3. To avoid cumbersome notations, only the one-dimensional version of the code is presented, except for the function F3, which is presented also in two dimensions. The code is not intended for optimized usage in terms of CPU time or memory allocation.

For any $a \in \mathbb{R}$, and $i, j \in \mathbb{Z}$, we define

$$a^+ := \begin{cases} a & \text{if } a \geq 0 \\ 0 & \text{if } a < 0, \end{cases} \qquad a^- := \begin{cases} -a & \text{if } a \leq 0 \\ 0 & \text{if } a > 0, \end{cases} \qquad \delta_{ij} := \begin{cases} 1 & \text{if } i = j \\ 0 & \text{if } i \neq j. \end{cases}$$

We use the following indexes:

E. Cristiani et al., *Multiscale Modeling of Pedestrian Dynamics*, MS&A 12,
DOI 10.1007/978-3-319-06620-2,

| | |
|---|---|
| $k$ | for microscopic pedestrians |
| $i$ (and $j$, in 2D) | for spatial cells |
| $r$ (and $s$, in 2D) | for auxiliary indexes for spatial cells |
| $n$ | for time steps |

For the reader's convenience, we recall here the expressions of the approximate multiscale velocity at a generic point $x$ and time $t_n$:

$$v[\tilde{\mu}_n](x) = v_{\mathrm{d}}(x) + \theta \underbrace{\sum_{\substack{k=1,\dots,N \\ X_n^k \neq x}} f(|X_n^k - x|) g(\alpha_{x X_n^k}) \frac{X_n^k - x}{|X_n^k - x|}}_{:=\varphi(x)} + (1-\theta)\Lambda \underbrace{\sum_{j \in \mathbb{Z}^d} \rho_j^n \int_{E_j} f(|y-x|) g(\alpha_{xy}) \frac{y-x}{|y-x|}\, dy}_{:=\psi(x)} \quad \text{(B.1)}$$

## B.2 The Pseudo-code

**Grid definition**
Spatial domain $\Omega$,
final time $T$,
space step $\Delta x$,
time step $\Delta t$,
number of space steps $N_x$,
number of time steps $N_t$,
number of pedestrians $N_p$,
vector of space nodes $x = (x_1, \dots, x_{N_x})$.
In 2D, define also $\Delta y$, $N_y$, and $y$ in analogous manner.

**Data structures**

| Name | Type | Size | Symbol (from Chap. 5) |
|---|---|---|---|
| `v_desired` | Vector | $N_x$ | $v_{\mathrm{d}}$ |
| `v_micro` | Vector | $N_p$ | $v_{\mathrm{i}}^{\text{micro},k}$ |
| `v_micro_for_micro` | Vector | $N_p$ | $v_{\mathrm{i}}^{\text{micro-for-micro},k}$ |
| `v_micro_for_macro` | Vector | $N_x$ | $v_{\mathrm{i}}^{\text{micro-for-macro},i}$ |
| `v_macro` | Vector | $N_x$ | $v_{\mathrm{i}}^{\text{macro},i}$ |
| `v_macro_for_macro` | Vector | $N_x$ | $v_{\mathrm{i}}^{\text{macro-for-macro},i}$ |
| `v_macro_for_micro` | Vector | $N_p$ | $v_{\mathrm{i}}^{\text{macro-for-micro},k}$ |
| `rho` | Matrix | $N_t \times N_x$ | $\rho$ |
| `X` | Matrix | $N_t \times N_p$ | $X$ |

**Algorithm 1:** MAIN code

**Initial conditions**
$n \leftarrow 1$
**for** $k = 1, \ldots, N_p$ **do**
  | $\texttt{X}(n, k) \leftarrow$ user's choice;
**end**
**for** $i = 1, \ldots, N_x$ **do**
  | $\texttt{rho}(n, k) \leftarrow \frac{\text{number of agents around cell } i}{\text{maximum number of agents around cell } i}$;
**end**

**Computation**
**for** $n = 1, \ldots, N_t$ **do**
  | F1 compute `v_micro_for_micro` and `v_micro_for_macro`;
  | F2 compute `v_macro_for_macro` and `v_macro_for_micro`;
  | **for** $i = 1, \ldots, N_x$ **do**
  |  | $\texttt{v\_macro}(i) \leftarrow \theta\ \texttt{v\_micro\_for\_macro}(i) +$
  |  |  $(1-\theta)\Lambda\ \texttt{v\_macro\_for\_macro}(i) + \texttt{v\_desired}(i)$;
  | **end**
  | **for** $k = 1, \ldots, N_p$ **do**
  |  | find cell $i_k$ containing the position $\texttt{X}(n, k)$ of agent $k$;
  |  | $\texttt{v\_micro}(k) \leftarrow \theta\ \texttt{v\_micro\_for\_micro}(k) +$
  |  |  $(1-\theta)\Lambda\ \texttt{v\_macro\_for\_micro}(k) + \texttt{v\_desired}(i_k)$;
  | **end**
  | check if $\Delta t$ satisfies CFL condition (5.40) (or use a variable $\Delta t$);
  | $\texttt{X}(n+1, k) \leftarrow \texttt{X}(n, k) + \Delta t\ \texttt{v\_micro}(k)$;
  | F3 update `rho`;
**end**

**Algorithm 2:** Function F1

**for** $k = 1, \ldots, N_p$ **do**
  | $\texttt{v\_micro\_for\_micro}(k) \leftarrow$ evaluate $\varphi$ for $x = \texttt{X}(n, k)$;
**end**
**for** $i = 1, \ldots, N_x$ **do**
  | $\texttt{v\_micro\_for\_macro}(i) \leftarrow$ evaluate $\varphi$ for $x = x_i$;
**end**

**Algorithm 3:** Function F2

**for** $i = 1, \ldots, N_x$ **do**
  v_macro_for_macro($i$) $\leftarrow$ evaluate $\psi$ for $x = x_i$;
**end**
**for** $k = 1, \ldots, N_p$ **do**
  find the cell $i_k$ containing the position X($k$, $n$) of the agent $k$;
  v_macro_for_micro($k$) $\leftarrow$ v_macro_for_macro($i_k$);
**end**

**Algorithm 4:** function F3

**for** $i = 2, \ldots, N_x - 1$ **do**
  rho$(n+1, i) \leftarrow 0$;
  **for** $r = i-1, i, i+1$ **do**
    D $\leftarrow \Delta t$ v_macro($r$);
    temp=D$^{+}\delta_{r,i-1}$+D$^{-}\delta_{r,i+1} + (\Delta x - |\mathrm{D}|)\delta_{r,i}$;
    rho$(n+1, i) \leftarrow$ rho$(n+1, i)$+rho$(n, r)\frac{1}{\Delta x}$temp;
  **end**
**end**

**Algorithm 5:** Function F3 in two dimensions

**for** $i = 2, \ldots, N_x - 1$ **do**
  **for** $j = 2, \ldots, N_y - 1$ **do**
    rho$(n+1, i, j) \leftarrow 0$;
    **for** $r = i-1, i, i+1$ **do**
      **for** $s = j-1, j, j+1$ **do**
        Dx $\leftarrow \Delta t$ v_macro.x($r$);
        Dy $\leftarrow \Delta t$ v_macro.y($s$);
        temp.x=Dx$^{+}\delta_{r,i-1}$+Dx$^{-}\delta_{r,i+1} + (\Delta x - |\mathrm{Dx}|)\delta_{r,i}$;
        temp.y=Dy$^{+}\delta_{s,j-1}$+Dy$^{-}\delta_{s,j+1} + (\Delta y - |\mathrm{Dy}|)\delta_{s,j}$;
        rho$(n+1, i, j) \leftarrow$ rho$(n+1, i, j)$+
        rho$(n, r, s)\frac{1}{\Delta x \Delta y}$temp.x temp.y;
      **end**
    **end**
  **end**
**end**

# References


1. Adamatzky, A.: Dynamics of Crowd-Minds. Patterns of Irrationality in Emotions, Beliefs and Actions. World Scientific Series on Nonlinear Science, vol. 54. World Scientific, Hackensack (2005)
2. Ailisto, H.J., Lindholm, M., Mantyjarvi, J., Vildjiounaite, E., Makela, S.M.: Identifying people from gait pattern with accelerometers. In: Proceedings of the SPIE 5779, Biometric Technology for Human Identification II, Orlando, vol. 7, pp. 7–14 (2005)
3. Al-nasur, S., Kachroo, P.: A microscopic-to-macroscopic crowd dynamic model. In: Proceedings of the IEEE ITSC 2006, Toronto, pp. 606–611 (2006)
4. Amadori, D., Di Francesco, M.: The one-dimensional Hughes model for pedestrian flow: Riemann-type solutions. Acta Math. Sci. **32B**(1), 259–280 (2012)
5. Ambrosio, L., Gangbo, W.: Hamiltonian ODEs in the Wasserstein space of probability measures. Commun. Pure Appl. Math. **61**(1), 18–53 (2008)
6. Ambrosio, L., Gigli, N., Savaré, G.: Gradient Flows in Metric Spaces and in the Space of Probability Measures. Lectures in Mathematics ETH Zürich, 2nd edn. Birkhäuser Verlag, Basel (2008)
7. Aminian, K., Rezakhanlou, K., De Andres, E., Fritsch, C., Leyvraz, P.F., Robert, P.: Temporal feature estimation during walking using miniature accelerometers: an analysis of gait improvement after hip arthroplasty. Med. Biol. Eng. Comput. **37**(6), 686–691 (1999)
8. Antonini, G., Bierlaire, M., Weber, M.: Discrete choice models of pedestrian walking behavior. Transp. Res. B **40**, 667–687 (2006)
9. Arechavaleta, G., Laumond, J.P., Hicheur, H., Berthoz, A.: An optimality principle governing human walking. IEEE Trans. Robot. **24**(1), 5–14 (2008)
10. Aw, A., Rascle, M.: Resurrection of "second order" models of traffic flow? SIAM J. Appl. Math. **60**, 916–938 (2000)
11. Ballerini, M., Cabibbo, N., Candelier, R., Cavagna, A., Cisbani, E., Giardina, I., Lecomte, V., Orlandi, A., Parisi, G., Procaccini, A., Viale, M., Zdravkovic, V.: Interaction ruling animal collective behavior depends on topological rather than metric distance: evidence from a field study. Proc. Natl. Acad. Sci. U.S.A. **105**(4), 1232–1237 (2008)
12. Ballerini, M., Cabibbo, N., Candelier, R., Cavagna, A., Cisbani, E., Giardina, I., Orlandi, A., Parisi, G., Procaccini, A., Viale, M., Zdravkovic, V.: Empirical investigation of starling flocks: a benchmark study in collective animal behaviour. Anim. Behav. **76**, 201–215 (2008)
13. Bardi, M., Capuzzo Dolcetta, I.: Optimal Control and Viscosity Solutions of Hamilton-Jacobi-Bellman Equations. Birkhäuser, Boston/Basel/Berlin (1997)
14. Bellomo, N., Bellouquid, A.: On the modeling of crowd dynamics: looking at the beautiful shapes of swarms. Netw. Heterog. Media **6**(3), 383–399 (2011)



E. Cristiani et al., *Multiscale Modeling of Pedestrian Dynamics*, MS&A 12,
DOI 10.1007/978-3-319-06620-2,

15. Bellomo, N., Dogbé, C.: On the modelling crowd dynamics from scaling to hyperbolic macroscopic models. Math. Models Methods Appl. Sci. **18**, 1317–1345 (2008)
16. Bellomo, N., Dogbé, C.: On the modeling of traffic and crowds: a survey of models, speculations, and perspectives. SIAM Rev. **53**, 409–463 (2011)
17. Bellomo, N., Piccoli, B., Tosin, A.: Modeling crowd dynamics from a complex system viewpoint. Math. Models Methods Appl. Sci. **22**, 1230004/1–29 (2012)
18. Bellomo, N., Soler, J.: On the mathematical theory of the dynamics of swarms viewed as complex systems. Math. Models Methods Appl. Sci. **22**(suppl. 1), 1140006/1–29 (2012)
19. Blue, V.J., Adler, J.L.: Emergent fundamental pedestrian flows from cellular automata microsimulation. Transp. Res. Rec. **1644**, 29–36 (1998)
20. Blue, V.J., Adler, J.L.: Cellular automata microsimulation of bidirectional pedestrian flows. Transp. Res. Rec. **1678**, 135–141 (1999)
21. Blue, V.J., Adler, J.L.: Modeling four-directional pedestrian flows. Transp. Res. Rec. **1710**, 20–27 (2000)
22. Braess, D.: Über ein Paradoxon aus der Verkehrsplanung. Unternehmensforschung **12**, 258–168 (1969)
23. Braess, D., Nagurney, A., Wakolbinger, T.: On a paradox of traffic planning. Transp. Sci. **39**(4), 446–450 (2005)
24. Bresch, D., Choquet, C., Chupin, L., Colin, T., Gisclon, M.: Roughness-induced effect at main order on the Reynolds approximation. Multiscale Model. Simul. **8**(3), 997–1017 (2010)
25. Bressan, A., Piccoli, B.: Introduction to the Mathematical Theory of Control. AIMS on Applied Mathematics, vol. 2. American Institute of Mathematical Sciences, Springfield (2007)
26. Bruno, L., Corbetta, A., Tosin, A.: From individual behaviors to an evaluation of the collective evolution of crowds along footbridges arXiv:1212.3711
27. Bruno, L., Tosin, A., Tricerri, P., Venuti, F.: Non-local first-order modelling of crowd dynamics: a multidimensional framework with applications. Appl. Math. Model. **35**, 426–445 (2011)
28. Burger, M., Di Francesco, M., Markowich, P.A., Wolfram, M.T.: Mean field games with nonlinear mobilities in pedestrian dynamics. arXiv:1304.5201
29. Burger, M., Markowich, P.A., Pietschmann, J.F.: Continuous limit of a crowd motion and herding model: analysis and numerical simulations. Kinet. Relat. Models **4**, 1025–1047 (2011)
30. Burstedde, C., Klauck, K., Schadschneider, A., Zittartz, J.: Simulation of pedestrian dynamics using a two-dimensional cellular automaton. Physica A **295**, 507–525 (2001)
31. Canuto, C., Fagnani, F., Tilli, P.: A Eulerian approach to the analysis of rendez-vous algorithms. In: Proceedings of the 17th IFAC World Congress (IFAC'08), Seoul, pp. 9039–9044. The International Federation of Automatic Control, IFAC World Congress, Seoul (2008)
32. Canuto, C., Fagnani, F., Tilli, P.: An Eulerian approach to the analysis of Krause's consensus models. SIAM J. Control Optim. **50**(1), 243–265 (2012)
33. Carrillo, J.A., Fornasier, M., Toscani, G., Vecil, F.: Particle, kinetic, and hydrodynamic models of swarming. In: Naldi, G., Pareschi, L., Toscani, G. (eds.) Mathematical Modeling of Collective Behavior in Socio-economic and Life Sciences. Modeling and Simulation in Science, Engineering and Technology, pp. 297–336. Birkhäuser, Boston (2010)
34. Cepolina, E., Tyler, N.: Understanding capacity drop for designing pedestrian environments. In: The 6th International Conference on Walking in the 21st Century, Zurich (2005)
35. Chitour, Y., Jean, F., Mason, P.: Optimal control models of goal-oriented human locomotion. SIAM J. Control Optim. **50**(1), 147–170 (2012)
36. Chraibi, M., Kemloh, U., Schadschneider, A., Seyfried, A.: Force-based models of pedestrian dynamics. Netw. Heterog. Media **6**, 425–442 (2011)
37. Chraibi, M., Seyfried, A., Schadschneider, A.: Generalized centrifugal-force model for pedestrian dynamics. Phys. Rev. E **82**, 046111/1–9 (2010)

38. Colombo, R.M., Garavello, M., Lecureux-Mercier, M.: A class of nonlocal models of pedestrian traffic. Math. Models Methods Appl. Sci. **22**, 1150023/1–34 (2012)
39. Colombo, R.M., Herty, M., Mercier, M.: Control of the continuity equation with a non local flow. ESAIM Control Optim. Calc. Var. **17**, 353–379 (2011)
40. Colombo, R.M., Piccoli, B.: Special issue on "crowd dynamics: results and perspectives". Netw. Heterog. Media **6**(3), i–iii (2011)
41. Colombo, R.M., Rosini, M.D.: Pedestrian flows and non-classical shocks. Math. Methods Appl. Sci. **28**, 1553–1567 (2005)
42. Colombo, R.M., Rosini, M.D.: Existence of nonclassical solutions in a pedestrian flow model. Nonlinear Anal. Real World Appl. **10**, 2716–2728 (2009)
43. Coscia, V., Canavesio, C.: First-order macroscopic modelling of human crowd dynamics. Math. Models Methods Appl. Sci. **18**, 1217–1247 (2008)
44. Cristiani, E. Coupling Brownian motion and heat equation: Toward a new description of multi-nature phenomena. arXiv:1406.1814
45. Cristiani, E., Engquist, B.: Hamilton-Jacobi equations. In: Engquist, B., Chan, T., Cook, W.J., Hairer, E., Hastad, J., Iserles, A., Langtangen, H.P., Le Bris, C., Lions, P.L., Lubich, C., Majda, A.J., McLaughlin, J., Nieminen, R.M., Oden, J., Souganidis, P., Tveito, A. (eds.) Encyclopedia of Applied and Computational Mathematics. Springer, Berlin/Heidelberg (2013)
46. Cristiani, E., Frasca, P., Piccoli, B.: Effects of anisotropic interactions on the structure of animal groups. J. Math. Biol. **62**, 569–588 (2011)
47. Cristiani, E., Piccoli, B., Tosin, A.: Modeling self-organization in pedestrians and animal groups from macroscopic and microscopic viewpoints. In: Naldi, G., Pareschi, L., Toscani, G. (eds.) Mathematical Modeling of Collective Behavior in Socio-economic and Life Sciences. Modeling and Simulation in Science, Engineering and Technology, pp. 337–364. Birkhäuser, Boston (2010)
48. Cristiani, E., Piccoli, B., Tosin, A.: Multiscale modeling of granular flows with application to crowd dynamics. Multiscale Model. Simul. **9**, 155–182 (2011)
49. Cristiani, E., Piccoli, B., Tosin, A.: How can macroscopic models reveal self-organization in traffic flow? In: 51st IEEE Conference on Decision and Control, Maui, 10–13 Dec 2012
50. Cristiani, E., Priuli, F.S., Tosin, A.: Modeling rationality to control self-organization of crowds: an environmental approach. arXiv:1406.7246
51. Cucker, F., Smale, S.: Emergent behavior in flocks. IEEE Trans. Autom. Control **52**(5), 852–862 (2007)
52. Cucker, F., Smale, S.: On the mathematics of emergence. Jpn. J. Math. **2**(1), 197–227 (2007)
53. Daamen, W., Hoogendoorn, S.P.: Experimental research of pedestrian walking behavior. Transp. Res. Rec. **1828**, 20–30 (2003)
54. Dabbs, J.M., Jr., Stokes, N.A., III: Beauty is power: the use of space on the sidewalk. Sociometry **38**(4), 551–557 (1975)
55. Daganzo, C.F.: Requiem for second-order fluid approximations of traffic flow. Transp. Res. B **29**, 277–286 (1995)
56. Dalton, R.C.: The secret is to follow your nose: route path selection and angularity. Environ. Behav. **35**(1), 107–131 (2003)
57. De Angelis, E.: Nonlinear hydrodynamic models of traffic flow modelling and mathematical problems. Math. Comput. Model. **29**, 83–95 (1999)
58. Degond, P., Dimarco, G., Mieussens, L.: A multiscale kinetic-fluid solver with dynamic localization of kinetic effects. J. Comput. Phys. **229**(13), 4907–4933 (2010)
59. Degond, P., Liu, J.G., Mieussens, L.: Macroscopic fluid model with localized kinetic upscaling effects. Multiscale Model. Simul. **5**(3), 940–979 (2006)
60. Degond, P., Motsch, S.: Continuum limit of self-driven particles with orientation interaction. Math. Models Methods Appl. Sci. **18**(suppl.), 1193–1215 (2008)
61. Di Francesco, M., Fagioli, S.: Measure solutions for non-local interaction PDEs with two species. Nonlinearity **26**(10), 2777–2808 (2103)

62. Di Francesco, M., Markowich, P.A., Pietschmann, J.F., Wolfram, M.T.: On the Hughes' model for pedestrian flow: the one-dimensional case. J. Differ. Equ. **250**, 1334–1362 (2011)
63. Dogbé, C.: On the numerical solutions of second order macroscopic models of pedestrian flows. Comput. Math. Appl. **56**, 1884–1898 (2008)
64. Dogbé, C.: Modeling crowd dynamics by the mean-field limit approach. Math. Comput. Model. **52**, 1506–1520 (2010)
65. Dogbé, C.: On the modelling of crowd dynamics by generalized kinetic models. J. Math. Anal. Appl. **387**(2), 512–532 (2012)
66. Donev, A., Bell, J.B., Garcia, A.L., Alder, B.J.: A hybrid particle-continuum method for hydrodynamics of complex fluids. Multiscale Model. Simul. **8**(3), 871–911 (2010)
67. Duives, D.C., Daamen, W., Hoogendoorn, S.P.: State-of-the-art crowd motion simulation models. Transp. Res. C **37**, 193–209 (2013)
68. El-Khatib, N., Goatin, P., Rosini, M.D.: On entropy weak solutions of Hughes' model for pedestrian motion. Z. Angew. Math. Phys. **64**, 223–251 (2013)
69. Falcone, M., Ferretti, R.: Semi-Lagrangian Approximation Schemes for Linear and Hamilton-Jacobi Equations. SIAM, Philadelphia (2014)
70. Fermo, L., Tosin, A. A fully-discrete-state kinetic theory approach to traffic flow on road networks. arXiv:1406.4257
71. Fermo, L., Tosin, A.: A fully-discrete-state kinetic theory approach to modeling vehicular traffic. SIAM J. Appl. Math. **73**(4), 1533–1556 (2013)
72. Fruin, J.J.: Designing for pedestrians: a level-of-service concept. Highw. Res. Rec. **355**, 1–15 (1971)
73. Goatin, P., Mimault, M.: The wave-front tracking algorithm for Hughes' model of pedestrian motion. SIAM J. Sci. Comput. **35**(3), B606–B622 (2013)
74. Goffman, E.: Relations in Public: Microstudies of the Public Order. Basic Books, New York (1971)
75. Golledge, R.G.: Human wayfinding and cognitive maps. In: Golledge, R.G. (ed.) Wayfinding Behavior, chap. 1, pp. 5–45. The Johns Hopkins University Press, Baltimore (1999)
76. Golson, H.L., Dabbs, J.M.: Line-following tendencies among pedestrians: a sex difference. Pers. Soc. Psychol. B **1**(1), 16–18 (1974)
77. Guéant, O., Lasry, J.M., Lions, P.L.: Mean field games and applications. In: Carmona, R.A., Cinlar, E., Ekeland, I., Jouini, E., Scheinkman, J.A., Touzi, N. (eds.) Paris-Princeton Lectures on Mathematical Finance 2010. Lecture Notes in Mathematics, pp. 205–266. Springer, Heidelberg/Dordrecht/London/New York (2011)
78. Ha, S.Y., Tadmor, E.: From particle to kinetic and hydrodynamic descriptions of flocking. Kinet. Relat. Models **1**(3), 415–435 (2008)
79. Hankin, B.D., Wright, R.A.: Passenger flow in subways. Oper. Res. Q. **9**(2), 81–88 (1958)
80. Hartmann, D., von Sivers, I.: Structured first order conservation models for pedestrian dynamics. Netw. Heterog. Media **8**(4), 985–1007 (2013)
81. Helbing, D.: A mathematical model for the behavior of pedestrians. Behav. Sci. **36**, 298–310 (1991)
82. Helbing, D.: A fluid-dynamic model for the movement of pedestrians. Complex Syst. **6**, 391–415 (1992)
83. Helbing, D.: Traffic and related self-driven many-particle systems. Rev. Mod. Phys. **73**, 1067–1141 (2001)
84. Helbing, D., Buzna, L., Johansson, A., Werner, T.: Self-organized pedestrian crowd dynamics: experiments, simulations, and design solutions. Transp. Sci. **39**(1), 1–24 (2005)
85. Helbing, D., Farkas, I., Vicsek, T.: Simulating dynamical features of escape panic. Nature **407**, 487–490 (2000)
86. Helbing, D., Johansson, A.: Quantitative agent-based modeling of human interactions in space and time. In: Proceedings of the Fourth Conference of the European Social Simulation Association, Toulouse, pp. 623–637 (2007)
87. Helbing, D., Johansson, A., Zein Al-Abideen, H.: Dynamics of crowd disasters: an empirical study. Phys. Rev. E **75**, 046109/1–7 (2007)

88. Helbing, D., Molnàr, P.: Social force model for pedestrian dynamics. Phys. Rev. E **51**, 4282–4286 (1995)
89. Helbing, D., Molnár, P., Farkas, I.J., Bolay, K.: Self-organizing pedestrian movement. Environ. Plann. B Plann. Des. **28**(3), 361–383 (2001)
90. Helbing, D., Vicsek, T.: Optimal self-organization. New J. Phys. **1**, 13.1–13.17 (1999)
91. Henderson, L.F.: On the fluid mechanics of human crowd motion. Transp. Res. **8**, 509–515 (1974)
92. Herty, M., Moutari, S.: A macro-kinetic hybrid model for traffic flow on road networks. Comput. Methods Appl. Math. **9**(3), 238–252 (2009)
93. Ho, H.W., Wong, S.C.: Two-dimensional continuum modeling approach to transportation problems. J. Transp. Syst. Eng. Inf. Technol. **6**, 53–72 (2006)
94. Hoogendoorn, S.P., Bovy, P.H.L.: Gas-kinetic modeling and simulation of pedestrian flows. Transp. Res. Rec. **1710**, 28–36 (2000)
95. Hoogendoorn, S.P., Bovy, P.H.L.: Simulation of pedestrian flows by optimal control and differential games. Optim. Control Appl. Meth. **24**, 153–172 (2003)
96. Hoogendoorn, S.P., Bovy, P.H.L.: Dynamic user-optimal assignment in continuous time and space. Transp. Res. B **38**, 571–592 (2004)
97. Hoogendoorn, S.P., Bovy, P.H.L.: Pedestrian route-choice and activity scheduling theory and models. Transp. Res. B **38**, 169–190 (2004)
98. Hoogendoorn, S.P., Daamen, W.: Self-organization in pedestrian flow. In: Hoogendoorn, S.P., Luding, S., Bovy, P.H.L., Schreckenberg, M., Wolf, D.E. (eds.) Traffic and Granular Flow '03, Springer, Berlin Heidelberg 373–382 (2005)
99. Hoogendoorn, S.P., Daamen, W., Bovy, P.H.L.: Extracting microscopic pedestrian characteristics from video data. In: Transportation Research Board Annual Meeting 2003, Washington, DC, pp. 1–15. National Academy Press, Washington, DC (2003)
100. Huang, L., Wong, S.C., Zhang, M., Shu, C.W., Lam, W.H.K.: Revisiting Hughes' dynamic continuum model for pedestrian flow and the development of an efficient solution algorithm. Transp. Res. B **43**, 127–141 (2009)
101. Hughes, R.L.: The flow of large crowds of pedestrians. Math. Comput. Simul. **53**, 367–370 (2000)
102. Hughes, R.L.: A continuum theory for the flow of pedestrians. Transp. Res. B **36**, 507–535 (2002)
103. Ishikawa, T., Fujiwara, H., Imai, O., Okabe, A.: Wayfinding with a GPS-based mobile navigation system: a comparison with maps and direct experience. J. Environ. Psychol. **28**(1), 74–82 (2008)
104. Ishikawa, T., Montello, D.R.: Spatial knowledge acquisition from direct experience in the environment: individual differences in the development of metric knowledge and the integration of separately learned places. Cogn. Psychol. **52**(2), 93–129 (2006)
105. Jacod, J., Protter, P.: Probability Essentials. Universitext, 2nd edn. Springer, Berlin (2003)
106. Jiang, Y., Zhang, P., Wong, S.C., Liu, R.: A higher-order macroscopic model for pedestrian flows. Physica A **389**, 4623–4635 (2010)
107. Kachroo, P., Al-nasur, S.J., Wadoo, S.A., Shende, A.: Pedestrian Dynamics. Feedback Control of Crowd Evacuation. Understanding Complex Systems. Springer, Berlin/Heidelberg (2008)
108. Kamareddine, A.M., Hughes, R.L.: Towards a mathematical model for stability in pedestrian flows. Netw. Heterog. Media **6**(3), 465–483 (2011)
109. Kirchner, A., Schadschneider, A.: Simulation of evacuation processes using a bionics-inspired cellular automaton model for pedestrian dynamics. Physica A **312**, 260–276 (2002)
110. Klar, A., Wegener, R.: Traffic flow: models and numerics. In: Degond, P., Pareschi, L., Russo, G. (eds.) Modeling and Computational Methods for Kinetic Equations. Modeling and Simulation in Science, Engineering and Technology, pp. 219–258. Birkhäuser, Boston (2004)
111. Koshak, N., Fouda, A.: Analyzing pedestrian movement in Mataf using GPS and GIS to support space redesign. In: The 9th International Conference on Design and Decision Support Systems (DDSS) in Architecture and Urban Planning, The Netherlands (2008)

112. Köster, G., Treml, F., Gödel, M.: Avoiding numerical pitfalls in social force models. Phys. Rev. E **87**, 063305/1–13 (2013)
113. Kraft, T.: An efficient method for coupling microscopic and macroscopic calculations in solidification modelling. Model. Simul. Mater. Sci. Eng. **5**(5), 473–480 (1997)
114. Lachapelle, A.: Quelques problèmes de transport et de contrôle en économie: aspects théoriques et numériques. Ph.D. thesis, Université Paris-Dauphine, France (2010)
115. Lachapelle, A., Wolfram, M.T.: On a mean field game approach modeling congestion and aversion in pedestrian crowds. Transp. Res. B **45**, 1572–1589 (2011)
116. Levine, M.: You-are-here maps: psychological considerations. Environ. Behav. **14**(2), 221–237 (1982)
117. Levine, M., Marchon, I., Hanley, G.: The placement and misplacement of you-are-here maps. Environ. Behav. **16**(2), 139–157 (1984)
118. Lighthill, M.J., Whitham, G.B.: On kinematic waves. II. A theory of traffic flow on long crowded roads. Proc. R. Soc. Lond. Ser. A **229**, 317–345 (1955)
119. Lloyd, R., Heivly, C.: Systematic distortions in urban cognitive maps. Ann. Assoc. Am. Geogr. **77**(2), 191–207 (1987)
120. Maury, B., Roudneff-Chupin, A., Santabrogio, F.: A macroscopic crowd motion model of gradient flow type. Math. Models Methods Appl. Sci. **20**, 1787–1821 (2010)
121. Maury, B., Roudneff-Chupin, A., Santabrogio, F., Venel, J.: Handling congestion in crowd motion modeling. Netw. Heterog. Media **6**, 485–519 (2011)
122. Maury, B., Venel, J.: Un modèle de mouvements de foule. ESAIM Proc. **18**, 143–152 (2007)
123. Maury, B., Venel, J.: A mathematical framework for a crowd motion model. C. R. Acad. Sci. Paris Ser. I **346**, 1245–1250 (2008)
124. Mogilner, A., Edelstein-Keshet, L., Bent, L., Spiros, A.: Mutual interactions, potentials, and individual distance in a social aggregation. J. Math. Biol. **47**, 353–389 (2003)
125. Montello, D.: The perception and cognition of environmental distance: direct sources of information. In: Spatial Information Theory: A Theoretical Basis for GIS, Laurel Highlands. Lecture Notes in Computer Science, vol. 1329, pp. 297–311. Springer, Berlin/Heidelberg (1997)
126. Moussaïd, M., Guillot, E.G., Moreau, M., Fehrenbach, J., Chabiron, O., Lemercier, S., Pettré, J., Appert-Rolland, C., Degond, P., Theraulaz, G.: Traffic instabilities in self-organized pedestrian crowds. PLoS Comput. Biol. **8**(3), e1002442/1–10 (2012)
127. Moussaïd, M., Helbing, D., Theraulaz, G.: How simple rules determine pedestrian behavior and crowd disasters. Proc. Natl. Acad. Sci. U.S.A. **108**(17), 6884–6888 (2011)
128. Moussaïd, M., Perozo, N., Garnier, S., Helbing, D., Theraulaz, G.: The walking behaviour of pedestrian social groups and its impact on crowd dynamics. Plos One **5**(4), e10047/1–7 (2010)
129. Navin, F.P., Wheeler, R.J.: Pedestrian flow characteristics. Traffic Eng. **19**(7), 30–33 (1969)
130. Okazaki, S.: A study of pedestrian movement in architectural space, Part 1: pedestrian movement by the application of magnetic model. Trans. A.I.J. **283**, 111–119 (1979)
131. Okazaki, S.: A study of pedestrian movement in architectural space, Part 2: concentrated pedestrian movement. Trans. A.I.J. **284**, 101–110 (1979)
132. Okazaki, S.: A study of pedestrian movement in architectural space, Part 3: along the shortest path, taking fire, congestion and unrecognized space into account. Trans. A.I.J. **285**, 137–147 (1979)
133. Okazaki, S., Matsushita, S.: A study of pedestrian movement in architectural space, Part 5: a proubing walk and a guide walk by a guideboard. Trans. A.I.J. **302**, 87–93 (1981)
134. Okazaki, S., Yamamoto, C.: A study of pedestrian movement in architectural space, Part 4: pedestrian movement represented in perspective. Trans. A.I.J. **299**, 105–113 (1981)
135. O'Neill, E., Kostakos, V., Kindberg, T., Schiek, A., Penn, A., Fraser, D., Jones, T.: Instrumenting the city: developing methods for observing and understanding the digital cityscape. In: Dourish, P., Friday, A. (eds.) UbiComp 2006: Ubiquitous Computing. Lecture Notes in Computer Science, vol. 4206, pp. 315–332. Springer, Berlin/Heidelberg (2006)

136. Ozbay, K., Yang, H., Bartin, B.: Calibration of an infrared-based automatic counting system for pedestrian traffic flow data collection. In: Transportation Research Board 89th Annual Meeting, Washington, DC (2010)
137. Papadimitriou, E., Yannis, G., Golias, J.: A critical assessment of pedestrian behaviour models. Transp. Res. F **12**(3), 242–255 (2009)
138. Payne, H.J.: Models of freeway traffic and control. Math. Models Publ. Syst. Simul. Counc. Proc. **28**, 51–61 (1971)
139. Pelechano, N., Allbeck, J.M., Badler, N.I.: Virtual Crowds: Methods, Simulation, and Control. Synthesis Lectures on Computer Graphics and Animation. Morgan & Claypool, San Rafael (2008)
140. Piccoli, B., Rossi, F.: On properties of the generalized Wasserstein distance arXiv:1304.7014
141. Piccoli, B., Rossi, F.: Transport equation with nonlocal velocity in Wasserstein spaces: convergence of numerical schemes. Acta Appl. Math. **124**(1), 73–105 (2013)
142. Piccoli, B., Rossi, F.: Generalized Wasserstein distance and its application to transport equations with source. Arch. Ration. Mech. Anal. **211**(1), 335–358 (2014)
143. Piccoli, B., Sussmann, H.J.: Regular synthesis and sufficiency conditions for optimality. SIAM J. Control Optim. **39**(2), 359–410 (2000)
144. Piccoli, B., Tosin, A.: Pedestrian flows in bounded domains with obstacles. Contin. Mech. Thermodyn. **21**, 85–107 (2009)
145. Piccoli, B., Tosin, A.: Time-evolving measures and macroscopic modeling of pedestrian flow. Arch. Ration. Mech. Anal. **199**, 707–738 (2011)
146. Plamondon, R., Guerfali, W.: The $2/3$ power law: when and why? Acta Psychol. **100**(1), 85–96 (1998)
147. Prigogine, I.: A Boltzmann-like approach to the statistical theory of traffic flow. In: Theory of Traffic Flow, Warren, pp. 158–164. Elsevier, Amsterdam (1961)
148. Prigogine, I., Herman, R.: Kinetic Theory of Vehicular Traffic. American Elsevier, New York (1971)
149. Quarteroni, A., Veneziani, A.: Analysis of a geometrical multiscale model based on the coupling of ODE and PDE for blood flow simulations. Multiscale Model. Simul. **1**(2), 173–195 (2003)
150. Rachev, S.T.: Probability Metrics and the Stability of Stochastic Models. Wiley, Chichester/New York (1991)
151. Richards, P.I.: Shock waves on the highway. Oper. Res. **4**, 42–51 (1956)
152. Roggen, D., Wirz, M., Tröster, G., Helbing, D.: Recognition of crowd behavior from mobile sensors with pattern analysis and graph clustering methods. Netw. Heterog. Media **6**(3), 521–544 (2011)
153. Rosini, M.D.: Macroscopic Models for Vehicular Flows and Crowd Dynamics: Theory and Applications. Understanding Complex Systems. Springer, Switzerland (2013)
154. Rudin, W.: Real and Complex Analysis, 3rd edn. McGraw-Hill, New York (1987)
155. Schaal, S., Sternad, D.: Origins and violations of the $2/3$ power law in rhythmic three-dimensional arm movements. Exp. Brain Res. **136**(1), 60–72 (2001)
156. Schadschneider, A., Seyfried, A.: Empirical results for pedestrian dynamics and their implications for modeling. Netw. Heterog. Media **6**, 545–560 (2011)
157. Seyfried, A., Passon, O., Steffen, B., Boltes, M., Rupprecht, T., Klingsch, W.: New insights into pedestrian flow through bottlenecks. Transp. Sci. **43**(3), 395–406 (2009)
158. Seyfried, A., Steffen, B., Klingsch, W., Boltes, M.: The fundamental diagram of pedestrian movement revisited. J. Stat. Mech. Theory Exp. **2005**(10), P10002 (2005)
159. Thalmann, D.: Crowd Simulation. Wiley Online Library (2007)
160. Tosin, A., Frasca, P.: Existence and approximation of probability measure solutions to models of collective behaviors. Netw. Heterog. Media **6**, 561–596 (2011)
161. Twarogowska, M., Goatin, P., Duvigneau, R.: Macroscopic modeling and simulations of room evacuation. Appl. Math. Model. (In press)
162. Venuti, F., Bruno, L.: Crowd-structure interaction in lively footbridges under synchronous lateral excitation: a literature review. Phys. Life Rev. **6**, 176–206 (2009)

163. Vickers, D., Bovet, P., Lee, M.D., Hughes, P.: The perception of minimal structures: performance on open and closed versions of visually presented Euclidean travelling salesperson problems. Perception **32**(7), 871–886 (2003)
164. Vicsek, T., Czirók, A., Ben-Jacob, E., Cohen, I., Shochet, O.: Novel type of phase transition in a system of self-driven particles. Phys. Rev. Lett. **75**(6), 1226–1229 (1995)
165. Vieilledent, S., Kerlirzin, Y., Dalbera, S., Berthoz, A.: Relationship between velocity and curvature of a human locomotor trajectory. Neurosci. Lett. **305**(1), 65–69 (2001)
166. Villani, C.: Topics in Optimal Transportation. Graduate Studies in Mathematics Series, vol. 58. American Mathematical Society, Providence (2003)
167. Villani, C.: Optimal Transport. Old and New. Grundlehren der Mathematischen Wissenschaften (Fundamental Principles of Mathematical Sciences), vol. 338. Springer, Berlin/Heidelberg (2009)
168. Viviani, P., Flash, T.: Minimum-jerk, two-thirds power law, and isochrony: converging approaches to movement planning. J. Exp. Psychol. Hum. **21**(1), 32–53 (1995)
169. Weimar, J.R.: Coupling microscopic and macroscopic cellular automata. Parallel Comput. **27**(5), 601–611 (2001)
170. Whitham, G.B.: Linear and Nonlinear Waves. Pure and Applied Mathematics. Wiley, New York (1974)
171. Willis, A., Kukla, R., Kerridge, J., Hine, J.: Laying the foundations: the use of video footage to explore pedestrian dynamics in PEDFLOW. In: Schreckenberg, M., Sharma, S.D. (eds.) Pedestrian and Evacuation Dynamics, pp. 181–186. Springer, Berlin/Heidelberg (2002)
172. Wolff, M.: Notes on the behaviour of pedestrians. In: Birenbaum, A., Sagarin, E. (eds.) People in Places: The Sociology of the Familiar, pp. 35–48. Praeger, New York (1973)
173. Xia, Y., Wong, S.C., Shu, C.W.: Dynamic continuum pedestrian flow model with memory effect. Phys. Rev. E **79**, 066113/1–8 (2009)
174. Yu, W.J., Chen, R., Dong, L.Y., Dai, S.Q.: Centrifugal force model for pedestrian dynamics. Phys. Rev. E **72**, 026112/1–7 (2005)
175. Zhang, H.M.: A non-equilibrium traffic model devoid of gas-like behavior. Transp. Res. B **36**, 275–290 (2002)

# Index




E. Cristiani et al., *Multiscale Modeling of Pedestrian Dynamics*, MS&A 12,
DOI 10.1007/978-3-319-06620-2,

# MS&A – Modeling, Simulation and Applications

7. B. Maury
   The Respiratory System in Equations
   2013, XVIII+276 pp, ISBN 978-88-470-5213-0

8. A. Quarteroni
   Numerical Models for Differential Problems, 2nd Edition
   2014, XX+656pp, ISBN 978-88-470-5521-6

9. A. Quarteroni, G. Rozza (Eds.)
   Reduced Order Methods for modeling and computational reduction
   2014, X+332pp, ISBN 978-3-319-02089-1

10. J. Xin, Y. Qi
    An Introduction to Mathematical Modeling and Signal Processing in Speech and Hearing Sciences
    2014, XII+208pp, ISBN 978-3-319-03085-2

11. L. Beirão da Veiga, K. Lipnikov, G. Manzini
    The Mimetic Finite Difference Method for Elliptic Problems
    2014, XVI+392pp, ISBN 978-3-319-02662-6

12. E. Cristiani, B. Piccoli, A. Tosin
    Multiscale Modeling of Pedestrian Dynamics
    2014, XVI+260pp, ISBN 978-3-319-06619-6

For further information, please visit the following link:
http://www.springer.com/series/8377